

Copyright

by

Matthew Robert O'Callaghan

2007

**Tensile Stresses in the End Regions of Pretensioned I-Beams at
Release**

by

Matthew Robert O'Callaghan, B.S.C.E.

Thesis

Presented to the Faculty of the Graduate School of
The University of Texas at Austin
in Partial Fulfillment
of the Requirements
for the Degree of

Master of Science in Engineering

**The University of Texas at Austin
August 2007**

**Tensile Stresses in the End Regions of Pretensioned I-Beams at
Release**

**Approved by
Supervising Committee:**

Oguzhan Bayrak, Supervisor

John E. Breen

Acknowledgements

This research project was made possible by generous support from the Texas Department of Transportation. A special thanks to the project director, John Holt, as well as Amy Eskridge at the Texas Department of Transportation for allowing me to test their new Tx family of girders.

Special thanks go to Dr. Michael Engelhardt for offering his guidance and expertise with the design of the pretensioning bed. Dr. John Breen's consultations were also greatly appreciated for without them the quality of this thesis would have suffered greatly. To Dr. Bayrak, my supervising professor, without your guidance and constant concern for quality, this project and my engineering abilities would never have reached their full potential.

I would also like to thank those that helped me while I worked in Ferguson Laboratory. Alejandro Avendano, without your countless hours and helpful insights in support of this project I would most likely still be working at Ferguson today. Sean Clifton, your hours spent in support of this project helped make it more complete. I would also like to thank David Birrcher, Robin Tuchscherer, and Matt Huizinga for being sounding boards and guaranteed help whenever I needed them. To all those additional students that helped during casts, I am grateful. Lastly, the assistance of the technical support and administrative staff at FSEL including Blake Stasney, Dennis Phillip, Eric Schell, Mike Wason, Greg Harris, Barbara Howard, Ella Schwartz, and Cari Billingsley is truly appreciated.

The most important thanks I have to give are owed to my parents. Thank you for pushing me when I needed pushed and offering wisdom when I had no answers. Without your continued love and support, I would not be who I am today.

Tensile Stresses in the End Regions of Pretensioned I-Beams at Release

Matthew Robert O'Callaghan, M.S.E.

The University of Texas at Austin, 2007

SUPERVISOR: Oguzhan Bayrak

An experimental research study was conducted at the Phil M. Ferguson Structural Engineering Laboratory at the University of Texas at Austin to investigate the cracking in end regions of pretensioned I-beams at prestress transfer. This horizontal cracking near the end face of the girder is caused by the tensile forces that develop perpendicular to the line of action of the prestressing force after it has been applied. After seeing this cracking occur in multiple girders throughout the state of Texas and in the process of developing design standards for a new family of prestressed concrete I-beams (Tx family of beams), the Texas Department of Transportation sponsored this research to investigate this end region cracking problem. The goals of this research were to:

- i. Ensure that the cracks forming in the end regions of new I-Beams are comparable to or less severe than those in conventional AASHTO girders or TxDOT beams.
- ii. Quantify the amount of end region reinforcement that should be used in the new I-Beams to ensure that the quality of the new I-Beams, that have larger bottom flanges and greater prestressing force, is comparable to or better than the conventional AASHTO girders or TxDOT beams.

To achieve these research objectives, four full scale beams from the new Tx family of girders were fabricated. More specifically, two 28", one 46", and one

70” deep girders were tested to examine transverse stresses in the end regions of pretensioned beams. The testing of four 30-ft-long full-scale beams resulted in 8 test regions. The test regions at the two ends of each girder had different transverse reinforcement details. Each end region was comprehensively instrumented by strain gauges to capture the most critical strains. The strain gauge data collected at the release of the prestressing strands was used to prepare new reinforcement details to control the widths of the cracks that form in the end regions of pretensioned I-girders at release.

Table of Contents

CHAPTER 1 INTRODUCTION.....	1
1.1 Background	1
1.1.1 Florida DOT	1
1.1.2 Washington DOT	3
1.1.3 Texas DOT	4
1.2 Objectives of Research.....	6
1.3 Scope of Research	6
1.4 Research Overview: Chapter Outline.....	7
CHAPTER 2 LITERATURE REVIEW	8
2.1 Overview	8
2.2 Historical Review of Pretensioned Anchorage Zone Research	12
2.2.1 U.S. Research	13
2.2.1.1 Marshall and Mattock, 1962.....	13
2.2.1.2 Gergely, Sozen, and Siess, 1963	18
2.2.1.3 Breen, Burdet, Roberts, Sanders, and Wollmann, 1994	25
2.2.1.4 Tuan, Yehia, Jonpitaksseel, and Tadros, 2004.....	28
2.2.2 European Research.....	33
2.2.2.1 Uijl, 1983.....	33
2.2.2.2 Comité Euro-International Du Béton, 1987	44
2.2.2.3 Comité Euro-International Du Béton, 1992	47
2.3 Code Development.....	51
2.3.1 United States Design Specifications and Guidelines	53
2.3.1.1 AASHTO Specifications for Highway Bridges, 1961 ...	53
2.3.1.2 AASHTO LRFD Bridge Design Specifications, 2007...	53

2.3.1.3	AASHTO LRFD Bridge Design Specifications, 2007...	54
2.3.1.4	PCI Design Handbook, 6 th Edition, 2004.....	55
2.3.2	A European Code: CEB-FIP Model Code, 1990	55
2.4	Summary	62
CHAPTER 3 EXPERIMENTAL PROGRAM		66
3.1	Overview	66
3.2	Specimen Design.....	66
3.2.1	Prestressed Beam Theory	66
3.2.1.1	Transfer Length	67
3.2.1.2	Beam Theory	69
3.2.1.3	Elastic Shortening	71
3.2.2	Tx Girder Design.....	72
3.3	Concrete Properties	76
3.3.1	Concrete Testing	76
3.3.2	Temperature Match Cure	78
3.3.2.1	Temperature Match Curing Facility: Sure Cure System	80
3.4	Mechanical Properties of Reinforcing Steel.....	82
3.4.1	Prestressing Steel.....	82
3.4.2	Welded Deformed Wire	84
3.4.3	Grade 60 Rebar.....	87
3.5	Pretensioning Facility.....	87
3.5.1	Design	87
3.5.2	Construction of Pretensioning Facility.....	92
3.6	TxDOT New I Beam Sections	94
3.7	Instrumentation.....	97
3.7.1	General	97

3.7.2	Strain Gauge Installation on Reinforcing Bars	98
3.7.2.1	Tx28-I and II Rebar Gauge Locations.....	100
3.7.2.2	Tx46 Rebar Gauge Locations.....	103
3.7.2.3	Tx70 Rebar Gauge Locations.....	106
3.7.3	Strain Gauge Installation on Strands	109
3.7.4	Temperature Monitoring	114
3.8	Specimen Fabrication	115
3.8.1	General	115
3.8.2	Pretensioning the Strands	116
3.8.3	Mixing and Placing Concrete	121
3.8.4	Releasing the Strands	126
CHAPTER 4 TEST RESULTS AND DISCUSSION		130
4.1	Introduction	130
4.2	Preliminary Analysis	133
4.2.1	AASHTO LRFD Bridge Design Specifications (2007).....	137
4.2.2	PCI Design Handbook (6 th Edition) Guidelines.....	138
4.2.3	CEB-FIP Model Code 1990 Provisions	138
4.2.4	Design Guideline Comparison Summary.....	144
4.3	Tx28-I Results	148
4.3.1	Tx28-I Release	148
4.3.1.1	Strand Stress before Release	149
4.3.2	Tx28-I Strand Stresses	150
4.3.3	Tx28-I Transverse Reinforcing Bar Stresses	153
4.3.4	Tx28-I Summary	160
4.4	Tx 28-II Results.....	161
4.4.1	Tx28-II Release	161
4.4.1.1	Strand Stress before Release	162

4.4.2 Tx28-II Strand Stresses	163
4.4.3 Tx28-II Transverse Reinforcing Bar Stresses	165
4.4.4 Tx28-II Summary	172
4.5 Tx46 Results.....	173
4.5.1 Tx46 Release	173
4.5.1.1 Strand Stresses before Release	174
4.5.2 Tx46 Strand Stresses	174
4.5.3 Tx46 Transverse Reinforcing Bar Stresses	176
4.5.4 Tx46 Summary	182
4.6 Tx70 Results.....	183
4.6.1 Tx70 Release	183
4.6.1.1 Strand Stress before Release	184
4.6.2 Tx70 Strand Stresses	185
4.6.3 Tx70 Transverse Reinforcing Bar Stresses	187
4.6.4 Tx70 Summary	195
4.7 Results Summary.....	195
4.7.1 Spalling Stresses: Summary	197
4.7.1.1 Spalling Stresses: Recommendations	198
4.7.2 Bursting Stresses: Summary.....	199
4.7.2.1 Bursting Stresses: Recommendations	202
CHAPTER 5 SUMMARY, CONCLUSIONS, AND RECOMMENDATIONS.....	210
5.1 Summary of the Research Program.....	210
5.2 Conclusions and Recommendations.....	211
5.2.1 Spalling Stresses: Concluding Observations.....	214
5.2.2 Bursting Stresses: Concluding Observations	214

5.3 Recommendations For Future work.....	215
APPENDIX A.....	216
APPENDIX B.....	227
APPENDIX C.....	243
APPENDIX D.....	248
APPENDIX E.....	252
APPENDIX F.....	257
BIBLIOGRAPHY	262
VITA	266

List of Tables

Table 3-1: Tx girder design summary	75
Table 3-2: Concrete Mixture designs for each Tx girder constructed.....	76
Table 4-1: Code provision comparison for Tx28 end region reinforcement.....	145
Table 4-2: Code provision comparison for Tx46 end region reinforcement.....	146
Table 4-3: Code provision comparison for Tx70 end region reinforcement.....	147
Table 4-4: Stresses in prestressing strands before release.....	149
Table 4-5: Stresses in prestressing strands before release.....	162
Table 4-6: Stresses in prestressing strands before release.....	174
Table 4-7: Stresses in prestressing strands before release.....	184
Table 4-8: Tx girder design summary	196
Table 4-9: Spalling forces	198
Table 4-10: Transverse rebar stresses and crack widths in the end regions.....	200
Table 4-11: Bursting forces.....	203
Table A-1: Tx girder design summary	218
Table A-2: Applied prestressing stress for all Tx girders	221
Table A-3: Total applied prestressing force for all Tx girders.....	221
Table B-1: AASHTO LRFD (2007) Spalling steel provision comparison	228
Table B-2: PCI (6 th Edition) Spalling steel provision comparison.....	229
Table B-3: Tx End region transverse reinforcement details (live end)	241
Table B-4: Tx End region transverse reinforcement details (dead end).....	241
Table B-5: Transverse end region reinforcement comparison (dead end)	242
Table B-6: Transverse end region reinforcement comparison (live end).....	242
Table C-1: Tx28-I cylinder strengths	244
Table C-2: Tx82-II cylinder tests	245
Table C-3: Tx46 cylinder tests	246
Table C-4: Tx70 cylinder tests	247

List of Figures

Figure 1-1: Bursting and Spalling Cracks in Florida Bulb Tees: Jensen Beach (Courtesy of Jonathan Van Hook, Florida DOT).....	2
Figure 1-2: Bursting and Spalling Cracks in AASHTO Type VI Beams: Galveston Causeway Expansion Project.....	5
Figure 2-1: Transverse stresses in the anchorage zone of a pretensioned member (CEB-FIP, 1998).	12
Figure 2-2: Exaggerated deformations of end block with fictitious discontinuities (Lenschow and Sozen, 1965).	12
Figure 2-3: Distribution of vertical tension strains over the depth of the web at the end face of a typical A-series girder (Marshall and Mattock, 1962).....	15
Figure 2-4: Distribution of vertical tension strain at the level of the centroidal axis in the end zone of a typical A-series girder (Marshall and Mattock, 1962)..	16
Figure 2-5: Typical variation of stirrup strains with distance from end face of girder (Marshall and Mattock, 1962).	17
Figure 2-6: Contours of equal transverse stress (Gergely et al., 1963).....	19
Figure 2-7: Magnitudes and points of action of tensile forces on longitudinal sections in the tension zone (Gergely et al., 1963).....	20
Figure 2-8: Forces on free body (Gergely et al., 1963).....	22
Figure 2-9: Tensile stress zones (Breen et al., 1994)	27
Figure 2-10: Typical D-region for a post-tensioned beam: (a) elastic stress trajectories; (b) elastic stresses; (c) strut-and-tie models. (Schlaich et al., 1987).....	27
Figure 2-11: Moment diagram at the end zone of NU1600 girder.....	29
Figure 2-12: End zone reinforcement with strain gauge locations for typical Nebraska I-girder (Tuan et al., 2004).....	30
Figure 2-13: Variation of maximum vertical reinforcement stress over end zone (Tuan et al., 2004)	31
Figure 2-14: Subdivision of the tensile stresses in the transmission zone of a pretensioned member (Uijl, 1983)	34
Figure 2-15: For calculation of the bursting force: (a) dimensions of the symmetrical prism; (b) moment equilibrium along section A-A (Uijl, 1983)	36
Figure 2-16: The spalling forces follow from the equilibrium of internal forces. (Uijl, 1983)	37
Figure 2-17: Position of the maximum spalling stress along the end face for different eccentricities (Uijl, 1983)	38
Figure 2-18: Distribution of the spalling stress (Uijl, 1983)	39
Figure 2-19: Bursting stress as a function of the eccentricity (Uijl, 1983)	40

Figure 2-20: Cross sectional dimensions of the investigated members (Uijl, 1983)	41
Figure 2-21: Spalling deformation versus prestress level from measurements and calculations for different bond stress distributions (Uijl, 1983)	42
Figure 2-22: Typical cracks at release and its growth afterwards (Uijl, 1983)	43
Figure 2-23: Superposition of splitting and bursting stresses (Uijl, 1983)	43
Figure 2-24: Schematic figure for stresses and potential cracks in transmission zone (CEB, 1987)	45
Figure 2-25: Definition of relative rib area for strand (CEB, 1992)	48
Figure 2-26: Bond stress as a function of slip for different tendon types (CEB, 1992)	48
Figure 2-27: Maximum spalling stress as a function of the cross-sectional dimensions, the eccentricity, and the transmission length (CEB-FIP, 1990)	51
Figure 2-28: For calculation of the bursting force: (a) dimensions of the symmetrical prism; (b) moment equilibrium along section A-A (CEB-FIP, 1998)	59
Figure 2-29: For calculation of the spalling force: (a) definition of the equivalent prism; (b) moment equilibrium along section B-B (CEB-FIP, 1998)	61
Figure 3-1: Transfer Length for Prestressing Strand	68
Figure 3-2: Typical D-region for a post-tensioned beam: (a) elastic stress trajectories; (b) elastic stresses; (c) strut-and-tie models. (Schlaich et al. 1987)	68
Figure 3-3: Bernoulli's hypothesis; plane sections remain plane (Beer and Johnston, 1992)	69
Figure 3-4: TxDOT's typical Tx Girder loaded eccentrically showing elastic stress distribution	70
Figure 3-5: Forney concrete cylinder testing machine	77
Figure 3-6: Concrete maturity for two different temperature concretes (Kehl and Carrasquillo, 1998)	78
Figure 3-7: Curing temperature profile in an AASHTO Type IV girder (Kehl and Carrasquillo, 1998)	80
Figure 3-8: Sure Cure Controller and Cylinders	81
Figure 3-9: Wireless Sure Cure I/O Box	81
Figure 3-10: Wireless Sure Cure Schematic	82
Figure 3-11: Universal Test Machine Used to Obtain Stress-Strain Curve of Strands	83
Figure 3-12: Typical Stress-Strain curve for low-relaxation 0.6" diameter strand	84
Figure 3-13: Typical deformed wire from WWR fabrics	85
Figure 3-14: Typical vertical reinforcement in WWR fabric with deformed bars	86
Figure 3-15: Longitudinal elevation view of pretensioning bed with Tx70 girder	88
Figure 3-16: Completed pretensioning bed from dead end	89

Figure 3-17: Completed pretensioning bed at the live end	90
Figure 3-18: SAP 2000 output for 12” thick plate with 70, 44 kip loads. Maximum stress shown = 28 ksi. (SAP 2000)	91
Figure 3-19: Completed Pretensioning Bed	93
Figure 3-20: Live end stressing bulkhead with rams	94
Figure 3-21: Tx Girder sections	96
Figure 3-22: Strain gauges of reinforcing bars and strands	98
Figure 3-23: Strain gauge on WWR.....	99
Figure 3-24: Tx28-I Rebar gauge locations for live end.....	100
Figure 3-25: Tx28-I Rebar gauge locations for dead end	101
Figure 3-26: Tx28-II Rebar gauge locations for dead end.....	102
Figure 3-27: Tx28-II rebar gauge locations for live end.....	102
Figure 3-28: Tx46 Rebar gauge locations for the live end.....	104
Figure 3-29: Tx46 Rebar gauge locations for the dead end	105
Figure 3-30: Tx70 Rebar gauge locations for the dead end	107
Figure 3-31: Tx70 Rebar gauge locations for the live end.....	108
Figure 3-32: Strain gauge orientation for 0.6” diameter strand	109
Figure 3-33: Sample strain gauge calibration curve for 0.6” strand	110
Figure 3-34: Application of microcrystalline wax onto strand strain gauges	111
Figure 3-35: Completed strain gauge on 0.6”diameter strand	112
Figure 3-36: Possible strand locations within the bottom flange	113
Figure 3-37: Typical locations for strand strain gauges in elevation view	113
Figure 3-38: Typical locations for strand strain gauges in plan view	114
Figure 3-39: Typical thermocouple locations in Tx girders.....	115
Figure 3-40: Individual strand stressing with mono-strand stressing jack.....	116
Figure 3-41: Hydraulic pumps used to control the application of prestressing force through four 400-ton rams	117
Figure 3-42: Three Linear Potentiometers measuring strand elongations	119
Figure 3-43: Dial gauges used at dead end of pretensioning bed to measure frame deflection.....	120
Figure 3-44: Flow-meter used to measure water placed into truck.....	122
Figure 3-45: Cement being added to the ready mix truck with a 1 cy hopper	123
Figure 3-46: Concrete placement using a 1 cy hopper.....	124
Figure 3-47: Form vibrator being used on a Tx28 girder.....	125
Figure 3-48: Use of an internal rod type vibrator: Tx28 girder	126
Figure 3-49: Typical time-temperature curve for Tx28-II girder.....	127
Figure 3-50: Cylinder strength vs. Time for the Tx70 girder.....	128
Figure 4-1: Typical end region reinforcement details for Tx family of girders..	132
Figure 4-2: Typical location of bundled spalling reinforcement in Tx28 girders	134
Figure 4-3: Typical location of bundled spalling reinforcement for a Tx46 girder	135

Figure 4-4: Typical location for bundled spalling reinforcement for a Tx70 girder.	136
Figure 4-5: For calculation of the bursting force: (a) dimensions of the symmetrical prism; (b) moment equilibrium along section A-A (CEB-FIP, 1998)	141
Figure 4-6: For calculation of the spalling force: (a) definition of the equivalent prism; (b) moment equilibrium along section B-B (CEB-FIP, 1998).....	143
Figure 4-7: Typical strand locations.....	151
Figure 4-8: Tx28-I Strand stresses at release for the live end.....	151
Figure 4-9: Tx28-I Strand stresses at release for the dead end	152
Figure 4-10: Tx28-I Live end transverse reinforcement stresses	154
Figure 4-11: Tx28-I Dead end transverse reinforcement stresses.....	155
Figure 4-12: Tx28-I Live end crack pattern	157
Figure 4-13: Tx28-I Live end photo with crack pattern.....	157
Figure 4-14: Tx28-I Dead end crack pattern.....	158
Figure 4-15: Tx28-I Dead end photo with crack pattern.....	158
Figure 4-16: Crack width measurement	160
Figure 4-17: Tx28-II Strand stresses after release for the live end	163
Figure 4-18: Tx28-II Strand stresses after release for the dead end.....	164
Figure 4-19: Tx28-II Live end transverse reinforcing bar stresses	166
Figure 4-20: Tx28-II Dead end transverse reinforcing bar stresses	167
Figure 4-21: Tx28-II Live end crack pattern.....	170
Figure 4-22: Tx28-II Live end photo with crack pattern	170
Figure 4-23: Tx28-II Dead end crack pattern.....	171
Figure 4-24: Tx28-II Dead end photo with crack pattern	171
Figure 4-25: Tx46 Strand stresses at release for the live end.....	175
Figure 4-26: Tx46 Strand stresses at release for the dead end	175
Figure 4-27: Tx46 Dead end transverse reinforcing bar stresses	177
Figure 4-28: Tx46 Live end transverse reinforcing bar stresses	178
Figure 4-29: Tx46 Live end crack pattern.....	180
Figure 4-30: Tx46 Live end photo with crack pattern	180
Figure 4-31: Tx46 Dead end crack pattern.....	181
Figure 4-32: Tx46 Dead end photo with crack pattern	181
Figure 4-33: Tx70 Strand stresses after release for the live end	185
Figure 4-34: Tx70 Strand stresses after release for the dead end.....	186
Figure 4-35: Tx70 Transverse reinforcing bar stresses for the live end.....	188
Figure 4-36: Tx70 Transverse reinforcing bar stresses for the dead end	189
Figure 4-37: Tx70 Live end crack pattern.....	191
Figure 4-38: Tx70 Live end photo with crack pattern	192
Figure 4-39: Tx70 Dead end crack pattern.....	193
Figure 4-40: Tx70 Dead end photo with crack pattern	194
Figure 4-41: Live end bursting stresses for all Tx girders	201

Figure 4-42: Dead end bursting stresses for all Tx girders	202
Figure 4-43: Recommended locations for additional transverse steel	204
Figure 4-44: Original end region reinforcement: a) Dead end; b) Live end	205
Figure 4-45: Suggested end region detail (Bars S refer to spalling and bursting reinforcement - No.6 bars)	206
Figure 4-46: Tensile stress zones (Breen et al., 1994)	209
Figure 4-47: Typical strut-and-tie model for a post-tensioned beam. (Schlaich et al., 1987).....	209
Figure A-1: Tx girder sections	219
Figure B-1: For calculation of the bursting force: (a) dimensions of the symmetrical prism; (b) moment equilibrium along section A-A (CEB-FIP, 1998)	232
Figure B-2: For calculation of the spalling force: (a) definition of the equivalent prism; (b) moment equilibrium along section B-B (CEB-FIP, 1998).....	236
Figure D-1: Strand calibration curve for Tx70 girder	249
Figure D-2: Strand calibration curve for Tx28-I, Tx28-II, and Tx46 girder.....	249
Figure D-3: Time-temperature curve for Tx28-I.....	250
Figure D-4: Time-temperature curve for Tx46	250
Figure D-5: Time-temperature curve for Tx70	251
Figure E-1: High capacity prestressing bed design drawing (Plan View)	253
Figure E-2: High capacity prestressing bed design drawing (Elevation View) ..	254
Figure E-3: High capacity prestressing bed design drawing (Elevation View) ..	255
Figure E-4: High capacity prestressing bed design drawing (Typical detail drawing)	256

CHAPTER 1

Introduction

1.1 BACKGROUND

In the process of developing design standards for a new family of pretensioned concrete I-beams, the Texas Department of Transportation noticed some inconsistencies between research results and code provisions for spalling and bursting reinforcement. In addition, they recognized the fact that the current end region reinforcement used in the TxDOT standard I-beams was based on experimental research. With these facts and impetus, an interagency testing contract was established between the University of Texas at Austin and the Texas Department of Transportation to investigate end region stresses and to arrive at simple details that can be used in the new TxDOT I-Beams.

In modern pretensioned concrete highway girder designs, higher strength concretes are being used in conjunction with larger diameter strands. These two adjustments allow designers to optimize beams to accommodate longer spans and fewer beam lines in bridges. The better optimization of modern I-beams, including the new TxDOT I-Beams, has raised the level of prestress force that is being applied to pretensioned beams and has therefore increased the level of transverse tensile stresses. It will be revealed in the next few sections that this problem is not just limited to the state of Texas, but rather is a problem throughout the United States.

1.1.1 Florida DOT

The Florida Department of Transportation experienced bursting and spalling cracks in numerous pretensioned I-girders and Bulb Tees throughout the

state of Florida. An example of some of the end region cracking is shown in Figure 1-1.



Figure 1-1: Bursting and Spalling Cracks in Florida Bulb Tees: Jensen Beach
(Courtesy of Jonathan Van Hook, Florida DOT)

The widths of the cracks shown in Figure 1-1 are somewhere between 0.003” and 0.005”. Some of these cracks extend to just over 3 feet into the beam from its end face. There are numerous memorandums that have been issued by the Florida DOT discussing this issue and how best to resolve it. One of those memorandums, written by William N. Nickas on February 3, 2004, is included below:

Cracking in the ends of AASHTO and Florida Bulb-Tee beams has been observed with vertical bursting reinforcing designed to 20 ksi stress, based on 4% of the bonded prestressing force and distributed over a distance of $h/5$, in accordance with the LRFD (2001) Section 5.10.10.1. To minimize these cracks and accommodate the longer distribution length ($h/4$) adopted by LRFD in 2002, the maximum prestressing force in the ends of these beams has been limited.

Additionally the maximum design concrete strength at release has been limited to 6000 psi to control the amount of prestress in the ends of these beams. The maximum prestressing force is based on 13 ksi bursting steel stress for AASHTO and Florida Bulb-Tee beams. This is approximately equivalent to a 20% decrease in allowable stress from the LRFD (2001) requirements. Florida-U beams and Inverted-T beams have not shown similar problems, so the maximum prestress force is based on 18 ksi and 20 ksi bursting steel stress respectively, which provides equivalent resistance to the previous LRFD (2001) requirements.”

As is seen in the above memorandum the cracks that form in the end regions of pretensioned beams at release have drawn some interest and caused Florida DOT to limit stresses in this region above and beyond that of the requirements of AASHTO LRFD Bridge Design Specifications (2007).

1.1.2 Washington DOT

In the state of Washington, end zone cracking has become an issue as well. A technical memorandum authored by Bijan Khaleghi of Washington State DOT on December 23, 2006 shows the state of bursting and spalling (what is defined as splitting within this memorandum) stresses in the state of Washington:

...“The provisions of LRFD Article 5.10.10.1 are to resist “splitting” of pretensioned members rather than “bursting”. LRFD article 5.10.10.1 requires the vertical splitting reinforcement uniformly distributed within the distance $h/4$ from end of the girder, where “h” is the overall depth of precast member. To satisfy this requirement some designers tend to use #6 bars or bundled bars for vertical splitting reinforcement, that is not practical for girder fabrication and bridge deck construction. For ease of fabrication and deck construction, it is acceptable to place the remaining splitting reinforcement beyond the code

prescribed $h/4$ zone. Please note that the $h/4$ zone is an approximation of the extent of the splitting zone apprehended from the stress contours of finite element analysis or other refined methods. It is therefore safe and reasonable to extend the splitting zone beyond the code prescribed $h/4$ zone if required for girder fabrication and bridge deck construction. The current reinforcement requirement is defined for pretensioned members with vertical webs. However, splitting reinforcement is clearly required in other pretensioned members such as slabs, double tees, tri-beams, tubs and box girders, where the primary splitting reinforcement may not be vertical. For pretensioned slab members, the width of the member is greater than the depth. A tensile zone is then formed in the horizontal direction perpendicular to the centerline of the member. For tub and box girders, prestressing strands are located in both the bottom flange and webs. Tensile zones are then formed in both the vertical and horizontal directions in the webs and flanges. Reinforcement is required in both directions to resist the splitting forces.”...

This memorandum shows the concerns that many state DOTs are dealing with in relation to transverse tensile (bursting and spalling) stresses and associated provisions in AASHTO LRFD Bridge Design Specifications.

1.1.3 Texas DOT

Similar to other states discussed above, within the state of Texas the formation of bursting and spalling cracks at release is of concern as well. Beams with horizontal or inclined end region cracks are not typically rejected provided that the widths of the cracks that form in the end regions are small enough ($w < 0.01$ ”). If the crack widths get to be larger, epoxy injection is typically required.

If a large number of wide end region cracks form at release (Figure 1-2) the beam is typically rejected by TxDOT inspectors.

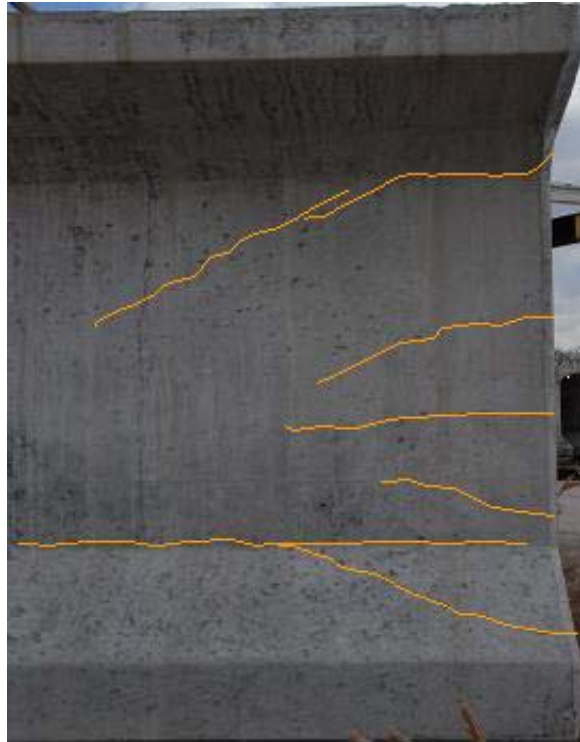


***Figure 1-2: Bursting and Spalling Cracks in AASHTO Type VI Beams:
Galveston Causeway Expansion Project***

Considering the facts outlined above, the investigation of bursting and spalling cracks for the new TxDOT I-Beams (Tx-family of beams) is of significance to ensure that:

- i. The cracks forming in the end regions of new I-Beams are comparable to those that formed in conventional AASHTO girders or TxDOT beams (e.g. Type IV beams, Type VI beams, C-Beams, A-beams etc.).

- ii. A sufficient amount of end region reinforcement is used in the new I-Beam standards to ensure that the quality of the new I-Beams that have larger bottom flanges and greater amounts of prestressing force is comparable to or better than the conventional AASHTO girders or TxDOT beams.

1.2 OBJECTIVES OF RESEARCH

To address the cracking problems in the end zones of pretensioned beams at release, a research project was funded by the Texas Department of Transportation. The research was performed at the University of Texas Phil M. Ferguson Structural Engineering Laboratory. The main goals of this research were a) to investigate the causes of the end region cracks and b) to optimize the end region reinforcement such that the widths of the end region cracks can be minimized without creating congestion that may result in concrete consolidation problems.

1.3 SCOPE OF RESEARCH

A literature review and an experimental program on full-scale girders were completed to more fully address end region cracking in pretensioned girders. The experimental program involved the construction of a pretensioning bed frame within Ferguson Lab as well as the construction of four full scale pretensioned beams. Referred to as the Tx family of beams, these girders were designed by TxDOT. The new girders were optimized to ensure that the compressive and tensile stresses in the end regions were near the maximum allowable release stresses as per AASHTO LRFD Bridge Design Specifications (2007). This helped ensure that bursting and spalling stresses were maximized at release, representing the most critical field conditions.

1.4 RESEARCH OVERVIEW: CHAPTER OUTLINE

Chapter 2 includes a thorough review of research done in the area of pretensioned anchorage zone tensile stresses. While there are significantly more works that have been done on post-tensioning anchorage zone stresses, primarily pretensioned works are reviewed because they more closely relate to the research being done. In addition the relevant provisions of AASHTO LRFD Bridge Design Specifications (2007), PCI Design Handbook (6th Edition), and the CEB-FIP Model Code 1990 were also reviewed.

Chapter 3 covers the experimental program and includes details of the test specimens and typical concrete and reinforcing steel properties. A brief explanation of the design and construction of the high-capacity pretensioning facility is also provided. The three section sizes tested from the Tx-family of beams were 28", 46", and 70" deep girders. These beam specimens were each extensively instrumented to capture the strain state in the end regions of each specimen.

The results for each end of each girder are presented and discussed in Chapter 4. Cracks that formed due to bursting stresses and spalling stresses are examined. Transverse reinforcing bar stresses arresting bursting cracks and spalling cracks are presented and examined in relation to the provisions of AASHTO LRFD Bridge Design Specifications (2007). A simple bursting reinforcement design recommendation to complement AASHTO LRFD provisions for spalling reinforcement is presented.

A summary of the work completed during the course of this investigation and primary conclusions of the study are presented in Chapter 5.

CHAPTER 2

Literature Review

2.1 OVERVIEW

Since the inception of prestressed technology, engineers have been aware of the concept of prestressed anchorage zone tensile stresses. In 1961, Professor Fritz Leonhardt of the Technological University of Stuttgart published the second edition of his book titled *“Prestressed Concrete Design and Construction”*. Although the first edition of the book was published in 1954, it was never translated to English. In 1964 the second edition was translated to English. In this textbook, prior to expressing his views on the state-of-the-art of prestressed concrete, Professor Leonhardt summarized the most important principles of prestressed concrete in a section titled *“Ten Commandments for the prestressed concrete engineer”*. This section preceded the main text. Item number 5 of that section reads:

... “ 5. *Provide non-tensioned reinforcement preferably in a direction transverse to the prestressing direction and, more particularly, in those regions of the member where the prestressing forces are transmitted to the concrete* ”...

As evidenced by the fifth principle given above, the need to provide reinforcement in the end regions of prestressed concrete beams was understood since the introduction of prestressing technology in Europe. One of the earliest U.S. recommendations on this subject appeared in the *Journal of the American*

Concrete Institute in its January 1958 proceedings. These tentative recommendations for prestressed concrete read:

“Reinforcing is necessary to resist tensile and spalling forces induced by the concentrated loads of the prestressing steel... Closely spaced reinforcement should be placed both vertically and horizontally throughout the length of the end block to resist tensile forces” (567).

Several years before this paper was published, some theoretical models were developed to explain the stresses that develop in the end regions of prestressed concrete beams during the transfer of prestressing force. In late 1950s and early 1960s much of the practical research was completed and published to establish code recommendations for the tensile stresses that developed in the end regions of pretensioned concrete beams at release.

Much of the early theoretical work was completed overseas by a number of researchers including Guyon (1953), Iyengar (1962), and Sievers (1956). Guyon’s work is heavily referenced in many of the other research papers reviewed during the course of this research study and hence it will not be reviewed as a stand alone reference. Iyengar (1962) and Sievers’ (1956) work are very theoretical and are considered to be beyond the scope of this investigation. Once initial conclusions were reached based on the extensive analytical work conducted primarily in Europe by Mörsch (1924), Guyon (1953), Sievers (1956), and Christodoulides (1956), and Iyengar (1962), papers discussing code provisions began to appear. Marshall and Mattock (1962) published one of the first U.S. papers on anchorage zone stresses in pretensioned girders. Gergely, Sozen, and Seiss (1963) conducted in-depth experimental and analytical research

on the tensile stresses that develop in the end regions of prestressed concrete beams. Their work offers some of the background theory as well as the technical data that supports the data generated during the course of this research study. The CEB-FIP Model Code (1990) and Bulletins are extensively referenced and used in interpreting the experimental data. CEB-FIP MC 90, and the background research supporting it, offers a detailed and up-to-date perspective on anchorage zone stresses in pretensioned concrete beams and how to control them. Before beginning the historical review of anchorage zone stresses, some terms and basic concepts associated with these stresses must first be understood.

In many early research studies (Guyon (1953), Iyengar (1962), Bleich (1923)) it was assumed that an elastic analysis could best predict the distribution of stresses in the end region. Some researchers (Gergely et al. (1963), Magnel (1949)) dispelled this idea and attempted other approaches. With the development of computers more advanced analytical work was done using lattice analogies (Ramaswamy, 1957), and finite element models (Uijl (1983), Breen et al. (1994)).

Gergely, Sozen, and Seiss (1963) conducted a thorough review of the early research on prestressed anchorage zone stresses. Breen et al. (1994) provided a more up to date review of the research conducted on post-tensioned anchorage zones between 1963 and 1994. The summary of the literature provided herein focuses on the most pertinent research work conducted since 1962 relating to the current research program.

In some of the early research there was not the distinction between pretensioned and post-tensioned beams (Gergely et al. (1963), Magnel (1949)), they were often both called prestressed beams. Pretensioned beams involve pretensioning groups of strands and then releasing those strands after they have

bonded to concrete. Post-tensioned applications involve unbonded strands being stressed after the concrete has set around some post-tensioning duct.

Guyon analyzed the end regions of both pretensioned and post-tensioned I-girders. He used Airy stress functions to model the end region of prestressed beams. In his pioneering work, Guyon (1953) devoted a section to pretensioned concrete beams. The importance of designating a difference between the pretensioned and post-tensioned beams relates to the application of the prestressing load onto the beam. In post-tensioned beams the load is applied directly to the face of the girder. In pretensioned beams the load is applied due to the bond between 7-wire strands and surrounding concrete. The prestressing force does not fully develop until after the transfer length, i.e. first few feet of the girder. U.S. building codes, ACI 318-05 and AASHTO LRFD Bridge Design Specifications (2007), use 60 times the diameter of the strand as the transfer length.

In Guyon's prestressed beam analysis he calls out two types of end region stresses: Bursting stresses and spalling stresses. It is important to understand what is being discussed when bursting and spalling stresses are referenced throughout the remainder of this text. Figure 2-1 clearly illustrates these forces. While the location of the bursting cracks follow through the location of the strands, spalling cracks occur due to the complicated nature of the stresses (and hence compatibility of strains) in the anchorage zone of a typical pretensioned beam. In a slightly more intuitive manner, Lenschow and Sozen (1965) illustrated the physical analog of the bursting and spalling phenomena in the end region of a post-tensioned beam.

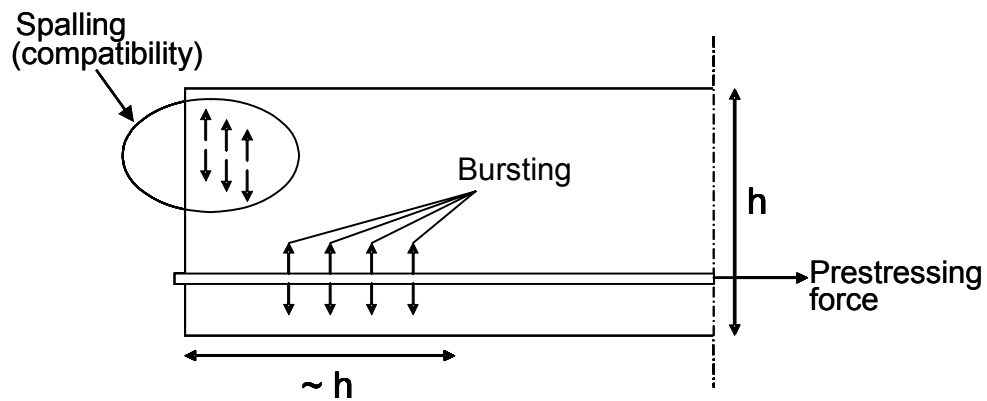


Figure 2-1: Transverse stresses in the anchorage zone of a pretensioned member (CEB-FIP, 1998).

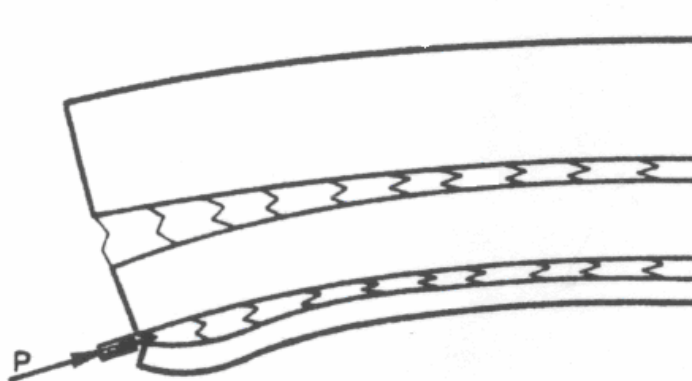


Figure 2-2: Exaggerated deformations of end block with fictitious discontinuities (Lenschow and Sozen, 1965).

2.2 HISTORICAL REVIEW OF PRETENSIONED ANCHORAGE ZONE RESEARCH

In order to put the data generated during the course of this research study in perspective, the research papers reviewed in this section predominately focus on the experimental work as opposed to purely theoretical work.

2.2.1 U.S. Research

2.2.1.1 Marshall and Mattock, 1962

Marshall and Mattock (1962) reported on their work that focused on controlling the horizontal cracks in pretensioned concrete girders. They investigated the stresses in the end regions of the pretensioned beams at transfer as well as the stresses that developed in the vertical steel when cracking occurred. An equation was developed to help facilitate design of the end regions of these girders that will be shown later in this review.

The authors completed a survey of the pretensioned concrete bridge beams in the United States and found that over half had some level of horizontal end cracking. They acknowledged that these cracks were forming due to the large tensile stresses that develop from the application of the prestress force. It is also important to note that the authors saw no benefit in casting end blocks on pretensioned girders as the end blocks had horizontal cracking as well. Their belief was that the end blocks on girders did not prevent cracking and also did not restrict the growth of the cracks once they had formed. Their suggestion was to remove these end blocks and replace them with vertical stirrups to control the end cracking. The main goal of Mattock and Marshall (1962) was to develop some design criteria for these vertical stirrups.

Marshall and Mattock's (1962) investigation into previous research revealed that no research had been conducted directly related to horizontal cracking or anchorage zone design in pretensioned girders. The only investigation that had some results of significance was done by G.D. Base (1958) of the Portland Cement Association. Base's 1958 research was on the transfer length of wires in pretensioned concrete beams, but he also measured strains due to vertical tension in the end zones of the pretensioned beams that were tested. In

Base's tests it was noted that high tensile stresses occurred near the bottom of the web of inverted T beams close to the face of the beam. It is also important to note that stresses in transverse reinforcement did not diminish until at least 20 inches into the beam. Marshall and Mattock (1962) concluded from this report that higher tensile stresses resulted from concentrated groups of strands and the magnitude of these stresses was affected by the transfer length.

Marshall and Mattock tested two series of beams: One to investigate concrete stresses at the time of prestress transfer, the other to investigate the stresses in the vertical reinforcement at prestress transfer. The first test series involved the construction of ten short girders to establish the strain distribution at the end face of the girder. Strand diameter as well as arrangement of the strands in the beam was varied. The results of the tests are shown in Figure 2-3 and Figure 2-4.

Figure 2-3 shows that the tensile strains varied over the depth of the beam at its end face, reaching a maximum near the centroid of the beam. In Figure 2-4 the strain values are shown at the centroidal axis over varying distances from the face of the beam. The stages shown in these figures are simply points where the release process was stopped to take measurements from the girder. Stage 5 represents full release. The maximum strain values occur near the face of the beam (Figure 2-4) thus supporting Base's conclusion.

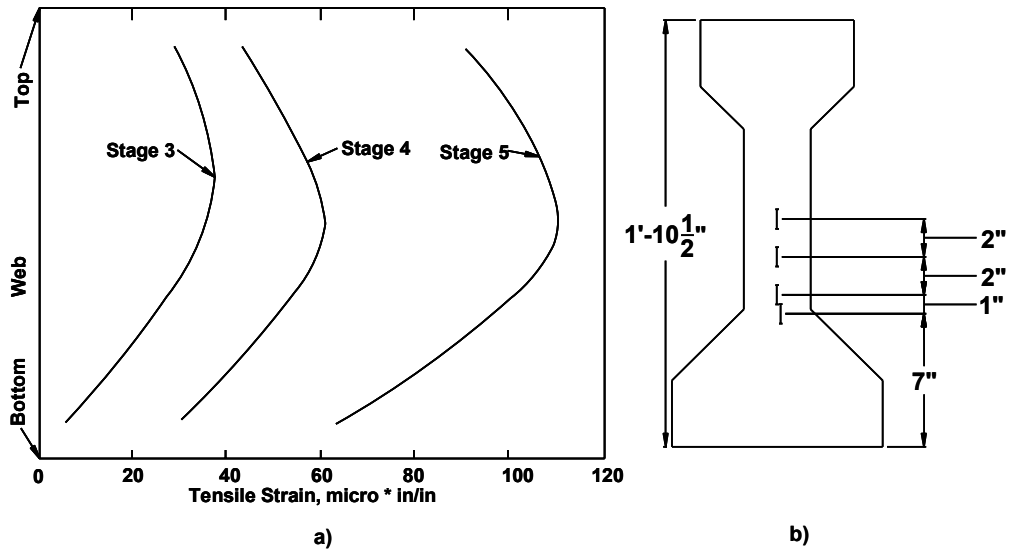


Figure 2-3: Distribution of vertical tension strains over the depth of the web at the end face of a typical A-series girder (Marshall and Mattock, 1962).

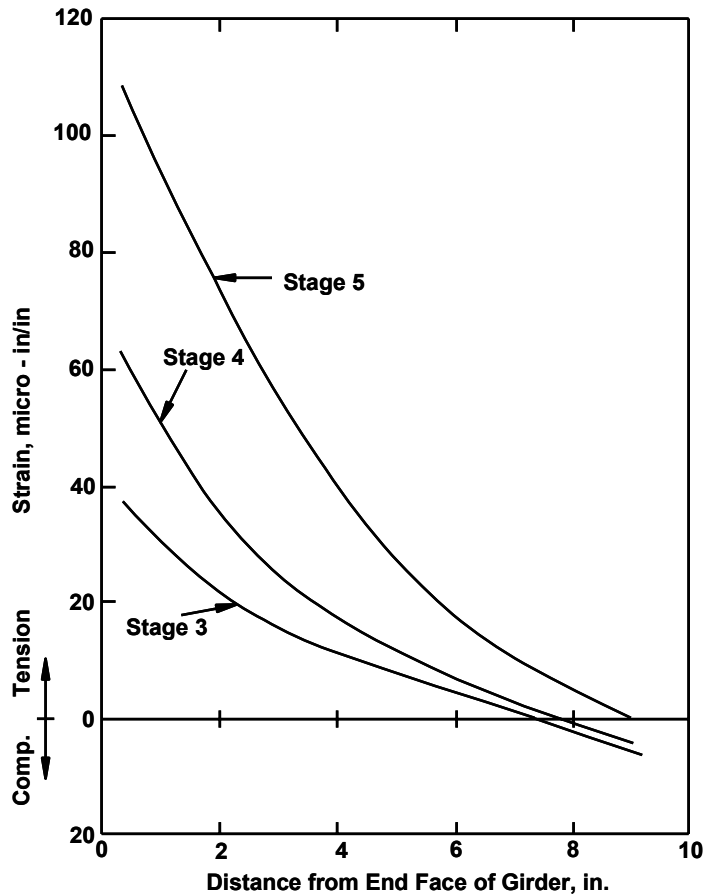


Figure 2-4: Distribution of vertical tension strain at the level of the centroidal axis in the end zone of a typical A-series girder (Marshall and Mattock, 1962).

Within the second phase of this research, 25 specimens with end reinforcement were tested. The resulting strain values supported the conclusions reached while unreinforced beams were tested. The highest stress levels occurred near the face of the girder and dissipated quickly further into the beam. Figure 2-5 shows typical results from these girders. The results shown are strains that occur at the centroidal axis of the beam.

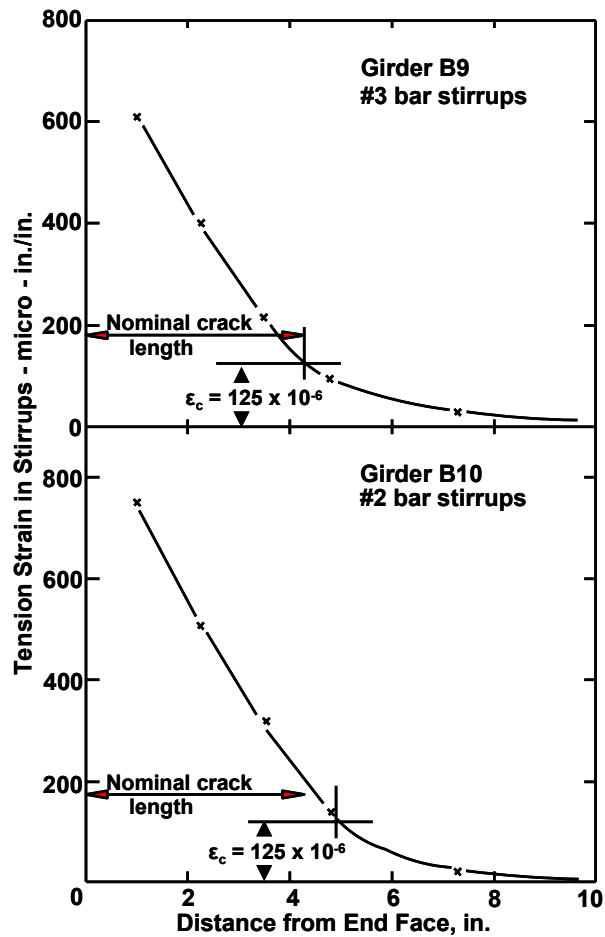


Figure 2-5: Typical variation of stirrup strains with distance from end face of girder (Marshall and Mattock, 1962).

Their test results indicated that the magnitude of the vertical stirrup stresses was a function of the transfer length of the strand as well as the total prestressing force applied. Using these results as a base, the authors formulated a design equation to help designers provide adequate quantities of steel in the end regions of pretensioned girders to reduce horizontal cracking. The resulting

equation shown below includes total prestressing force, depth of the girder, transfer length, and an allowable stress in the vertical reinforcement:

$$A_t = \frac{S}{(f_s/2)} = 0.021 \frac{T}{f_s} * \frac{h}{l_t} \quad \text{Equation 2-1}$$

where:

- S = total force resisted by stirrups
- f_s = maximum allowable stress in the stirrups
- T = Total prestressing force
- h = height of beam
- l_t = transfer length

Marshall and Mattock (1962) recommended that the amount of steel calculated should be evenly spread out over a length of one fifth of the girder depth or $h/5$. The authors concluded their paper by reminding readers that the use of end blocks in pretensioned concrete girders was not necessary. Instead, a minimal amount of vertical reinforcement could be used to limit the crack widths.

2.2.1.2 Gergely, Sozen, and Siess, 1963

One of the more thorough early research studies on transverse stresses in the end regions of prestressed I-girders was conducted by Gergely, Sozen, and Siess (1963). Before examining their research and its results some terminology must be clarified. Gergely, Sozen, and Siess (1963) often refer to their beams as prestressed beams. It should be noted that what they generally define as prestressed beams, were more specifically post-tensioned beams. While the primary focus of the current research project is not on post-tensioned beams, Gergely et al. lay important ground work and theory that must be understood, if

the transverse stresses in the end regions of pretensioned I-girders are to be understood as well.

The main goal of Gergely et al.'s 1963 work was to investigate the behavior of the anchorage zones of post-tensioned beams after the formation of the first crack. The focus of this summary will be on the research associated with reinforced end regions. Gergely et al. (1963) used a finite difference solution to analyze the end region of their post-tensioned girders to establish the correct stress distribution in this region. The stress contours obtained in their analyses are shown in Figure 2-6 and Figure 2-7.

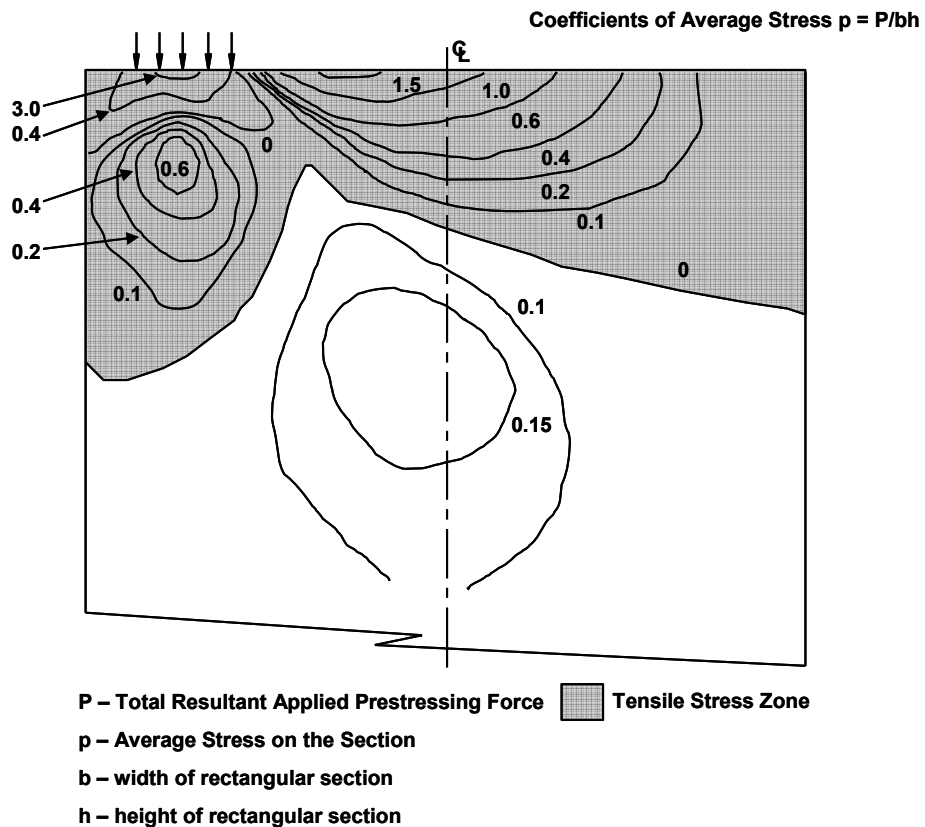


Figure 2-6: Contours of equal transverse stress (Gergely et al., 1963).

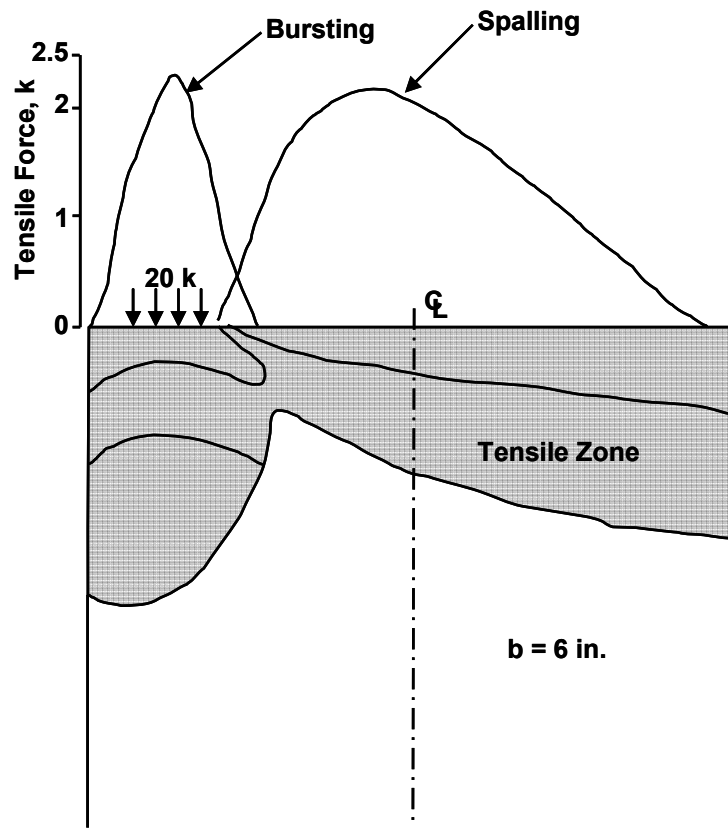


Figure 2-7: Magnitudes and points of action of tensile forces on longitudinal sections in the tension zone (Gergely et al., 1963).

Figures 2-6 and 2-7 show an eccentrically loaded post-tensioned beam. Gergely et al. (1963) defined the bursting and spalling stresses shown in Figure 2-7 as follows:

”...The tensile stresses under the load occur at a distance from the end face and are called bursting stresses while the tensile stresses at the top of the region are called spalling stresses...” (9).

This definition agrees with the earlier definition from Guyon’s (1953) work. For their research, the expected spalling stresses were higher than bursting stresses

and the first cracks formed near the centerline of the beam at the surface of the end region. It was also noted that as eccentricity decreased, bursting stresses became the controlling transverse stress. When comparing their analytical results from the finite difference solution to other earlier researchers, Gergely, Sozen, and Siess (1963) most closely identified with Guyon (1953) as having the most accurate analytical results up to the time when their research was conducted. It was noted that the boundary conditions used by Guyon better quantified the actual stress conditions in a typical post-tensioned beam than most other early works. The inconsistencies between the analytical results in Gergely, Sozen, and Siess' (1963) work and Guyon's (1953) were attributed to the loading conditions and inability to accurately interpolate (or extrapolate) the maximum values from the published stress values for Guyon's results. Guyon's method for calculating tensile stresses using a "*symmetrical prism*" cut from the end block, led to the simplified method for transverse stress calculation discussed below.

To gain a better understanding of how the tensile stresses could best be arrested by reinforcement in the end regions of post-tensioned beams, Gergely et al. (1963) developed a simplified method for estimating the location of the first crack as well as the internal forces that must be resisted by the reinforcement. Most of the early research (Iyengar (1962), Bleich (1923), Guyon (1953)) examined by Gergely, Sozen, and Siess (1963) used elastic solutions to calculate tensile stresses and then offered reinforcement patterns based on these solutions. Gergely, Sozen, and Siess pointed out the fact that the reinforcement did not act until a crack formed in the beam. Once a crack formed in the beam the end region was no longer elastic and an elastic solution was not appropriate. To accommodate the fact that a crack existed in the beam and the reinforcement was acting to keep the tensile stresses from splitting the beam apart, a free body diagram of the end region bounded by the face of the girder and the longitudinal

crack gave the researchers a starting point to begin a simplified analysis of the end region. This prism is somewhat similar to Guyon's symmetrical prism cut from the center of a concentrically loaded beam, but is different because it is based on a cracked beam assumption. The forces acting on the free body are shown in Figure 2-8.

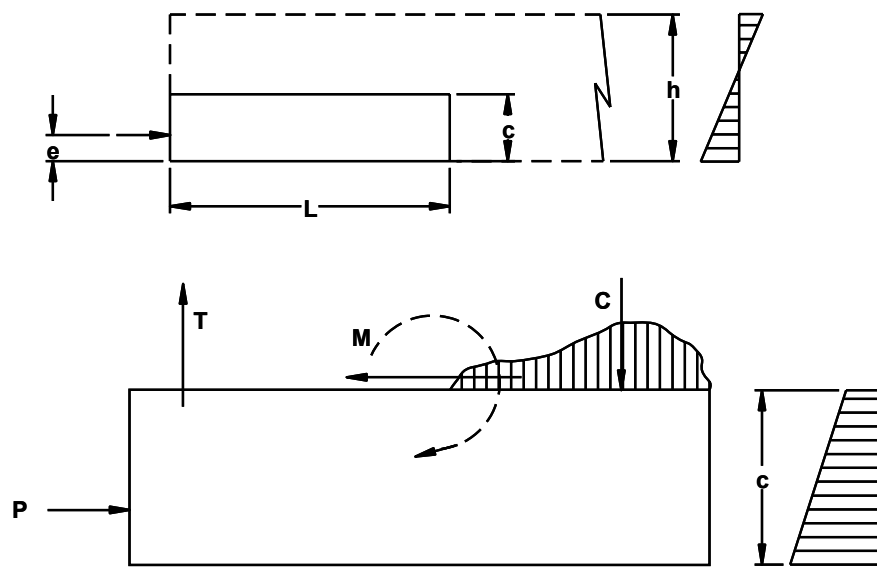


Figure 2-8: Forces on free body (Gergely et al., 1963).

The applied force P produces a linear stress distribution on the free body at a distance L from the end. The tensile force T in the stirrups and the compression force C in the concrete counteract the moment created by the aforementioned stress distribution. The height of the free body is determined by the position of the crack. This means that T and C will change as the position of the crack changes. This also means that the maximum moment can be calculated that will have to be offset by a maximum tensile force T in the stirrups.

To check the analytical model they had developed, the researchers tested 14 rectangular beams and 11 I-beams with reinforcement in their end regions. Since the work on the 11 I-beams most closely correlate to the I-beams tested during the course of this research study, the results of those tests will be examined further. In the I-beams tested by Gergely et al. (1963) reinforcement was placed at varying locations from the end face of the girder. Strains in the reinforcement were measured using strain gauges placed directly onto the reinforcement, while strains in the concrete were measured using mechanical gauges placed on the outside of the beam. Testing was done by gradually applying load to an unbonded steel rod within the concrete beam until the beam failed. Crack lengths, crack widths, and steel stresses were monitored throughout this loading process. The detailed results of these tests can be found in the Gergely, Sozen, and Siess (1963) report. After testing, the authors compared their original analytical model to their empirical results from testing. Using the free body model to calculate the location of maximum moment the most likely crack location was found. Of the original 11 tests that were conducted, only 9 of these proved to provide valid results. The results matched the actual crack locations on the I-beams in 7 of the 9 valid tests. This location on the beam is related to spalling stresses and is the maximum tensile stress in the end region as mentioned earlier in this review. Using the free body model as a basis and assuming a maximum crack length for ease of calculations and to serve as a conservative lower bound, a design method was developed.

This design method used the free body diagram explained above as well as the experimental bond slip relationship developed by Gergely, Sozen, and Siess (1963). Using the experimental evidence and the theoretical model a design guideline was developed. The design guideline reported by Gergely, Sozen, and Siess (1963) is as follows:

Total force F_T given within $h/2$ that must be resisted by transverse reinforcement:

$$F_T = \frac{M_m}{h - z} \quad \text{Equation 2-2}$$

and the stress in the steel shall be:

$$f_s \leq 10^5 \sqrt{\frac{w}{A_s}} \text{ but not greater than } 30,000 \text{ psi} \quad \text{Equation 2-3}$$

where:

A_s = Area of one stirrup

F_T = Total stirrup force

h = height of beam

z = distance from end of beam to centroid of the areas of the stirrups that are within $h/2$ from the end.

w = permissible nominal crack width, in.

M_m = maximum unbalanced moment caused by forces acting on the free body bounded by a transverse section and a longitudinal section within the member considered.

Gergely, Sozen, and Siess (1963) recommended that the maximum moment M_m found in I-girders must be calculated by trial and error using the free body diagram described above.

Using these equations Gergely, Sozen, and Siess (1963) suggested that this method was best applied to anchorage zones with large eccentricities. In such cases the conditions of the anchorage zone do not affect spalling stresses. Anchorage zones with smaller eccentricities are influenced by the size of loading plate. Nonetheless, Gergely, Sozen, and Siess (1963) reported that their equations would give a conservative estimate of forces for those cases as well.

2.2.1.3 Breen, Burdet, Roberts, Sanders, and Wollmann, 1994

A more recent research study was completed in 1994 by Breen et al. in the area of post-tensioned anchorage zone reinforcement. This thorough review of post-tensioned anchorage zones yielded valuable, up-to-date insights into anchorage zone detailing that carry over well into the review of pretensioned anchorage zones. While a complete review of this study will be avoided for sake of brevity, key points that help establish the state-of-the-art in the anchorage zone detailing of post-tensioned beams will be drawn out.

Breen et al. (1994) summarized the early research studies (e.g. Guyon (1953), Mörsch (1924)) on the analysis of post-tensioned anchorage zones. The authors then reported on the recent nonlinear finite element analysis that was conducted to estimate the state of stress for the anchorage region (Adeghe and Collins (1986), Fenwick and Lee (1986)). Breen et al. (1994) concluded that most of the research reviewed lacked a general design method that would support a variety of post-tensioned anchorage zone problems. With that motivation a comprehensive research into the reinforcing bar detailing in post-tensioned anchorage zones was conducted.

Two main anchorage zone areas were researched within this NCHRP report: (i) the local zone, “*the region of very highly compressive stresses immediately ahead of the anchorage zone*”, and (ii) the general zone, “*the region subjected to tensile stresses due to spreading of the concentrated tendon force in the structure.*” Stress conditions in the local zone, or the zone adjacent to the post-tensioning anchorage, are uniquely associated with post-tensioning and they are not reviewed here since their applicability to pretensioned beams is not obvious. On the other hand, a brief look into the analysis and tests conducted on the general zone provide a good background for similar stresses in pretensioned beams.

Breen et al. (1994) described three types of tensile stresses in the general zone: longitudinal edge tension stresses, spalling stresses, and bursting stresses. The spalling and bursting stresses are identical to those described in Gergely et al. (1963), while the edge tension stresses are the stresses that develop due to the eccentricity of the load. Figure 2-9 shows these stresses and their locations in the end region of a post-tensioned beam. 36 specimens were tested to investigate each of these stresses in relation to first crack prediction and ultimate strength prediction. The primary method used to design the specimens and predict ultimate capacity was the strut-and-tie model. A typical strut and tie model for an eccentrically loaded post-tensioned beam is shown in Figure 2-10 (c). Note that each of the forces shown in Figure 2-9 are related to a tie force shown in Figure 2-10: T_1 = spalling force; T_2 = edge tensile force; and T_3 = bursting force. This correlation revealed that STM was an advanced method for calculating bursting and spalling forces. This understanding helped the authors develop a comprehensive research study by using STM to show how tensile forces could be analyzed and how reinforcement can be detailed in a more generalized fashion to accommodate all problems associated with post-tensioned anchorage zones.

The primary test variables included the eccentricity of post-tensioning load, the inclination of post-tensioning load, anchor types and single versus multiple loads. STM was used to design each of the specimens and then each test specimen was loaded to failure with special attention paid to cracking loads and ultimate loads. The results of the general zone study revealed two key points. First, in agreement with STM predictions, the bursting force yielded the reinforcing bar tension tie as the primary method of failure. Second, STM proved to be a very conservative design method that could be very useful for reinforcement detailing to the trained engineer.

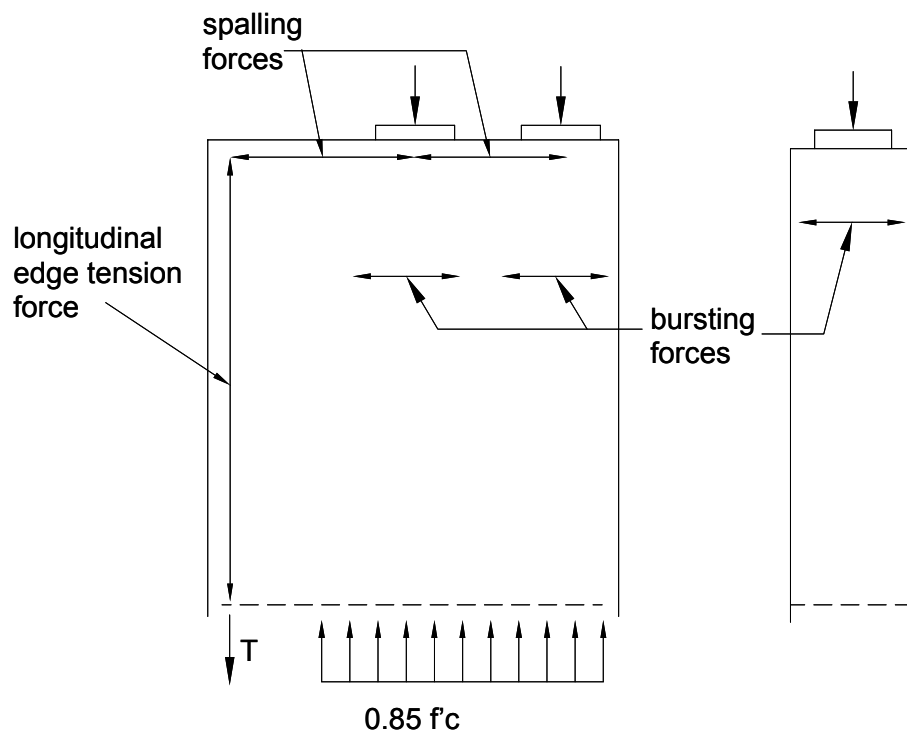


Figure 2-9: Tensile stress zones (Breen et al., 1994)

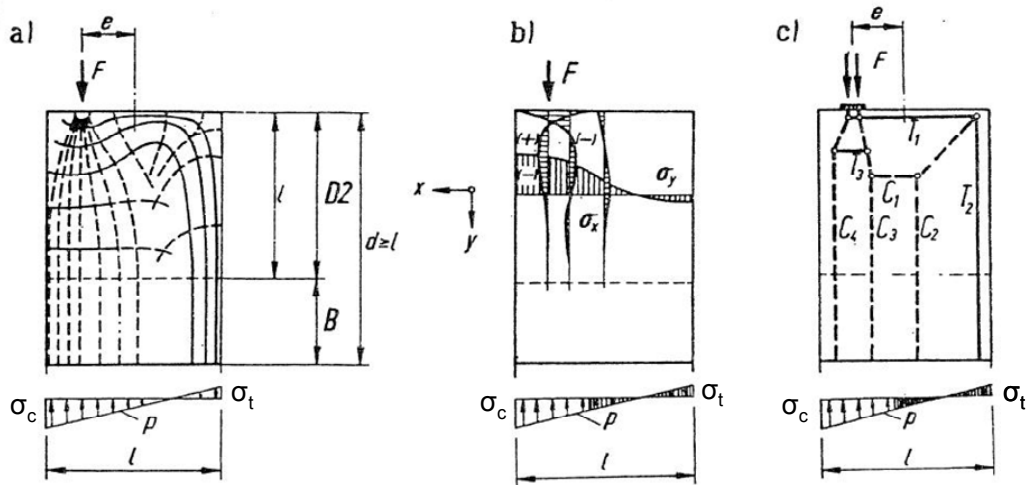


Figure 2-10: Typical D-region for a post-tensioned beam: (a) elastic stress trajectories; (b) elastic stresses; (c) strut-and-tie models. (Schlaich et al., 1987)

2.2.1.4 Tuan, Yehia, Jonpitaksseel, and Tadros, 2004

Tuan et al. (2004) investigated end zone reinforcement in pretensioned highway girders. The authors pointed out the fact that cracks were frequently present in the end zone regions of many pretensioned members. Tuan et al. (2004) stated that *“These cracks are caused primarily by the concentration of prestressing forces at the time of release”* (68). Tuan et al. (2004) noted that the AASHTO LRFD Bridge Design Specifications (2002) required the steel used to resist the end region cracks be placed within $h/4$ of the end of the beam and be designed for a stress less than 20 ksi. The authors further stated that as larger diameter strands were being used in combination with higher strength concretes more commonly, an impractical amount of transverse steel was required to be placed at the end of the pretensioned girders designed according to the AASHTO LRFD Bridge Design Specifications (2002). Their research focused on solving this problem.

The researchers began by conducting a literature review on the subject. The two major research projects that were discussed in their literature review are also reviewed within the text of the current research project: Marshall and Mattock’s (1962) and Gergely, Sozen and Siess (1963). Based on their literature review Tuan et al. (2004) suggested that AASHTO LRFD (2002) provisions were developed primarily from Marshall and Mattock’s (1962) work. Tuan et al. (2004) suggested that design guidelines proposed by Gergely, Sozen and Siess (1963) (Equations 2-2 and 2-3) provided the best method for analyzing the end regions of pretensioned members. Strut-and-tie models as well as finite element analysis were also looked at as viable options for analyzing the end regions of pretensioned beams. Tuan et al. (2004) suggested that the finite element analysis did not lend itself toward designing reinforcement for crack control. The researchers suggested that, *“...the STM in pretensioned end zones could yield a*

splitting force between 4 to 13 percent of the pretensioning force” (71). As other methods yielded spalling forces that are less than or equal to 4 percent of the prestressing force, the authors did not want to analyze their specimens using STM. Instead, they used the equations proposed by Gergely, Sozen and Siess (1963) (Equations 2-2 and 2-3) due to their simplicity and practicality. Tuan et al. (2004) used these equations to find where the maximum moment in the end regions occur within the depth of their pretensioned beams. A summary of their work is provided in Figure 2-11.

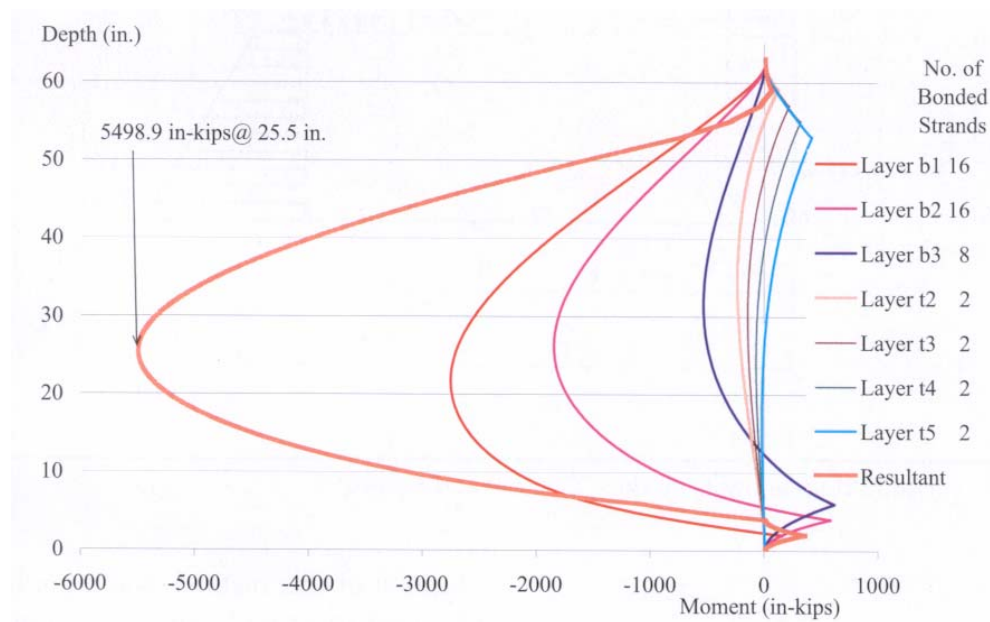
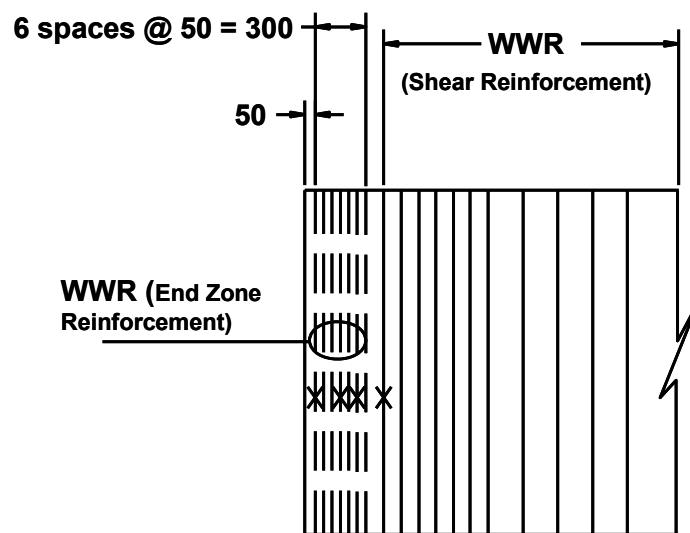


Figure 2-11: Moment diagram at the end zone of NU1600 girder

(Tuan et al., 2004).

Tuan et al. (2004) tested 3 specimens of each for two sizes of inverted-tees and two sizes of I-girders for a total of 12 beams. The authors divided their experimental research into two phases. Both phases included I-girders with both

draped and straight strands as well as some debonded straight strands. In Phase I girders designed to meet AASHTO LRFD 2002 Specifications were tested and as such vertical reinforcement was placed within $h/4$ from the end of the beam. In Phase II girders with end zone reinforcement details that were developed in their research were tested. The strain gauges were installed on the vertical reinforcement at the critical section predicted through the use of Gergely, Sozen and Siess method (1963). Bars located within the first 16 inches from the face of the member were strain gauged. The locations of these gauges are shown in Figure 2-12.



End Zone Reinforcement Elevation

Figure 2-12: End zone reinforcement with strain gauge locations for typical Nebraska I-girder (Tuan et al., 2004)

Once the strain gauges were installed on the reinforcing steel, the beams were cast and released following conventional practices. The compressive strength of

concrete at release averaged about 6500 psi and release was done by flame cutting draped strands and gradual release of straight strands with a hydraulic jack.

The authors found that in their beams designed in accordance with AASHTO LRFD (2002), the stresses in the vertical reinforcement were consistent with the values obtained through the use of Marshall and Mattock method (1962). In other words, the stresses in the vertical reinforcement were at their maximum value near the face of the girder and decreased as the distance measured from the face of the beam increased (Figure 2-13).

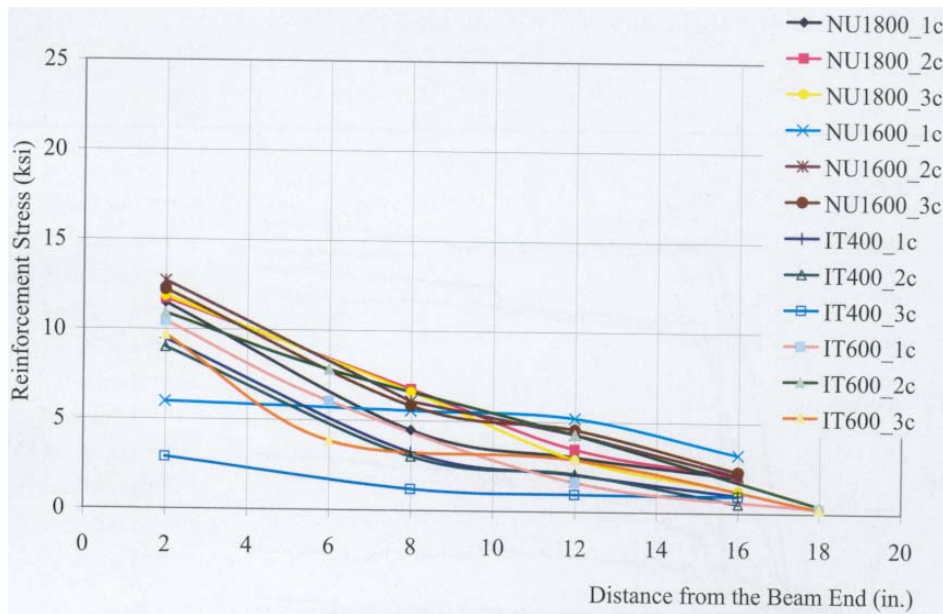


Figure 2-13: Variation of maximum vertical reinforcement stress over end zone (Tuan et al., 2004)

It was shown that the maximum stress value reached in these I-girders was 12.9 ksi in the reinforcement closest to the end of the member. This is well below the allowable stress of 20 ksi limit of the AASHTO LRFD provisions (2002). The

average spalling force inferred from measured strains in the end regions of these I-girders was approximately 2 percent of the prestressing force. This force was calculated using the sum of the products of steel strains, modulus of elasticity, and provided steel area. The authors found similar results in the inverted-tee members that were tested.

Tuan et al. (2004) based their Phase II redesign of the test specimens on the results obtained during the Phase I testing. The researchers felt that end zone reinforcement should be concentrated at the end of the girder and the first bar should be placed as close to the end face as possible. They also note that reinforcement within the first $h/8$ of the member experienced most significant stresses. The phase II designs were adjusted to achieve the full steel stress of 20 ksi. The reinforcement was then designed for a spalling resistance of approximately 2 percent of the prestressing force. The redesign of the I-beams for phase II resulted in less total transverse steel in the end regions of the beams than the amounts employed in phase I testing –which were based on AASHTO LRFD Bridge Design Specifications (2002). After testing these beams the researchers found similar results to Phase I. The beams cracked at the same locations predicted by the Gergely-Sozen-Siess Method (1963), and the first bar in the member experienced the highest level of stress. The stresses in these bars were significantly higher reaching 25.8 ksi. The researchers suggested that the high stresses recorded for the first bar indicated that the first bar was placed in a more optimal location to resist the tensile stresses. The researchers also reported that the crack widths and lengths were smaller in phase II specimens although no formal verification was presented.

Tuan et al. (2004) made recommendations based on their comparisons between the results obtained in the two phases of testing. They suggested that the AASHTO LRFD code provision 5.10.10.1 “Factored Bursting Resistance” remain

unchanged. They further recommended that at least 50 percent of the calculated area of steel be placed within the first $h/8$ from the members end. They also recommended that these bars should be welded to plates at the top and bottom of the bar to ensure anchorage of the reinforcement. The researchers recommended that the clear cover and spacing should be 1 inch within the first $h/8$ of the member. Their final recommendation was to distribute the remaining required transverse steel over a distance $3h/8$ from the end of the member. This means that the total amount of reinforcement should be placed over the first $h/2$ of the beam. It is interesting to note that the maximum spalling force value inferred from strain gauge readings was 3 percent of the total prestressing force and the maximum stress in the splitting reinforcement was close to 25 ksi in bars near the end of the members. The researchers suggested that the future research might push the stress limit in the splitting reinforcement to 30 or 36 ksi.

2.2.2 European Research

Several comprehensive research studies on anchorage zones in prestressed members were conducted in Europe in the early life of prestressed concrete (Guyon (1953), Magnel (1949), Bleich (1923)). Most of these early studies were on post-tensioned applications, but a more recent, in-depth study was completed by J.A. den Uijl in 1983 on pretensioned beams and led to the development of the CEB-FIP Model Code 1990 provisions. This study will be reviewed in depth since it offers the most up to date perspective on anchorage zone stresses in pretensioned concrete and ultimately led to the current code provisions in Europe for detailing these stresses.

2.2.2.1 Uijl, 1983

Uijl's report on the tensile stresses in the "transmission" zones of pretensioned hollow-core slabs helped the CEB-FIP develop its thorough

provisions on handling these stresses. Uijl identified three different types of tensile stresses that develop due to the application of the prestressing force. These stresses are bursting, spalling and splitting. Figure 2-14 shows the location of these stresses in relation to the prestressing force.

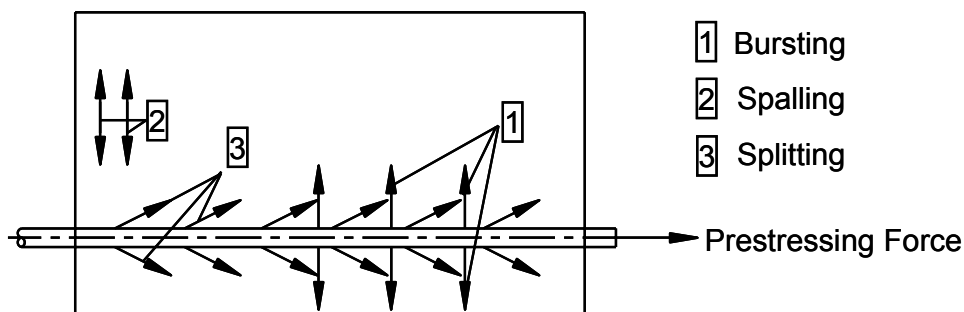


Figure 2-14: Subdivision of the tensile stresses in the transmission zone of a prestressed member (Uijl, 1983)

Uijl defined the three types of tensile stresses shown in Figure 2-12 as follows:

1 – Bursting.

Bursting stresses occur along the line of action of the force and perpendicular to it. The maximum bursting stress is located at some distance beyond the loading point.

2 – Spalling.

Spalling stresses are developed beside the loading point along the border of the member.

3 – Splitting.

Splitting stresses are circumferential tensile stresses reacting to the radially directed compressive stresses due to bond.

Splitting stress defined above is a stress component that was not considered in the research projects summarized up to this point in this chapter. During the review of Uijl's work it will become apparent that this additional stress component contributes noticeably to the state of stress in pretensioned anchorage zones. In order to calculate the magnitude of the bursting stresses Uijl used Guyon's "symmetrical prism rule" which was originally developed for post-tensioned members. The only difference in its application to pretensioned members was the change in "transmission" length, which this author defined as the distance from the loaded face to the location in the member where the applied force was uniformly distributed over the depth of the member. This difference was accounted for by lengthening the prism to accommodate the change in loading conditions. The author used the term β to extend the length of the prism. The equation for this term originated from Ruhnau and Kupfer (1977) equation for transmission length:

$$l_m = \{s^2 + (0.6l_t)^2\}^{\frac{1}{2}} \quad \text{Equation 2-4}$$

where:

$s =$ length of the disturbed area, which equals the depth of the prism

$l_t =$ transfer length

The equation for β given by the Uijl was derived directly from Equation 2-4:

$$\beta = \{d_p^2 + (0.6l_t)^2\} / d_p \quad \text{Equation 2-5}$$

where:

$d_p =$ depth of the prism

Equation 2-5 is also included in the CEB-FIP code in calculating the length of the symmetric prism for bursting forces. The bursting force was then calculated using the following equation:

$$R_b / P_o = 0.25 / \beta \quad \text{Equation 2-6}$$

where:

R_b = the bursting force

P_o = the initial prestressing force

Figure 2-15 shows the use of the symmetrical prism to calculate bursting stresses.

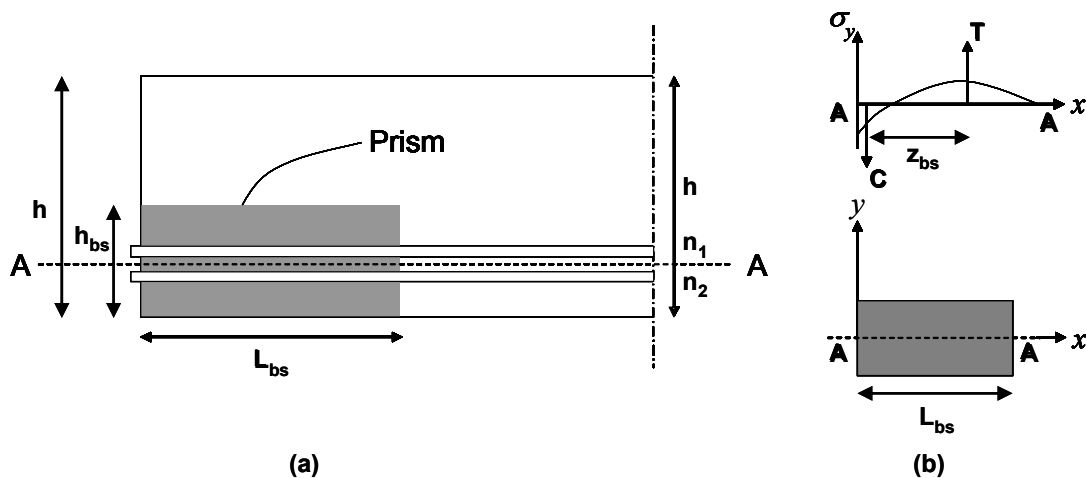


Figure 2-15: For calculation of the bursting force: (a) dimensions of the symmetrical prism; (b) moment equilibrium along section A-A (Uijl, 1983)

Uijl stated that the symmetrical prism rule was found to overestimate the bursting stresses in a member, recommended a more accurate FEM-analysis to calculate the bursting stresses.

The spalling stresses that develop in the end zone of a pretensioned girder were found to be similar to that of a post-tensioned beam with the exception of

the load application point. The internal forces in a post-tensioned member are shown in Figure 2-16 to act as a starting point for the pretensioned girder analysis.

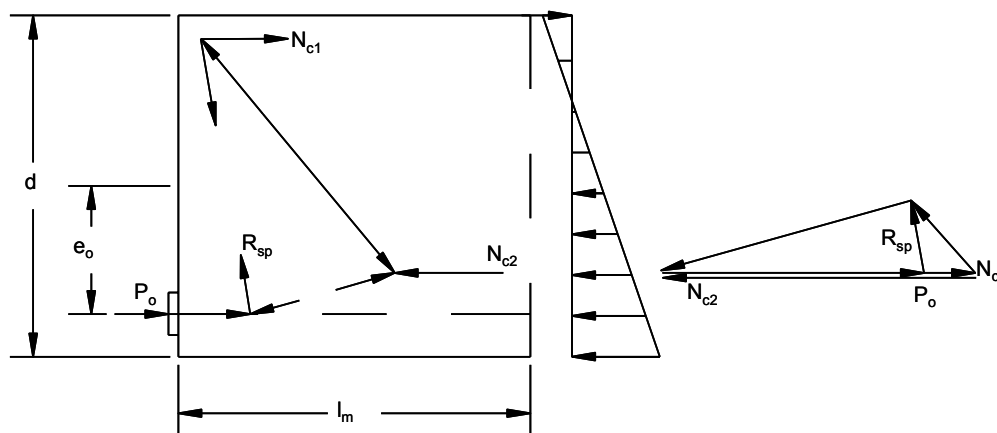


Figure 2-16: The spalling forces follow from the equilibrium of internal forces.
(Uijl, 1983)

After the manipulation of the post-tensioned solution for R_{sp} a solution for the spalling force was derived by Uijl and is given in Equation 2-7:

$$R_{sp} / P_o = 2(e_o / d - 1/6)^2 / \{\gamma(e_o / d)\} \quad \text{Equation 2-7}$$

where:

R_{sp} = the spalling force

e_o = the eccentricity of the prestressing load

d = the depth of the member

γ = exactly the same as β except a function of the depth of the member and transfer length

Uijl pointed out that Equation 2-7 established an important relationship between the spalling force and the eccentricity of the load. This concept agrees with much

of the research reviewed earlier in this chapter. Uijl also reviewed an additional method for calculating spalling stress values that is presented by another European researcher (Kupfer, 1981). Kupfer's research is the basis for the CEB-FIP MC 90 provisions for spalling stress. The method summarized in Uijl's (1983) report is identical to the Gergely, Sozen, and Siess equivalent prism method (1963) presented earlier in this chapter so it will not be shown again here.

Uijl conducted extensive finite element analyses and the most important results that can be drawn out of that component of Uijl's work are the relationships between transfer length, eccentricity of load, and the bond stress distribution. As was mentioned before, the spalling stresses are highly influenced by the eccentricity of load. Not only spalling stresses increase with increasing eccentricity, but the location of the maximum spalling stress also changes with changes in eccentricity. This relationship is shown in Figure 2-17, while the relationship between stress and eccentricity is shown in Figure 2-18.

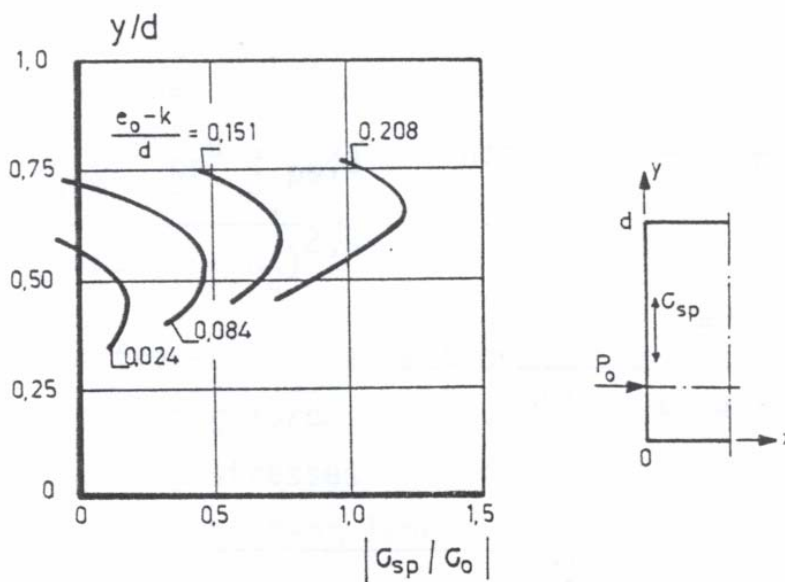


Figure 2-17: Position of the maximum spalling stress along the end face for different eccentricities (Uijl, 1983)

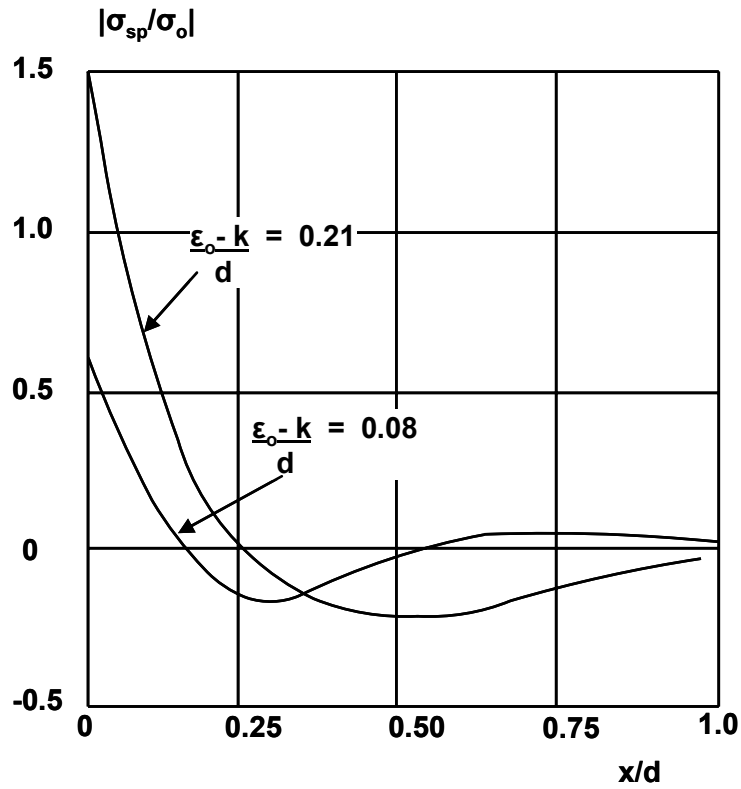


Figure 2-18: Distribution of the spalling stress (Uijl, 1983)

Uijl conducted finite element analyses on both I-sections and rectangular sections and found that the shape of the section did not change the values of the spalling stress so long as the eccentricity remained the same. Bursting stresses were also affected by the eccentricity of the load as shown by in Figure 2-19.

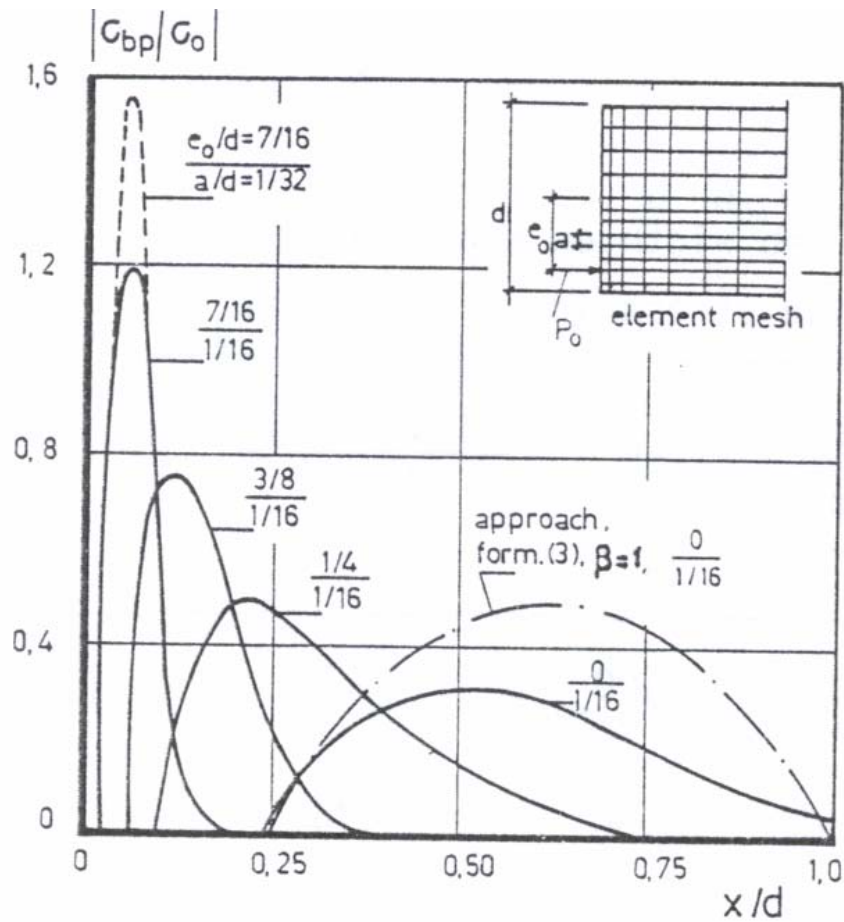


Figure 2-19: Bursting stress as a function of the eccentricity (Uijl, 1983)

Uijl also studied the type of bond stress distribution as well as the transfer length by conducting finite element analyses. Two types of bond stress distribution were examined: uniform bond stress and linear bond stress. While the bond stresses ramp up with “linear bond stress” assumption, they are assumed to be constant in “uniform bond stress” assumption. Uijl pointed out that both the spalling and bursting stresses were higher in the analyses conducted with linear bond assumption in comparison to those conducted with uniform bond assumption.

Uijl also reported that with increasing transfer length, both spalling and bursting stresses decreased in the analytical research done.

Uijl completed a number of tests on small I shaped sections that were to resemble one bay of a hollow core slab. Since these are very similar to I-beams it is felt that the research conducted by Uijl provides useful information for the current research project. The geometry of the test specimens are shown in Figure 2-20.

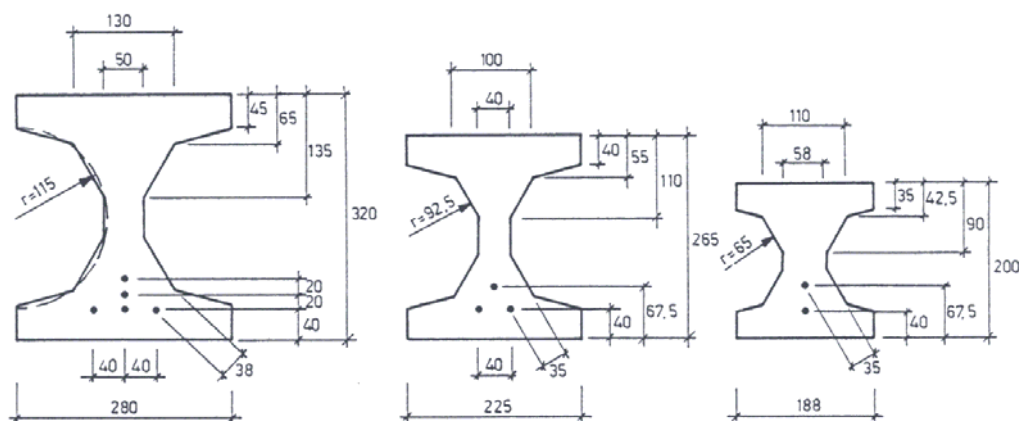


Figure 2-20: Cross sectional dimensions of the investigated members (Uijl, 1983)

While the experimentally obtained transfer length and effective prestressing force matched the pretest calculations, spalling cracks did not occur in the end zones of these beams as was expected by Uijl. Nevertheless, important data were gathered regarding the type of bond stress distribution. Figure 2-21 shows that for typically low values of prestressing force a linear stress distribution is the best match, while at higher prestressing loads (which most codes permit) a uniform bond stress distribution is a better representation of experimentally obtained stresses.

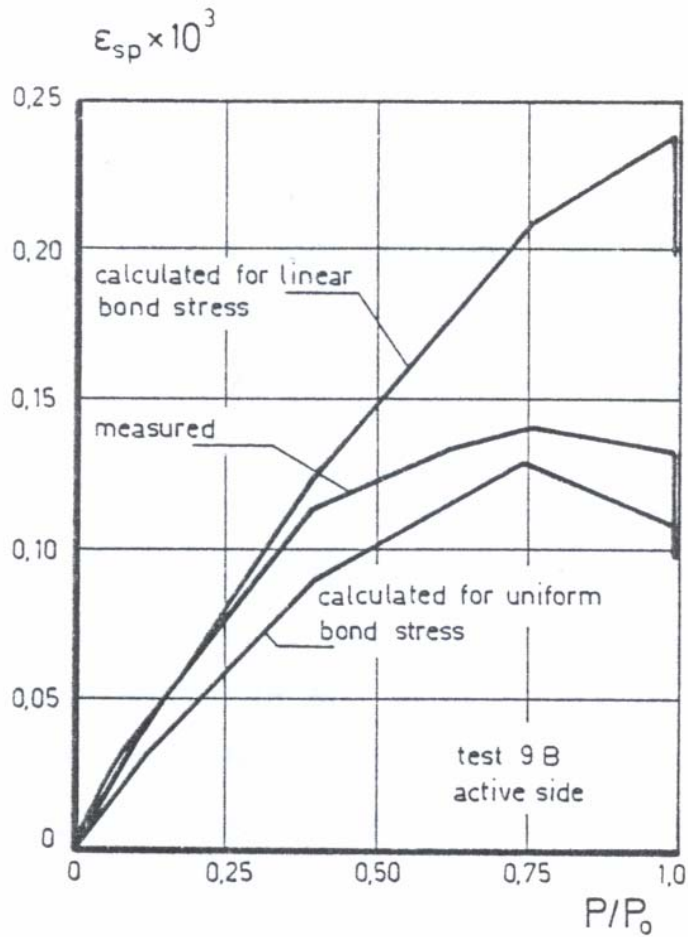


Figure 2-21: Spalling deformation versus prestress level from measurements and calculations for different bond stress distributions (Uijl, 1983)

While there were no cracks in the spalling zone of the beams, there were cracks in the bursting/splitting zone of the beam. Figure 2-22 shows the location of these cracks.

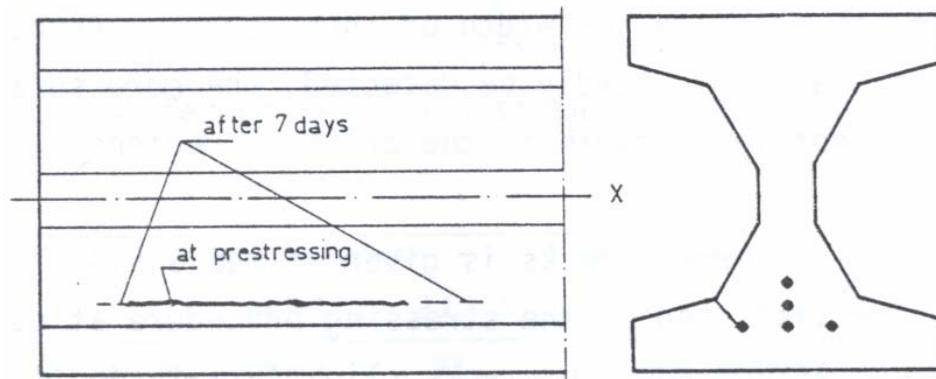


Figure 2-22: Typical cracks at release and its growth afterwards (Uijl, 1983)

It is important to note that these cracks did not extend all the way to the face of the beam. This is most likely due to the superposition of the bursting and splitting stresses. Splitting stresses alone would probably have caused cracking if not for the fact that the bursting stresses compressed the beam near the face of the girder. Once the bursting stresses were tensile the cracks appeared on the beam. This phenomenon is shown in Figure 2-21.

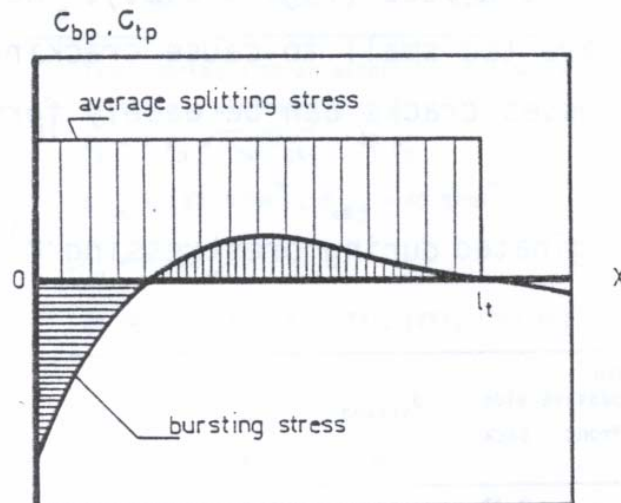


Figure 2-23: Superposition of splitting and bursting stresses (Uijl, 1983)

Uijl reported one equation to calculate the spalling stress in a pretensioned member with respect to its prestressing force, web width, eccentricity, and transfer length. Including these parameters agrees with Marshall and Mattock's (1962) research reviewed earlier in this chapter. Uijl suggested that since it was difficult to distinguish what may be bursting stresses and what may be splitting stresses, these two stress components should be superimposed for ease of calculation. The superposition of these two stresses yields a simple equation shown below:

$$\sigma_{ip} = 0.05(\phi_p / c)\sqrt{\sigma_{po}f_{ckj}} \quad \text{Equation 2-8}$$

where:

σ_{ip} = the total splitting/bursting stress

ϕ_p = the diameter of the prestressing strand

c = clear cover of strands

f_{ckj} = concrete strength at release

Uijl recommended that calculated spalling and bursting stresses be kept lower than the permissible stresses. These permissible stresses were based on the characteristic tensile strength of the concrete at release:

Spalling Stress Limit

$$\sigma_{sp} \leq f_{ckj} \quad \text{Equation 2-9}$$

Bursting/Splitting Stress Limit

$$1.4\sigma_{ip} \leq f_{ckj} \quad \text{Equation 2-10}$$

2.2.2.2 Comité Euro-International Du Béton, 1987

A major work that summarized much of the research into prestressed anchorage zone design in Europe was the Comité Euro-International Du Béton's Bulletin d'Information N° 181. An in-depth look into post-tensioned anchorage

zones was included in this report but will not be completely reviewed here for sake of brevity. Two important details that are defined at the beginning of this bulletin are revisited here. The first point is that the anchorage zone design for both post-tensioned and pretensioned members is the same in its goal to resist the tensile forces that develop due to the application of the load. The only difference in the two is how the load is applied. The second point this bulletin makes distinguishes the three types of transverse stresses in pretensioned members also shown in Section 2.2.2.1. Figure 2-24 once again shows the locations of these stresses as well as the locations of cracks in the ends of a pretensioned concrete member.

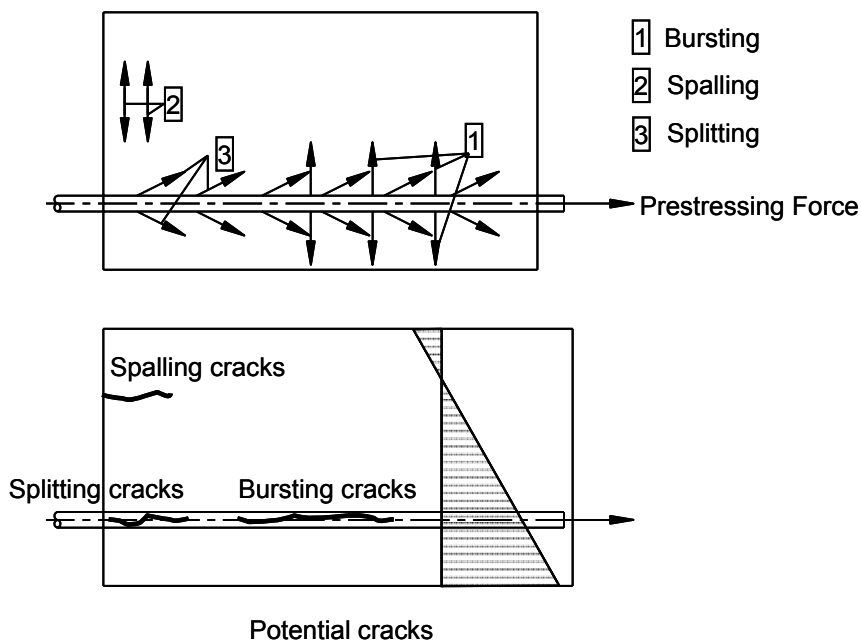


Figure 2-24: Schematic figure for stresses and potential cracks in transmission zone (CEB, 1987)

One of the important issues that the bulletin deals with is the transfer of the prestressing force into a member by bond action. As is stated in the report, bond is a very complex phenomenon that depends on numerous characteristics, including but not limited to:

- *Surface characteristics of the tendon*
- *type and size of prestressing tendon*
- *strength of concrete*
- *maturity of the concrete at release*
- *type of prestressing force release (gradual or sudden)*
- *confining effects*
- *concrete cover to tendons*
- *place of the tendon in beams (top or bottom)*

On some occasions it may be necessary to debond a few strands using plastic tube or tape until the beam can better handle the additional forces. Wherever this debonding ends is where the bond stresses begin. This CEB bulletin defined the transmission length as follows:

“...Transmission length is the length necessary to build up the prestressing force by bond stress between tendon and concrete...” (54).

This definition is similar to what is defined in the U.S. as transfer length. The main method used to experimentally find out what this value equals in pretensioned members is to apply strain gauges to the concrete surface of the end zones of pretensioned members. Two studies regarding transfer length were reviewed in this bulletin, both of which found similar results for the “transmission” length of pretensioned concrete. One of those investigations was conducted by J.A. den Uijl at Delft University of Technology and has been reviewed earlier in this thesis. The other was completed by G. Tassi at the Technical University of Budapest in 1985. One additional phenomenon related to

bond discussed in this CEB report is the tendon draw-in. This is simply the relative displacement between the end of the concrete member and the prestressing tendon. The end result of all the bond and draw-in research results in a step by step method for calculating transmission length using these two phenomena.

Since “transmission” length has an important effect on the transverse stresses that develop in the end region of pretensioned members the Comité Euro-International Du Béton did a review of the code provisions from various countries around the world to establish any major differences in its calculation. These code provisions are all very different in their method of calculation. Some give the transmission (transfer) length as a function of draw-in, while others use anchorage length or bond length, and some also use simple empirical formulae.

The committee recommended the use of the symmetric prism method developed by Guyon (1953) as the best method for calculating the stresses in the end regions of pretensioned and post-tensioned members. The committee concluded that pretensioned members see much lower levels of tensile stresses in the anchorage regions than post-tensioned members.

2.2.2.3 Comité Euro-International Du Béton, 1992

The CEB published one additional bulletin on prestressed anchorage zones to supplement the original Bulletin N° 181. This Bulletin N° 212 is very brief, but does an excellent job explaining two main topics; prestressing strand bond and transverse tensile stresses. One of the major references again was Uijl’s 1983 work at Delft University of Technology; additional research that was not covered in Bulletin N° 181 was included in the Bulletin N° 212. .

The authors of this bulletin indicated that in early versions of the CEB-FIP code, strands were viewed similar to deformed bars as far as bond was concerned.

A relative rib area equivalent to the rib area of a deformed bar was defined as the area between individual wires as shown in Figure 2-25.

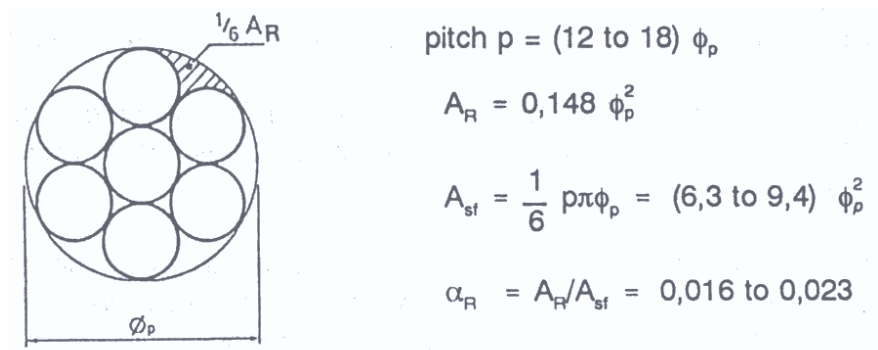


Figure 2-25: Definition of relative rib area for strand (CEB, 1992)

Some pull out tests done supporting the 1978 CEB Model Code were also reported (Figure 2-26).

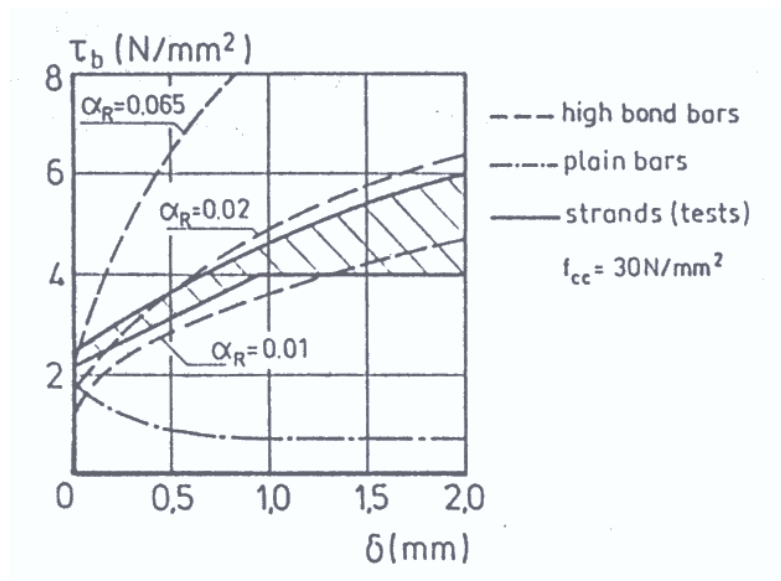


Figure 2-26: Bond stress as a function of slip for different tendon types (CEB, 1992)

Additional work completed on the bond mechanism proved that the equivalent rib assumption used in 1978 version of the CEB model code was inaccurate given that a strand moves through concrete in *“the pre-shaped helical channel and no concrete ribs are sheared off. Hence, the bond is rather based on friction.”* (CEB, 1992) To develop the friction, the committee indicated that at least three actions between the strand and concrete would occur:

- a) *Cross-sections of the strand change over the length of the strand, which causes the strand to wedge into the concrete with relative movement (Hoyer effect).*
- b) *Changes in the longitudinal stress deform the strand transversely within the concrete (Poisson effect).*
- c) *Changes in the longitudinal stress can cause changes in the stress between strand and concrete due to the shape of the wires*

The most important point to recognize is that the bond stress of prestressing strand is not just a function of the slip, but also the change in stress over the length of the wire. This gives prestressing strand somewhat different bond properties than plain bars. One result of this bond action results in different concrete stresses around the strand than are typically found around plain bars. The wedging effect described in part (a) above causes a radial compressive stress in the surrounding concrete. Tangential to these radial stresses are tensile stresses that have been referred to as splitting stress in the previously reviewed research. Some additional discussion on these radial stresses is done, but the main principles of strand bond have been covered.

The final section in CEB’s Bulletin d’Information N^o 212 included a brief review of transverse tensile stresses in pretensioned anchorage zones. Much of this section summarizes Uijl’s work that is reviewed in Section 2.2.2.1 so only a few key points will be touched on. The first is that much of the research that has

been done supporting the Bulletin as well as the CEB-FIP Model Code (1990) was done using only straight strand configurations. Stone and Breen (1984) conducted a comprehensive study of inclined and eccentric tendons in post-tensioned members and found that inclined or curved tendons have an adverse effect on cracking load, reducing it considerably. The authors of the Bulletin felt this research had limited applicability towards a specific class of problems in post-tensioned members and did not include them in support of their work. The second point that will be highlighted is that the committee felt that Uijl's recommendation to limit spalling stresses to $f_{ctk0.05} / 1.5$ could be overly conservative and was not satisfied by many existing pretensioned members. The committee stated that the calculation method discussed in Uijl (1983) gave a tensile stress limit that greatly differs from the real spalling stress. They further pointed out that a better estimation of the spalling stresses can be made using the results of Uijl's finite element model shown in Figure 2-27.

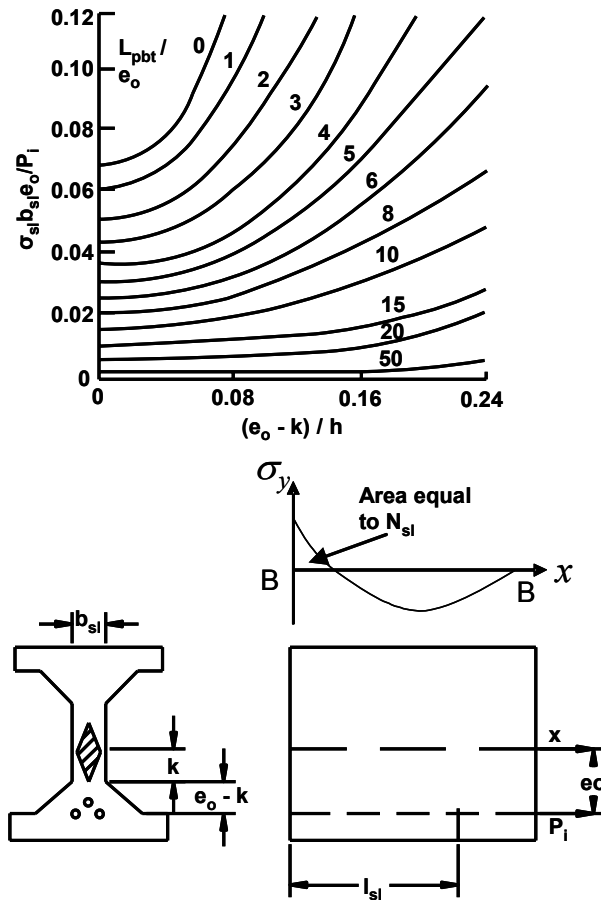


Figure 2-27: Maximum spalling stress as a function of the cross-sectional dimensions, the eccentricity, and the transmission length (CEB-FIP, 1990)

The committee indicated that bursting and spalling stresses in prestressed beams could be negligible as long as proper cover and normal transverse reinforcement was in place.

2.3 CODE DEVELOPMENT

In the United States there are two design specifications and one design guidelines for prestressed concrete members: AASHTO LRFD Bridge Design

Specifications (2007), ACI 318-05, and the PCI Design Handbook (6th Edition). The two main design codes in the United States, ACI 318 and AASHTO Standard Specifications, have existed since the beginning of prestressed concrete in the United States in the mid 1950's. ACI had existed in some form for nearly 50 years when prestressed concrete provisions were incorporated into the code in 1963. AASHTO first saw major provisions related to prestressed concrete in their 1961 Standard Specifications edition. PCI did not print its first edition until 1971. Each of these codes or design guidelines has had a major impact on the way designers detail prestressed concrete girders in the U.S. In Europe, it is difficult to tell exactly when the code provisions first started appearing related to prestressed concrete, but Europe was most certainly ahead of the curve in prestressed technology as compared to the U.S.

Looking through both European and United States codes, it can be somewhat difficult to deduce where the first pretensioned anchorage zone code requirements originated. Each major United States and European code described above was reviewed for their contributions to the design of pretensioned anchorage zone details. ACI-318 has not included any prescriptive provisions for the design of pretensioned anchorage zones although it has extensive provisions for post-tensioned anchorage zones. AASHTO LRFD (2007), PCI Design Handbook (6th Edition) and CEB-FIP MC 90 include explicit guidelines and provisions that can be used to design the anchorage zones of pretensioned girders. The guidelines reviewed here include the simplified calculation methods suggested by each of the codes and guidelines, since these are what most typical designers will use as opposed to STM. It is important to recognize that while the use of STM yields conservative designs of post-tensioned anchorage zones, its use for pretensioned beams present additional challenges regarding the difficult in

defining the geometry and actual location of internal nodes in the anchorage region.

2.3.1 United States Design Specifications and Guidelines

2.3.1.1 AASHTO Specifications for Highway Bridges, 1961

The first design provisions for end region reinforcement in AASHTO appeared in the interim provisions for the 1961 Standard Specifications. Article 1.13.15 of the interim specification was revised to specifically call out end blocks for post-tensioned and pretensioned beams separately. The pretensioned beam provisions read as follows:

In pretensioned beams, vertical stirrups acting at a unit stress of 20,000 psi to resist at least 4 percent of the total prestressing force shall be placed within a distance of $\frac{d}{4}$ of the end of the beam, the end stirrup being as close to the end as practicable.

This provision appears to be the first one in the U.S. for pretensioned members for anchorage zone rebar detailing. It is difficult to surmise exactly where this provision came from, but it appears to be a simplification of Marshall and Mattock's equation in their 1962 PCI paper.

2.3.1.2 AASHTO LRFD Bridge Design Specifications, 2007

In over 50 years the AASHTO provision for pretensioned anchorage zone detailing has changed very little. The only change is that the original provision has been taken out of verbal form and placed into equation form in Article 5.10.10.1 – Factored Bursting Resistance:

The bursting resistance of pretensioned anchorage zones provided by vertical reinforcement in the ends of pretensioned beams at the service limit state shall be taken as:

$$P_r = f_s A_s \qquad \text{Equation 2-11}$$

where:

f_s = *stress in steel not exceeding 20 ksi*

A_s = *total area of vertical reinforcement located within the distance $h/4$ from the end of the beam (in²)*

h = *overall depth of precast member (in)*

P_r = *bursting resistance force*

The resistance shall not be less than 4 percent of the prestressing force at transfer.

The end vertical reinforcement shall be as close to the end of the beam as practicable.

2.3.1.3 AASHTO LRFD Bridge Design Specifications, 2007

An additional design provision from AASHTO LRFD (2007) is used to help control splitting stresses. This provision is for the amount of confining steel that needs to be used around the prestressing strand in the end region. Article 5.10.10.2 reads:

For the distance of $1.5d$ from the end of the beams other than box beams reinforcement shall be placed to confine the prestressing steel in the bottom flange. The reinforcement shall not be less than No. 3 deformed bars, with spacing not exceeding 6.0 in. and shaped to enclose the strands.

At this point, it is important to appreciate the fact that the AASHTO provisions are aimed at handling spalling (incorrectly referred to as bursting in the code) and splitting stresses while bursting stresses are not addressed.

2.3.1.4 PCI Design Handbook, 6th Edition, 2004

The Precast and Prestressed Concrete Institute followed suit with AASHTO and placed its first pretensioned anchorage zone provision in its 6th Edition. The provision is also based on Marshall and Mattock's original 1962 PCI paper. This provision however, mirrors the equation Marshall and Mattock (1962) suggested with the exception of the design stress for the steel. It states that at the time of prestress transfer, tensile stresses develop transverse to the line of action of the strands and elaborates further as follows:

These forces can be resisted by vertical reinforcement calculated by the following equation:

$$A_{vt} = \frac{0.021P_o h}{f_s l_t} \qquad \text{Equation 2-12}$$

where:

A_{vt} = required area of stirrups at the end of a member uniformly distributed over a length $h/5$ from the end

P_o = prestress force at transfer

h = depth of member

f_s = design stress in the stirrups, usually assumed to be 30 ksi

l_t = strand transfer length

2.3.2 A European Code: CEB-FIP Model Code, 1990

CEB-FIP Model Code 90 has much more thorough provisions for pretensioned anchorage zone detailing. A suggested method for detailing both

pretensioned and post-tensioned anchorage zones is the use of STM. As with AASHTO LRFD (2007) there is an understanding that STM is not well-understood universally, so simplified design methods are supplied. These provisions are more commonly used by designers of pretensioned beams, so they are the primary focus of this code review. The origins of the provisions first included in the 1990 version of the code were reviewed earlier in this text under the Bulletin d'Information N° 181 and N° 212 as well as Uijl's work at Delft University of Technology. The first provisions shown will provide the equations for calculating the “transmission” length of prestressing steel. Transmission length in CEB FIP MC 90 is an equivalent term to transfer length in U.S. codes, but the distances that can be calculated in the two codes are very different. The following provisions will be the requirements for anchorage zone detailing in pretensioned members. The CEB-FIP Model Code has two different provisions for detailing the end region of pretensioned members. One handles the reinforcement detailing requirements for bursting/splitting stress and is based on Guyon's (1953) symmetrical prism. The other handles the spalling stress requirements and is based on a similar “equivalent prism” method to that of Gergely, Sozen, and Siess (1963):

6.9.11.2 Bond Strength

$$f_{bpd} = \eta_{p1} \eta_{p2} f_{ctd} \quad \text{Equation 2-13}$$

where

$f_{ctd} = f_{ctk}(t)/1.50$ is the lower design concrete tensile strength; for the transmission length the strength at the time of release

$\eta_{p1} =$ takes into account the type of prestressing tendon: $\eta_{p1} = 1.4$ for indented or crimped wires, and $\eta_{p1} = 1.2$ for 7-wire strands

η_{p2} = takes into account the position of the tendon: $\eta_{p2} = 1.0$ for all tendons with an inclination of 45° - 90° with respect to the horizontal during concreting, $\eta_{p2} = 1.0$ for all horizontal tendons which are up to 250 mm from the bottom or at least 300 mm below the top of the concrete section during concreting, and $\eta_{p2} = 0.7$ for all other cases.

6.9.11.3 Basic Anchorage Length

The basic anchorage length of an individual pretensioned tendon is

$$l_{bp} = \frac{A_{sp} f_{ptd}}{\phi\pi f_{bpd}} \quad \text{Equation 2-14}$$

where

$f_{ptd} = f_{ptk}/1.15$, where f_{ptk} is yield strength of prestressing tendon

$$\frac{A_{sp}}{\phi\pi} = \phi/4 \text{ for tendons with a circular cross-section}$$

$$= 7\phi/36 \text{ for 7-wire strands}$$

6.9.11.4 Transmission Length

The transmission length of a pretensioned tendon is

$$l_{bpt} = \alpha_8 \alpha_9 \alpha_{10} l_{bp} \frac{\sigma_{pi}}{f_{pd}} \quad \text{Equation 2-15}$$

where

α_8 = considers the way of release: $\alpha_8 = 1.0$ for gradual release and $\alpha_8 = 1.25$ for sudden release;

α_9 considers the action effect to be verified: $\alpha_9 = 1.0$ for calculation of anchorage length when moment and shear

capacity is considered, and $\alpha_9 = 0.5$ for verification of transverse stresses in anchorage zone

α_{10} considers the influence of bond situation: $\alpha_{10} = 0.5$ for strands and $\alpha_{10} = 0.7$ for indented or crimped wires;

σ_{pi} is the steel stress just after release

6.9.12 Transverse stresses in the anchorage zone of prestressed tendons

6.9.12.1 General

The anchorage zone of prestressed tendons is a discontinuity region that should be treated according to section 6.8. Should the use of the strut-and-tie model be too problematic because of the complexity of the stress field, the verification may be performed on the basis of the stresses in a linear, uncracked member. For design purposes, the tensile stresses, due to the development and distribution of the prestressing force, are subdivided into three groups (Fig. 2.2.a).

If the strut-and-tie model is not applicable due to lack of transverse reinforcement, the verification may be performed on the basis of stress and strain analysis.

6.9.12.2 Bursting

For the calculation of the bursting force the symmetric prism analogy may be used (Figure 2-28).

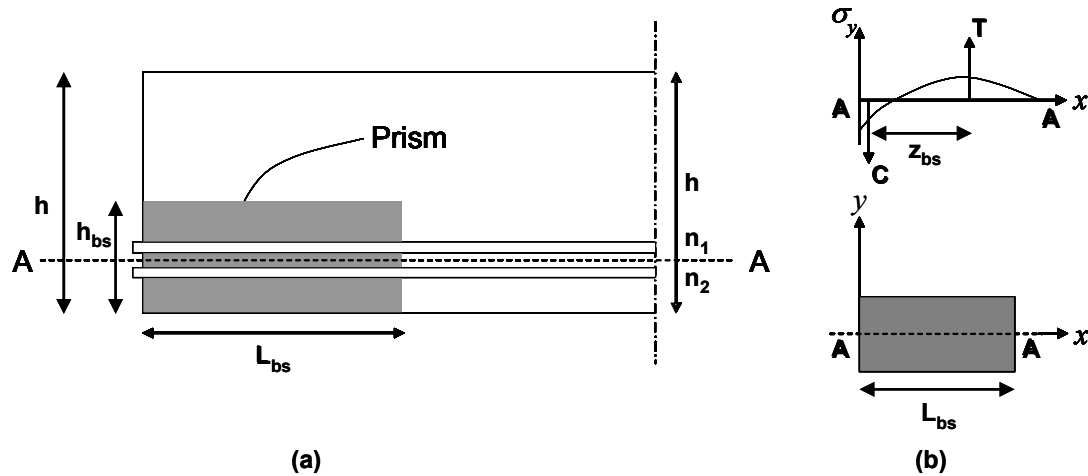


Figure 2-28: For calculation of the bursting force: (a) dimensions of the symmetrical prism; (b) moment equilibrium along section A-A (CEB-FIP, 1998)

The height and the width of the prism follow from the possible enlargement of the anchor plates (post-tensioning) or the tendon pattern (pretensioning). For multiple tendons the most unfavorable situations shall be considered: a single tendon or a group of tendons. The bursting action shall be determined both in the vertical and in the horizontal direction.

The length of the prism is for the end anchored tendons

$$l_{bs} = h_{bs} \quad \text{Equation 2-16}$$

And for tendons anchored by bond

$$l_{bs} = \sqrt{[h_{bs}^2 + (0.6l_{bpt})^2]} < l_{bpt} \quad \text{Equation 2-17}$$

The internal lever arm for the bursting force is

$$z_{bs} = 0.5l_{bs} \quad \text{Equation 2-18}$$

The bursting force follows from the moment equilibrium along section A-A of Figure 2-28 (b).

$$N_{bs} = \frac{1}{2} \frac{(n_1 + n_2)t_2 - n_1 t_1}{z_{bs}} \gamma_1 F_{sd} \quad \text{Equation 2-19}$$

where

t_1 is the distance between the centroid of tendons above section A-A to the centroid of the prism

t_2 is the distance between the centroid of the concrete stress block above section A-A to the centroid of the prism

n_1, n_2 are the numbers of tendons above and below section A-A, respectively

F_{sd} is the design force per tendon

$\gamma_1 = 1.1$ is the supplementary partial safety factor against overstressing by overpumping

The maximum bursting stress follows from

$$\sigma_{bs} = 2N_{bs} / b_{bs} l_{bs} \quad \text{Equation 2-20}$$

where b_{bs} is the width of the prism.

For $\sigma_{bs} > f_{ctd}$ the bursting force shall be resisted by confining or net reinforcement distributed within $l_{bs}/3$ to l_{bs} from the end face, with

$$A_{bsb} = N_{bs} / f_{sy} \quad \text{Equation 2-21}$$

6.9.12.3 Spalling

The spalling force may be calculated with the equivalent prism analogy (Figure 2-29(a)).

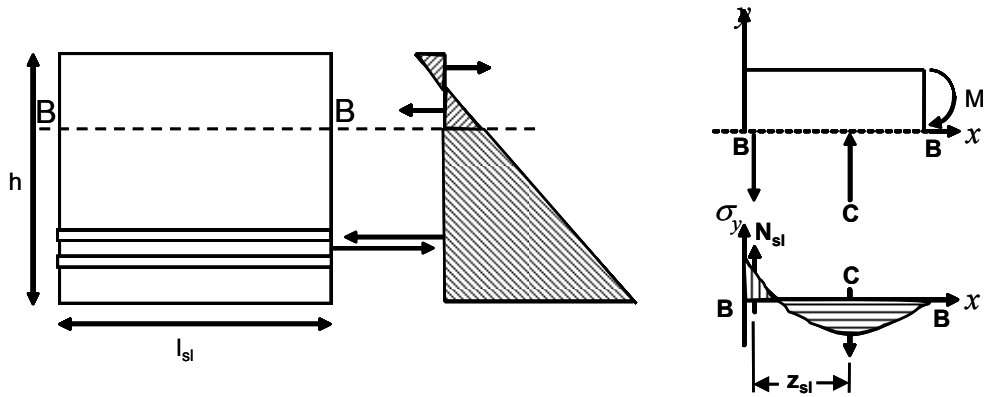


Figure 2-29: For calculation of the spalling force: (a) definition of the equivalent prism; (b) moment equilibrium along section B-B (CEB-FIP, 1998)

The length of the prism is defined as, for end anchored tendons

$$l_{sl} = h \quad \text{Equation 2-22}$$

And for tendons anchored by bond

$$l_{sl} = \sqrt{[h^2 + (0.6l_{bpt})^2]} < l_{bpt} \quad \text{Equation 2-23}$$

The internal lever arm for the spalling force is

$$z_{sl} = 0.5l_{sl} \quad \text{Equation 2-24}$$

Section B-B shall be chosen so that along this section no shear force results. The spalling force results from the moment equilibrium along section B-B

$$N_{sl} = M / z_{sl} \quad \text{Equation 2-25}$$

With the moment M given by concrete stresses above section B-B.

The maximum spalling stress follows from

$$\sigma_{sl} = 8N_{sl} / b_{sl}l_{sl} \quad \text{Equation 2-26}$$

With b_{sl} width of the cross section at section B-B.

For $\sigma_{sl} \leq f_{ct,fl} / \gamma_c$, where

$$\gamma_c = 1.5$$

$f_{ct,fl}$ is the flexural tensile strength of concrete

the spalling force shall be resisted by reinforcement

$$A_{s,sl} = N_{sl} / f_{sy} \qquad \text{Equation 2-27}$$

The spalling force resisting reinforcement shall be put parallel to the end face in its close vicinity.

The final spalling stress provision is supplemented by the following simplified, but also more accurate method:

The equivalent prism approach overestimates the spalling stress. For shallow members (i.e. hollow core slabs) a more accurate value may be obtained from Figure 2-27.

2.4 SUMMARY

Much of the experimental work that has been used in developing pretensioned beam anchorage zone design guidelines or code provisions is reviewed in this chapter. In addition, some analytical work is reviewed to gain a better understanding of the state of stress in the end zones of typical pretensioned and post-tensioned members. Post-tensioned members are examined because much more research has been conducted in this area and the research offers a starting point for most of the analytical work on pretensioned concrete. As stated within multiple reviews, the only difference between post-tensioned and pretensioned concrete applications is the method in which the load is applied to

the beam. Pretensioned beams build up prestressing load as the bond between concrete and strand develops. The application of the load on the end region of a prestressed member creates transverse tensile stress as the applied load spreads to become a linear stress distribution. The distance required for the prestressing force to build up to its full value is defined as the transfer length. It is within this distance that researchers have found the worst transverse stresses occur. Most researchers agree that there are at least two types of stresses occurring in the end regions: bursting and spalling. The third type of transverse stress that is primarily discussed in European research is splitting stress. All of these stresses are discussed in Section 2.2.2.1.

U.S. design specifications and guidelines for pretensioned members have included provisions for what has been defined as bursting stress and minimal splitting stress. This “bursting” stress term in AASHTO Article 5.10.10.1 is not consistent with most research which defines that same stress as spalling stress. Even within the U.S. design codes there is inconsistency in these terms. In the post-tensioned code provisions from AASHTO (§5.10.9), that were primarily based on the research conducted by Breen et al. (1994), the bursting and spalling stresses are correctly called out in their respective locations. This has been the case since these provisions were first adopted by the AASHTO Bridge Design Specifications. ACI 318-05 has almost identical provisions for post-tensioned anchorage zones and also correctly defines these two types of stresses. This indicates that while there is not a lack of knowledge in the U.S. on the post-tensioned anchorage zone detailing side, the pretensioned anchorage zone provisions appear to not have benefited from this knowledge.

Research summarized in Sections 2.2.1.1 and 2.2.1.4 examines pretensioned spalling stresses, their magnitude, and how best to design and detail reinforcing bars to control these stresses. The researchers (Marshall and Mattock

(1962), Tuan et al. (2004)) focusing on tensile stresses in anchorage zones of pretensioned beams found that spalling stresses occur near the centroid of the beam and are at their maximum at the end face of the beam. Since the researchers in the U.S., Marshall and Mattock (1962) and Tuan et al. (2004)), did not investigate bursting stresses or splitting stresses, reinforcing bar detailing received no attention in their reports. Breen et al. (1994) , used strut-and-tie modeling to detail both spalling and bursting regions of post-tensioned anchorage zones. As reported by Tuan et al. (2004), the use of STM can sometimes be overly conservative (requiring 3 times as much reinforcement in some cases). Nevertheless, Breen et al. (1994) found that bursting forces were the most common failure mechanism in post-tensioned applications. European research (Uijl (1983), CEB-FIP (1987, 1992)) reviewed here looked at all three types of stresses (bursting, splitting, and spalling) and how best to control them. Bond, transfer length, magnitude of prestressing load, eccentricity of load, and concrete cover are some of the topics that are reviewed that are found to contribute to the level of transverse stresses. Uijl (1983) in Section 2.2.2.1 discusses most of these topics within the text of his report. Uijl found that cracking typically occurred in the bursting/splitting regions of the girders that he tested. This agrees with Breen et al.'s (1994) work in post-tensioning and begins to show the importance of this region within a pretensioned concrete beam. Uijl also indicated that while bursting/splitting cracks did reveal higher levels of stress, spalling stresses should be monitored as eccentricity increases. The idea that eccentricity increases spalling stresses agrees with Gergely, Sozen and Siess (1963) as well as Stone and Breen (1984). This agreement shows the level of common understanding that exists between U.S. and European research. Even in post-tensioned design provisions that apply to anchorage zone reinforcing detailing, the terminology and design guidelines using STM are very similar between the U.S. and Europe.

While the researchers and post-tensioned code provisions are in agreement, the U.S. codes and European codes differ on the subject of pretensioned beams. The United States codes have provisions only for spalling stresses in pretensioned beams. While these can be an important stress to monitor, bursting stresses are overlooked and can cause problems in pretensioned girders. Due to Uijl's in depth review and research of end zone stresses in pretensioned beams, CEB-FIP Model Code 1990, has much deeper content on how to control the majority of transverse end zone stresses in pretensioned beams. This is shown in Section 2.3.2.

Splitting stresses acting alone in the bottom flange are only touched on in this review. The AASHTO LRFD Code Provision (2007) in Section 2.3.1.3 shows that a minimal amount of reinforcement must be included around the strands to oppose the splitting force of the strands. This provision seems to have been developed from experience rather than analytical or empirical research as no U.S. background research could be found for it. The European code provision simply bulks bursting and splitting reinforcement together.

CHAPTER 3

Experimental Program

3.1 OVERVIEW

The design of pretensioned beams tested in the experimental research program, design and construction of a prestressing facility, and instrumentation and construction of each test specimen is discussed in this chapter. All of this work was completed at the University of Texas at Austin's J.J. Pickle Research Campus in Austin, Texas. The construction of the pretensioning bed and I-girders was completed at the Phil M. Ferguson Structural Engineering Laboratory. This research was conducted through funding from the Texas Department of Transportation.

3.2 SPECIMEN DESIGN

Before constructing each specimen to be tested, the strand pattern had to be designed to maximize prestressing force applied to each beam. Background theory on how pretensioned beams are designed and what provisions typically control designs is shown to help the reader understand the process. Once the theory is presented, some typical design equations are shown with supporting calculations in the Appendices.

3.2.1 Prestressed Beam Theory

Before beginning an in depth look into bursting, splitting, and spalling stresses, some basic theory on pretensioned beams is addressed here. Many of the equations used in this section are directly from AASHTO LRFD Bridge Design Specifications (2007) and ACI 318-05.

3.2.1.1 Transfer Length

As clearly stated in Chapter 2, the application of prestressed force into a typical pretensioned beam happens over a specified length in a beam. This length is referred to as the transfer length. Over this length prestressing force builds up to its initial prestress minus some losses due to elastic shortening. These losses will be covered in further detail later in this chapter. A typical development length equation looks much like §12.9 of ACI 318-05:

$$l_d = \left(\frac{f_{se}}{3}\right)d_b + (f_{ps} - f_{se})d_b \quad \text{Equation 3-1}$$

where:

l_d = development length of prestressing strand (in)

f_{se} = effective stress in the prestressing steel after losses (ksi)

d_b = nominal strand diameter (in)

f_{ps} = average stress in prestressing steel at members nominal strength (ksi)

This is a typical strand development equation that is used in the U.S. AASHTO LRFD Bridge Design Specifications also has a similar equation, but suggests simply that the use of 60 strand diameters be used for transfer length. Assuming a typical prestressing force after losses, reveals the same equation for strands from ACI and AASHTO given a lack of information at nominal strength:

$$l_d = \left(\frac{180(ksi)}{3}\right) \cdot 0.6" = 60 \cdot 0.6" = 36" \quad \text{Equation 3-2}$$

This gives a practical value for transfer length for 0.6" strand which was the main type of strand used in this research. This length is approximately the distance it takes to build up to the full prestressing force after initial losses. To be consistent with AASHTO LRFD (2007) and ACI 318-05 specifications a linear variation in this force can be assumed as shown in Figure 3-1.

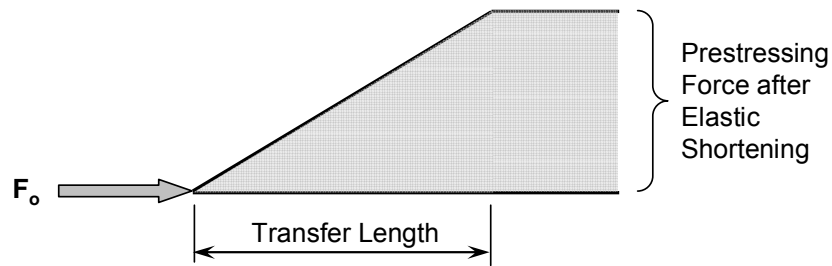


Figure 3-1: Transfer Length for Prestressing Strand

Until the prestressing force reaches its full value the zone within the transfer length is often referred to as a disturbed region. This simply means that the stress distribution over the depth of the beam is not linear. The disturbed region, or “D-region”, usually extends into the beam a distance equal to the depth of the beam. Once the disturbed region ends, Bernoulli’s beam theory becomes valid and simple beam theory can be applied. These regions are commonly referred to as “B-regions”. A figure showing how the elastic stress trajectories travel from D to B regions is shown in Figure 3-2.

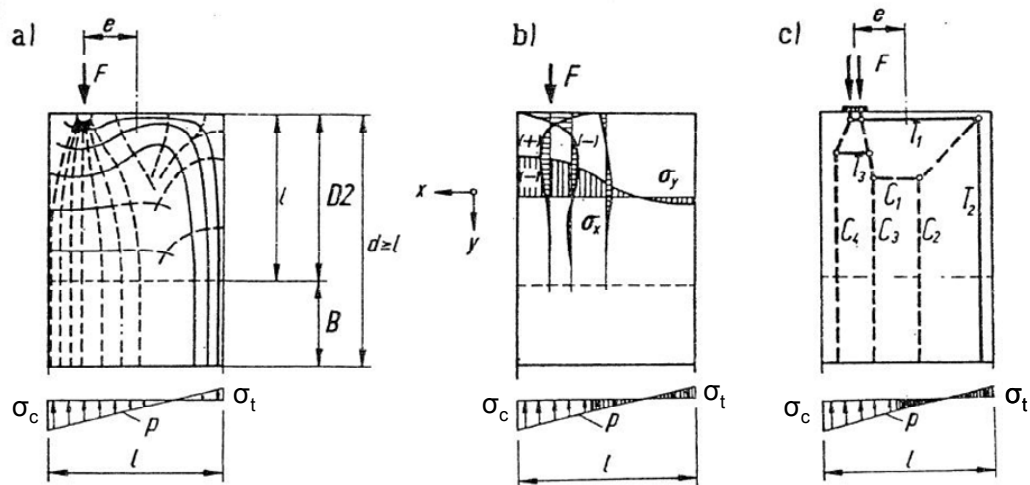


Figure 3-2: Typical D-region for a post-tensioned beam: (a) elastic stress trajectories; (b) elastic stresses; (c) strut-and-tie models. (Schlaich et al. 1987)

3.2.1.2 Beam Theory

Basic beam theory utilizes Bernoulli's hypothesis that as a beam bends in flexure sections within the beam remain plane. As shown in Figure 3-3, the bending moment across each cross-section is the same and the member bends uniformly throughout its cross-section.

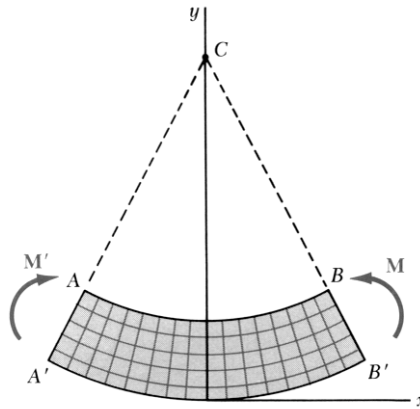


Figure 3-3: Bernoulli's hypothesis; plane sections remain plane (Beer and Johnston, 1992).

Since line AB and line A'B' are bent about the same center point C, any cross-section that was perpendicular to the original line will remain plane as the member bends.

In prestressed beams, the application of an axial load is present that produces a uniform axial deformation, and if the load is eccentric, a bending moment is applied. The bottom and top fiber stresses in a pretensioned beam can be calculated by using plane sections remain plane assumption. These calculations require the materials being used to remain within their elastic state to be valid. Since this is true (i.e. permissible release stresses are met), the following elastic flexure formula can be used to calculate the maximum stresses in a prestressed beam.

$$f_{\max} = \frac{P}{A} \pm \frac{Mc}{I} = \frac{P}{A} \pm \frac{Pec}{I} \quad \text{Equation 3-3}$$

where:

f_{\max} = maximum stress (ksi)

P = applied prestressing force (kips)

A = cross-sectional area of beam

M = moment induced by eccentric application of P

I = moment of inertia

e = eccentricity of applied load P

These stresses can now be calculated to meet code requirements for allowable stresses due to prestressing. Calculations for typical stresses in the Tx girders tested are shown in Appendix A. A graphical representation of what is being calculated is shown in Figure 3-4.

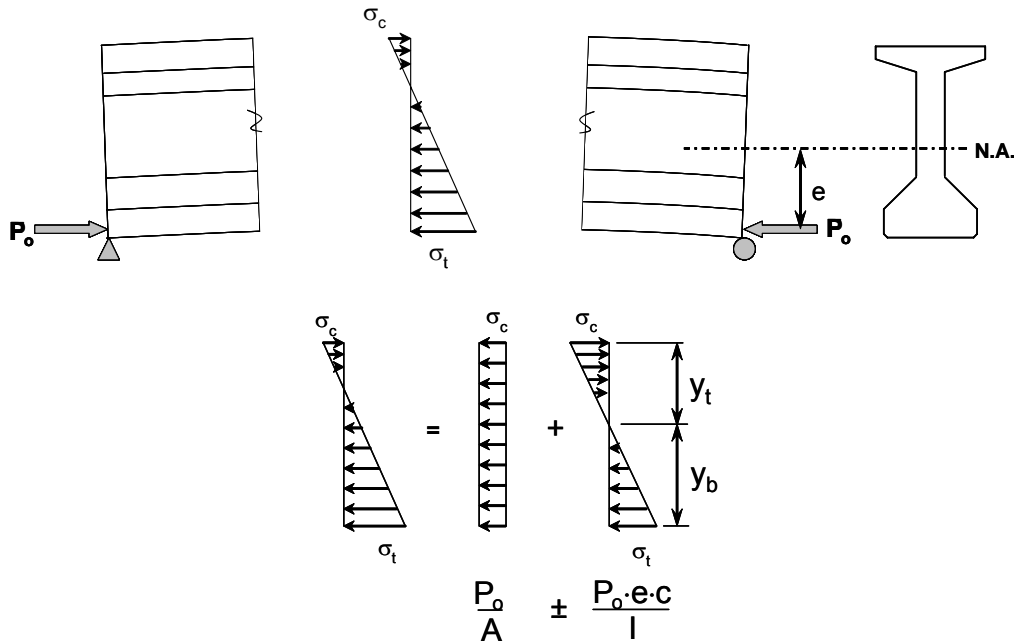


Figure 3-4: TxDOT's typical Tx Girder loaded eccentrically showing elastic stress distribution

3.2.1.3 Elastic Shortening

As was mentioned in earlier, there are some losses that occur during prestressed force transfer. These are often referred to as elastic shortening. When an axial load is applied a beam, it will deform axially as well as flexurally as seen in Figure 3-4. These deformations experienced by the concrete, relieve some portion of the prestressed force and make the actual prestressed force applied to the beam somewhat smaller. AASHTO LRFD 2007 §5.9.5.2.3a offers a simple calculation for finding the elastic shortening losses in a pretensioned member.

$$\Delta f_{pES} = \frac{E_p}{E_{ct}} f_{cgp} \quad \text{Equation 3-4}$$

where:

Δf_{pES} = elastic shortening losses (ksi)

E_p = modulus of elasticity of prestressing steel (ksi)

E_{ct} = modulus of elasticity of concrete at transfer (ksi)

f_{cgp} = the concrete stress at the center of gravity of prestressing tendons due to prestressing force immediately after transfer and the self weight of the member at the section of maximum moment.

A quick sample calculation for a Tx28 beam is shown below. A typical release stress for concrete was 6,500 psi, while the typical force in a prestressed 0.6” strand before release was 44 kips. The eccentricity of the prestressing force in these smaller section beams was 5”.

$$\begin{aligned}
E_p &= 29,000ksi \\
E_{ct} &= 57000 \cdot \sqrt{6500} = 4595ksi \\
f_{cgt} &= \frac{44k \cdot (36strands)}{585in^2} + \frac{44k \cdot (36strands) \cdot (5.01in)^2}{52,772in^4} \quad \text{Equation 3-5} \\
f_{cgt} &= 3.46ksi \\
\Delta f_{pES} &= \frac{29,000}{4595} \cdot 3.46ksi = 21.82ksi
\end{aligned}$$

This is a fairly typical elastic loss for the beams that are tested in this report. This means that after an initial stress of 200 ksi, the actual force imparted into the beam can be calculated using a stress of 178 ksi. Additional calculations for all sections are shown in Appendix A.

3.2.2 Tx Girder Design

Before any prestressing could begin, each girder section had to have a strand pattern designed for it. The strand patterns used for each beam are shown later in this chapter. Each pattern was designed to maximize the amount of prestressing force that could be applied to the section without violating the code limits for allowable stresses at release. For the deeper sections, consideration was given to maximizing the prestressing load and the eccentricity simultaneously. In this way, a more critical scenario for obtaining spalling cracks was created as discussed in Chapters 2 and 4.

ACI provision §18.5.1 states that the stress in the strands shall not exceed $0.74f_{pu}$ during prestressing operations and beam fabrication. AASHTO LRFD (2007) provision §5.9.3-1 allows this stress to be slightly higher at $0.75f_{pu}$. These are both equivalent to a stress of 200 ksi in the strands. The beams were designed to meet AASHTO LRFD Specifications (2007) except for the allowable compressive stresses in concrete after release. These provisions for maximum tensile and compressive stresses on a pretensioned member after release are

located in §5.9.4. Maximum compressive stresses for this project were limited to slightly higher values than are permitted in the code for two reasons: (i) In an ongoing research project funded by TxDOT and conducted by researchers at the Ferguson laboratory, a compressive release stress of $0.65 f'_{ci}$ was found to be feasible. (ii) Subjecting the beams to slightly higher compressive stresses created a slightly increased demand on the transverse reinforcement resisting bursting, spalling and splitting cracks. In short, the compressive stresses were limited to:

$$\sigma_c \leq 0.65 f'_{ci} \qquad \text{Equation 3-6}$$

where:

σ_c = allowable compressive stress

f'_{ci} = specified compressive strength at time of release

The compressive strength of concrete at release was specified by TxDOT as 6500 psi, which limited compressive stresses to $0.65 \cdot 6500 = 4225$ psi; 325 psi higher than the compressive stresses currently permitted by AASHTO LRFD (2007). Tensile stresses did not control the design of Tx28-I, Tx28-II, and Tx46. In Tx70 both the prestressing force and the tendon eccentricity were maximized, as a result additional bonded reinforcement had to be provided within the top flange. The tensile stress limit (AASHTO LRFD (2007)) used to design this beam is shown below for beams with bonded reinforcement sufficient to resist the tensile force:

$$\sigma_t \leq 0.24 \sqrt{f'_{ci}} \qquad \text{Equation 3-7}$$

where:

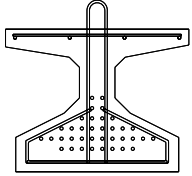
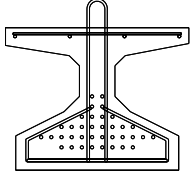
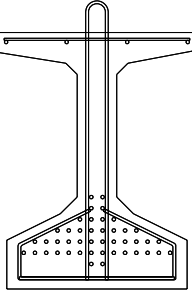
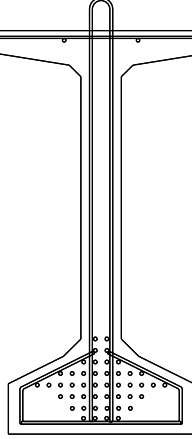
σ_t = allowable tensile stress

f'_{ci} = specified compressive strength in ksi at time of release

This equation yields a tensile stress limit of 612 psi. Additional reinforcement in the form of three #6 bars across the top flange was needed to

adequately counteract the full tensile force in the beam. Detailed equations for this and the design of other beam strand patterns are shown in Appendix A. Table 3-1 below shows the cross-sectional properties for each girder with their appropriate strand pattern. This table also summarizes the results of the equations found in the Appendix by giving prestressing force before and after release, tendon eccentricity, concrete strength at release, and final concrete strength. Section dimensions can be found in Figure 3-21 as well as in Appendix A.

Table 3-1: Tx girder design summary

Section Sketch	Section Properties	Actual Applied P/S Force	Tendon Eccentricity	Cylinder Strength
<p style="text-align: center;">Tx28-I</p> 	<p>Height = 28" $A_g = 585\text{in}^2$ $I_x = 52,772\text{in}^4$ $I_y = 40,692\text{in}^4$ $y_t = 15.02''$ $y_b = 12.98''$</p>	<p>Initial: 1,591 kips</p> <p>After Losses: 1,466 kips</p>	5.01"	<p>Release: 10,025 psi</p> <p>Final: 13,825 psi</p>
<p style="text-align: center;">Tx28-II</p> 	<p>Height = 28" $A_g = 585\text{in}^2$ $I_x = 52,772\text{in}^4$ $I_y = 40,692\text{in}^4$ $y_t = 15.02''$ $y_b = 12.98''$</p>	<p>Initial: 1,692 kips</p> <p>After Losses: 1,522 kips</p>	5.01"	<p>Release: 6,475 psi</p> <p>Final: 11,375 psi</p>
<p style="text-align: center;">Tx46</p> 	<p>Height = 46" $A_g = 761\text{in}^2$ $I_x = 198,089\text{in}^4$ $I_y = 46,603\text{in}^4$ $y_t = 25.90''$ $y_b = 20.10''$</p>	<p>Initial: 1,945 kips</p> <p>After Losses: 1,732 kips</p>	10.67"	<p>Release: 6,500 psi</p> <p>Final: 13,200 psi</p>
<p style="text-align: center;">Tx70</p> 	<p>Height = 70" $A_g = 966\text{in}^2$ $I_x = 628,747\text{in}^4$ $I_y = 57,720\text{in}^4$ $y_t = 38.09''$ $y_b = 31.91''$</p>	<p>Initial: 1,974 kips</p> <p>After Losses: 1,754 kips</p>	22.91"	<p>Release: 6,675 psi</p> <p>Final: 11,575 psi</p>

3.3 CONCRETE PROPERTIES

The concrete used in this project was designed to mirror that which is used in the field in the construction of pretensioned I-girders. Type-III, high early strength cement is typically used in these mixes to allow for a fast turnover rate in the construction of these beams. The concrete mixture designs used in this project are shown here in Table 3-2 for each beam.

Table 3-2: Concrete Mixture designs for each Tx girder constructed

	<i>Tx28-I</i>	<i>Tx28-II</i>	<i>Tx46</i>	<i>Tx70</i>
<i>Course Aggregate</i>	<i>1799 lb/cy, Round River Gravel</i>			
<i>Fine Aggregate</i>	<i>1429 lb/cy</i>			
<i>Type III Cement</i>	<i>611 lb/cy</i>			
<i>Water</i>	<i>214 lb/cy</i>			
<i>Water/Cement Ratio</i>	<i>0.35</i>			
<i>HRWR Admixture</i>	<i>10 oz/Cwt</i>	<i>14.6 oz/Cwt</i>	<i>12 oz/Cwt</i>	
<i>Retarder</i>	<i>11 oz/Cwt</i>	<i>4 oz/Cwt</i>		

3.3.1 Concrete Testing

To ensure that the pretensioned concrete beam specimens were released at the proper strength, cylinder tests were conducted from approximately 8 hours after the concrete placement until 6,500 psi compressive strength was reached. This was done using a Forney universal cylinder test machine (Figure 3-5).



Figure 3-5: Forney concrete cylinder testing machine

The tests were conducted using ASTM C39 Standard Test Method for Compressive Strength of Cylindrical Concrete Specimen. Standard 4" x 8" cylinders were capped with neoprene bearing pads, talcum powder, and a steel retaining ring before testing. Compressive capacities were recorded for each cylinder and then compressive stress values were calculated using Equation 3-8. All cylinder test values are reported in Appendix C for each beam. Table 3-1 summarizes the compressive strength values at release for each girder.

$$f'_c = \frac{P \cdot 4}{\pi \cdot D^2}$$

Equation 3-8

where:

f'_c = cylinder compressive strength (psi)

P = applied load (lbs)

D = diameter of cylinder (in)

3.3.2 Temperature Match Cure

To ensure cylinder strength accurately represented the curing conditions of concrete in a pretensioned concrete beam specimens cast with Type III cement, temperature match curing technology was used. The idea behind match curing technology is fairly simple. Concrete maturity theory states that temperature is a critical factor in the strength development of concrete, especially within the first 24 hours (Kehl and Carrasquillo, 1998). Maturity is found by multiplying an interval of time by the temperature of the concrete. This means that concrete curing at a lower temperature will have to cure longer to reach the same maturity as concrete curing at a higher temperature. As seen in Figure 3-8, the maturity is simply the area under the time temperature curve.

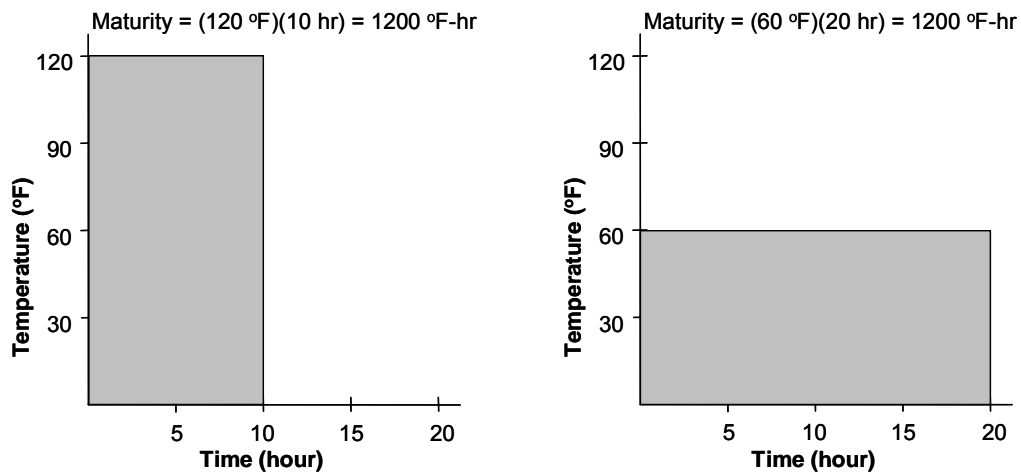


Figure 3-6: Concrete maturity for two different temperature concretes (Kehl and Carrasquillo, 1998)

The idea behind temperature match-curing cylinders is to better match the concrete maturity within a pretensioned concrete beam. Since the beam has a much greater mass of concrete it heats up at a much faster rate and often to higher temperatures than a typical 4" x 8" cylinder and the two would achieve very different strengths within the first 24 hours. Temperature match-curing avoids this problem by heating up the cylinders to match the temperature of a pretensioned concrete beam and therefore the maturity of concrete in the beam is replicated. In its simplest form, match-curing can be accomplished by placing cylinders next to the beam under a tarp to use heat generated from the beam to heat the cylinders. Otherwise, thermocouples placed within the concrete beam may be used to measure the temperature. Then a computer-controlled temperature match-curing system can be used to drive the heat in specialty cylinder molds to match the temperature in the beam. Since the temperatures within the beam can easily get in upwards of 160° F and maturity correlates directly to strength within the first 24 hours, the match-cured cylinders tend to provide the best representation of the true concrete strength. Examples of the possible differences in temperature between ambient, member cured (set next to the beam), and true beam temperatures are shown in Figure 3-7.

During the experimental research conducted as part of this research project, a computer controlled temperature match-curing system was used. Through the use of this system, accurate measurements of compressive strength of concrete were accomplished. A brief explanation of the match curing system (*Sure Cure*) used in this project is provided within the next section.

Since this setup was originally positioned close to a low-capacity pretensioning bed that was utilized in another research project, it was roughly 150 feet away from the high capacity pretensioning bed used in this project. In order to communicate the temperature information collected through the use of the

thermocouples positioned in test specimens the system was modified to include a wireless communication system. The wireless system, shown in Figure 3-9, allowed 6 temperature readings to be taken within a typical beam specimen and then relayed those temperature readings to the original system to match the cylinder temperatures. A schematic of the process is shown in Figure 3-10.

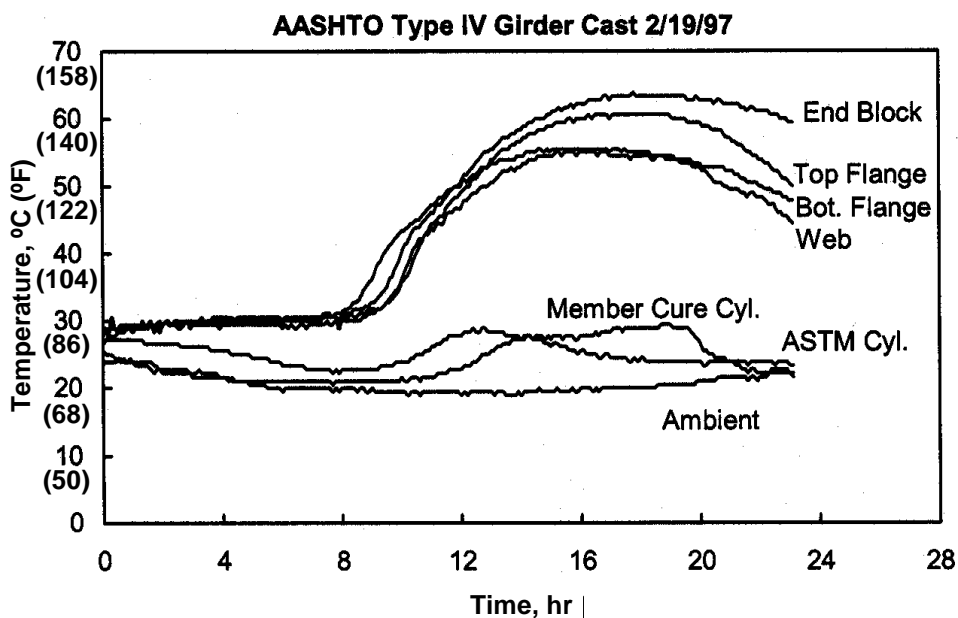


Figure 3-7: Curing temperature profile in an AASHTO Type IV girder (Kehl and Carrasquillo, 1998)

3.3.2.1 Temperature Match Curing Facility: Sure Cure System

The *Sure Cure*, temperature match curing facility allowed cylinders to be match cured to the time-temperature curves experienced by several points in beam specimens. A picture of the setup used is shown in Figure 3-8.



Figure 3-8: Sure Cure Controller and Cylinders



Figure 3-9: Wireless Sure Cure I/O Box

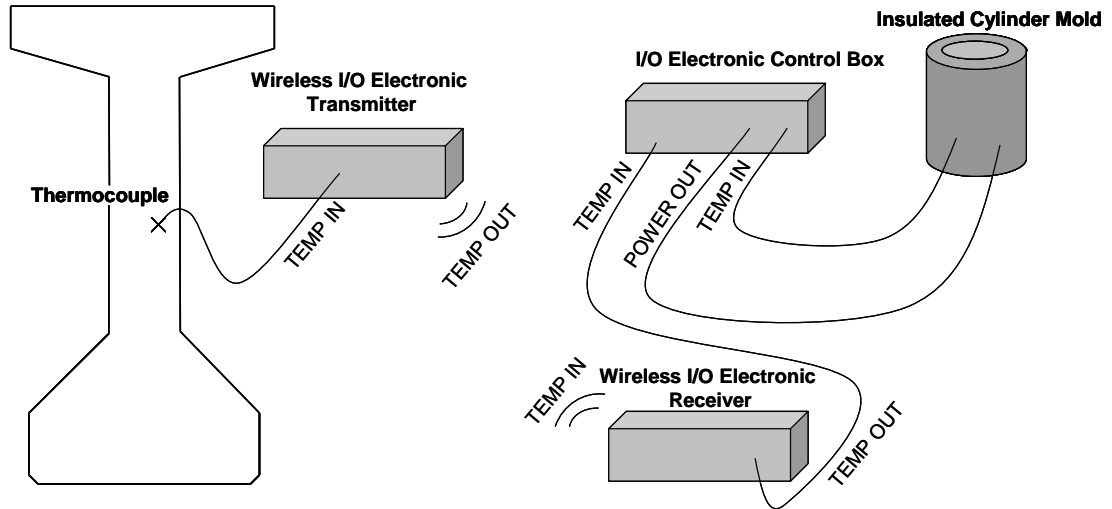


Figure 3-10: Wireless Sure Cure Schematic

A more thorough review of thermocouple locations within each beam as well as temperature plots are given in Section 3.7.4.

3.4 MECHANICAL PROPERTIES OF REINFORCING STEEL

Within this section the stress-strain properties of reinforcing materials used in fabricating the test specimens are reported. Mechanical properties of 0.6” diameter strands, welded deformed wire, and reinforcing bars are reported in this section.

3.4.1 Prestressing Steel

Standard low-relaxation 0.6” diameter strands were used in all specimens. Naturally, the use of 0.6” strands created a more critical condition or a “worst-case scenario” for the test specimens in regards to bursting, spalling, and splitting cracks. Strands were cut from within the same spool and tested in a 600-kip universal testing machine to determine the stress-strain curve of the strands. To gain accurate strength values for the strand it had to be encased in epoxy within a

steel pipe at each end. This was done to ensure that there was no failure at the grips of the 600 kip machine, but instead within the middle of the strand. Figure 3-11 shows the strand in the universal testing machine, while Figure 3-12 shows a typical stress-strain plot. The stress-strain plot was developed using a 24" gauge length extensometer from Epsilon Technology Corp. As seen in Figure 3-12, yield stress for the strands used in this study was 245 ksi. The ultimate strength was 285 ksi.



Figure 3-11: Universal Test Machine Used to Obtain Stress-Strain Curve of Strands

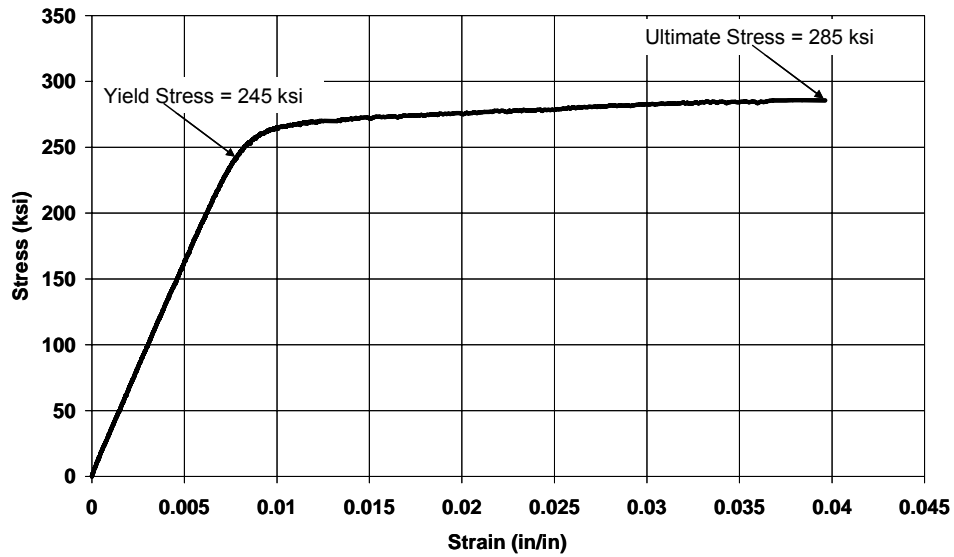


Figure 3-12: Typical Stress-Strain curve for low-relaxation 0.6" diameter strand

3.4.2 Welded Deformed Wire

In all but the first Tx28 girder, prefabricated welded-deformed rebar cages were used to simplify the rebar cage construction for the vertical reinforcement in the beam specimens. A typical bar in the welded fabric of reinforcing bars is shown in Figure 3-13. A typical fabric of reinforcing bars is shown in Figure 3-14.



Figure 3-13: Typical deformed wire from WWR fabrics



Figure 3-14: Typical vertical reinforcement in WWR fabric with deformed bars

Welded rebar cages are sometimes an option for the pretensioned beam fabricators as they provide a slightly easier installation method than typical reinforcing bars that need to be tied together to form a cage. The bars used in welded rebar fabrics are typically slightly higher strength bars, and they provide less plasticity than typical Grade 60 reinforcing bars. In order to check this preliminary assessment, bars were tested in a 600-kip, hydraulically actuated, universal testing machine. All of the vertical bars used in the beam were designated D19.7. This welded-wire designation gives information on the thickness of the bars. The D signifies deformed wire, while the 19.7 signifies a cross-sectional area of 0.197 in^2 . These wires are very close in size comparison to standard # 4rebars. The average yield strength of the deformed wires/rebars was

75 ksi, with an ultimate strength close to 90 ksi. These bars typically had a modulus of elasticity of 29,000 ksi.

3.4.3 Grade 60 Rebar

The additional bars used as spalling reinforcement in each beam were standard Grade 60, #6 reinforcing bars. A detailed look into the location of these bars is shown later in Section 3.7.2. These bars were tested similar to the deformed wires to ensure proper yield values. Typical yield stress values obtained for these bars were between 60 to 63 ksi. Ultimate strength of the bars ranged from about 100 to 105 ksi. The average modulus of elasticity value was 28,500 ksi which is very close to the typical assumed modulus of elasticity value of 29,000 ksi. Since this difference is almost negligible and can well be attributed to the gauge length or testing methods used, a value of 29,000 ksi will be used for these bars throughout the report for calculation purposes.

3.5 PRETENSIONING FACILITY

Before the construction of the specimens for this project could begin, the design and construction of a pretensioning bed was necessary. Once girder section sizes and strand patterns were finalized (Table 3-1) a preliminary design for the pretensioning bed was completed and the actual design process could start.

3.5.1 Design

The design load for this frame was 2,500 kips. It was with this information that a self reacting frame was designed and detailed. Tie downs were essentially unnecessary for the self reacting frame but they were designed to keep the frame in place in the event of a catastrophic failure. Additional members to stress top strands were designed to withstand top strand loads for up to 50 kips. An elevation view of the design is shown in Figure 3-15.

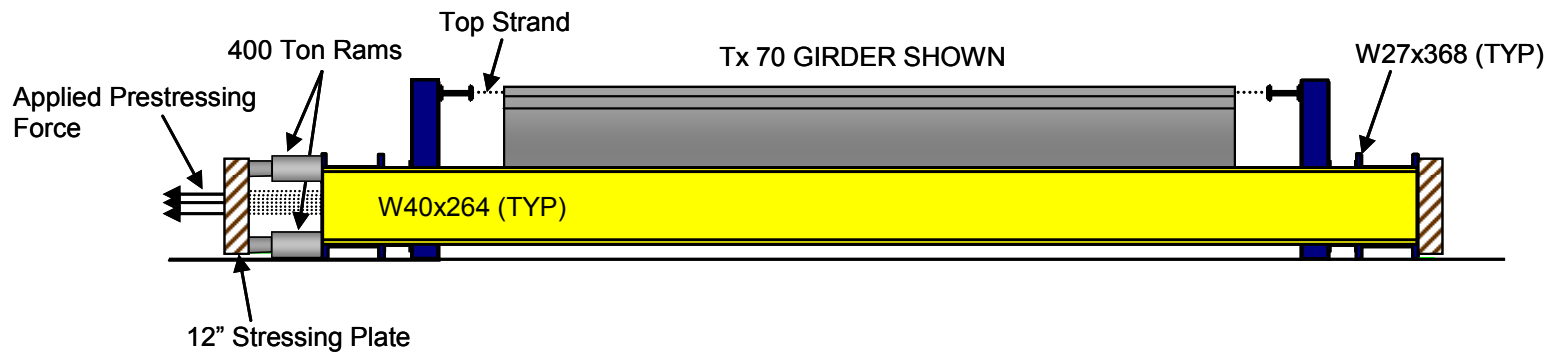


Figure 3-15: Longitudinal elevation view of pretensioning bed with Tx70 girder

As can be observed in Figure 3-15, two large bulkheads, or 12-in.-thick steel plates, as well as four 400-ton hydraulic rams were used to perform the stressing operation. Since four strands stressed to 5 kips/strand were utilized within the top flange of all test specimens, the design also allowed different size beams to be constructed by a movable top strand stressing frame. Additional design drawings showing details of this as well as other aspects of the pretensioning bed are shown in Appendix E. Additional pictures of the completed frame are shown below.



Figure 3-16: Completed pretensioning bed from dead end

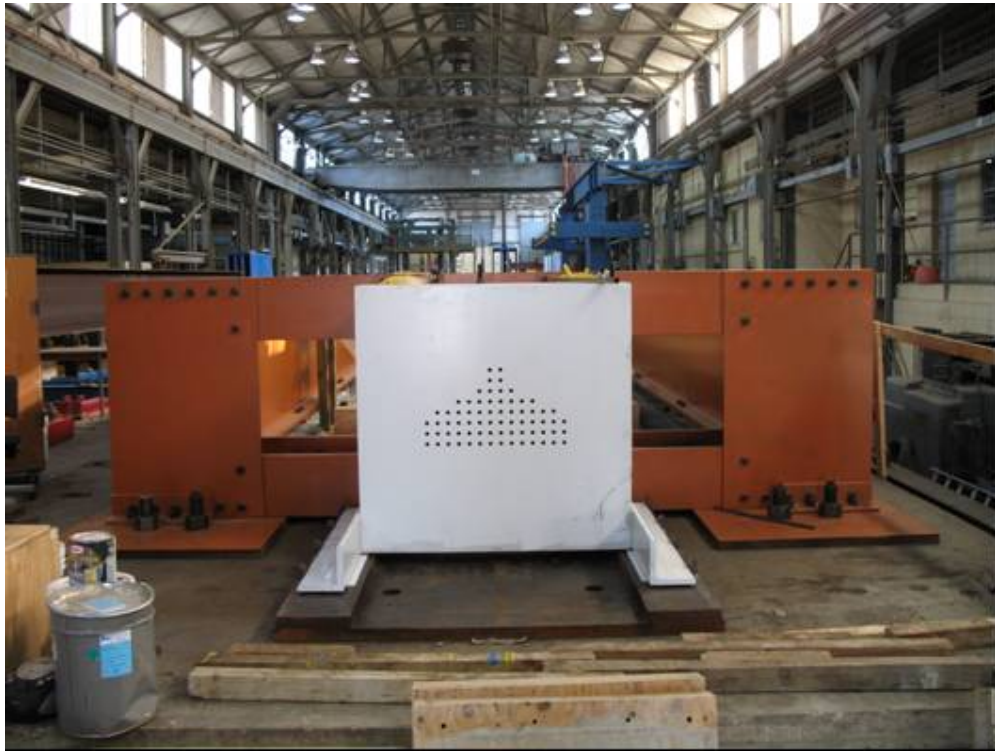
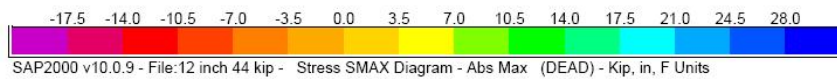
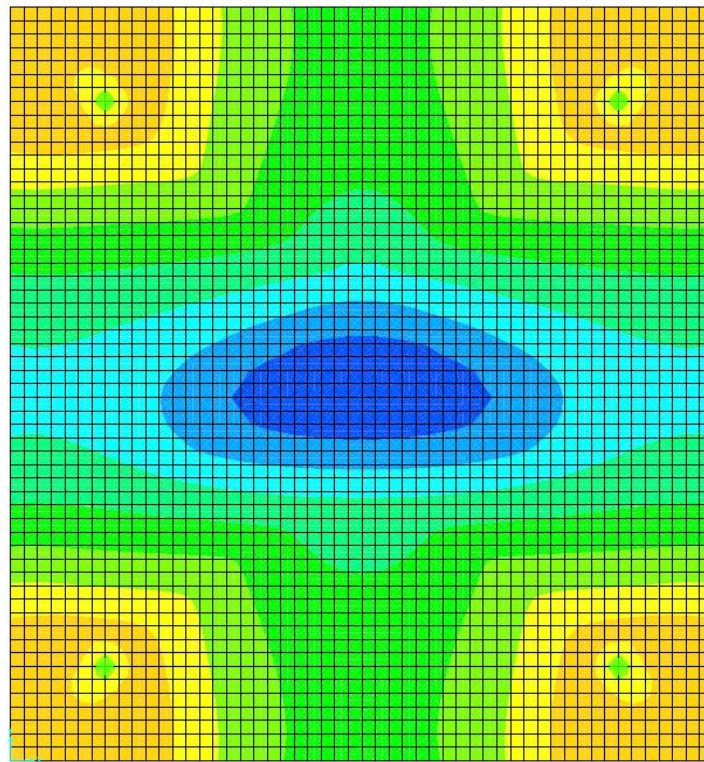


Figure 3-17: Completed pretensioning bed at the live end

One of the more time consuming design tasks was the design of the stressing bulkheads. These plates had to be able to withstand the full design load on their own in order to be effective. The use of a structural analysis software package (SAP2000) with plate modeling capabilities helped ensure that the plates were designed to meet this capacity. This design yielded a 12" thick, 4'x 4' plate to handle the loads needed. Even though a full strand pattern of 70 strands would never be used, especially with 0.6" strands, this pattern was also checked on the 12" thick plate giving a design load on the plate of 3,080 kips. The maximum stress resultants are shown in Figure 3-18, with the maximum stress being 28 ksi, which is still well below the yield stress of the plate (32 ksi). Once the plates,

main columns, and cross members were designed, they were ordered and the construction of the reaction frame began.



***Figure 3-18: SAP 2000 output for 12” thick plate with 70, 44 kip loads.
Maximum stress shown = 28 ksi. (SAP 2000)***

3.5.2 Construction of Pretensioning Facility

The pretensioning bed utilized in this project was built on an elevated slab at the north end of the Ferguson Laboratory. This allowed access underneath it to install tie downs where necessary. The construction of the frame began in November, 2005 and finished in early September, 2006. Much of the early construction consisted of drilling holes so that each part could be bolted together. Over 700 holes were drilled in the frame and over 300 bolts were used to assemble the frame. Construction of the stressing bulkheads was primarily completed through outside machine shops. Since 12” thick plates were hard to locate, they were purchased from a manufacturer in Ohio. They were shipped to Houston where holes were drilled through them to accommodate the strand pattern. Finally, some lifting holes were drilled into the plates after they arrived at Ferguson Laboratory. Once the frame and stressing bulkheads were completed the frame was painted. A picture of the final product is shown in Figure 3-19. The main stressing bulkheads as well as the top strand bulkheads were painted white whereas the rest of the frame was painted burnt orange.



Figure 3-19: Completed Pretensioning Bed

The live end of the bed is not shown in Figure 3-19, but instead shown in Figure 3-20. The 12-in. steel plate shown in white (Figure 3-20) is pushed by the four 400-ton hydraulic rams. The top two rams and bottom two rams were hooked up to separate hydraulic pumps such that various eccentricities could be accommodated. In order to reduce the total force that had to be applied to move the 12-in plate shown in Figure 3-20, the plate was placed on skids with Teflon placed underneath them. The riding surface was also coated with Teflon so that the plate was riding on a Teflon to Teflon contact surface. This cut down on the amount of friction to the point where it was negligible as compared to the forces that would be placed on the frame.



Figure 3-20: Live end stressing bulkhead with rams

3.6 TXDOT NEW I BEAM SECTIONS

The focus of the project was on bursting, splitting, and spalling stresses, in the end regions of new TxDOT beams that had recently been designed. These girders are similar to the AASHTO bulb tee's that are used throughout the country, but have much thinner and wider top flanges and wider bottom flanges. As part of this research project, three beams (Tx28, Tx46 and Tx70) were tested. The beams names are related to the beam depths. For example Tx28 is a 28" deep beam. 4 top strands were used in each beam's top flange for assisting rebar placement.

The smallest of beam section tested was Tx28 (Figure 3-21). The main differences between Tx46 and Tx28 are the increased web height and the increased depth of the bottom flange that allows for an additional row of strands.

As seen in Figure 3-21, going from Tx46 to Tx70 the height of the web and the width of the top flange is increased. One additional change to Tx70 included three No.6 bars in the top flange to help control tensile cracking from the application of the highly eccentric prestressed force. Additional section information including area, moments of inertia, tendon eccentricity, and applied prestressing force can be found in Table 3-1.

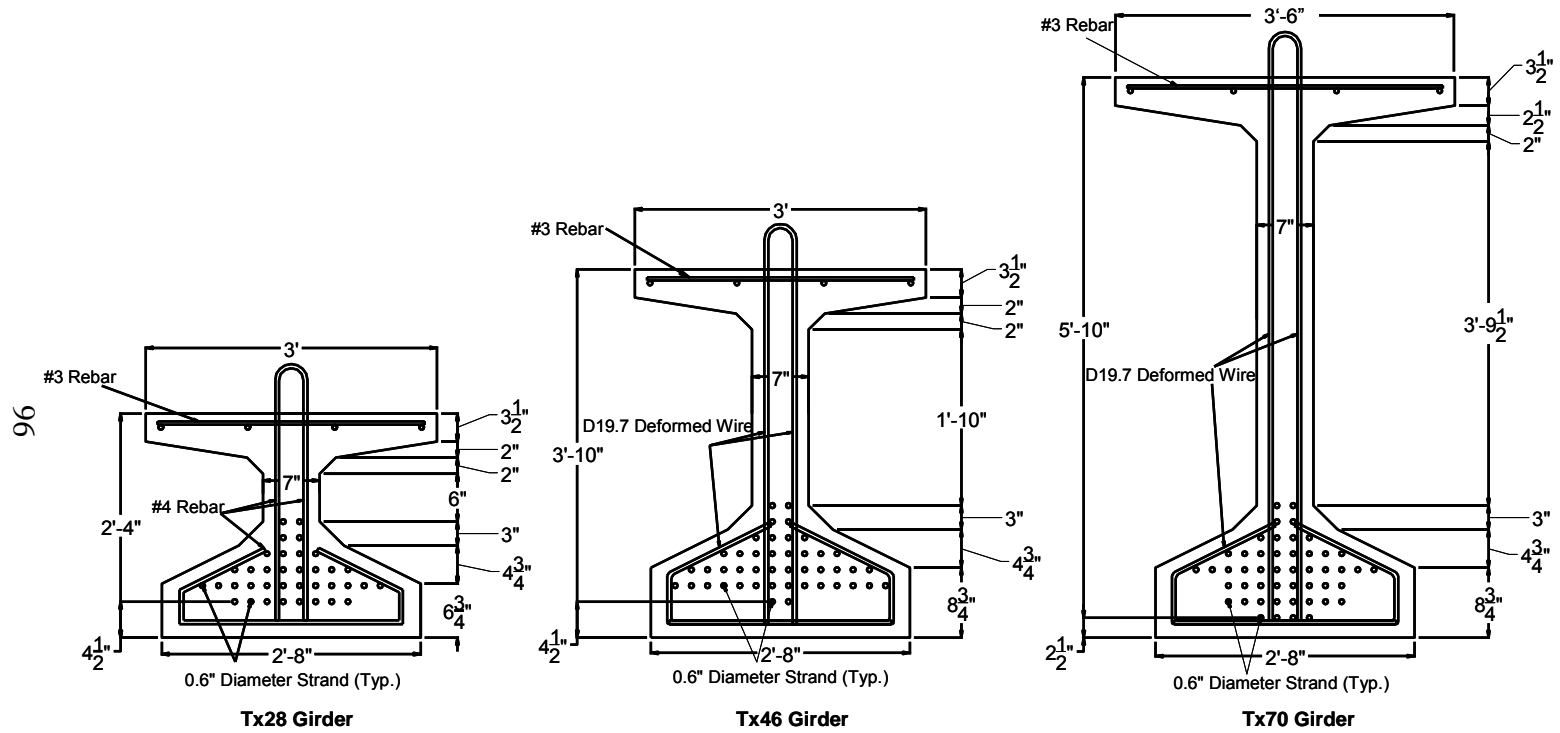


Figure 3-21: Tx Girder sections

3.7 INSTRUMENTATION

3.7.1 General

Previous research on cracks that form in the end regions of pretensioned concrete beams was examined in Chapter 2. The most critical locations for transverse tensile stresses due to bursting, spalling and splitting stresses as reported in previous research projects were studied. Since the experimental facts reported by other researchers were used in the instrumentation plan, pertinent parts of those research projects are discussed here.

As seen in Marshall and Mattock (1962) as well as Tuan et al. (2004), the most critical location for spalling stresses lies somewhere between the mid-height and the centroid of the beam within the web. These researchers monitored strains within the first 18 inches from the end face. Uijl (1983) showed that bursting stresses at the web to bottom flange connection could create cracking to a distance h from the end face. The crack locations from the Florida and Texas Department of Transportation beams also show substantial cracking at the top flange to web connection near the end face of typical I-girders. Since rebars do not develop significant strains prior to cracking of concrete and since the locations of typical bursting, spalling, and splitting cracks are reasonably well-defined. It was felt that placing strain gauges on the rebars at possible crack locations would give the best estimate of the maximum stresses experienced by rebars. It was also felt that since transfer length was discussed heavily within the reviewed literature, it would be of importance to monitor strand stress development within the end regions of the beams as well. In order to gather all these data anywhere from 48 to 63 strain gauges per test region were placed in the end of each girder. Typical placement of strain gauges within the end regions is shown in Figure 3-22. Six thermocouples were also placed in each girder to monitor temperature profiles in

the beam and to broadcast temperature information to the *Sure Cure* facility. A detailed discussion of instrumentation is provided within the next sections.



Figure 3-22: Strain gauges of reinforcing bars and strands

3.7.2 Strain Gauge Installation on Reinforcing Bars

The reinforcing bars throughout the end regions were comprehensively instrumented to ensure that the stresses can be inferred from the strain readings at critical locations. The strain gauges used in this research were TML Strain Gauges from Tokyo Sokki Kenkyujo Co., Ltd., Type FLA-5-11-5LT, with a gauge length of 5mm. These gauges were applied to the reinforcing bars and WWR by using the same installation protocol. Strain gauges were applied to spalling reinforcement wherever possible and on shear reinforcement everywhere else. One or two of the ribs were ground off from a typical reinforcing bar to

obtain a flat surface for strain gauge installation. In grinding the deformations off, careful attention was paid not to change the area of the base bar so that stress and force values could be accurately calculated after construction. Once the surface was smooth it was cleaned with two cleaning solutions. The first being a mild phosphoric acid, while the second was an ammonia based solvent that neutralized any chemical reactions. The strain gauge was then positioned and attached to the bar using a cyanoacrylate adhesive. A picture of the gauge after CN adhesive has dried is shown in Figure 3-23.



Figure 3-23: Strain gauge on WWR

Once the adhesive had dried, the gauge and lead wires were covered with an air-drying acrylic coating to protect and waterproof them. Finally, the strain

gauges were covered with foil tape and sealed with electrical tape to help protect them as well as create a water tight barrier for the gauge.

3.7.2.1 Tx28-I and II Rebar Gauge Locations

Each girder had slightly different patterns of rebar gauges in their end regions. Although the fundamental placement of the strain gauges remained the same, as the girder depth changed and more lessons were learned through the examination of strain gauge data some adjustments were made. The basic pattern was based on the assumption that the bulk of the transfer region tensile stresses happen within h of the end face of the girder. This comes from Marshall and Mattock’s original 1962 PCI paper. Then as stated earlier, the strain gauges were placed where the cracks were most expected to occur. Figure 3-24 and Figure 3-25 show the location of these rebar gauges for the first Tx28 constructed. The top and bottom gauges were always located on the opposite bar from the middle gauge. This pattern was then alternated on each set of vertical reinforcement for the full distance of bars that were gauged.

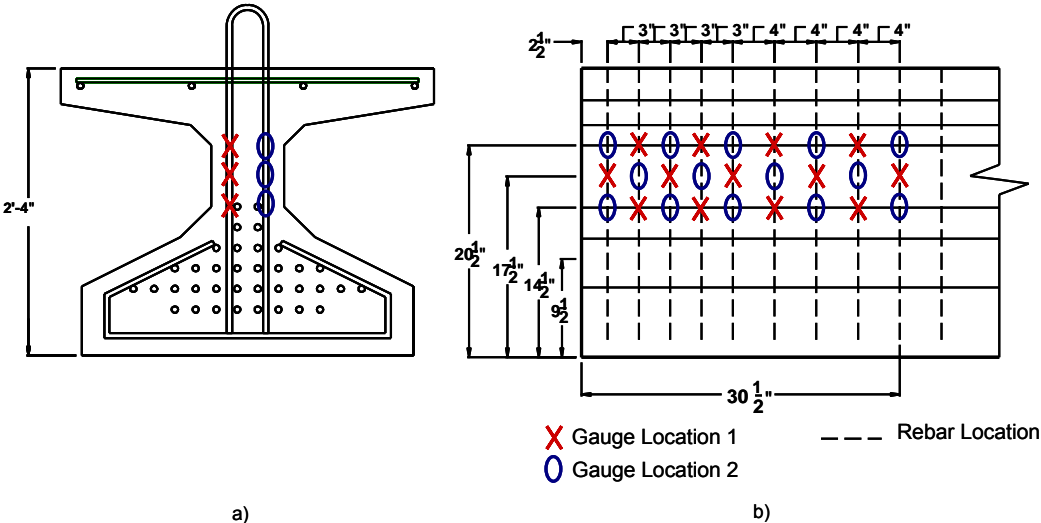


Figure 3-24: Tx28-I Rebar gauge locations for live end

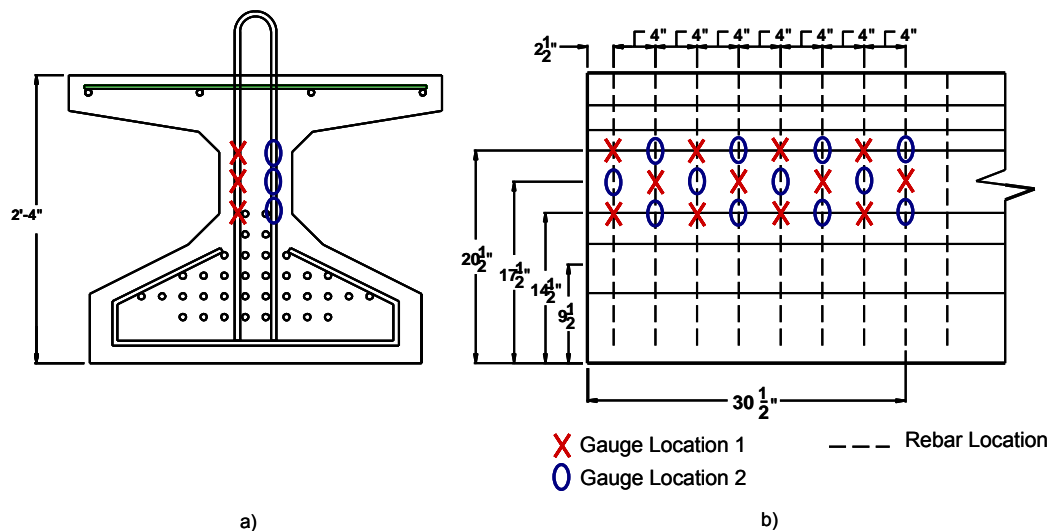


Figure 3-25: Tx28-I Rebar gauge locations for dead end

After the release of the prestressing force, it was found that a crack existed on the top face of the bottom flange in the first Tx28. In order to ensure that this crack was not continuous across the section of the beam and merely a localized crack, additional gauges were placed near the location of that crack from the first Tx28. These additional gauges are shown in Figure 3-26 and Figure 3-27. The strain readings indicated that the cracks observed on the top face of the bottom flange were localized and as such small strain readings were obtained. In the subsequent tests the additional strain gauges used in Specimen Tx28-II were not used.

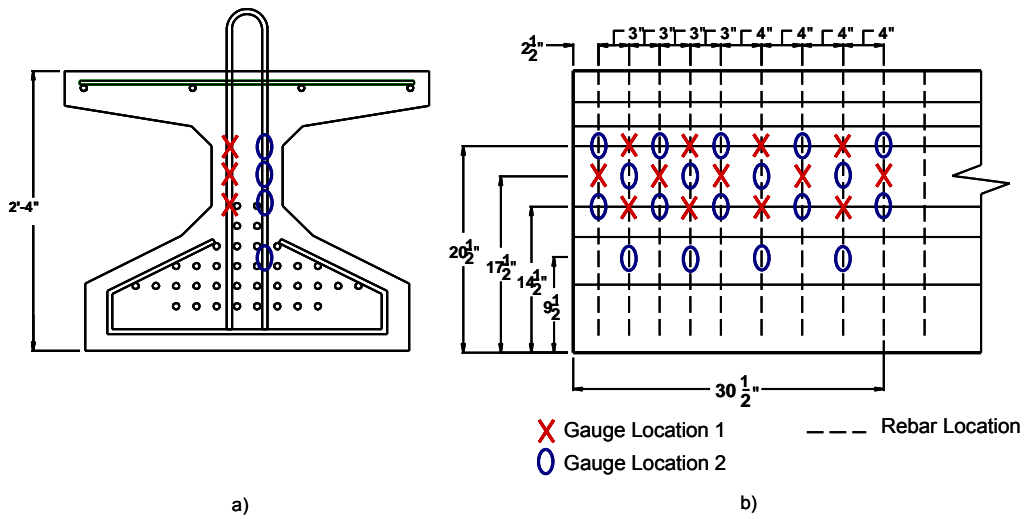


Figure 3-26: Tx28-II Rebar gauge locations for dead end

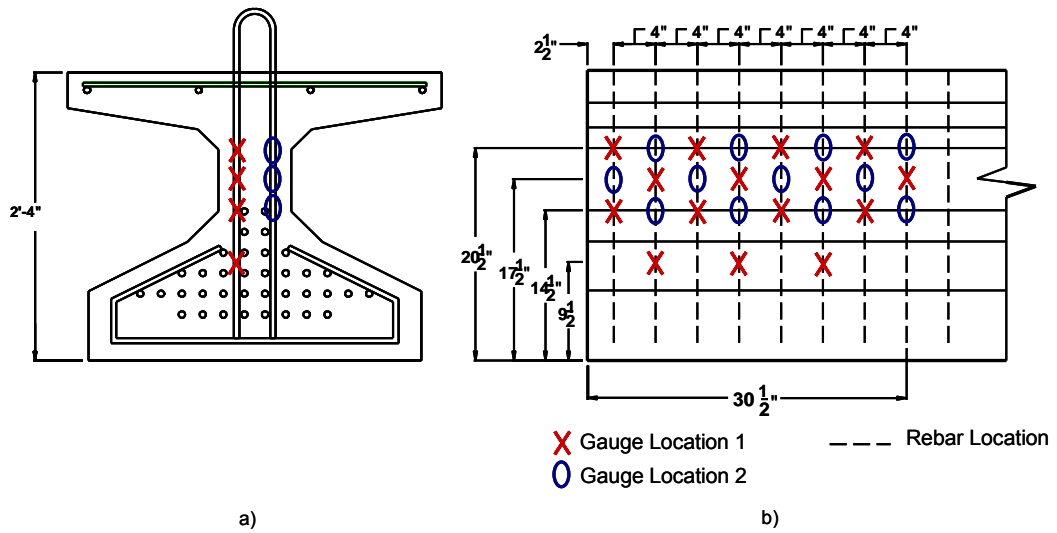


Figure 3-27: Tx28-II rebar gauge locations for live end

3.7.2.2 Tx46 Rebar Gauge Locations

Tx46 was similar to the Tx28-I in its gauge locations. Due to data acquisition computer constraints, i.e. number of channels available to monitor strains, every bar from the face of the beam to h could not be monitored. It was felt that this would be acceptable as long as the bars within the approximate transfer length of $50d_b - 60d_b$ were monitored. Once the transfer length was reached every other bar was monitored out to 46" or h . Figure 3-28 shows the strain gauge locations for the live end while Figure 3-29 shows the locations for the dead end.

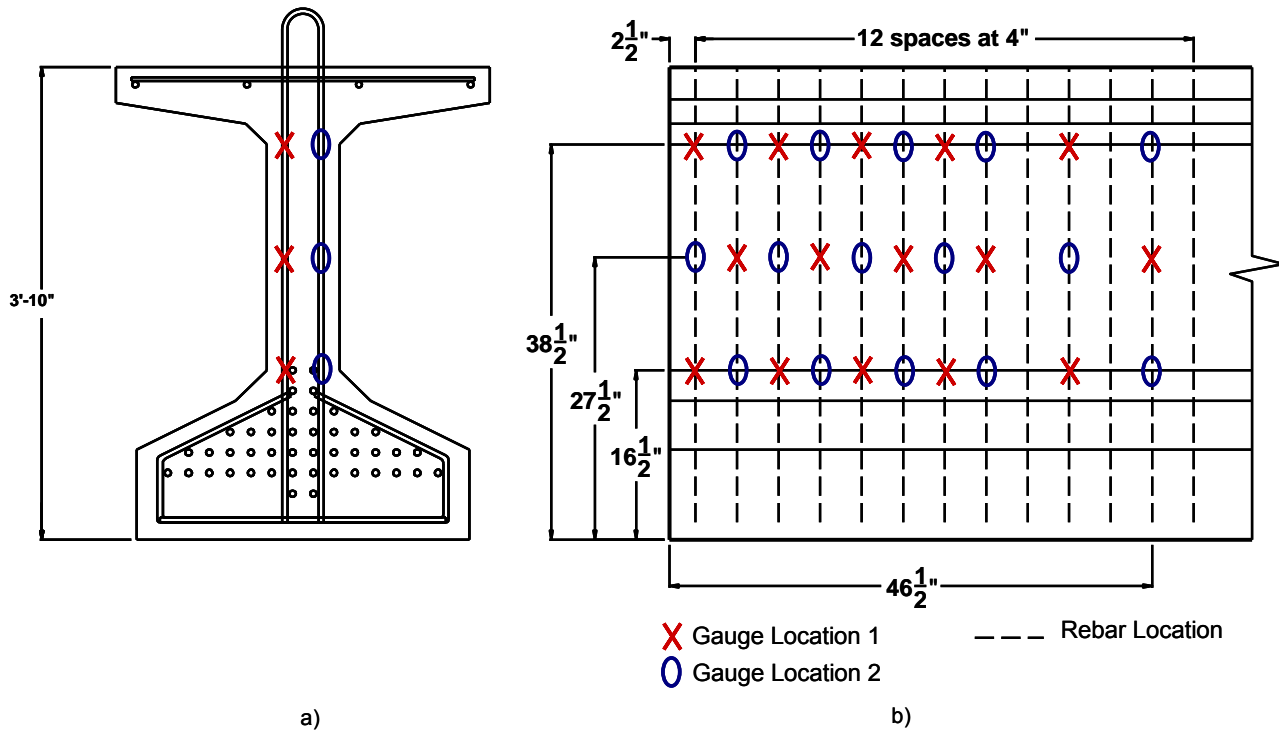


Figure 3-28: Tx46 Rebar gauge locations for the live end

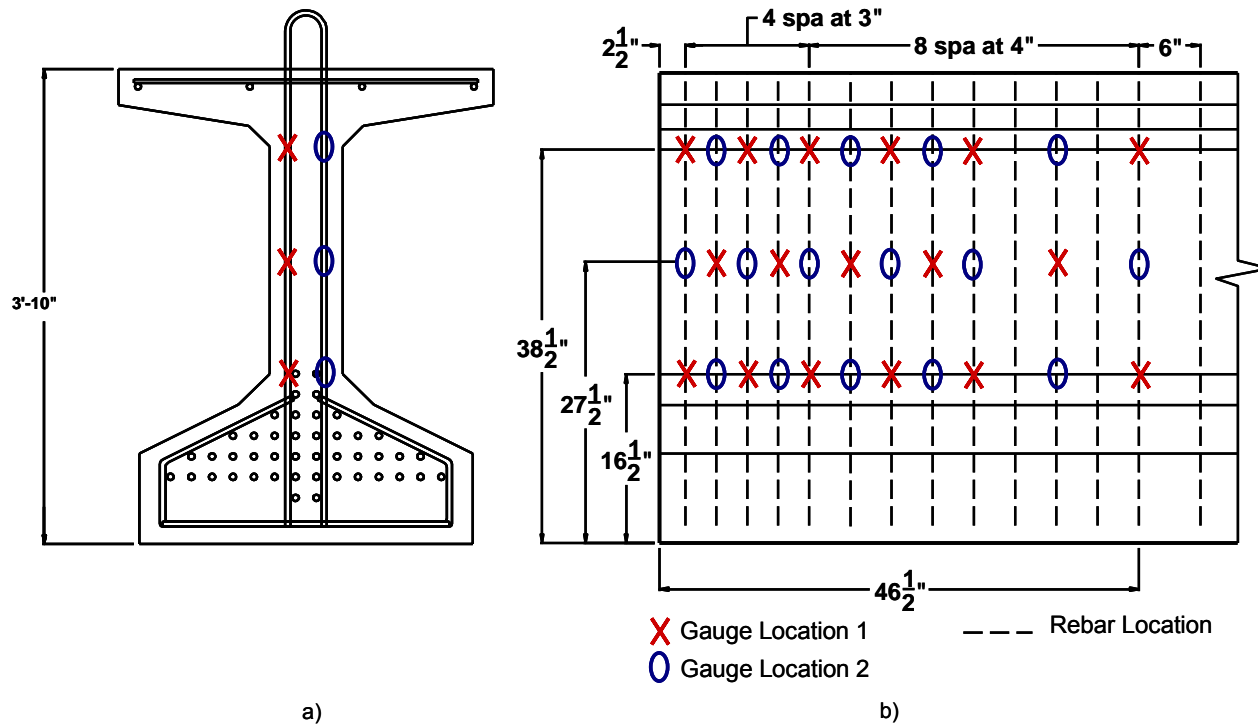


Figure 3-29: Tx46 Rebar gauge locations for the dead end

3.7.2.3 Tx70 Rebar Gauge Locations

Strain gauge locations in the Tx70 girder were almost identical to the Tx46. The transfer length was monitored with every bar being strain gauged. Then every other bar was monitored out to a maximum distance of h or 70". The only change from Tx46 lies in the location of the middle strain gauges (Figure 3-30 and Figure 3-31). As stated earlier, Marshall and Mattock (1962) and Tuan et al. (2004) both found that spalling cracks tended to appear at the centroid of the larger girders. Since this was confirmed with the pictures obtained from Florida DOT and TxDOT, the middle gauges were moved from the center of the web to the centroid of the beam.

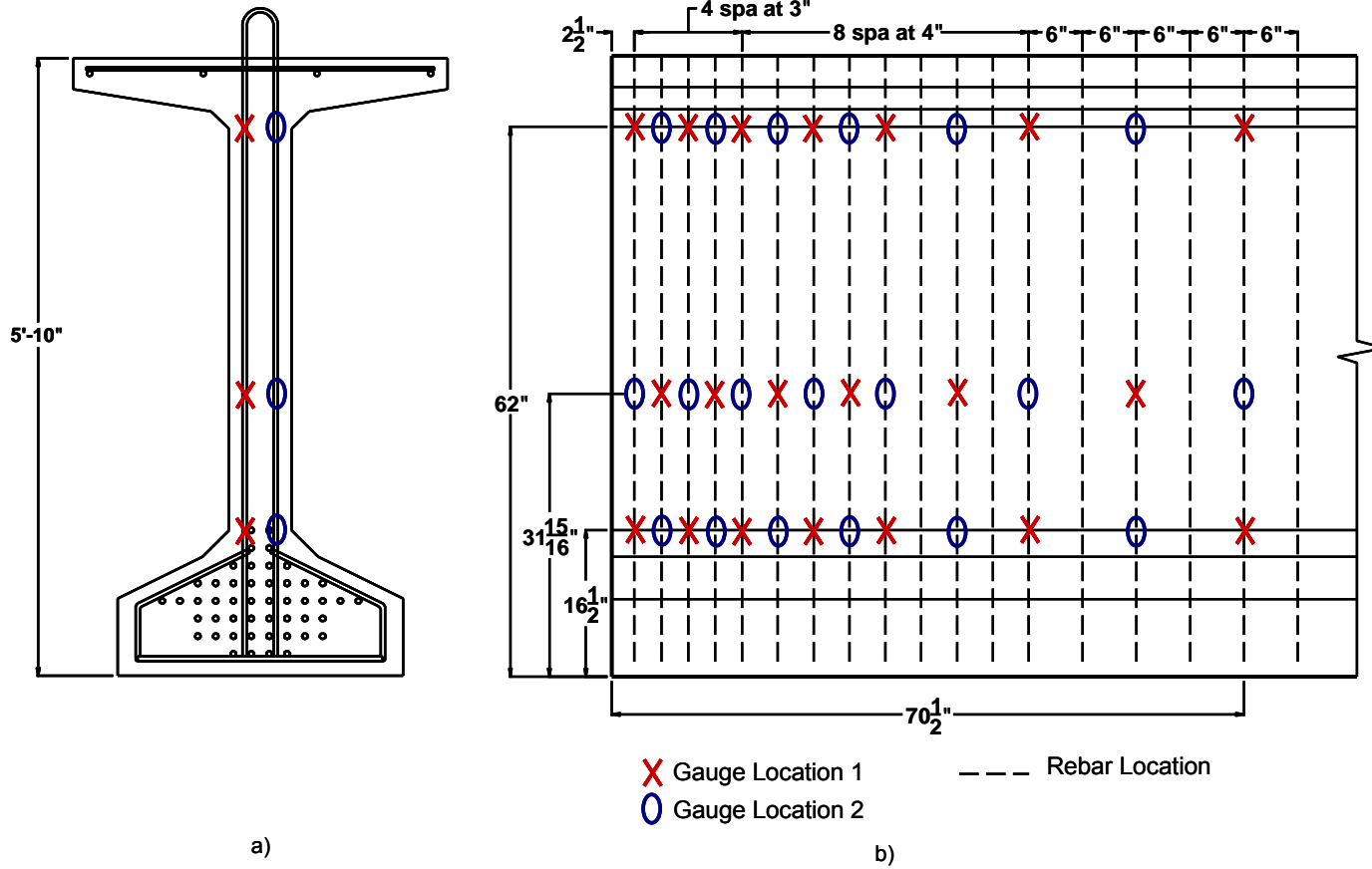


Figure 3-30: Tx70 Rebar gauge locations for the dead end

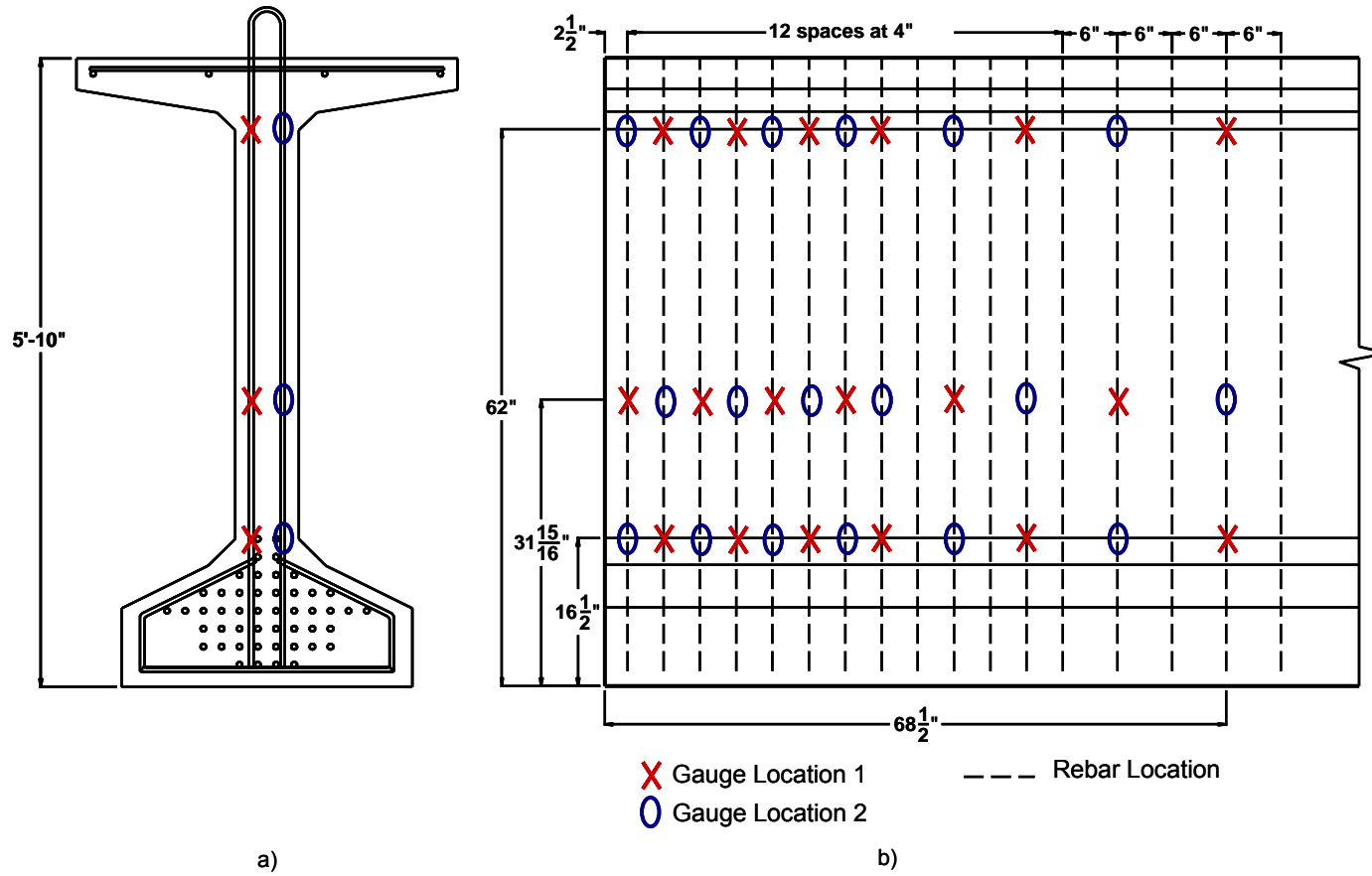


Figure 3-31: Tx70 Rebar gauge locations for the live end

3.7.3 Strain Gauge Installation on Strands

It must be first understood that strain gauges cannot be placed along the longitudinal axis of the strand because the 7-wire configuration does not line up directly in the axial direction. Instead, the six wires wrap helically around the center wire. This prevents the gauge from reading a true longitudinal strain value. In order to deal with this fact a simple solution was used. The strain gauge is first placed along the axis of one of the six outer strands. This puts the gauge slightly angled away from the line of action of the strand as seen in Figure 3-32.



Figure 3-32: Strain gauge orientation for 0.6" diameter strand

Since the gauge does not lie along the axis of the strand, strain readings are inaccurate unless a calibration curve is used to account for the difference. As such, a calibration curve was developed. It is important to note that in the calibration curve shown in Figure 3-33, a modified elastic modulus value for the strand is found, taking into account the off-axis orientation of the strain gauge.

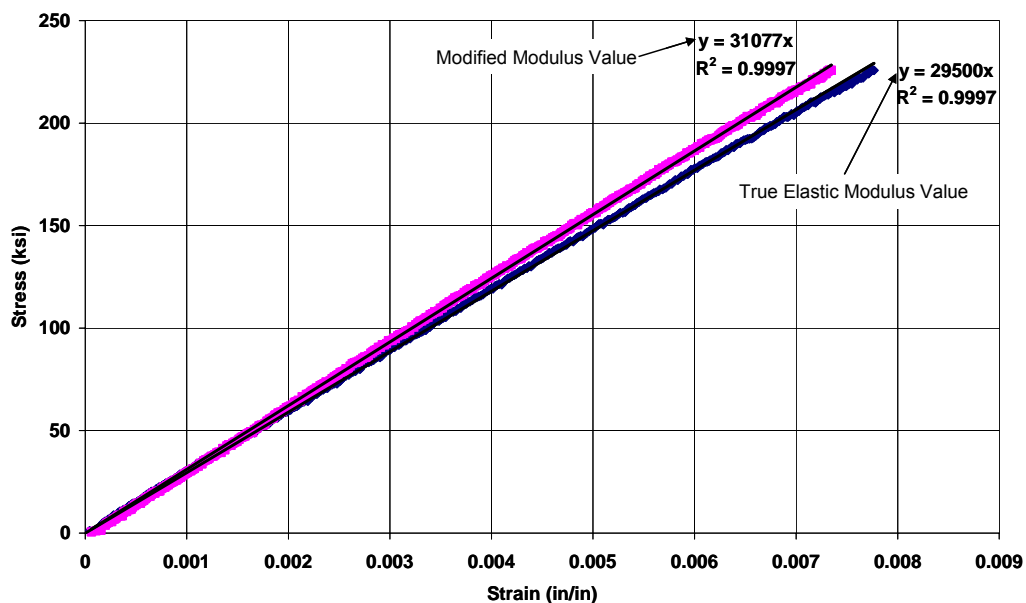


Figure 3-33: Sample strain gauge calibration curve for 0.6" strand

The use of this curve during stressing as well as after release was vital to the accurate assessment of strains and stresses inferred from those strain values. Installing strain gauges on prestressing strands presented a problem that was not apparent until after the data from the first beam was analyzed. After the construction of the first Tx28 beam, it became apparent that a number of strand strain gauges malfunctioned. It was felt that the major cause of this problem was the method of protection that was used on the strain gauges. It appeared as

though the acrylic coating and foil did not serve as an adequate water barrier or padding for the strain gauge. In order to provide better protection for the strain gauges, microcrystalline wax was heated until it was liquid and was then applied onto the gauges (Figure 3-34).



Figure 3-34: Application of microcrystalline wax onto strand strain gauges

Once the wax was set, a coating tape manufactured by Tokyo Sokki Kenkyujo Co., Ltd. was wrapped around the strand. The Type CT-D16 tape was then heated with a heat gun to activate the glue that is on its underside. The glue melted and the tape shrunk to completely seal off the gauge. After the glue and tape cooled, the gauge application process was complete (Figure 3-35).



Figure 3-35: Completed strain gauge on 0.6" diameter strand

While the location of the strain gauges installed on strands varied vertically and horizontally within each beam, the main goal of the strain gauge installation remained the same: To monitor strand stress development such that the transfer length of the strand could be verified. It is important to note that while multiple gauges were installed on some of the strands, only one gauge was installed on other strands (Figure 3-37 and Figure 3-38). By comparing the data from strands that were instrumented with a large number of strain gauges and those that were instrumented with only one gauge, the impact of excessive instrumentation on transfer length was evaluated. The research results chapter shows the values for these gauges and it is important to recognize that the large number of strain gauges used to monitor strains in the strands had an insignificant influence on the transfer length.

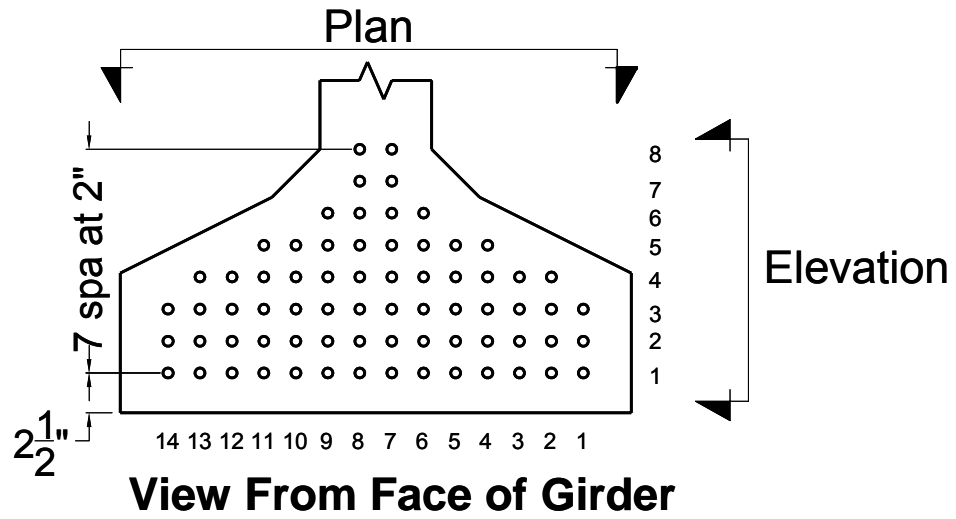


Figure 3-36: Possible strand locations within the bottom flange

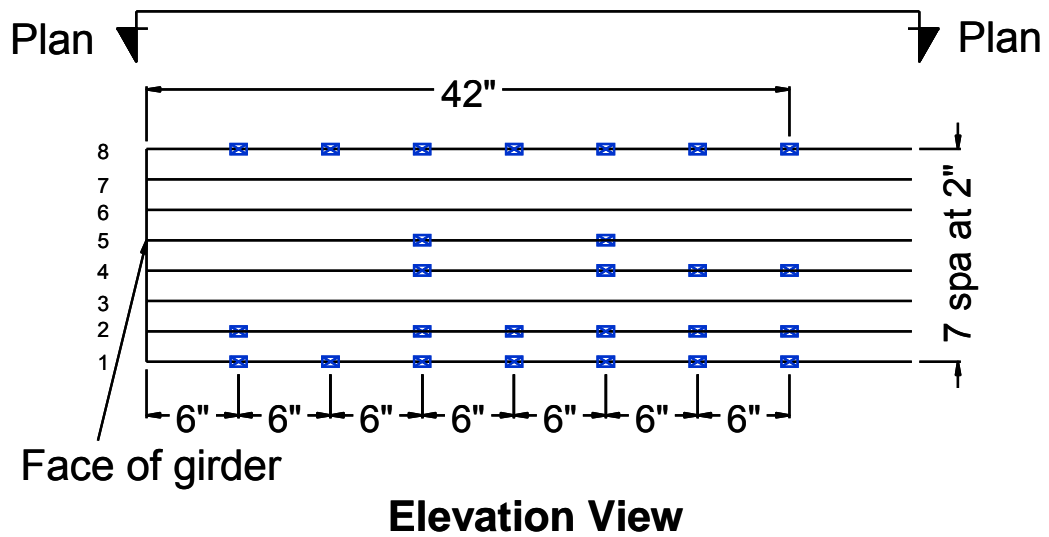


Figure 3-37: Typical locations for strand strain gauges in elevation view

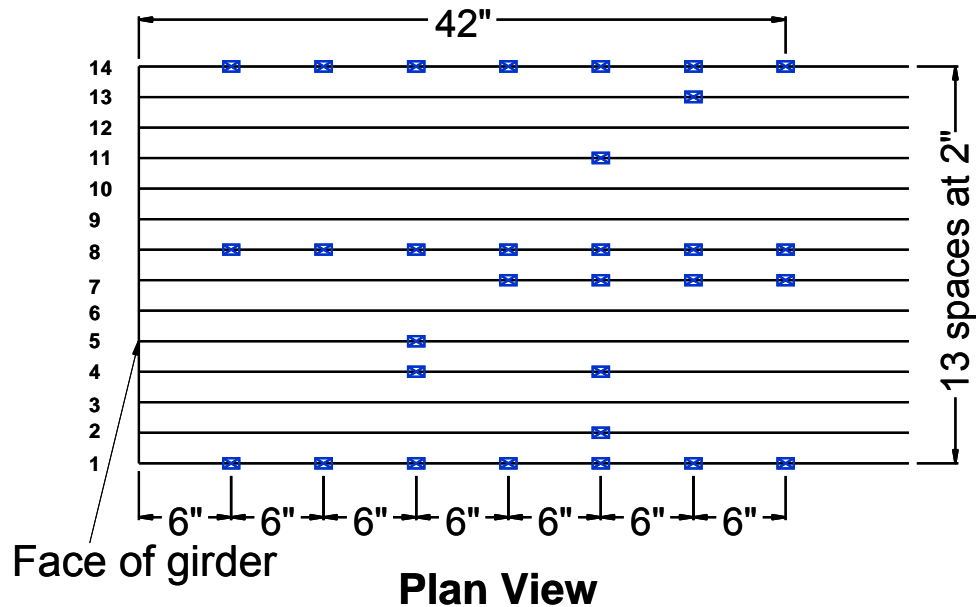


Figure 3-38: Typical locations for strand strain gauges in plan view

3.7.4 Temperature Monitoring

A set of thermocouples were installed within a section that was located 5-ft. from the end of the beam (Figure 3-39). These thermocouples measured temperature by measuring the voltage created by the temperature difference across two contacting, dissimilar metals. These metals are typically, welded, soldered, or twisted together. For this project, they were twisted together and then coated with a shrink tape to electrically isolate them from the water in the concrete. The wireless feature of the temperature match-curing system (*Sure Cure*) was used to match the curing temperatures of those locations marked in Figure 3-39. With each specimen a total of 48 cylinders were prepared and match-cured. Compressive strength of those cylinders was monitored and used to ensure that the 6500-psi release strength was achieved prior to releasing the strands. Typical

temperature plots for the girders tested in this project are shown in Section 3.8.4 and Appendix D.

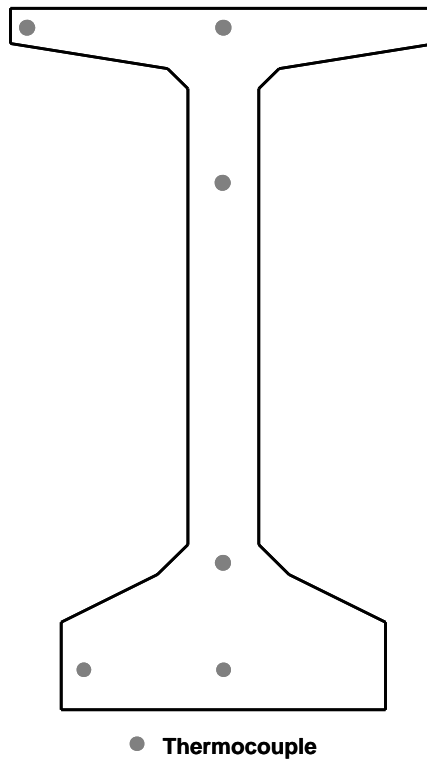


Figure 3-39: Typical thermocouple locations in Tx girders

3.8 SPECIMEN FABRICATION

3.8.1 General

The fabrication of a typical specimen involved several different activities: Pretensioning the strands, mixing and placing the concrete, and releasing the strands.

3.8.2 Pretensioning the Strands

Each strand was first strung through the pretensioning bed and individually stressed to take the slack out the strand. The strands were stressed to ~ 2 kips each so that strain gauges could be applied on them and reinforcing cage could be assembled. The strands were individually stressed to ~ 2 kips using a mono-strand stressing jack, shown in Figure 3-40.



Figure 3-40: Individual strand stressing with mono-strand stressing jack

In ACI 318-05 and PCI Design Handbook (6th Edition), there are requirements for at least 2 methods of verification for prestressing force in strands. As such, in a prestressed concrete fabrication plant the prestressing force

is typically verified by comparing hydraulic pressure or load measurements with expected strand elongations. Within the framework of this research project at least 3 and very often 4 methods to verify the amount of prestressing force being applied to the strands were used: (i) Pressure gauges on each hydraulic pump, (ii) pressure transducers on each hydraulic line, (iii) strain gauges on strands used in conjunction with strand load-vs.-strand wire strain calibration curves and (iv) linear potentiometers monitoring strand deformations. Figure 3-41 shows the two hydraulic pumps used to control the top 2 or bottom 2 rams. Pressure differences between the top and bottom sets of rams were due to the load being slightly eccentric to the center of the stressing plate.



Figure 3-41: Hydraulic pumps used to control the application of prestressing force through four 400-ton rams

At the live end, linear potentiometers measured the movement of the stressing plate while ram displacements were also measured to ensure accurate elongation measurements were taken. To make sure the most accurate values of elongation could be reported, dial gauges at the dead end measured the deflection of the frame. This deflection was subtracted from the live end elongation to get the true elongation value for the strands. Typical deflection of the reaction frame was approximately 0.25” for a load between 1500 and 2000 kips. A quick elongation calculation is shown below for one 0.6” diameter strand. Figure 3-42 shows the linear potentiometer setup, while Figure 3-43 shows the typical dial gauge setup to measure deflections of the frame.

$$\Delta = \frac{PL}{AE} \qquad \text{Equation 3-9}$$

where:

Δ = elongation

P = applied prestressing force

L = length of strand between anchorage points

A = area of strand

E = modulus of elasticity for prestressing strand

$$\Delta = \frac{(44\text{kips}) \cdot (604\text{in})}{(0.217\text{in}^2) \cdot (29,000\text{ksi})} \qquad \text{Equation 3-10}$$

$$\Delta = 4.22\text{in}$$

$$\text{Total Elongation Value} = 4.22 + .25 = 4.47\text{in}$$



Figure 3-42: Three Linear Potentiometers measuring strand elongations



Figure 3-43: Dial gauges used at dead end of prestensioning bed to measure frame deflection

Using the independent measurements described above the prestressing force was determined to a high level of accuracy. These independent measurements could then be compared to the design loads and elongations calculated before prestensioning began. Once full prestressing was applied, pumps were monitored until concrete was placed to ensure that no hydraulic pressure losses took place. It is believed that with the rigor associated with cross-referencing and double checking the prestressing force, the error in the reported prestressing forces is considerably below 3 % - whereas the industry standard tolerance is 5%.

3.8.3 Mixing and Placing Concrete

After the pretensioning operation was completed the morning of concrete placement, concrete mixing took place. The basic concrete mixture design used in this project had been used in previous pretensioned concrete research projects at the Ferguson Laboratory. This concrete mixture design was originally obtained from a precast pretensioned concrete beam producer in San Marcos, TX. The main attributes of the mixture design are illustrated in Table 3-2.

The precast, pretensioned concrete beam producer located in San Marcos, Texas donated the coarse aggregate, sand, and admixtures to the project while a ready mix truck was rented from a ready-mix company in the Austin area. In previous projects, the precast concrete producer had supplied adequate amounts of admixtures to meet the mix design requirements. Some problems related to the dosage of retarder arose in casting the first girder. The amount of retarder supplied was significantly higher than the dosage shown in the mix design approaching 12 oz/Cwt as shown in Table 3-2. This led to the concrete placed in the beam not setting up for almost 60 hours. While this proved to be unrepresentative of practical I-girder construction valuable data was gathered from it and so it is still included in the text of this thesis. After the experience with the concrete mixture used for the first beam, the amounts of admixtures supplied by the precast pretensioned concrete beam were measured at FSEL and no major problems were encountered.

The following are the major steps that were followed in preparing the concrete that was used to fabricate the test specimens:

1. Ready mix-truck was sent to San Marcos and charged with the correct amounts of fine and coarse aggregates at the precast, pretensioned concrete beam fabrication plant.

2. Upon the arrival at FSEL of the truck that was charged with aggregates, the admixtures were measured out and diluted in water in 5-gallon buckets for ease of pouring. While this was being done, the correct amount of water was added to the ready-mix truck using a flow-meter shown in Figure 3-44 to monitor exactly how much water was being added. This value was calculated beforehand using the moisture content of the aggregates reported in the batch ticket, and water ratios from the concrete mixture design.



Figure 3-44: Flow-meter used to measure water placed into truck

3. Once all the water had been added, Type-III cement was placed into a 1 cubic yard bucket and added to the ready mix truck (Figure 3-45). This was done quickly but evenly to ensure that the cement properly mixed with the water and aggregates without allowing too much time for the aggregates to soak up the water.



Figure 3-45: Cement being added to the ready mix truck with a 1 cy hopper

4. After all of the cement had been added, the diluted admixtures were poured in and the truck was set to turn at least 300 revolutions to properly mix the concrete. After 300 turns the concrete was checked for consistency. If it was felt that the concrete was mixed thoroughly enough and had a large enough slump to ensure workability then the concrete placing operation began.



Figure 3-46: Concrete placement using a 1 cy hopper

The placement process involved the use of the 1 cy concrete bucket to place the concrete in the girder. Anywhere from 6-10 buckets of concrete were placed in each girder throughout project. After the first bucket was placed into the beam, form vibrators mounted to the side of the forms were used to consolidate the concrete (Figure 3-47). This would ensure that the concrete in the bottom flange was consolidated before placing concrete into the web.



Figure 3-47: Form vibrator being used on a Tx28 girder

Once the bottom flange concrete was placed and consolidated, internal rod vibrators were used in conjunction with form vibrators to consolidate concrete placed in the web (Figure 3-48). This helped ensure that the concrete properly flowed around the reinforcing bars and strands without leaving any voids. Once the concrete had been placed, temperature monitors were turned on so that match curing of cylinders could take place.



Figure 3-48: Use of an internal rod type vibrator: Tx28 girder

3.8.4 Releasing the Strands

After a pour was completed each beam was covered with wet burlap and then covered with plastic to ensure that very little shrinkage cracks would take place. Then for the next 12 – 20 hours, temperatures were monitored and a large number of cylinders that were cured using the *Sure Cure* system. Once a spike in the time-temperature curve was observed, cylinder testing began. A typical time-temperature curve is given in Figure 3-49

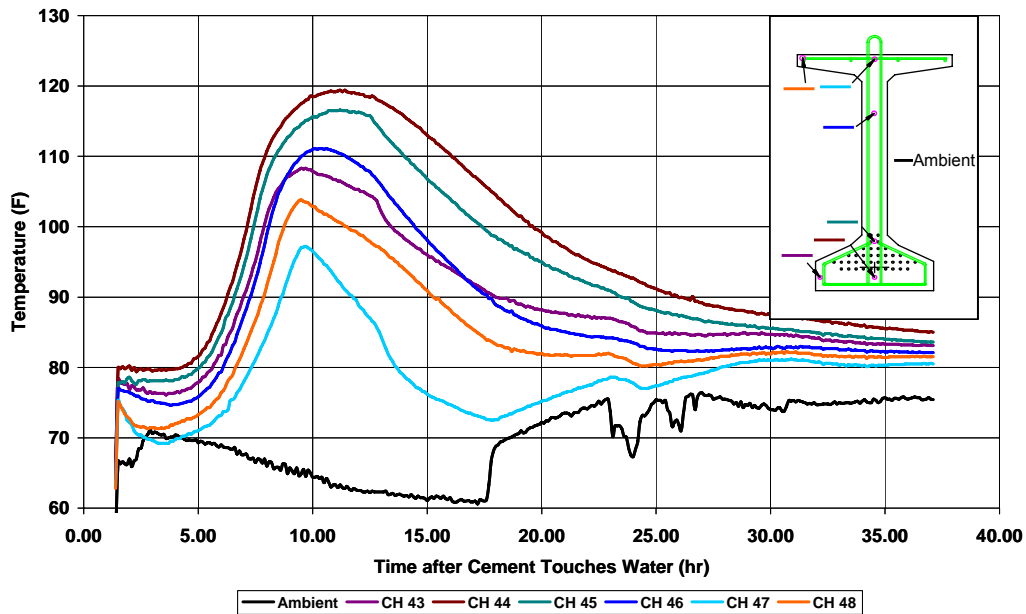


Figure 3-49: Typical time-temperature curve for Tx28-II girder

It can be seen in Figure 3-49 that the temperatures typically peaked out close to 10 hours after the concrete was mixed. These temperatures reached anywhere between 102 and 120 degrees Fahrenheit. The first cylinders were tested after approximately eight hours of curing. Using engineering judgment three different Sure Cure locations were used to test the first three cylinders. Typically cylinders match-cured to a hot, cold, and average temperature locations were tested with each batch. Once the first batch had been tested, three additional cylinders were tested approximately every hour until release strength was reasonably close. Once the release strength of 6,500 psi was close, a full set of 6 cylinders matching the six *Sure Cure* locations in the beam were tested. If the average strength for the six locations was slightly higher than 6,500 psi, strands were released. Cylinders were again tested immediately after release to give the best estimate of strength during release. Typically the coolest spots in the beam caught up to the

strength of the warmer spots by the time 6,500 psi release strength was achieved. This made it easier to decide exactly when to release the strands given that the scatter in the compressive strength of cylinders match-cured to different locations was very small at release. Figure 3-50 illustrates the fact that while during the early stages significant differences in the compressive strength of cylinders match-cured to hot and cold spots within the section were observed, when the compressive strength of concrete reached 6,000 psi, the scatter was significantly reduced.

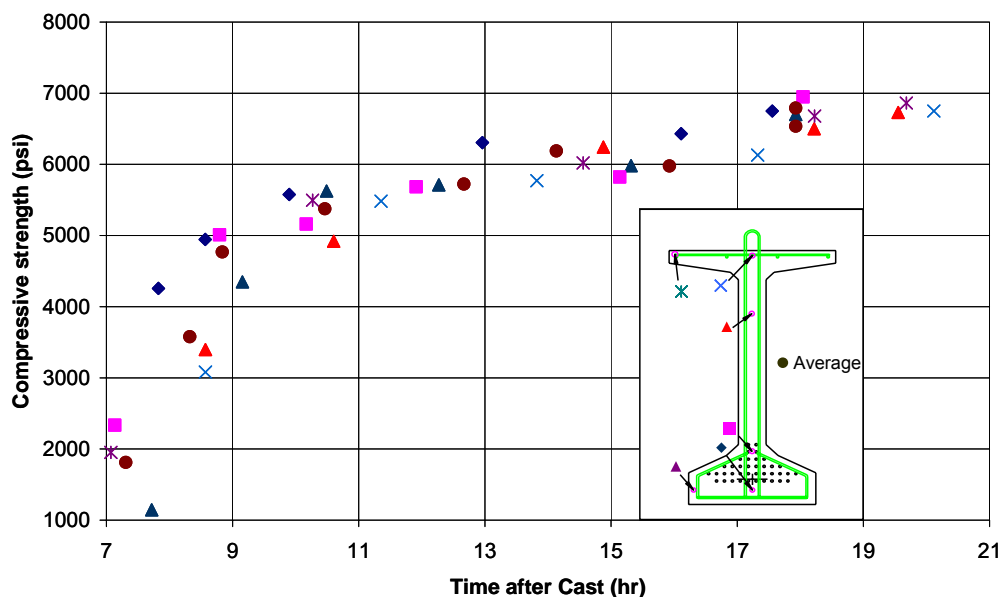


Figure 3-50: Cylinder strength vs. Time for the Tx70 girder

When the compressive strength of concrete reached 5,000 psi or so, the forms were removed. The beam was then re-covered until release took place. Once concrete reached release strength, data acquisition software was turned on to begin gathering data for the release. First the top four strands stressed to 5-kips

each (strands within the top flange) were cut individually. Next, the bottom strands were released using the same hydraulic pumps that were used to stress the strands. Using the pumps ensured that the release was done gradually. After the strands were released, data was continually gathered for another 30-45 minutes. In this way, strains in reinforcing bars were monitored while some of the cracks formed both at the dead and the live ends. During this time the beams also cambered up slightly, putting the beam in a simply supported end condition after release.

CHAPTER 4

Test Results and Discussion

4.1 INTRODUCTION

Examples illustrated in Chapters 2 and 3 make it apparent that cracking in the end zones of pretensioned concrete beams has become a common problem. The potential reasons for this cracking include increased use of higher strength concrete with increased utilization of 0.6" diameter strands. AASHTO LRFD Bridge Design Specifications (2007) and the PCI Design Handbook (6th Edition) both supply recommendations on how best to restrict these cracks in the spalling zone of pretensioned beams. These design guidelines are shown and discussed in Chapter 2. Only the CEB-FIP Model Code (1990) has provisions for detailing both spalling and bursting regions in pretensioned beams. The girders tested during the course of this project were designed by the Texas Department of Transportation with the AASHTO LRFD Bridge Design Specifications (2007) in mind. While within the actual TxDOT designs the code provisions are met, in order to examine the worst-case scenario, the prestressing force was maximized to a point that the spalling reinforcement provided in test specimens was slightly less than that required by AASHTO LRFD in some cases and more than that required by PCI guidelines. In essence, the spalling reinforcement provided in the test specimens, came from the field experience on existing beam designs and the practical amount of reinforcement that can be used in the end regions without creating congestion and construction issues. With these points in mind, four beams were constructed of varying sizes and reinforcement patterns. Two main reinforcement patterns shown in Chapter 3 and Figure 4-1 were used in the opposite ends of each specimen. This gave a total of eight test regions or four test

regions for each reinforcement pattern. Before taking an in depth look at the test results obtained in each one of the test regions, some preliminary analysis of the end regions will be done. This will give a better idea of what the design guidelines require and what is a reasonable estimate of steel that can be placed into the end regions.

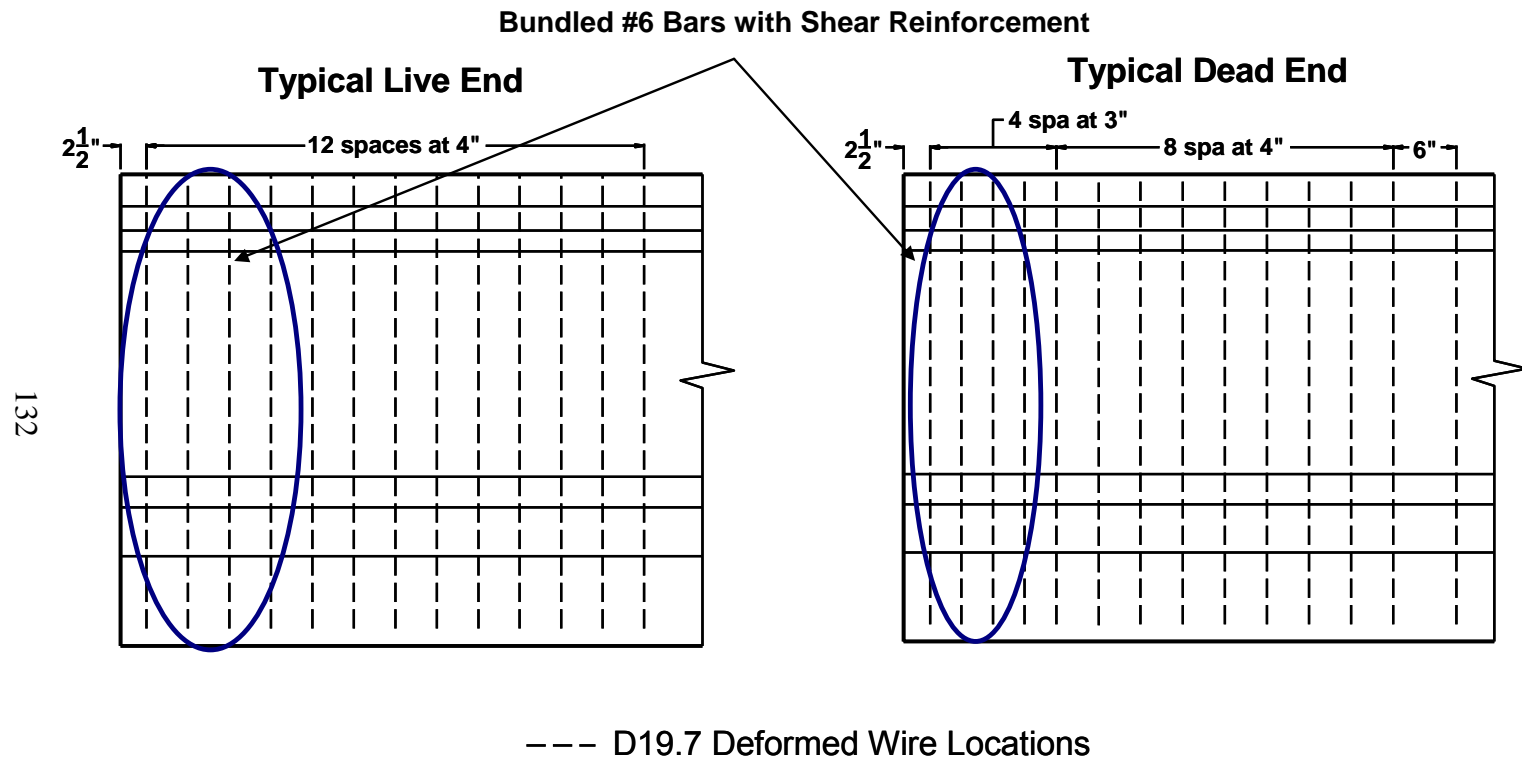


Figure 4-1: Typical end region reinforcement details for Tx family of girders

4.2 PRELIMINARY ANALYSIS

Each design specification or guideline, discussed at length in Chapter 2, will be briefly reviewed here for comparison. AASHTO LRFD Bridge Design Specifications (2007) and PCI Design Handbook (6th Edition) only have guidelines for spalling reinforcement and so the specimens were designed with this in mind. Additional steel was placed in the specimens bundled with the shear reinforcement to meet these designs. It was typically placed on the first 3 (Tx28) to 4 bars (Tx46 and Tx70) of the end regions. Figure 4-2, Figure 4-3, and Figure 4-4 below shows where this steel was bundled for the Tx28, Tx46, and Tx70 respectively.

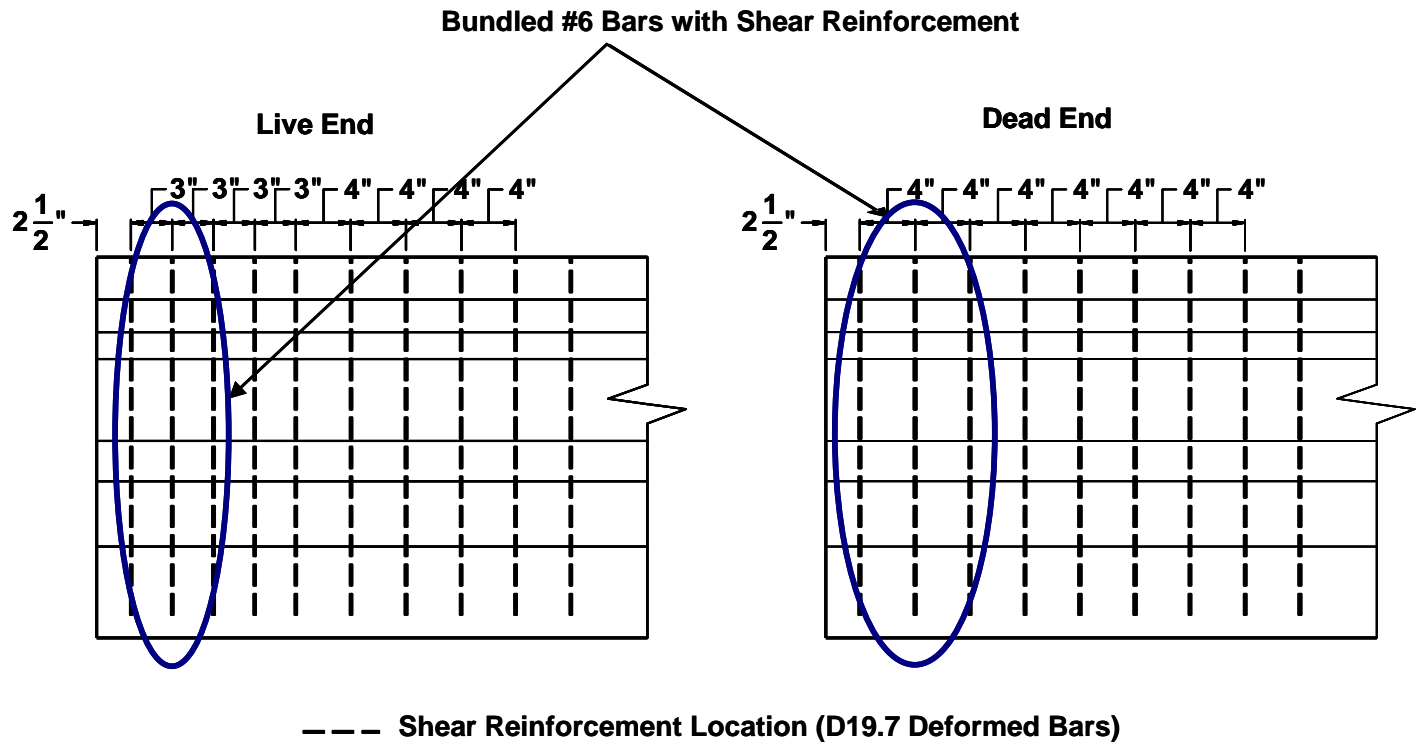


Figure 4-2: Typical location of bundled spalling reinforcement in Tx28 girders

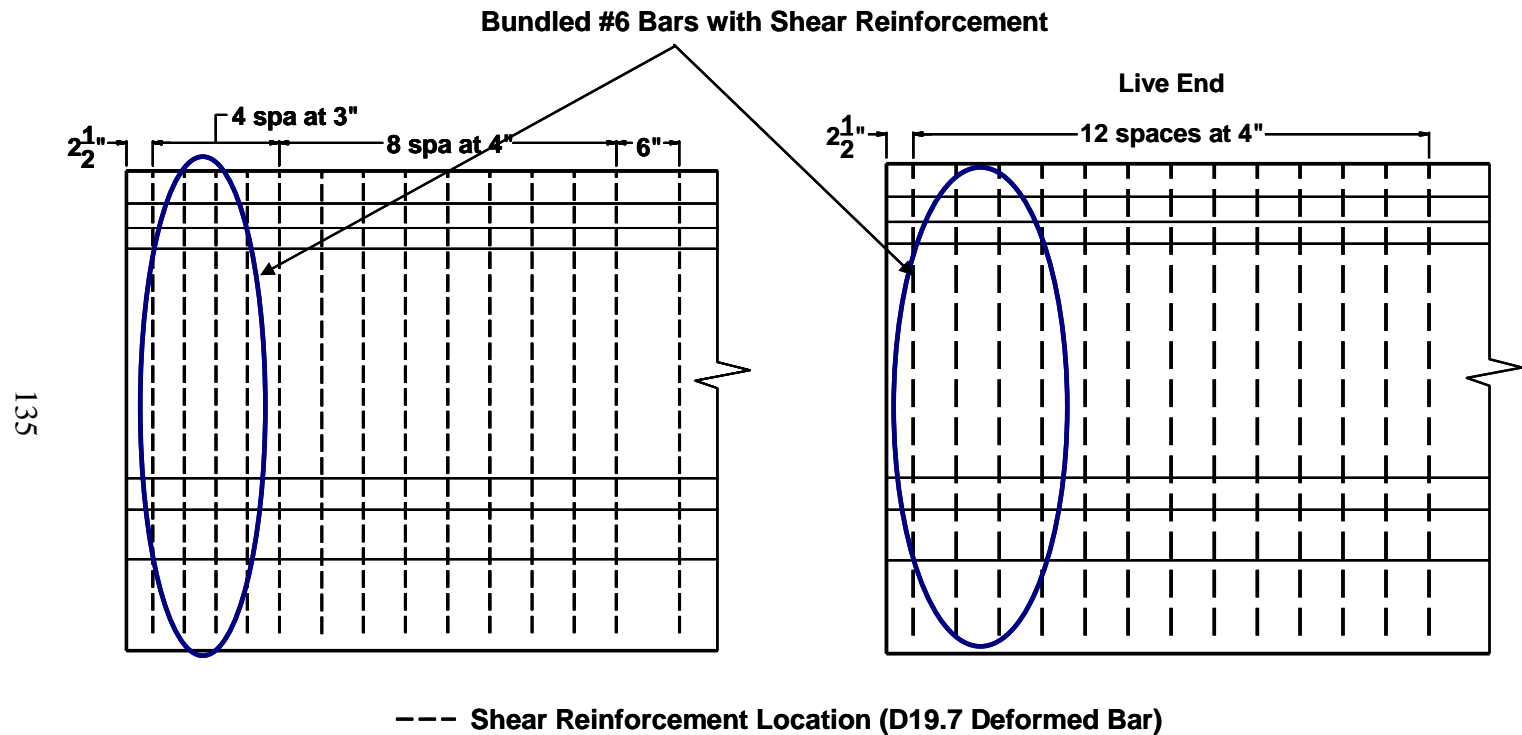


Figure 4-3: Typical location of bundled spalling reinforcement for a Tx46 girder

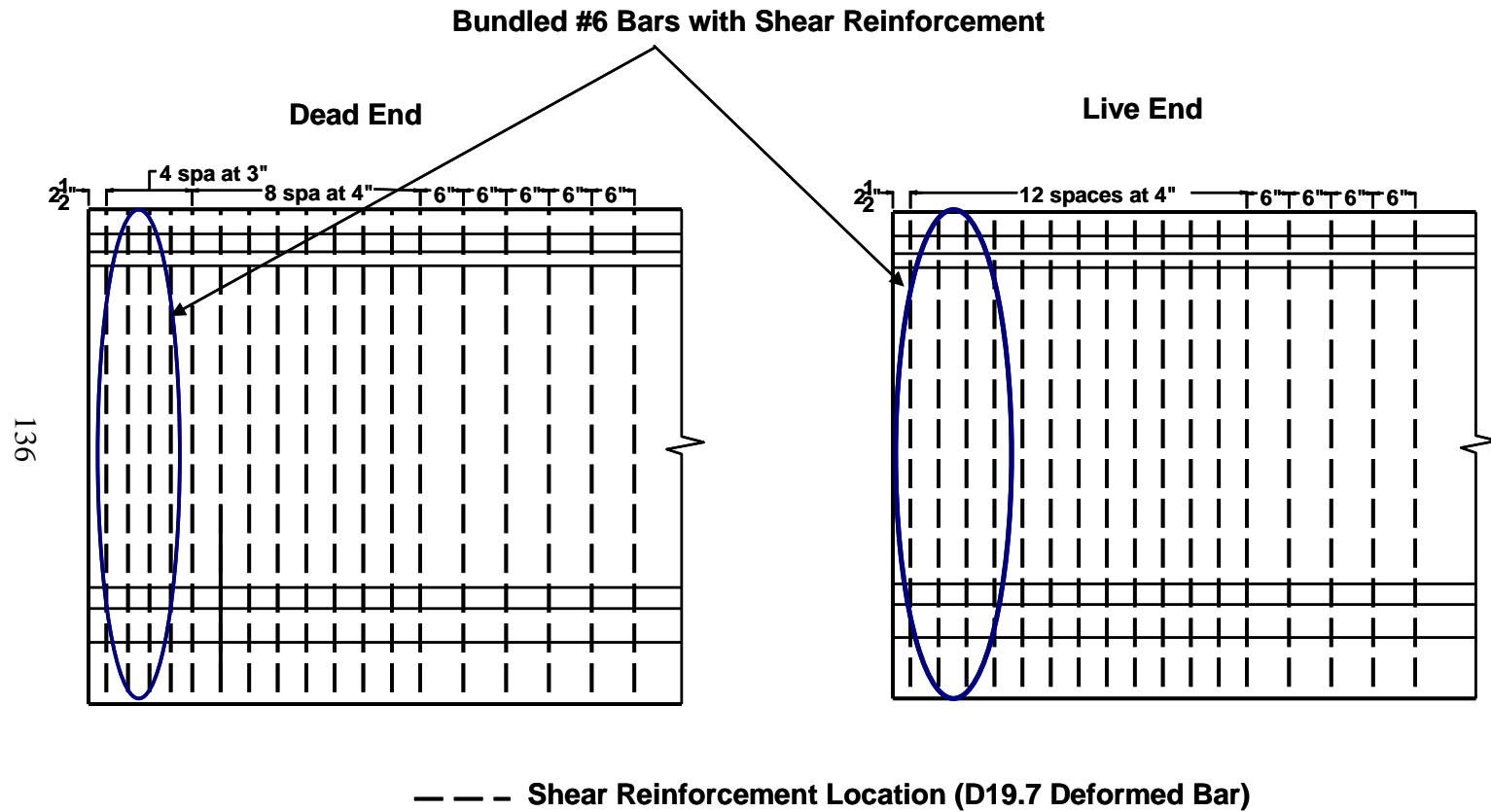


Figure 4-4: Typical location for bundled spalling reinforcement for a Tx70 girder.

The following sections below show a sample calculation for one girder to compare with the actual design shown above. In addition to this, design guidelines are compared and contrasted. Detailed calculations for these code provisions can be seen in Appendix B.

4.2.1 AASHTO LRFD Bridge Design Specifications (2007)

Code provision §5.10.10.1, incorrectly called “*Factored Bursting Resistance*”, is actually a provision for spalling reinforcement. The Tx46 girder will be the representative girder used for all calculations. Steel stress is limited to 20 ksi so that value will be used as the worst case scenario. The prestressing force at transfer for a Tx46 equals 1732 kips.

$$P_r = f_s A_s \Rightarrow A_s = \frac{P_r}{f_s}$$

$$A_s = \frac{0.04 \cdot (1732 \text{ kips})}{20 \text{ ksi}} = 3.46 \text{ in}^2$$

Equation 4-1

This amount of reinforcement is supposed to be placed within the first $h/4$ of the beam. This means that from the face of the girder to 11.5 inches into the beam, 3.46 in² of steel reinforcement should be stressed to 20 ksi. The actual design of the Tx46 at the dead end includes 8 - #6 reinforcing bars or 3.52 in² of spalling reinforcement in that distance. At this end of the beam the total amount of reinforcement, meets code requirements. The live end has slightly less spalling reinforcement in the end region of the beam. There are only 6 - #6 reinforcing bars or 2.64 in² of spalling reinforcement in that end zone. If shear reinforcement is included (6 - D19.7 bars or $0.197 \text{ in}^2 \cdot 6 = 1.18 \text{ in}^2$), the code requirements are met by having 3.82 in² of total vertical reinforcement within $h/4$. It should be noted that at the end of this chapter, the comparison between the live end and

dead end stresses and crack patterns will provide the best review of which reinforcement pattern works more effectively.

4.2.2 PCI Design Handbook (6th Edition) Guidelines

The provision in PCI Design Handbook (6th Edition) called “§4.2.4, *End Stresses at Transfer*” stipulates providing reinforcement for bursting or splitting stresses. As in AASHTO LRFD Bridge Design Specifications (2007), this provision is actually aimed at detailing reinforcement in the spalling region. The Tx46 girder will again be used as an example for this calculation using a prestress force of 1732 kips, a height of 46”, a steel stress of 30 ksi, and a transfer length of 36”.

$$A_{vt} = \frac{0.021P_o h}{f_s l_t} = \frac{0.021 \cdot 1732k \cdot 46''}{30ksi \cdot 36''} \quad \text{Equation 4-2}$$

$$A_{vt} = 1.55in^2$$

This amount of reinforcement must be placed within the first $h/5$ of the girder. For the dead end of the girder the first $h/5$, or 9.2 inches, includes 6 - #6 reinforcing bars or 2.64 in² of spalling reinforcement which easily meets the code requirements. The live end has slightly less reinforcement with 4 - #6 reinforcing bars which is equal to 1.76 in² but steel meets the recommendation of PCI Design Handbook. In short, both of these ends meet PCI design guidelines for spalling steel.

4.2.3 CEB-FIP Model Code 1990 Provisions

The CEB-FIP MC 90 provides the most extensive detailing requirements for spalling and bursting stress steel. Detailed calculations illustrating the use of the CEB-FIP MC 90 expressions are shown in Appendix B. A sample set of equations for quantities of transverse steel are shown below. The transmission

length (European terminology) or transfer length (U.S. Customary Terminology) used in these equations equals 41.3” with calculations shown below. The symmetrical prism method used to calculate bursting stresses is shown immediately after the transfer length equation followed by the equivalent prism method for calculating spalling stresses.

6.9.11.2 Bond Strength

$$f_{bpd} = \eta_{p1}\eta_{p2}f_{ctd} = 1.2 \cdot 0.7 \cdot \frac{242 \text{ psi}}{1.5} \quad \text{Equation 4-3}$$

$$f_{bpd} = 136 \text{ psi}$$

where

$f_{ctd} = f_{ctk}(t)/1.50$ is the lower design concrete tensile strength; for the transmission length the strength at the time of release

η_{p1} = takes into account the type of prestressing tendon: $\eta_{p1} = 1.4$ for indented or crimped wires, and $\eta_{p1} = 1.2$ for 7-wire strands

η_{p2} = takes into account the position of the tendon: $\eta_{p2} = 1.0$ for all tendons with an inclination of 45°-90° with respect to the horizontal during concreting, $\eta_{p2} = 1.0$ for all horizontal tendons which are up to 250 mm from the bottom or at least 300 mm below the top of the concrete section during concreting, and $\eta_{p2} = 0.7$ for all other cases.

6.9.11.3 Basic Anchorage Length

The basic anchorage length of an individual pretensioned tendon is

$$l_{bp} = \frac{A_{sp}}{\phi\pi} \cdot \frac{f_{ptd}}{f_{bpd}} = \frac{7 \cdot 0.6''}{36} \cdot \frac{245 \text{ ksi} / 1.15}{0.136 \text{ ksi}} \quad \text{Equation 4-4}$$

$$l_{bp} = 182''$$

where

$f_{ptd} = f_{ptk}/1.15$, where f_{ptk} is yield strength of prestressing tendon

$\frac{A_{sp}}{\phi\pi} = \phi/4$ for tendons with a circular cross-section

= $7\phi/36$ for 7-wire strands

6.9.11.4 Transmission Length

The transmission length of a pretensioned tendon is

$$l_{bpt} = \alpha_8 \alpha_9 \alpha_{10} l_{bp} \frac{\sigma_{pi}}{f_{pd}} = 1.0 \cdot 0.5 \cdot 0.5 \cdot 182'' \cdot \frac{178\text{ksi}}{196\text{ksi}} \quad \text{Equation 4-5}$$

$$l_{bpt} = 41.3''$$

where

α_8 = considers the way of release: $\alpha_8 = 1.0$ for gradual release and $\alpha_8 = 1.25$ for sudden release;

α_9 considers the action effect to be verified: $\alpha_9 = 1.0$ for calculation of anchorage length when moment and shear capacity is considered, and $\alpha_9 = 0.5$ for verification of transverse stresses in anchorage zone

α_{10} considers the influence of bond situation: $\alpha_{10} = 0.5$ for strands and $\alpha_{10} = 0.7$ for indented or crimped wires;

σ_{pi} is the steel stress just after release

6.9.12.2 Bursting

For the calculation of the bursting force the symmetric prism analogy may be used (Figure 4-5).

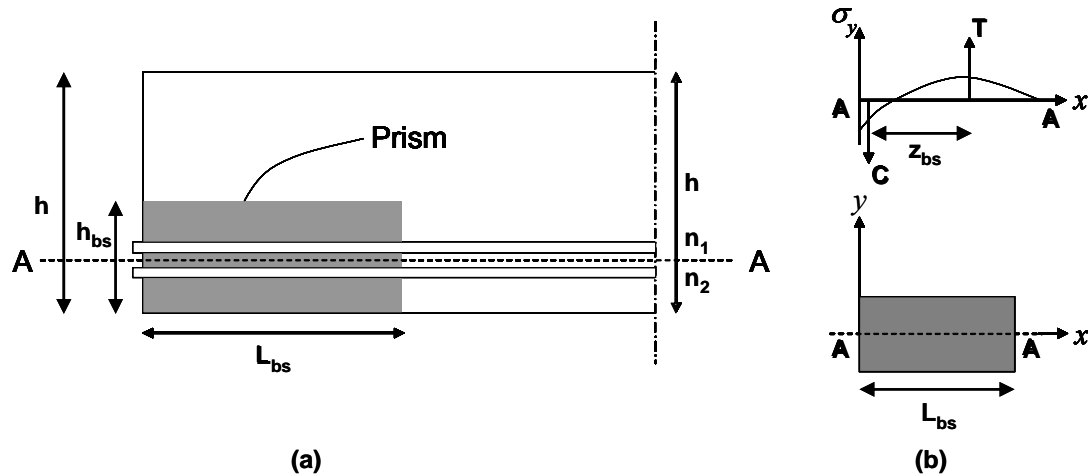


Figure 4-5: For calculation of the bursting force: (a) dimensions of the symmetrical prism; (b) moment equilibrium along section A-A (CEB-FIP, 1998)

The height and the width of the prism follow from the possible enlargement of the anchor plates (post-tensioning) or the tendon pattern (pretensioning). For multiple tendons the most unfavorable situations shall be considered: a single tendon or a group of tendons. The bursting action shall be determined both in the vertical and in the horizontal direction.

The length of the prism is for the end anchored tendons

$$l_{bs} = h_{bs} = 18.82" \quad \text{Equation 4-6}$$

And for tendons anchored by bond

$$l_{bs} = \sqrt{[h_{bs}^2 + (0.6l_{bpt})^2]} < l_{bpt} \quad \text{Equation 4-7}$$

$$l_{bs} = \sqrt{[18.82^2 + (0.6 \cdot 41.3")^2]} = 31.12"$$

The internal lever arm for the bursting force is

$$z_{bs} = 0.5l_{bs} = 0.5 \cdot 31.12 = 15.6" \quad \text{Equation 4-8}$$

The bursting force follows from the moment equilibrium along section A-A (Figure 4-5(b))

$$N_{bs} = \frac{\frac{1}{2}(n_1 + n_2)t_2 - n_1t_1}{z_{bs}} \gamma_1 F_{sd}$$

$$N_{bs} = \frac{\frac{1}{2}(44.46) \cdot 9.28" - 16.46 \cdot 3.73"}{15.56"} \cdot 1.1 \cdot 44.2 \text{kips} \quad \text{Equation 4-9}$$

$$N_{bs} = 412 \text{kips}$$

The maximum bursting stress follows from

$$\sigma_{bs} = 2N_{bs} / b_{bs}l_{bs} = 2 \cdot 412 \text{k} / 7" \cdot 31.12" \quad \text{Equation 4-10}$$

$$\sigma_{bs} = 3.78 \text{ksi}$$

where b_{bs} is the width of the prism.

For $\sigma_{bs} > f_{ctd}$ the bursting force shall be resisted by confining or net reinforcement distributed within $l_{bs}/3$ to l_{bs} from the end face, with

$$A_{bsb} = N_{bs} / f_{sy} = 412 \text{kips} / 60 \text{ksi} \quad \text{Equation 4-11}$$

$$A_{bsb} = 6.86 \text{in}^2$$

As is shown in Equations 4-10 and 4-11 the maximum expected stress in the bursting region is 3.78 ksi and the required reinforcement placed within $l_{bs}/3$ and l_{bs} is 6.86in^2 . The design of the live and dead ends have 2.36in^2 of shear reinforcement within the specified region ($l_{bs}/3$ to l_{bs} or 10.4" to 31.12"), but no reinforcement specifically designed to resist the bursting stresses. This begins to show the importance of bursting stresses in a pretensioned beam and why there is high potential for cracking. The spalling stress calculations are shown below:

6.9.12.3 Spalling

The spalling force may be calculated with the equivalent prism analogy (Figure 4-6(a)).

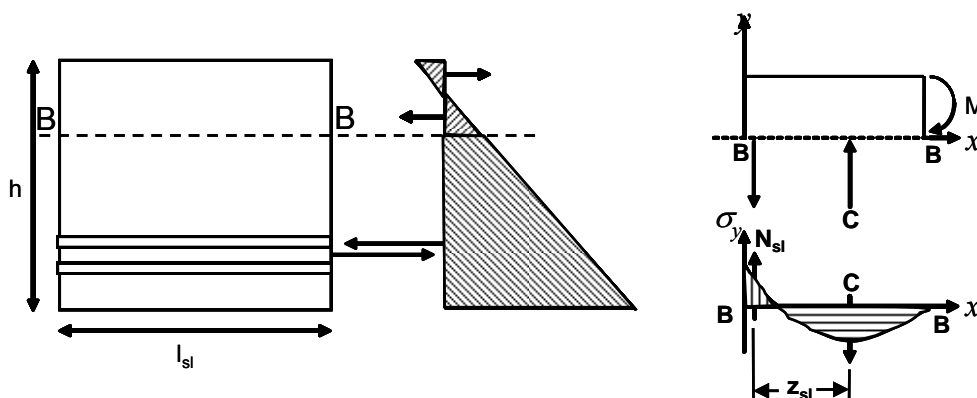


Figure 4-6: For calculation of the spalling force: (a) definition of the equivalent prism; (b) moment equilibrium along section B-B (CEB-FIP, 1998)

The length of the prism is defined as, for end anchored tendons

$$l_{sl} = h \quad \text{Equation 4-12}$$

And for tendons anchored by bond

$$l_{sl} = \sqrt{h^2 + (0.6l_{bpt})^2} < l_{bpt}$$

$$l_{sl} = \sqrt{46^2 + (0.6 \cdot 41.3)^2} = 52.25'' \quad \text{Equation 4-13}$$

$$l_{sl} = 41.3''$$

The internal lever arm for the spalling force is

$$z_{sl} = 0.5l_{sl} = 0.5 \cdot 41.3'' = 20.65'' \quad \text{Equation 4-14}$$

Section B-B shall be chosen so that along this section no shear force results. The spalling force results from the moment equilibrium along section B-B

$$N_{sl} = M / z_{sl} = 3.64k \cdot in / 20.65" \quad \text{Equation 4-15}$$

$$N_{sl} = 0.18kips$$

With the moment M given by concrete stresses above section B-B.

The maximum spalling stress follows from

$$\sigma_{sl} = 8N_{sl} / b_{sl}l_{sl} = 8 \cdot .18kips / 7" \cdot 41.3" \quad \text{Equation 4-16}$$

$$\sigma_{sl} = 0.005ksi$$

With b_{sl} width of the cross section at section B-B.

For $\sigma_{sl} \leq f_{ct,fl} / \gamma_c$, where

$$\gamma_c = 1.5$$

$f_{ct,fl}$ is the flexural tensile strength of concrete

the spalling force shall be resisted by reinforcement

$$A_{s,sl} = N_{sl} / f_{sy} = 0.18kips / 60ksi \quad \text{Equation 4-17}$$

$$A_{s,sl} = 0.003in^2$$

The spalling force resisting reinforcement shall be put parallel to the end face in its close vicinity.

This shows that in the CEB-FIP MC 90 does not find it necessary to provide spalling reinforcement for Tx46. With such low stresses and little required reinforcement it appears whatever shear steel might be in the end region would be more than sufficient to resist the transverse stresses.

4.2.4 Design Guideline Comparison Summary

Design calculations performed on Tx46 for bursting and spalling stresses are given in the preceding section. Detailed calculations are provided in

Appendix B. Table 4-1, Table 4-2, and Table 4-3 below give a comparison of all of the code provisions as well as the design of the beam.

Table 4-1: Code provision comparison for Tx28 end region reinforcement

Code	Spalling (in²)	Design (in²)	Req's Met?	Bursting (in²)	Design (in²)	Req's Met?
Live End						
AASHTO	2.93	1.76	N*	N/A	0.00	N/A
		2.55			2.76	
PCI	0.80	0.88	Y	N/A	0.00	N/A
		1.27			2.76	
CEB-FIP	0.00	0.88	Y	5.34	0.00	N
		1.27			2.76	
Dead End						
AASHTO	2.93	1.76	N*	N/A	0.00	N/A
		2.55			3.15	
PCI	0.80	1.76	Y	N/A	0.00	N/A
		2.55			3.15	
CEB-FIP	0.00	1.76	Y	5.34	0.00	N
		2.55			3.15	
Spalling or Bursting Reinforcement Only						
Spalling or Bursting Reinforcement + Shear Reinforcement						
* Code Provision cannot be met even if shear reinforcement is included						

Table 4-2: Code provision comparison for Tx46 end region reinforcement

Code	Spalling (in²)	Design (in²)	Req's Met?	Bursting (in²)	Design (in²)	Req's Met?
Live End						
AASHTO	3.46	2.64	N*	N/A	0.00	N/A
		3.82			2.36	
PCI	1.55	1.76	Y	N/A	0.00	N/A
		2.55			2.36	
CEB-FIP	0.00	1.76	Y	6.86	0.00	N
		2.55			2.36	
Dead End						
AASHTO	3.46	3.52	Y	N/A	0.00	N/A
		5.10			2.36	
PCI	1.55	2.64	Y	N/A	0.00	N/A
		3.82			2.36	
CEB-FIP	0.00	1.76	Y	6.86	0.00	N
		2.55			2.36	
	Spalling or Bursting Reinforcement Only					
	Spalling or Bursting Reinforcement + Shear Reinforcement					
	* Code Provision is met if shear reinforcement is included					

Table 4-3: Code provision comparison for Tx70 end region reinforcement

Code	Spalling (in ²)	Design (in ²)	Req's Met?	Bursting (in ²)	Design (in ²)	Req's Met?
Live End						
AASHTO	3.51	3.52	Y	N/A	0.00	N/A
		5.10			1.97	
PCI	2.39	2.64	Y	N/A	0.00	N/A
		3.82			1.97	
CEB-FIP	1.62	2.64	Y	4.19	0.00	N
		3.82			1.97	
Dead End						
AASHTO	3.51	3.52	Y	N/A	0.00	N/A
		5.10			1.97	
PCI	2.39	3.52	Y	N/A	0.00	N/A
		5.10			1.97	
CEB-FIP	1.62	3.52	Y	4.19	0.00	N
		5.10			1.97	
Spalling or Bursting Reinforcement Only						
Spalling or Bursting Reinforcement + Shear Reinforcement						

These tables show that spalling reinforcement requirements can be difficult to meet with AASHTO LRFD (2007) using only bundled spalling steel and not including shear steel. PCI (6th Edition) and CEB-FIP MC 90 spalling requirements are met in all of the girders used in this project. These tables also show a complete lack of information regarding bursting reinforcement in the U.S. codes and the emphasis placed on it by CEB-FIP MC 90. This preliminary analysis suggested that more problems would develop with bursting stresses in these beams than with spalling stresses. The subsequent sections presented in this chapter will support this preliminary conclusion.

4.3 Tx28-I RESULTS

The first beam that was cast was the Tx28. This 28” deep beam provided valuable information in spite of the concrete mixture design problems. As mentioned before this girder was not representative of typical precast beams as the concrete did not set up until 60 hours after placement. However, other than the delay seen in the initial set, all other attributes of the beam fabrication and concrete hydration were typical. The data collected helped make the casting and the instrumentation of the following three beams much easier and more accurate. It is with these in mind that the data will be reported here as a starting point for the research.

4.3.1 Tx28-I Release

Since the concrete used to construct this girder did not begin to set up until 60 hours after concrete placement, it was felt that release should be done after a few days so that all sections of the girder had a chance to gain strength. The prestressing strands were released 5 days after casting. Cylinder testing to determine concrete strength was done simultaneously with release. A full set of 6 *Sure Cure* cylinders gave an average concrete strength of 10,025 psi. Since the compressive strength of the concrete is known, a more accurate elastic shortening calculation could be done using AASHTO LRFD 2007 §5.9.5.2.3a:

$$E_p = 29,500ksi$$

$$E_{ct} = 57,000 \cdot \sqrt{10,025} = 5707ksi$$

$$f_{cgt} = \frac{44.2k \cdot (36strands)}{585in^2} + \frac{44.2k \cdot (36strands) \cdot (5.24in)^2}{52,772in^4} + \frac{5k \cdot (4strands)}{585in^2} - \frac{5k \cdot (4strands) \cdot (13.37in)^2}{52,772in^4}$$

$$f_{cgt} = 3.51ksi$$

$$\Delta f_{pES} = \frac{29,500}{5,707} \cdot 3.51ksi = 18.2ksi$$

As mentioned in Chapter 3 release was done by first cutting the top strands and then gradually releasing the bottom strands using hydraulic rams.

4.3.1.1 Strand Stress before Release

In order to evaluate the stresses in the end regions of the test specimens, the prestressing force has to be known. The prestressing force was determined by comparing the strain gauge readings and pressure gauge readings. While individual strands may have had slightly different stress levels, the total prestressing force was determined from pressure gauges readings and verified with strain gauge readings. Since the force in each strand was not identical, an average value was taken from all the readings, removing those which had obviously malfunctioning strain gauges. The average stress and force are reported for each end in Table 4-4. Average stress values were calculated using the calibration curves discussed in Chapter 3.

Table 4-4: Stresses in prestressing strands before release

Specimen	Avg. Strain (in/in)	Avg. Stress (ksi)	Avg. Force (kips)	Total Force (kips)
Tx28-I	0.006323	203.6	44.2	1,591

In order to support these stresses inferred from strain gauge readings, hydraulic pressure readings and elongations were also taken. The elongations measured by ram displacement were on average 4.5 inches. This value minus the deflection of the dead end, 0.2", gives an elongation of 4.3" which is only 1/8" away from the expected value. The pressure readings of 5,150 psi on the top two rams and 3,900 psi on the bottom two rams calculate out to a total force of 1,571 kips of initial prestress. With all of these values in such close agreement the strain gauge

readings could be confidently utilized for calculations of strand and rebar stresses after release.

4.3.2 Tx28-I Strand Stresses

An important part of understanding transverse tensile stresses has to do with the application of the load onto the beam. This was shown in many of the previous research studies reviewed in Chapter 2. This means that an important part of understanding spalling, bursting, and splitting stress has to do with the transfer length. Both live and dead ends were instrumented with strain gauges throughout the transfer length on the strand. This was done for two reasons. First, the measurement of transfer length could be seen once the values of stress in the strands peaked. Second, this peak value would help show the amount of elastic shortening taking place in the beam. In other words, theoretical calculations could be compared to measurements. Typical locations of the strand strain gauges are shown in Chapter 3. The graphs below show the increase in strand stress over the transfer length. In the figures below there is an unusually large scatter close to the beam ends. This can be attributed to each strand bonding to the concrete in a slightly different manner. With the data that does appear to be reasonable some trends and values should be noted. The strand stresses appear to both peak and converge at about 30” at slightly different values for the two ends. There are row and column numbers used in strand strain gauge designations used in Figure 4-8 and Figure 4-9 which are shown below in Figure 4-7. These locations refer to rows and columns of strand in the strand pattern - for example R2C8 in Figure 4-8 implies strand placed in the second row, eighth column.

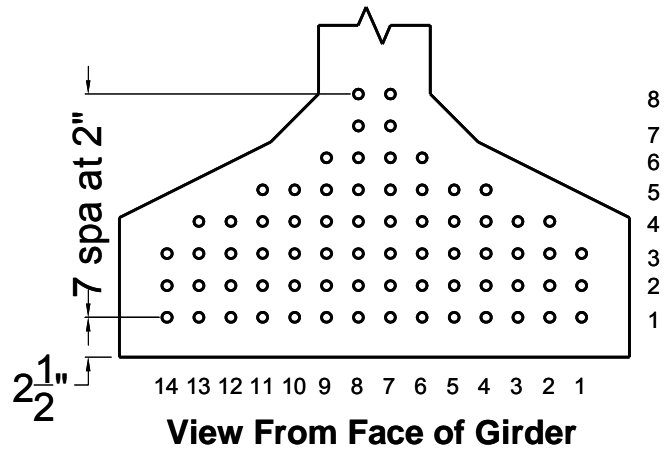


Figure 4-7: Typical strand locations

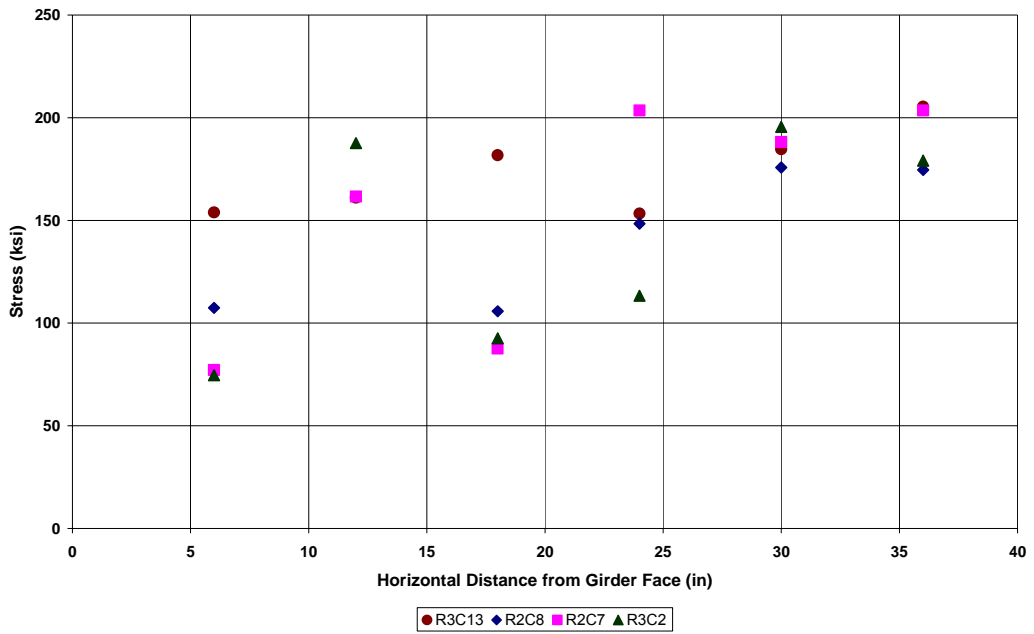


Figure 4-8: Tx28-I Strand stresses at release for the live end

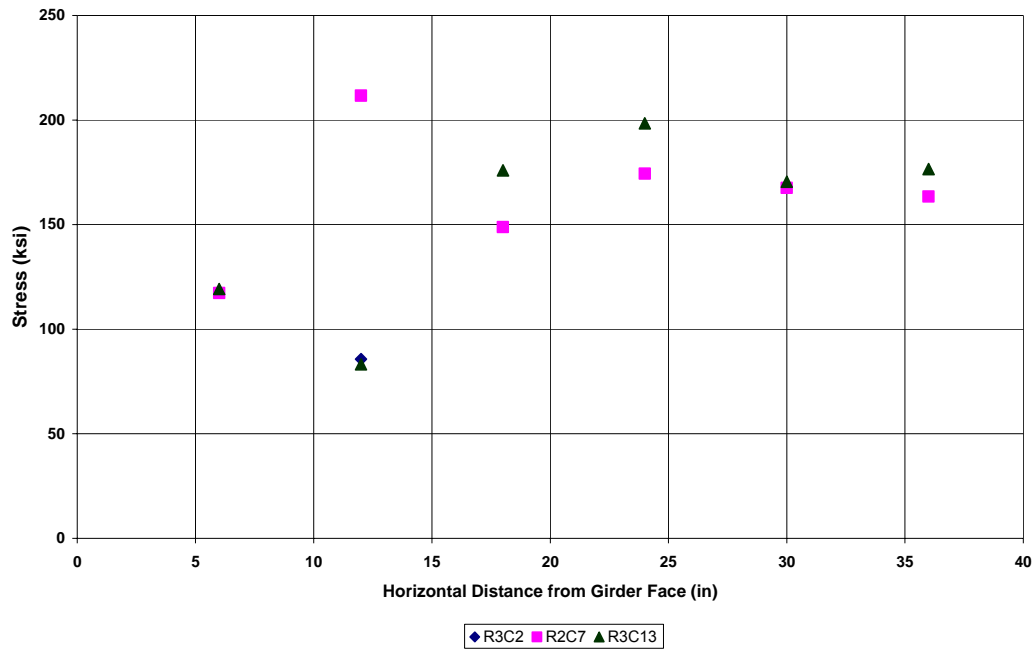


Figure 4-9: Tx28-I Strand stresses at release for the dead end

.As previously reported the average stress in strands was 203.6 ksi. At the live end, where there were a greater number of functional strain gauges, the average of the highest strand stresses inferred from strain gauge readings after release was 185.5 ksi, resulting in an elastic shortening loss of 18.1 ksi. As shown in Section 4.3.1 the estimated elastic losses were 18.2 ksi, which is very close to the measured losses in the beam after release. The approximate transfer length of 36 inches found in Chapter 3 is slightly higher than the measured transfer length of ~30 inches for this beam. As such, the AASHTO LRFD Bridge Design Specification (2007) value for transfer length is on the conservative side for transfer length.

4.3.3 Tx28-I Transverse Reinforcing Bar Stresses

With known values of compressive strength, transfer length, prestressing force applied, and elastic shortening losses, it is easier to interpret the transverse tensile stresses in the girder. The location of the strain gauges on each bar is shown in Chapter 3. Before the casting operation began a quality control check was done to make sure gauges were at the proper vertical and horizontal locations. Once the concrete placement was completed the horizontal distance was measured again using the protruding rebars as a guide. With the locations of the gauges known and the strain values recorded, a plot of the transverse reinforcement stresses for each test region could be compiled. The variations of the transverse rebar stresses within the live and dead ends of Tx28-I are shown in Figure 4-10 and Figure 4-11 respectively.

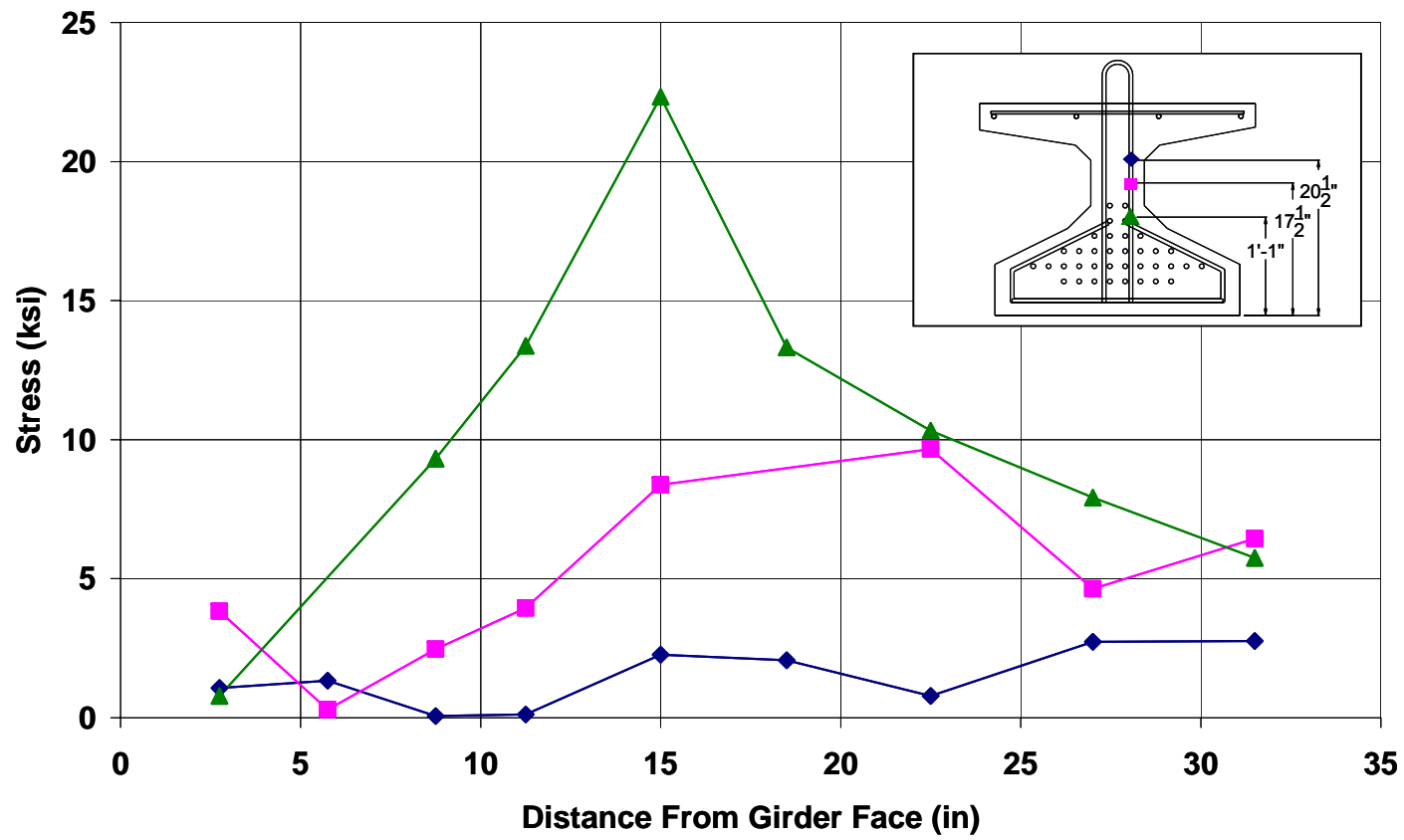


Figure 4-10: Tx28-I Live end transverse reinforcement stresses

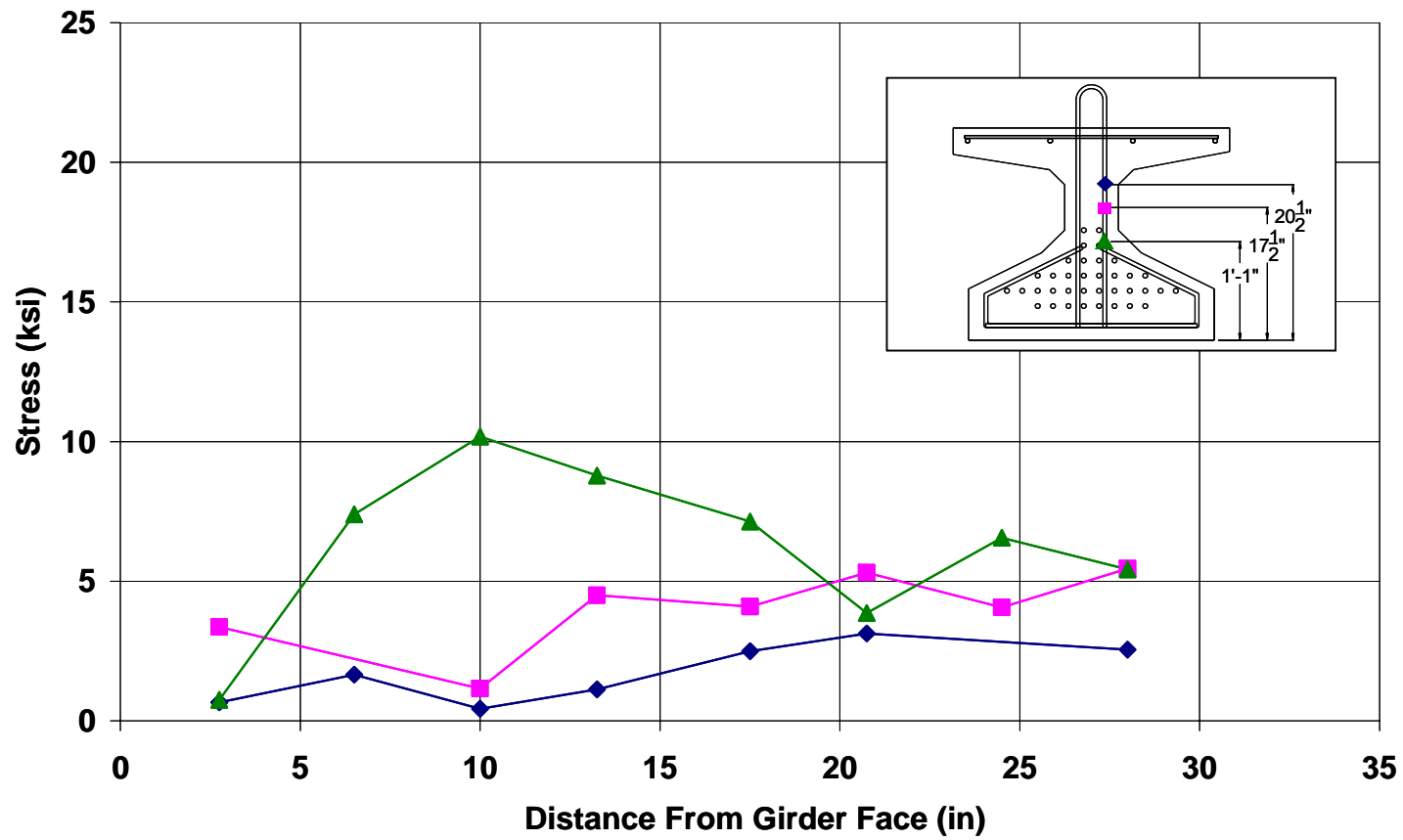


Figure 4-11: Tx28-I Dead end transverse reinforcement stresses

With these stresses, Tx28-I girder cracked primarily in the bottom flange to web connection with some additional cracking in the bottom flange itself. These crack patterns are shown in Figure 4-12 and Figure 4-14 (the spacing of the transverse #4 reinforcing bars are shown on the top of the drawings).

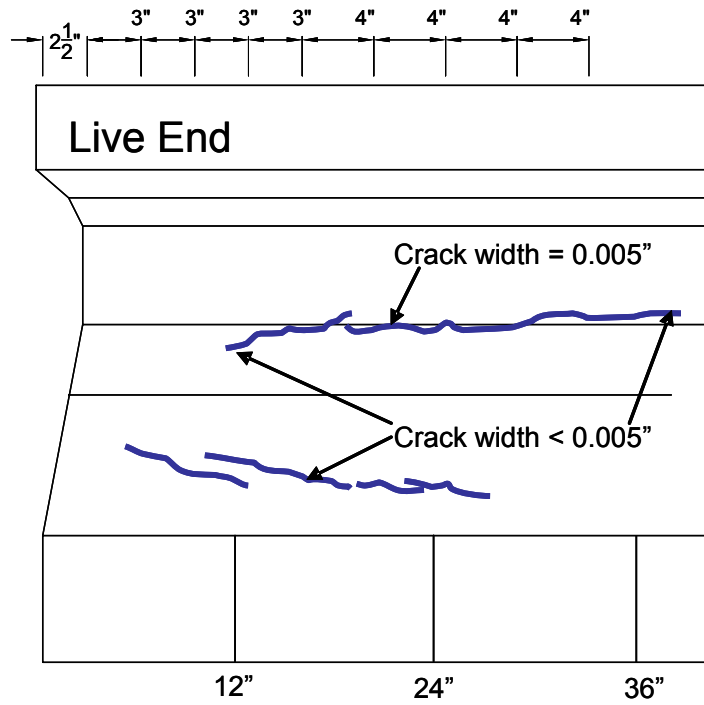


Figure 4-12: Tx28-I Live end crack pattern



Figure 4-13: Tx28-I Live end photo with crack pattern

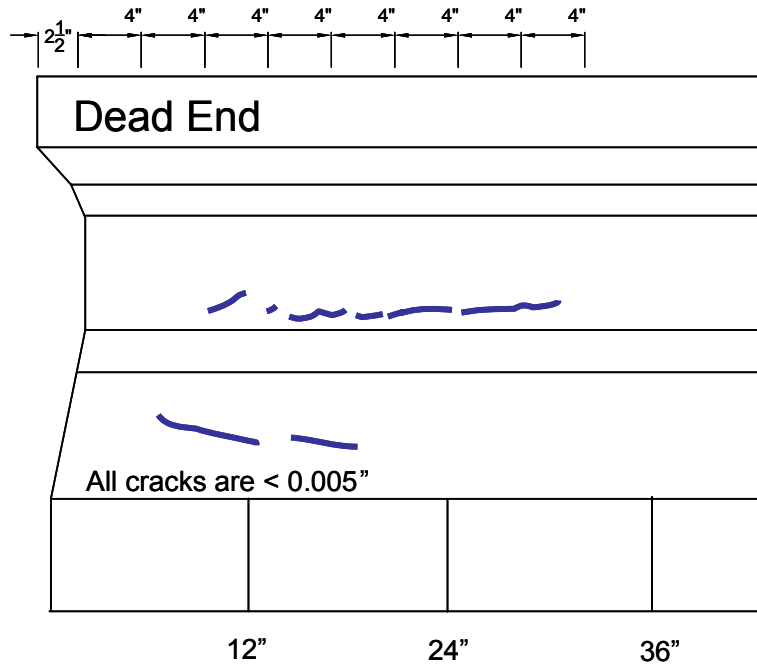


Figure 4-14: Tx28-I Dead end crack pattern



Figure 4-15: Tx28-I Dead end photo with crack pattern

These crack patterns show that in spite of the higher release strength of concrete (compressive strength of concrete was over 10,000 psi at release and the specified release strength was 6,500 psi) the girder still cracked. The crack patterns and stress plots show that the preliminary hypothesis that bursting stresses would present more of a problem in pretensioned girders is a valid statement. There was no cracking in the spalling region of the beam while there were some cracks within the bursting/splitting region of the beam. The maximum crack widths occurred reasonably close to the location of maximum stress in the rebar. At approximately 15" away from the beam end, the stress in the steel reached 22 ksi with a crack width of 0.005". This occurred at the live end, whereas the transverse reinforcement at the dead end was not stressed to higher than 10-11 ksi and all cracks were below the measurable crack width value of 0.005". Crack widths were measured using a crack comparator shown in Figure 4-16.

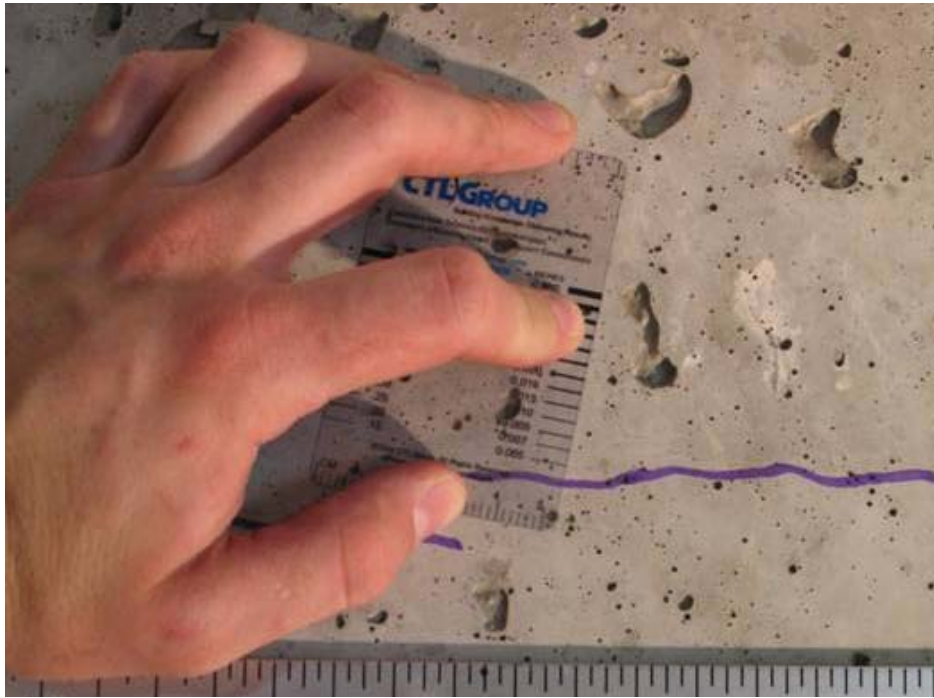


Figure 4-16: Crack width measurement

4.3.4 Tx28-I Summary

While concrete mixture design related problems caused this beam to be released five days after casting, the strength gain after the initial set was fairly typical. The strain gauge data proved that the bursting stresses pose a much greater problem than the spalling stresses. Since the eccentricity of the prestressing force (~5-in.) was not too high for Tx28-I, it is expected that spalling stresses are less of a concern than the bursting stresses. Theoretical work summarized in Chapter 2 and CEB-FIP MC 90 provisions support this observation. With increasing prestressing force eccentricities, spalling stresses will get to be much more significant with the two larger girders. The bursting and splitting stresses cause all of the cracking in this beam and are therefore the main set of transverse stresses that need to be addressed.

A maximum bursting stress over 22 ksi and crack widths at 0.005" raises some concerns about current design provision steel stress limits. To be more specific, it is of concern that the stress levels in shear reinforcement were as high as 22 ksi at release. The bursting stresses will be thoroughly reviewed after the data for all the test specimens are presented. While there are expected cracks at the web to bottom flange connection where the stresses get up over 22 ksi, the researchers felt like the cracks within the bottom flange required further attention. In order to make sure that these cracks were due to localized splitting stress associated with cover and confining steel, additional gauges were placed in the Tx28-II on the vertical reinforcement at the locations of these cracks. This would ensure that the crack was not continuous through the beam's bottom flange.

4.4 TX 28-II RESULTS

The concrete used to construct the second Tx28 girder performed much closer to a typical concrete used in a pretensioned girder cast in the field. Within 8 hours after concrete was batched, the beam began gaining strength and within 14 hours compressive strength increased to 6,500 psi and the strands were released. The addition of a few more strain gauges was the only major change besides the admixture dosage used in Tx28-II. Otherwise, Tx28-II was identical to Tx28-I in size, detailing, and applied prestressing force.

4.4.1 Tx28-II Release

The concrete in Tx28-II girder performed as expected and as such strands were released approximately 14 hours after concrete placement. Concrete cylinders were tested from all 6 *Sure Cure* locations and gave an average strength of 6,475 psi. Once again, elastic shortening can be better estimated with this known concrete strength.

$$E_p = 29,500 \text{ksi}$$

$$E_{ct} = 57000 \cdot \sqrt{6,475} = 4587 \text{ksi}$$

$$f_{cgt} = \frac{47.0k \cdot (36 \text{strands})}{585 \text{in}^2} + \frac{47.0k \cdot (36 \text{strands}) \cdot (5.24 \text{in})^2}{52,772 \text{in}^4} + \frac{5k \cdot (4 \text{strands})}{585 \text{in}^2} - \frac{5k \cdot (4 \text{strands}) \cdot (13.37 \text{in})^2}{52,772 \text{in}^4}$$

$$f_{cgt} = 3.74 \text{ksi}$$

$$\Delta f_{pES} = \frac{29,500}{4,587} \cdot 3.74 \text{ksi} = 24.0 \text{ksi}$$

Similar to Tx28-I the release procedure involved first cutting the top strands and then gradually releasing the bottom strands using hydraulic rams.

4.4.1.1 Strand Stress before Release

The waterproofing and impact protection of the strain gauges used in this specimen and subsequent specimens was improved as discussed in Chapter 3. The strain gauges used in Tx28-II performed much better than those used in the previous beam, i.e. only very few gauges malfunctioned. Knowing the value of the prestressing force in the strands is once again vital. Average strain values were measured and are reported in Table 4-5. As it can be seen in this table the strands were slightly overstressed as compared to the those used in Tx28-I.

Table 4-5: Stresses in prestressing strands before release

Specimen	Avg. Strain (in/in)	Avg. Stress (ksi)	Avg. Force (kips)	Total Force (kips)
Tx28-II	0.006729	216.6	47.0	1,692

Once again in support of the strain gauge readings, elongations and pressure readings were taken. The linear potentiometer frame discussed in Chapter 3 was used for this test and supplied good values for elongation. The central potentiometer failed, but the two outermost linear potentiometers worked giving an average elongation of 4.63". This value minus the deflection of the dead end

of 0.23” gives a total elongation of 4.40”. An elongation of 4.40” should give an initial prestressing force of 1,651 kips. This is reasonably close to the prestressing force inferred from strain gauge readings reported in Table 4-5.

4.4.2 Tx28-II Strand Stresses

A number of strands were instrumented with strain gauges both at the live and dead ends throughout the transfer length as before. The locations of the gauges are again called out by their location on a particular strand. These row and column numbers used in strand strain gauge designations used in Figure 4-17 and Figure 4-18 are shown above in Figure 4-7. Figure 4-17 and Figure 4-18 show the increase in strand stress over the transfer length for the Tx28-II.

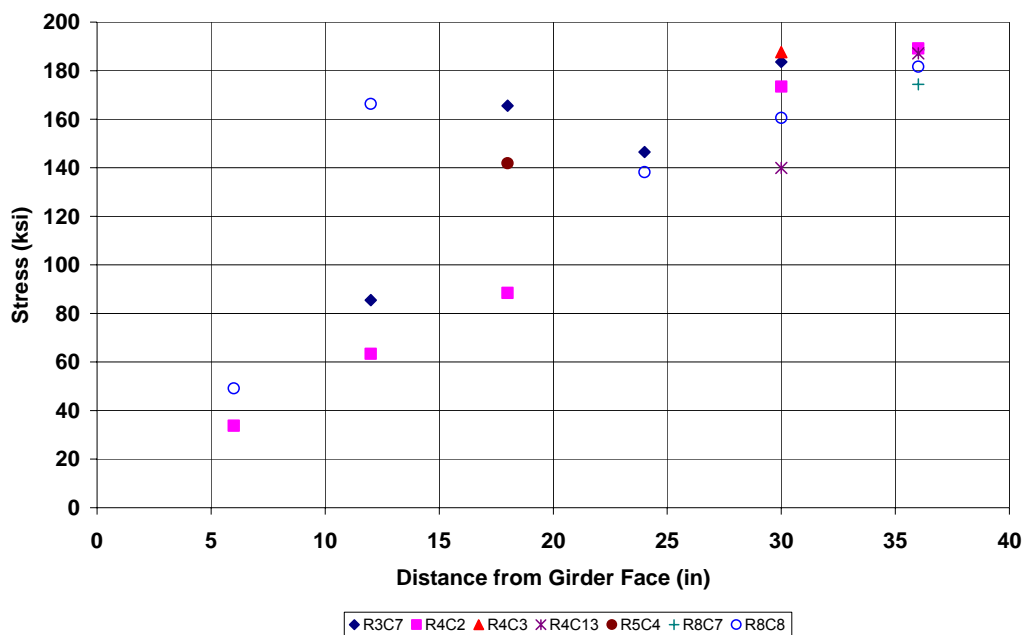


Figure 4-17: Tx28-II Strand stresses after release for the live end

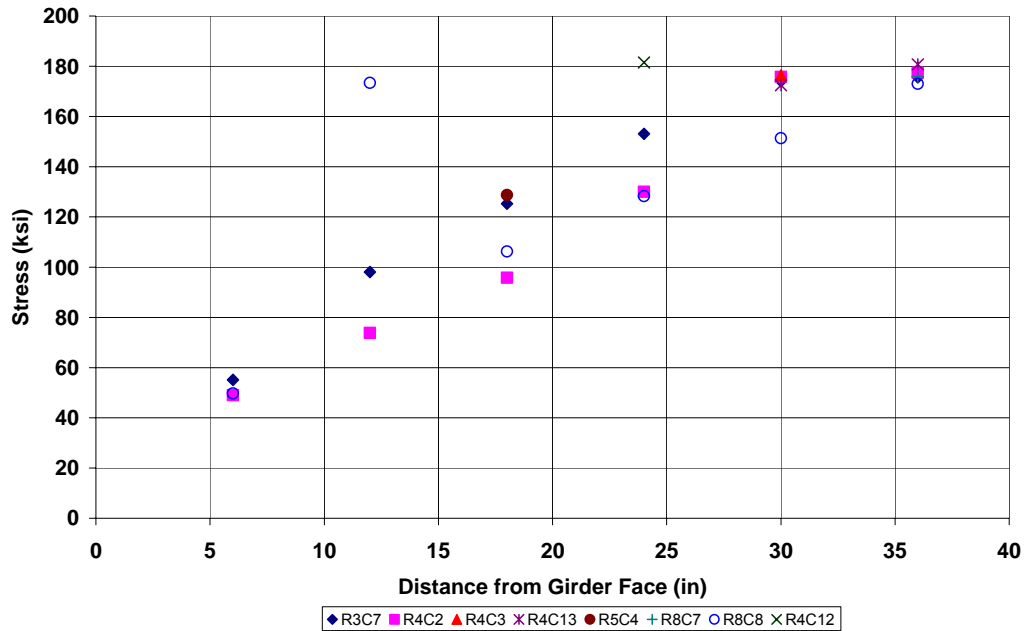


Figure 4-18: Tx28-II Strand stresses after release for the dead end

An examination of Figure 4-17 and Figure 4-18 reveals two facts: (i) the data scatter is reduced significantly in relation to the first test (ii) there is a more distinct pattern that can be used to identify the transfer length. Figure 4-17 and Figure 4-18 illustrate that both ends of Tx28-II have all strands reach the same stress level by 36” into the beam. This transfer length is in direct agreement with the AASHTO LRFD Bridge Design Specifications (2007) and ACI 318-05 code equations. The elastic shortening values found from the prestressing force in the strands is about 30 ksi and is somewhat higher than the expected value from Section 4.4.1 of 24.0 ksi. This discrepancy is mostly attributed to the slight overstressing of the prestressing strands to 47.0 kips each.

4.4.3 Tx28-II Transverse Reinforcing Bar Stresses

The strain gauge locations on the vertical reinforcement were shown in Chapter 3. These locations were verified before the cast. It is important to make note of the additional gauges placed within the bottom flange to check on the stress values in the region that cracked in the previous beam. Data from the strain gauges in these locations are also plotted on the transverse reinforcing bar stress plots shown in Figure 4-19 and Figure 4-20.

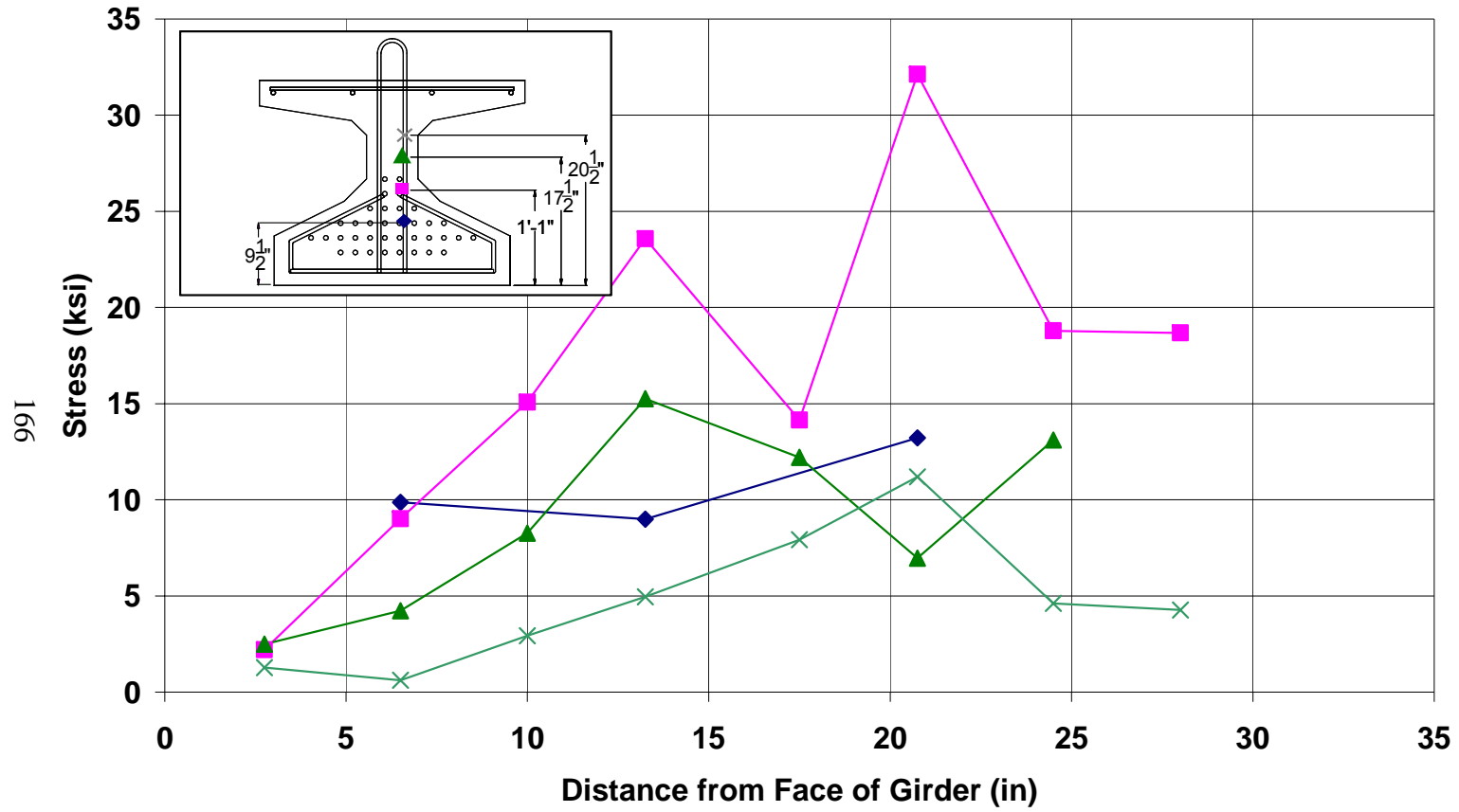


Figure 4-19: Tx28-II Live end transverse reinforcing bar stresses

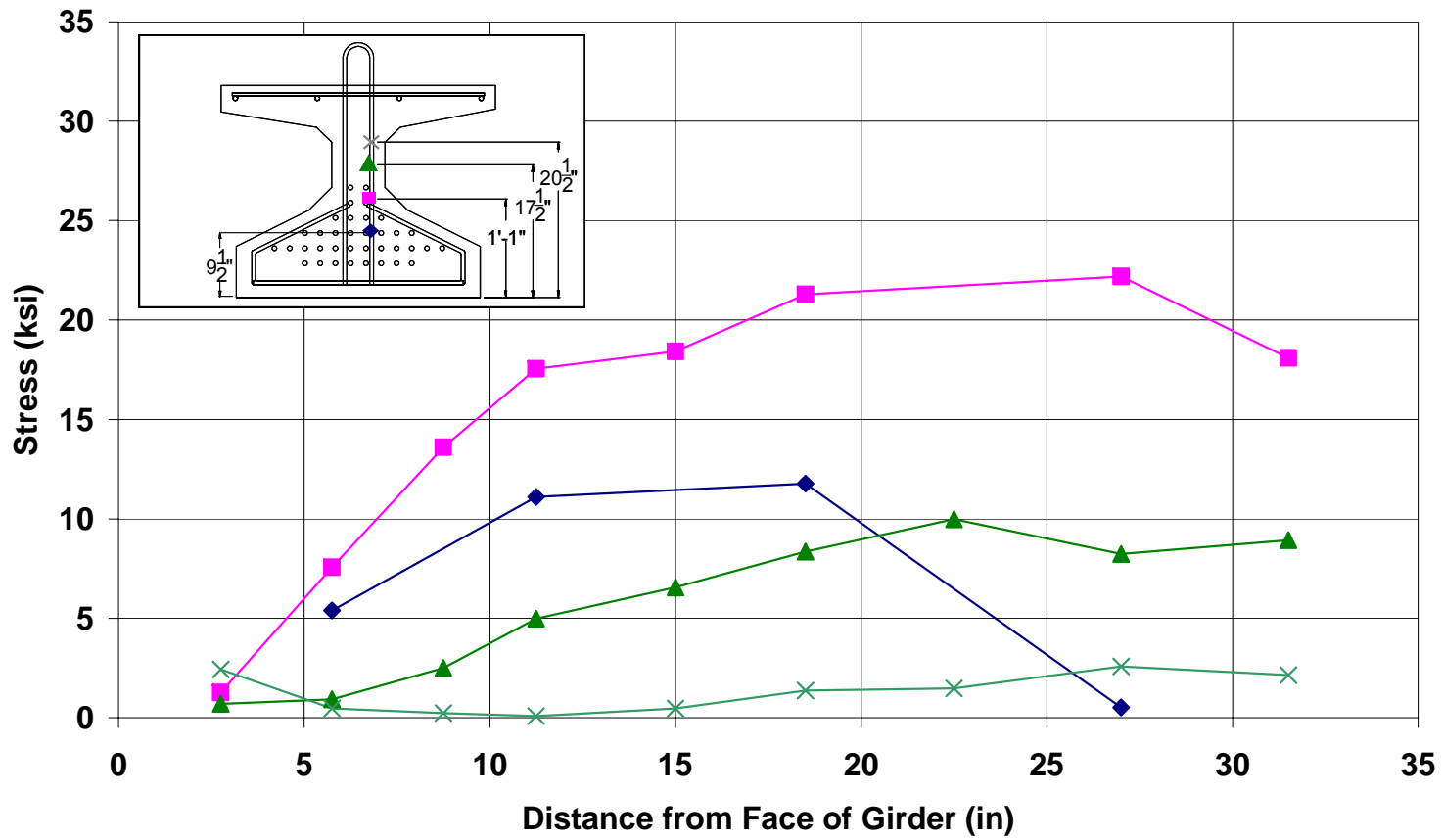


Figure 4-20: Tx28-II Dead end transverse reinforcing bar stresses

The reinforcing bar stresses at the top flange to web connection were less than 3 ksi and 12 ksi for the dead and live ends respectively. The mid-web rebar stresses at the live end got up to almost 15 ksi, but not until 12" into the beam. These were not spalling stresses but just the worst case scenario bursting stresses due to the slight overstressing of the strands. Largest reinforcing bar stresses were encountered at the bottom flange to web connection. The peak stress at the live end reached 32 ksi in the transverse reinforcing bars; well past the 20 ksi limit in AASHTO LRFD Bridge Design Specifications (2007) and slightly above the 30 ksi limit in PCI Design Handbook (6th Edition). The point right before the 32 ksi data point on the live end (Figure 4-19) is significantly less than the point before it or after it. It appears as though this gauge did not cross a crack and therefore did not pick up large strains. The lowest gauges placed in the bottom flange did reach 10 to 15 ksi, but these are low levels of stress as compared to the strain gauges placed at the bottom flange to web connection. These 10 to 15 ksi stresses are directly associated to the development of the transverse reinforcement at this particular location. The highest stresses measured at bottom flange to web connection do not develop immediately at a crack, but instead build up over the length of the reinforcement. The stresses found at the lowest gauges (10 to 15 ksi) illustrate the principle of reinforcing bar development. The crack maps given in Figure 4-21 and Figure 4-23 indicate that the beam had some cracks on the top side of the bottom flanges, yet the strain gauges placed on the vertical reinforcement did not pick up large strains, thus supporting the idea that the cracks were caused by the straining of bottom flange confining reinforcement. Since the primary focus of this research is on vertical reinforcement and not on local stresses with cover and confining reinforcement, and since critical readings were not obtained from the gauges placed on the vertical reinforcement within the

development length included in the bottom flange, these gauges were left out in the next two beams.

The crack patterns that developed in the end regions support the stresses inferred from strain gauge readings in the vertical reinforcement. These crack patterns for each end are shown in Figure 4-21, Figure 4-22, Figure 4-23, and Figure 4-24. Despite the fact that the strands were slightly over-stressed and that stresses in the vertical reinforcement reached 32 ksi, maximum crack width did not exceed 0.01". Beams with such cracks are typically accepted without any remediation, such as epoxy injection, by the TxDOT inspectors in pretensioned concrete beam fabrication plants.

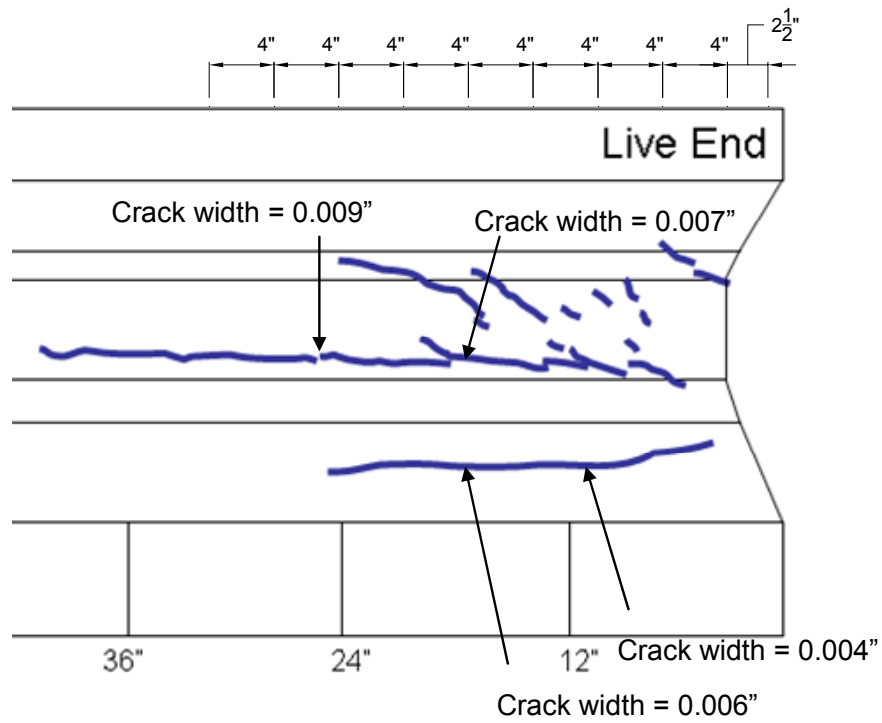


Figure 4-21: Tx28-II Live end crack pattern

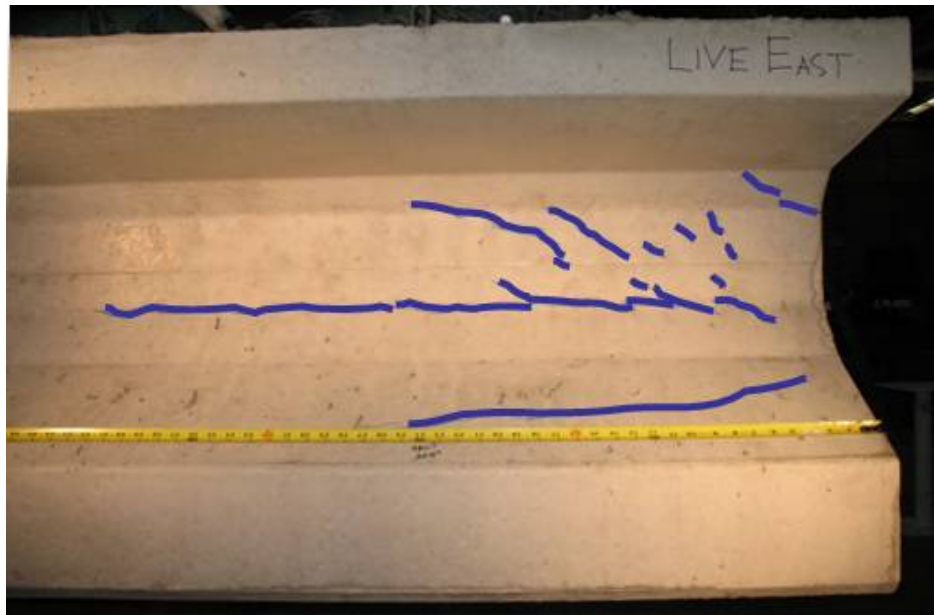


Figure 4-22: Tx28-II Live end photo with crack pattern

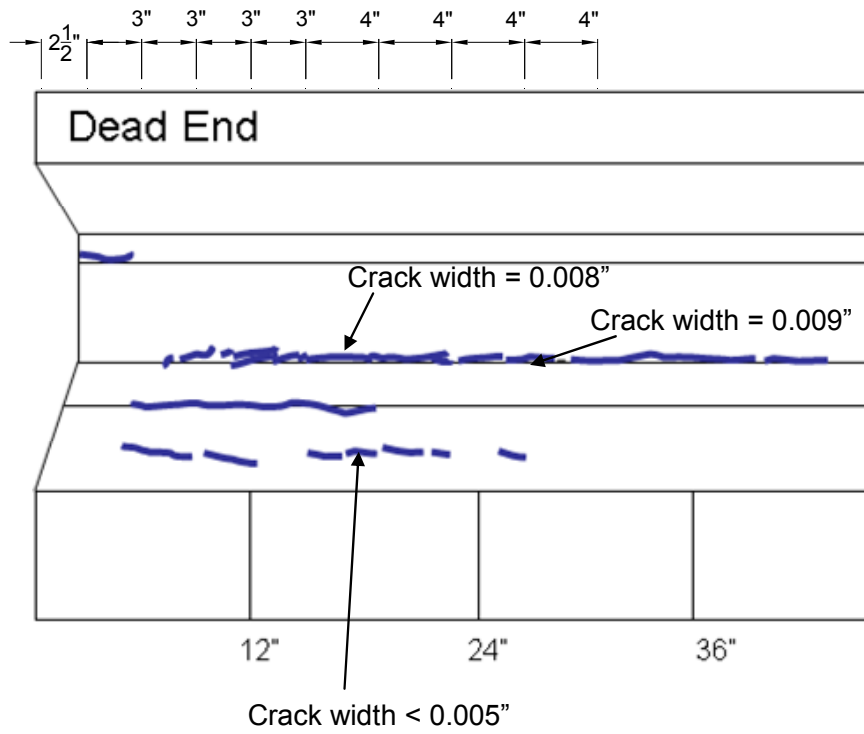


Figure 4-23: Tx28-II Dead end crack pattern

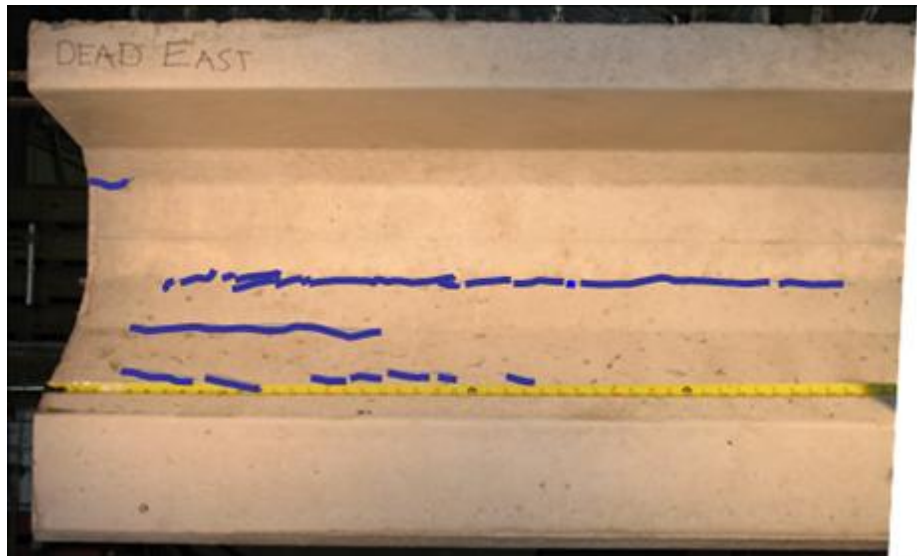


Figure 4-24: Tx28-II Dead end photo with crack pattern

The crack patterns on each end of the beam show that the primary location for cracks was along the bottom flange to web connection. The stresses shown earlier also agree with this statement. As with Tx28-I there were almost no cracks in the spalling region of the beam. While AASHTO LRFD provisions place emphasis on designing and detailing reinforcement within the first $h/4$ from the beam, the stresses in the transverse reinforcement within the first 7 inches ($28/4 = 7$ in.) were reasonably small. Much higher stresses were encountered $\sim 2 - 2.5$ ft. from the beam ends. The transverse reinforcing bar stresses and associated crack patterns presented earlier suggest that bursting stresses are a more significant source of cracking in these smaller girders as opposed to spalling stresses.

4.4.4 Tx28-II Summary

The maximum crack width at the live end was 0.009" at approximately 2-ft. into the beam. This crack width occurred when the transverse rebar stress reached the maximum value of 32 ksi. At the dead end the same crack width of 0.009" occurred at almost the identical location on the beam, but with a slightly lower stress in the rebar at 23 ksi. Both the crack maps and transverse reinforcing bar stress profiles reported earlier indicate that the spalling steel stipulated in AASHTO LRFD was not positioned effectively to counteract the bursting stresses. The shear reinforcement was instrumental in limiting the widths of the cracks that formed due to bursting stresses. The transverse rebar stresses increased with increasing distance measured from the beam ends within the first 2 feet. After this point the stresses began to drop off. By merely examining the data from 28-in. deep beams it is not possible to correlate this distance to the typical length of the disturbed region, $h = 28$ " into the beam, or to the transfer length, $l_t = 36$ ". This issue will be revisited when the data obtained from deeper beams is analyzed in the subsequent sections.

4.5 Tx46 RESULTS

Some important preliminary observations needed to be substantiated by testing the Tx46 girder. These included the effects of eccentricity on the spalling stresses and whether bursting stresses were a function of member depth or transfer length. The idea that the transfer length was closely associated to the bursting stresses needed supporting data. This was partially accomplished by placing some strain gauges on strands out to 42" away from the beam face. This location is past the ACI 318-05 and AASHTO LRFD Bridge Design Specifications (2007) transfer length of 36" and also meets the CEB-FIP Model Code (1990) definition of transmission length. As seen in Chapter 3, the vertical reinforcement was strain gauged out to 46" to again test the theory that the transverse stresses occur out to a distance of h from the beams' ends.

4.5.1 Tx46 Release

The Class H concrete used to fabricate Tx46 also performed as expected with respect to concrete curing time. It was cast and released at almost identical times to the Tx28-II girder. Concrete cylinders were tested from all 6 *Sure Cure* locations and gave an average strength of 6,500 psi at release. This concrete strength is used to estimate the elastic shortening:

$$E_p = 29,500 \text{ksi}$$

$$E_{ci} = 57,000 \cdot \sqrt{6,500} = 4,595 \text{ksi}$$

$$f_{cgt} = \frac{44.2k \cdot (44 \text{strands})}{761 \text{in}^2} + \frac{44.2k \cdot (44 \text{strands}) \cdot (11.03 \text{in})^2}{198,089 \text{in}^4} + \frac{5k \cdot (4 \text{strands})}{761 \text{in}^2} - \frac{5k \cdot (4 \text{strands}) \cdot (24.25 \text{in})^2}{198,089 \text{in}^4}$$

$$f_{cgt} = 3.72 \text{ksi}$$

$$\Delta f_{pES} = \frac{29,500}{4,595} \cdot 3.72 \text{ksi} = 23.9 \text{ksi}$$

4.5.1.1 Strand Stresses before Release

The Tx46 girder was stressed as all the other test beams. The values reported in Table 4-6 are the actual strain values in the strands before release.

Table 4-6: Stresses in prestressing strands before release

Specimen	Avg. Strain (in/in)	Avg. Stress (ksi)	Avg. Force (kips)	Total Force (kips)
Tx46	0.006322	203.5	44.2	1,945

The prestressing force obtained from the strain readings and calibration curves was verified by using the elongation measurements from the linear potentiometers and pressure gauges. The three linear potentiometers monitoring the movement of the stressing plate had an average value of 4.43" with a dead end deflection of .22". This gave a total elongation value of 4.21". The expected elongation value was 4.218". The expected total force in the strands from preliminary calculations is 1,953 kips; only 8 kips different from the actual value reported in Table 4-6. The top two hydraulic rams were pressurized to 6,300 psi and the bottom rams were pressurized to 4,800 psi. Using these hydraulic pressures and the areas of the hydraulic rams the prestressing force could be calculated as 1,927 kips. This value is also reasonably close to 1,945 kips reported in Table 4-6.

4.5.2 Tx46 Strand Stresses

As indicated earlier, strain gauges were installed on the strands at the live and dead ends of the girder. The first 42 inches measured from the end of the beam, of the strands were instrumented with strain gauges. The actual position of each gauge is shown in the legends of Figure 4-25 and Figure 4-26. The term R refers to the row and the C refers to the column, both of which can be cross-referenced by using the strand patterns illustrated in Figure 4-7.

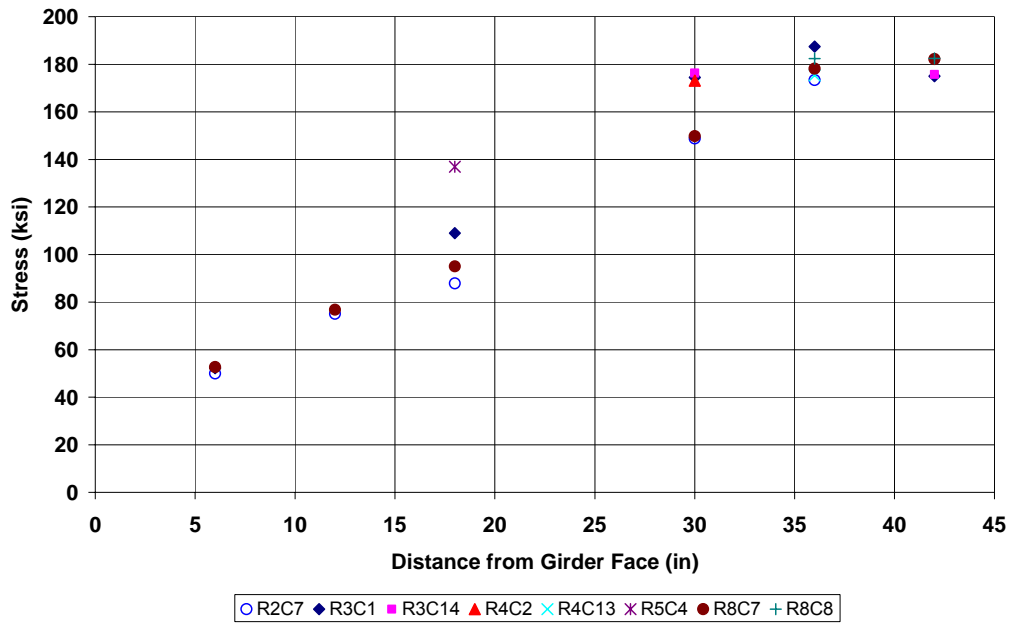


Figure 4-25: Tx46 Strand stresses at release for the live end

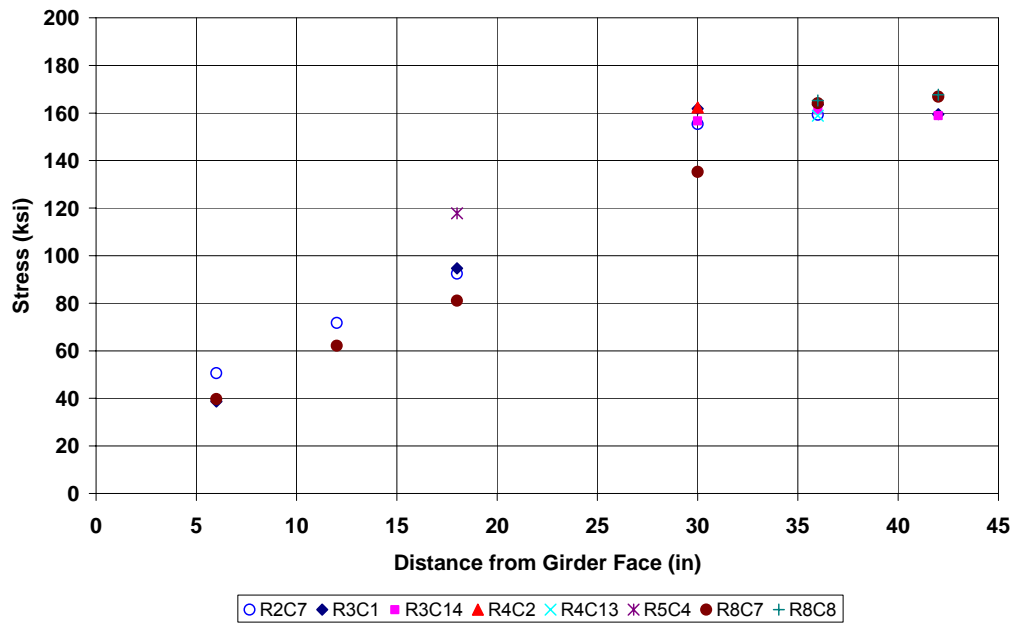


Figure 4-26: Tx46 Strand stresses at release for the dead end

While there is some scatter in the strand stress values initially, at around the transfer length all stress values converge and scatter is minimized. An examination of Figure 4-25 and Figure 4-26 indicates that the transfer length is approximately 36” at both ends. The elastic shortening related losses for the live end can be calculated by working out the difference between the previously reported average initial prestressing stress of 203.5 ksi and 179.3 ksi (from Figure 4-25). As a result, the experimentally obtained elastic shortening loss, 24.2 ksi, is very close to the previously calculated elastic shortening loss of 23.9 ksi.

4.5.3 Tx46 Transverse Reinforcing Bar Stresses

Vertical reinforcement was instrumented with strain gauges within the first 46” in each end. Within the first 30 inches every single bar was strain gauged. Every other bar located between a distance of 30-in. and 46-in. from the ends was strain gauged. The data gathered is shown in Figure 4-27 and Figure 4-28.

177

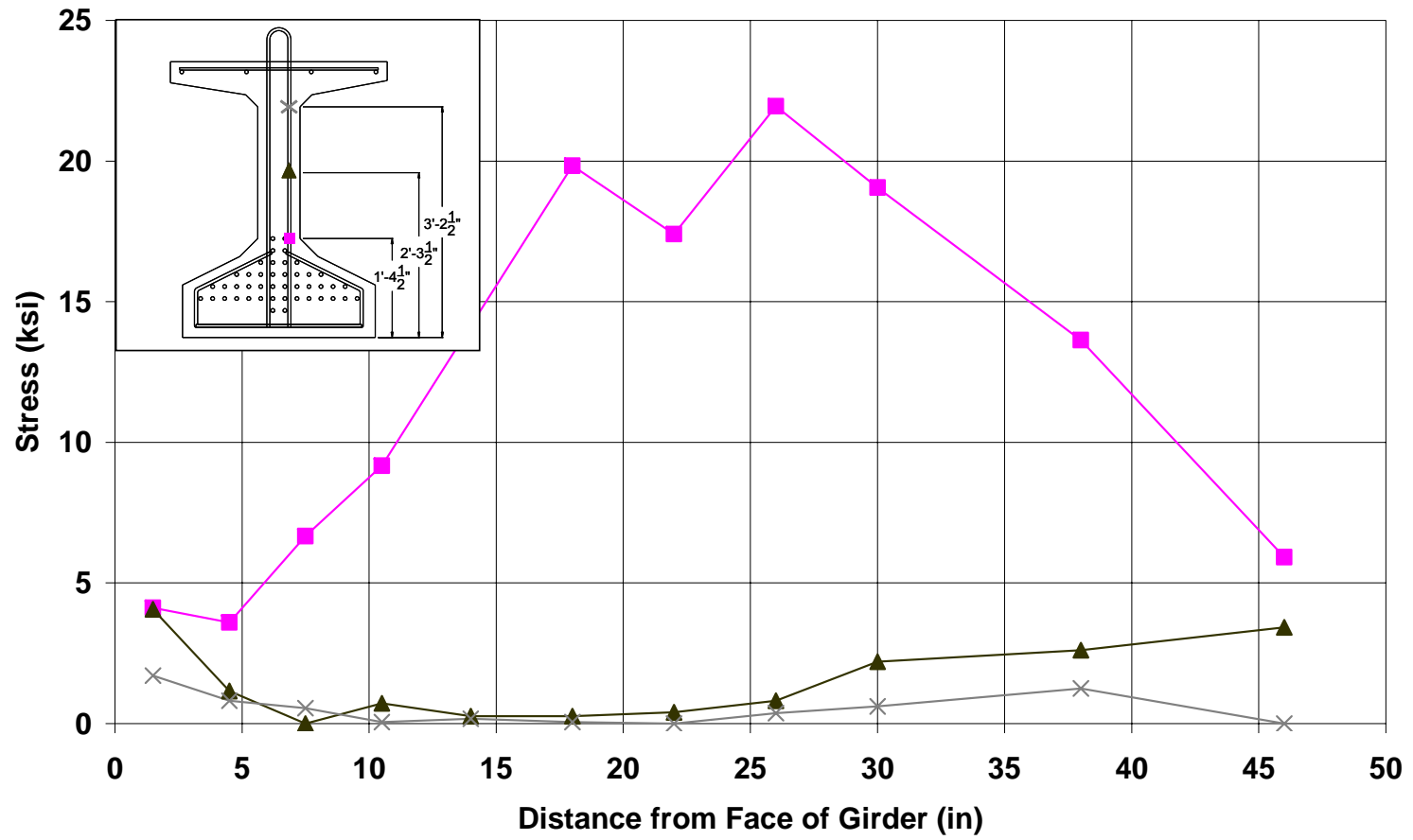


Figure 4-27: Tx46 Dead end transverse reinforcing bar stresses

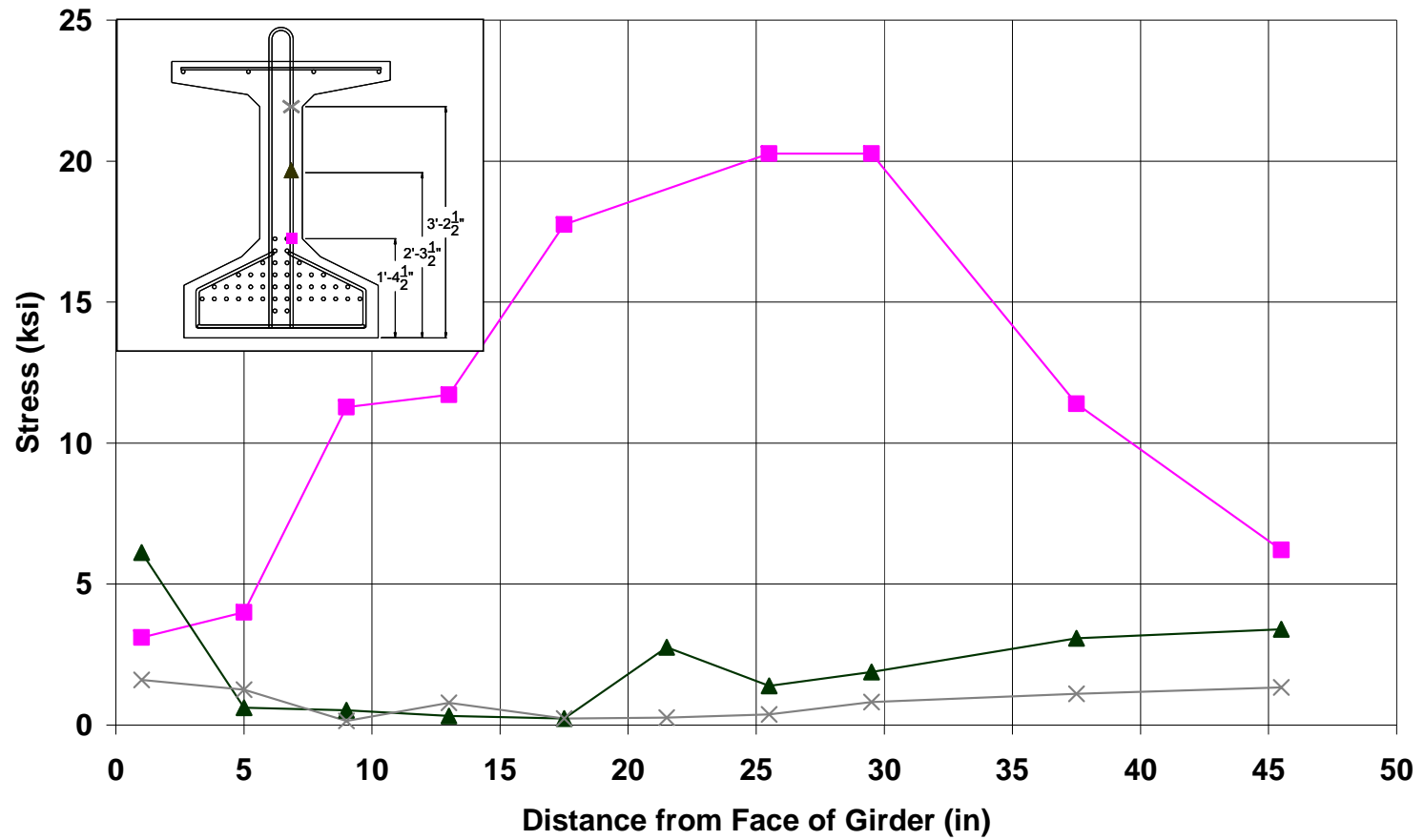


Figure 4-28: Tx46 Live end transverse reinforcing bar stresses

Data presented in Figure 4-27 and Figure 4-28 indicates that for Tx46, the dominant stresses were the bursting stress. The reinforcing bar stresses inferred from strain gauge readings reached a maximum value of 22 ksi and 20.3 ksi at the dead and live ends respectively. The maximum reinforcing bars stresses occurred at a distance of about 26" from the face of the girder.

It is also interesting to observe the trend of the reinforcing bar stresses at the mid height of the web. The reinforcing bar stresses at the mid-height of the web, close to the ends of the beams can be attributed to spalling stresses. Since the eccentricity of the prestressing force was roughly doubled in going from Tx28 ($e = 5.01$ in.) beam specimens to Tx46 ($e = 10.67$ in.), increased spalling stresses were recorded. While the stresses in the reinforcing bars at the mid height of the web close to the beam ends ranged from 4.1 ksi to 6.1 ksi for Tx46, these stresses quickly diminished to insignificantly small values. A quick review of the data obtained in testing Tx28-I and Tx28-II and presented earlier in this chapter indicates that the spalling induced stresses in Tx28-I and Tx28-II were a small fraction of 1 ksi for those beams.

An examination of the stresses plotted in Figure 4-27 and Figure 4-28 proves two facts: (i) the spalling reinforcement stipulated in AASHTO LRFD specifications is most effective close to the beam ends and as such the "h/4" distance referred to in AASHTO LRFD is appreciated. (ii) The magnitude of rebar stresses due to spalling ranging from 4.1 ksi to 6.1 ksi are far smaller than the magnitude of the bursting stresses ranging from 20.3 ksi to 22 ksi.

The cracks in Tx46 were less severe than the cracks observed in Tx28-II. Most, if not all, of the cracks observed in Tx46 were induced by bursting stresses. Only a few short and narrow (width < 0.005 ") cracks observed at the web the top flange connection and the mid-height of the web (Figure 4-29, Figure 4-30, Figure 4-31, and Figure 4-32) are attributed to spalling stresses.

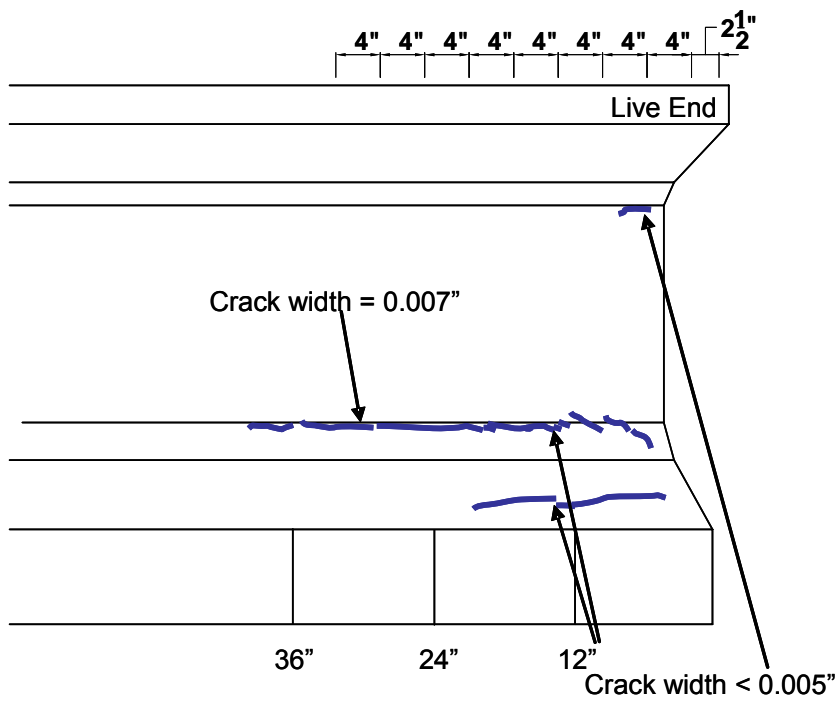


Figure 4-29: Tx46 Live end crack pattern

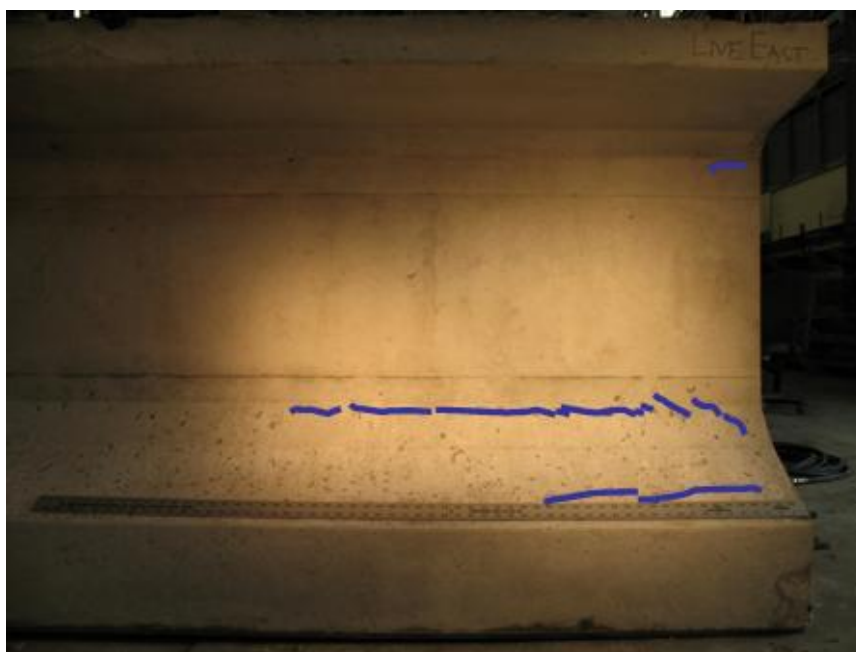


Figure 4-30: Tx46 Live end photo with crack pattern

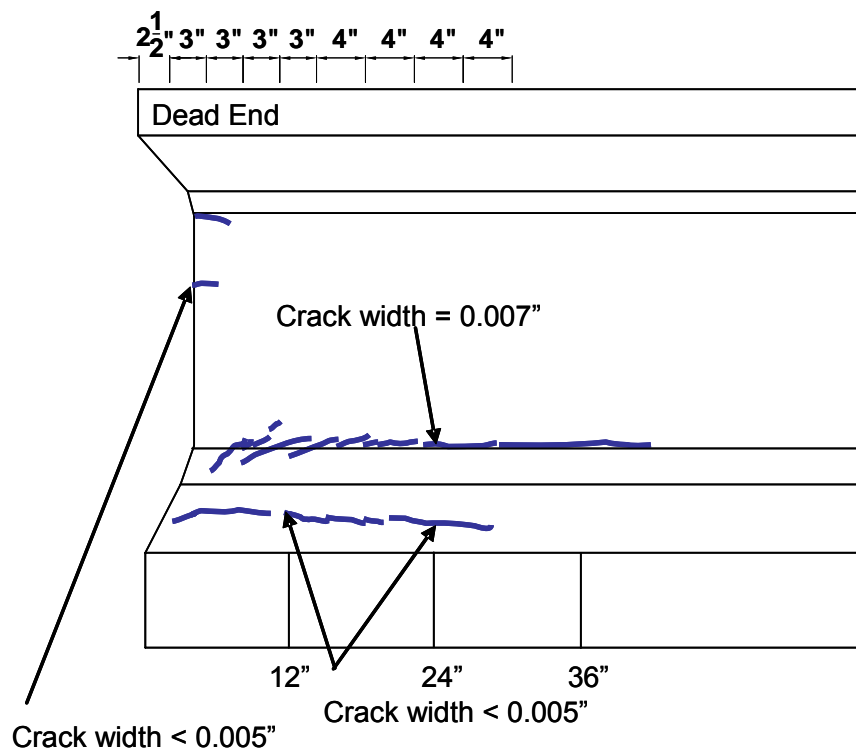


Figure 4-31: Tx46 Dead end crack pattern

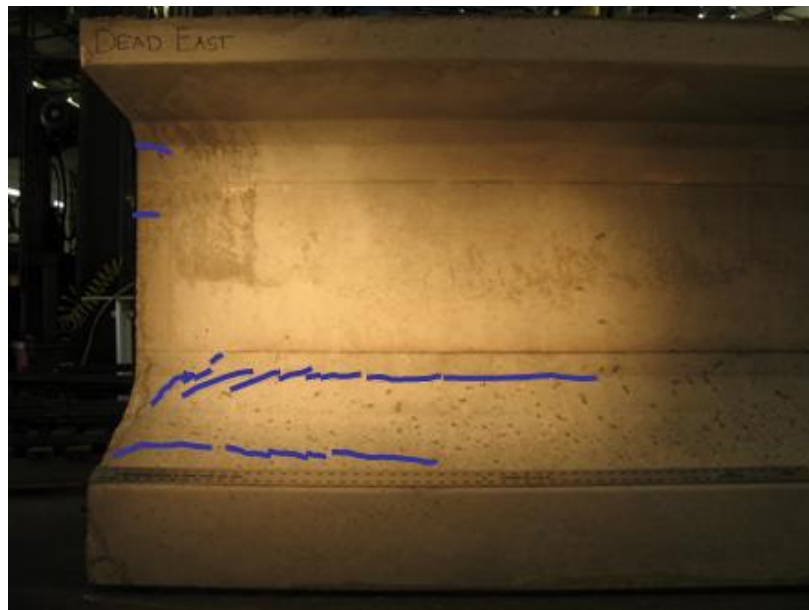


Figure 4-32: Tx46 Dead end photo with crack pattern

Crack patterns given in Figure 4-29, and Figure 4-31 on the two ends of the girder support the steel stress data shown in Figure 4-27 and Figure 4-28. A maximum crack width of 0.007" occurred at almost the exact location of maximum stress in the transverse steel. At 24" into the beam the bursting cracks reached their maximum width, but for the most part the widths of the bursting cracks remained at or below 0.005".

4.5.4 Tx46 Summary

The strand stresses inferred from strain gauges attached to the strands revealed that the transfer length of 36" calculated in accordance with AASHTO LRFD Bridge Design Specifications (2007) and ACI 318-05 is an accurate estimate. In addition, the elastic shortening values estimated using AASHTO LRFD Bridge Design Specifications (2007) are also realistic.

When it comes to the stresses in transverse reinforcing bars, some very interesting points can be made. Earlier estimations that the spalling stresses might increase with increasing eccentricity of applied load is supported by the data here. The transverse reinforcement near the end face was stressed to about 5 ksi and then the stress in the steel quickly diminished further into the end region. The bursting stresses once again controlled the primary cracks that formed in the end regions. Reaching a maximum stress in the steel of 22 ksi at 24" into the girder, the bursting stresses caused cracks that were typically 0.005" wide, with a maximum crack width of 0.007". When the stresses in the bars within the bursting region are examined, it can be seen that the stresses peak near the end of the transfer length and then drop off significantly by the time a distance of h is reached from the face of the beam. This observation supports the idea that the bursting stresses are directly affected by the transfer length and not the length of

the disturbed region. This observation will be revisited when data from Tx70 is interpreted in the subsequent sections.

4.6 TX70 RESULTS

The largest girder cast for this research project was 70 in. deep. Strain gauge, thermocouple, pressure and displacement transducer data was collected from almost 150 channels. The large number of channels required for data acquisition necessitated the use of 2 computers throughout the stressing, casting, and releasing process. The locations of the strain gauges did not change significantly from the test specimen Tx46. The vertical bars were strain gauged out to 70" from the end of the beam. The only other change involved installation of strain gauges at the centroid of the section rather than mid-height of the beam. The review of the technical literature indicated that most critical stresses were typically encountered at the centroid of the beam near the end face. It was with this information that strain gauges were installed along a line that followed the geometric centroid of the section in hopes of capturing the reinforcing bar strains exactly at the location of the maximum spalling stresses.

4.6.1 Tx70 Release

The concrete used to fabricate this beam also behaved well and reached the specified compressive release strength within 20 hours after placement. Concrete cylinders were tested from all 6 *Sure Cure* locations before and after release and gave an average strength of 6,675 psi. For the strand pattern shown in Chapter 3, and using AASHTO LRFD Bridge Design Specifications (2007), the elastic shortening can be calculated as follows:

$$E_p = 29,500 \text{ksi}$$

$$E_{ct} = 57,000 \cdot \sqrt{6,675} = 4,657 \text{ksi}$$

$$f_{egt} = \frac{42.9k \cdot (46 \text{strands})}{966 \text{in}^2} + \frac{42.9k \cdot (46 \text{strands}) \cdot (23.50 \text{in})^2}{628,747 \text{in}^4} + \frac{5k \cdot (4 \text{strands})}{966 \text{in}^2} - \frac{5k \cdot (4 \text{strands}) \cdot (36.42 \text{in})^2}{628,747 \text{in}^4}$$

$$f_{egt} = 3.75 \text{ksi}$$

$$\Delta f_{pES} = \frac{29,500}{4,657} \cdot 3.75 \text{ksi} = 23.8 \text{ksi}$$

4.6.1.1 Strand Stress before Release

Once again, the strands for this girder were gang-stressed using 4 hydraulic rams. As shown in Table 4-7, each strand was individually stressed by applying a ~2 kip load. After strands were taut, strain gauges were applied and reinforcing bars were installed. Just before concrete placement strands were gang-stressed to 42.9 kips / strand. The total prestressing force was 1,974 kips. It is important to note that this value was obtained through the stresses inferred from strain gauge readings and calibration curves.

Table 4-7: Stresses in prestressing strands before release

Specimen	Pre-Strain (in/in)	Avg. Strain (in/in)	Total Strain (in/in)	Avg. Stress (ksi)	Avg. Force (kips)	Total Force (kips)
Tx70	0.000373	0.005972	0.006345	197.8	42.9	1,974

As mentioned earlier prestressing force was always double checked and cross-referenced. The pressure readings recorded on each hydraulic line was multiplied by the area of the rams to calculate the total prestressing force to be equal to 2,048 kips. This value is slightly off (3.7%) the expected 1,974 kip value. The elongations measured from the linear potentiometers averaged to 4.46-in. The net elongation of the strands was calculated by subtracting out the 0.27” deflection

measured at the dead end. The net elongation of the strands was 4.19". This translated to an applied of 2,007 kips. This value more closely agrees (difference = 1.7%) with the prestressing force obtained from the strain gauge readings.

4.6.2 Tx70 Strand Stresses

As was the case for all test specimens, the transfer length was evaluated by analyzing the data from strain gauge readings. The strand stresses shown in Figure 4-33 and Figure 4-34 illustrate how the strand stresses ramp up within the first 42 inches of the beam.

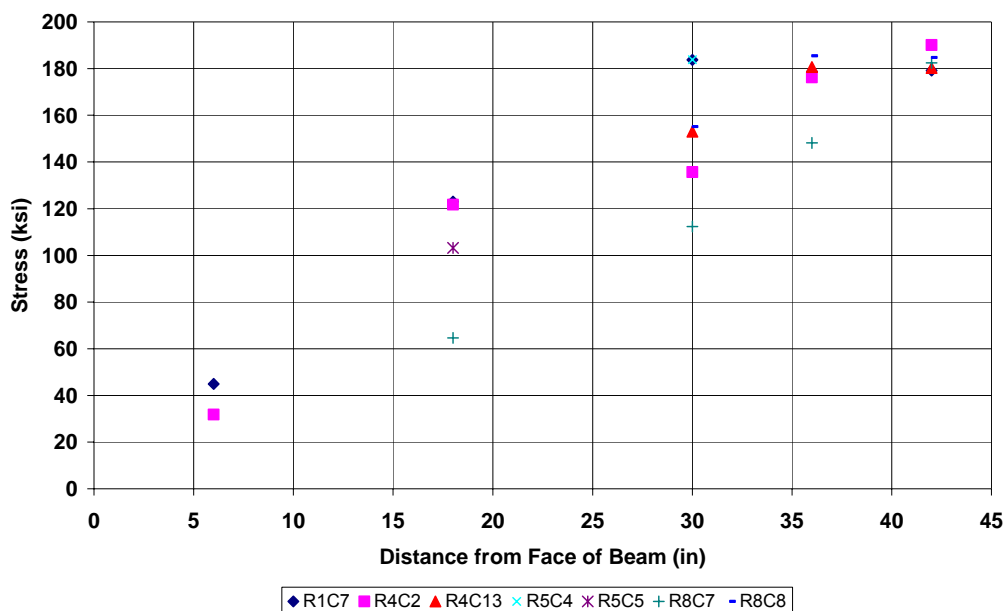


Figure 4-33: Tx70 Strand stresses after release for the live end

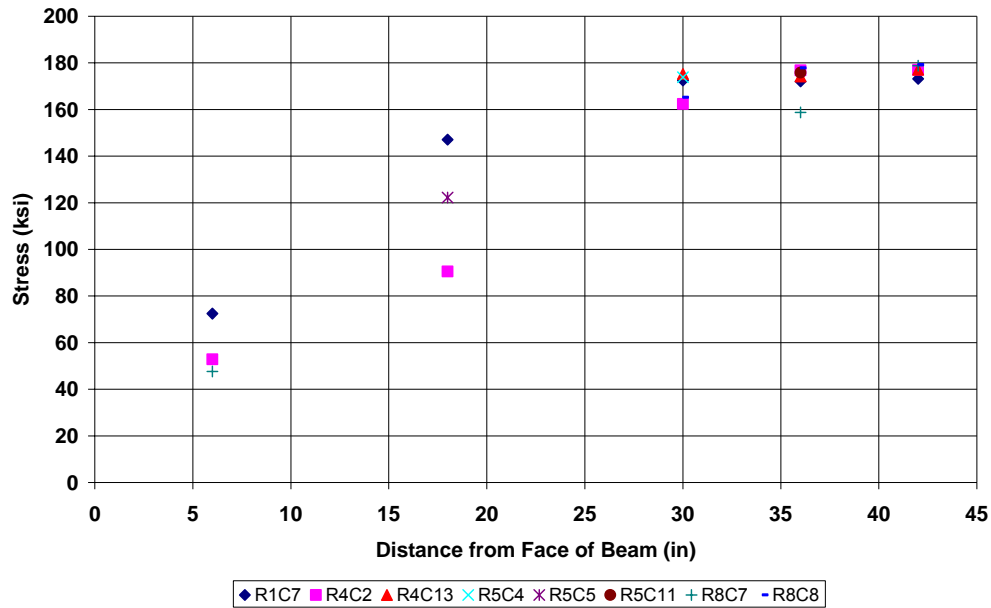


Figure 4-34: Tx70 Strand stresses after release for the dead end

The live and dead end strand stresses appear to ramp up and converge to a constant value at around 36". An examination of Figure 4-33 indicates that after release the maximum strand stresses is 183.4 ksi (calculated as an average of all of the measured values). As shown in Table 4-7, before release, the stress in the strands was equal to 197.8 ksi. Hence, the elastic shortening losses can be calculated as 14.4 ksi. It is important to note that the elastic shortening value is smaller than that calculated using AASHTO LRFD Bridge Design Specifications in Section 4.6.1 - 23.8 ksi. This discrepancy is attributed to the general scatter associated with the modulus of elasticity data. A lesser than predicted elastic shortening loss, implies that the prestressing force was slightly greater than the originally anticipated value. A slightly greater prestressing force after the elastic shortening creates a slightly more critical scenario for bursting and spalling stresses.

4.6.3 Tx70 Transverse Reinforcing Bar Stresses

Strain gauges were installed on vertical reinforcing bars within the first 70" measured from the beam's ends. The strain gauge line that was positioned at the mid-height of the previous girders where bursting stresses were more prevalent was moved down to the centroid of the cross-section so that rebar strains induced by spalling stresses could be captured at the most critical location, i.e. at the most critical horizontal spalling crack. The nearly 80 strain gauges used in the end regions did a thorough job of capturing the state of strain in the vertical steel at the end regions. The reinforcing bar strains captured after the release of the prestressing strands are summarized in Figure 4-35 and Figure 4-36.

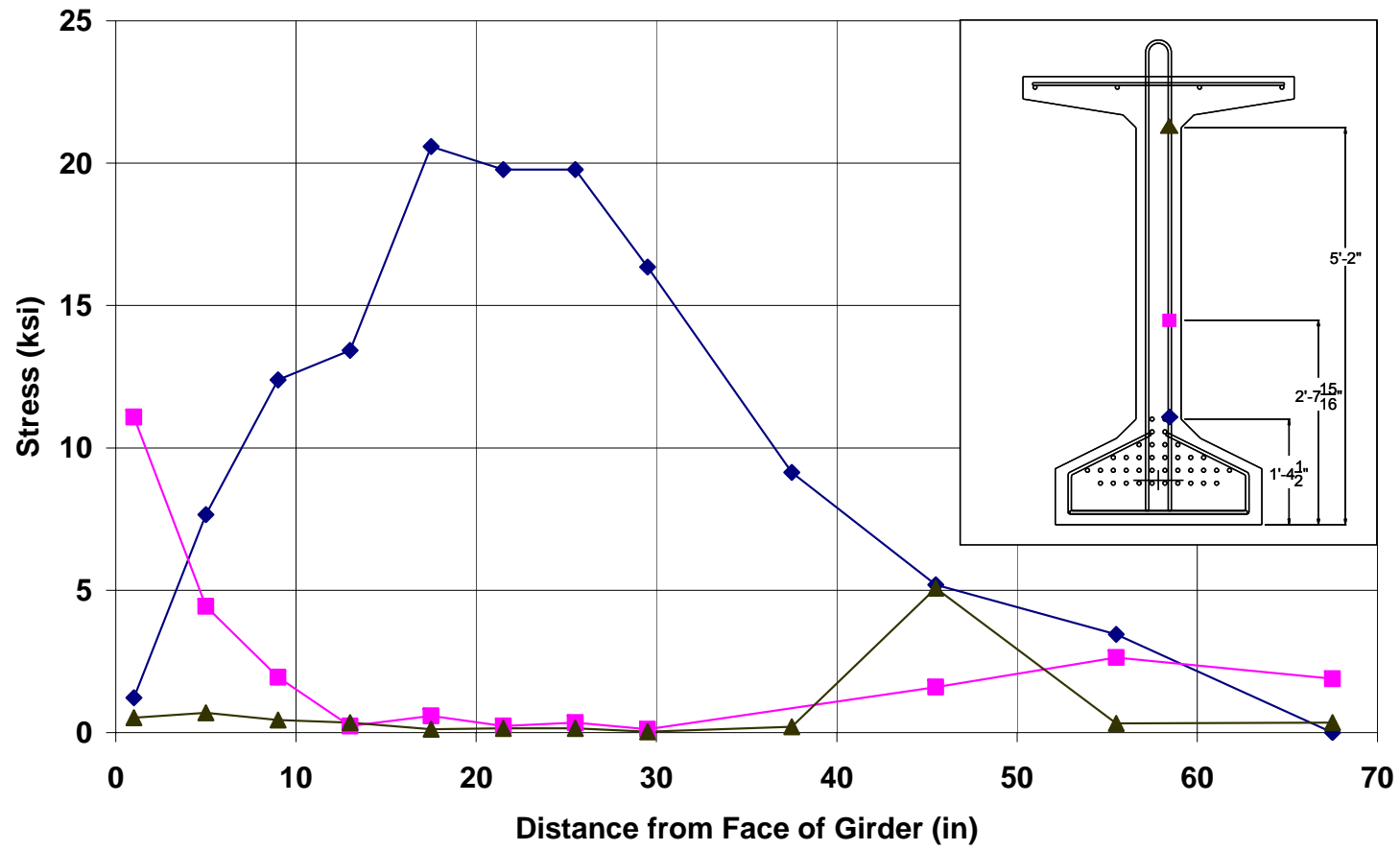


Figure 4-35: Tx70 Transverse reinforcing bar stresses for the live end

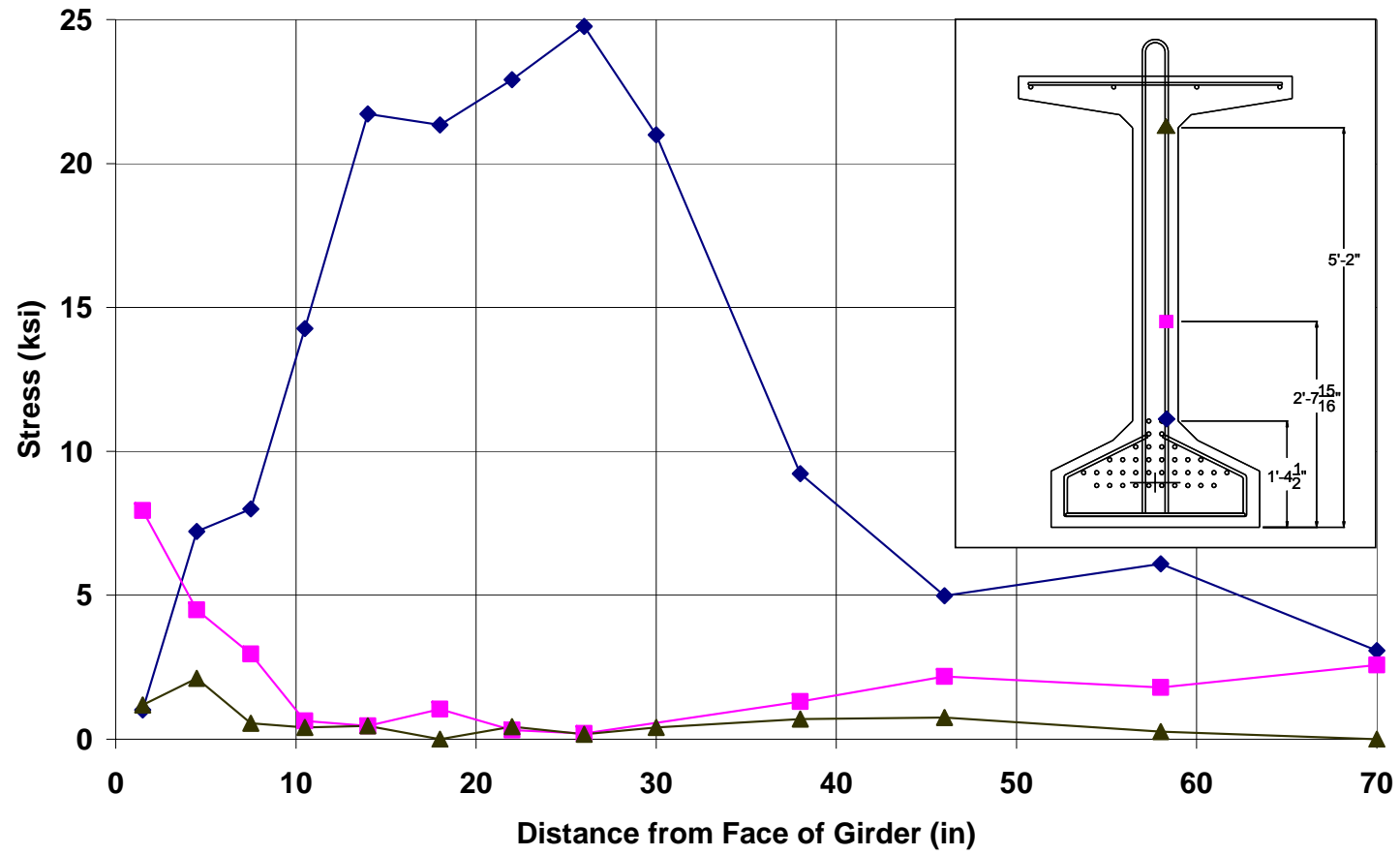


Figure 4-36: Tx70 Transverse reinforcing bar stresses for the dead end

Figure 4-35 and Figure 4-36 are considered to be the key figures shedding light to bursting and spalling stresses. An examination of these two figures highlight the following facts: (i) For both ends of the 70-in.-deep beam that was tested as part of this research study, bursting stresses, causing the large strains/stresses recorded at bottom flange to web connection, are more prevalent than the spalling stresses. (ii) As implied by the code provisions that make reference to the use of end region reinforcement within a distance of $h/4$ (AASHTO LRFD) or $h/5$ (PCI Design Handbook), spalling stresses were most critical within the first 12 inches.

The maximum stresses seen in Figure 4-35 and Figure 4-36 are 24.8 ksi in the dead end and 20.6 ksi at the live end. As usual, these stresses occur around 2 feet into the beam, i.e. close to the end of the transfer length, and then quickly taper off to very small values. These stresses, recorded at the bottom flange to web connection are directly attributed to bursting stresses.

The spalling stresses measured in Tx70 were the largest spalling stresses measured in any one of the test specimens. Transverse reinforcing bars closest to the face of the girders were stressed to 8-11 ksi at around the centroid of the cross-section. Since the prestressing force in Tx70 had the highest eccentricity, the spalling stresses were consequently maximized. In agreement with earlier research done by Tuan et al. (2004) and Marshall and Mattock (1962), spalling stresses taper off to nearly zero about 12 inches away from the face of the beam.

The crack patterns given in Figure 4-37, Figure 4-38, Figure 4-39, and Figure 4-40 are in substantial agreement with the reinforcing bar stresses reported in Figure 4-35 and Figure 4-36.

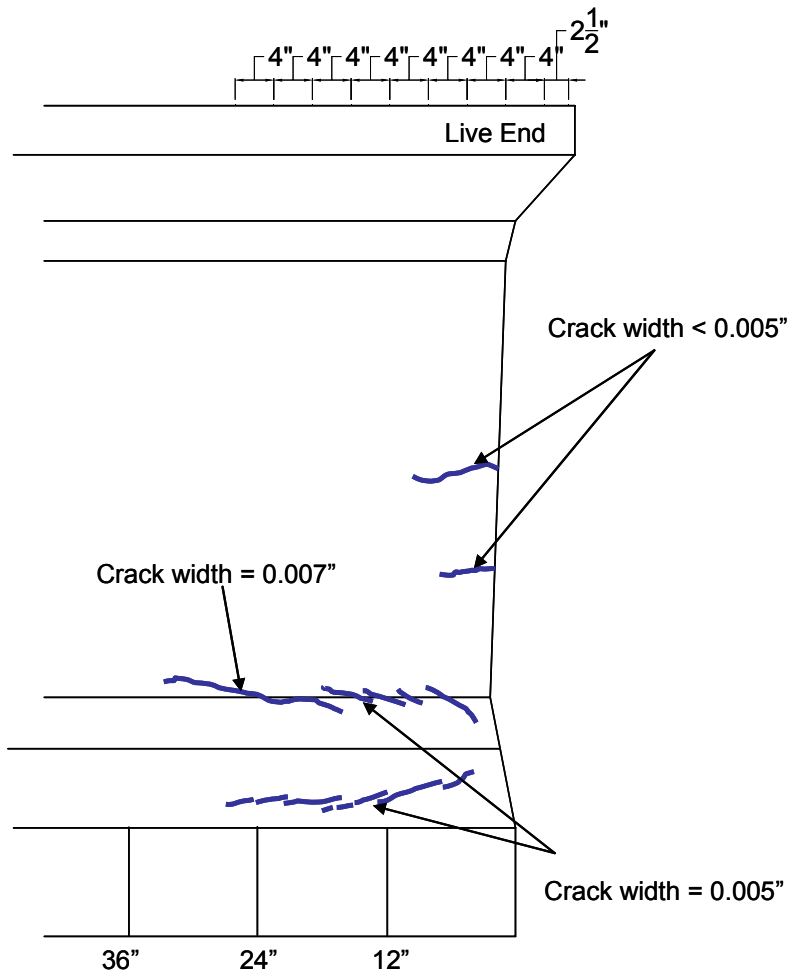


Figure 4-37: Tx70 Live end crack pattern



Figure 4-38: Tx70 Live end photo with crack pattern

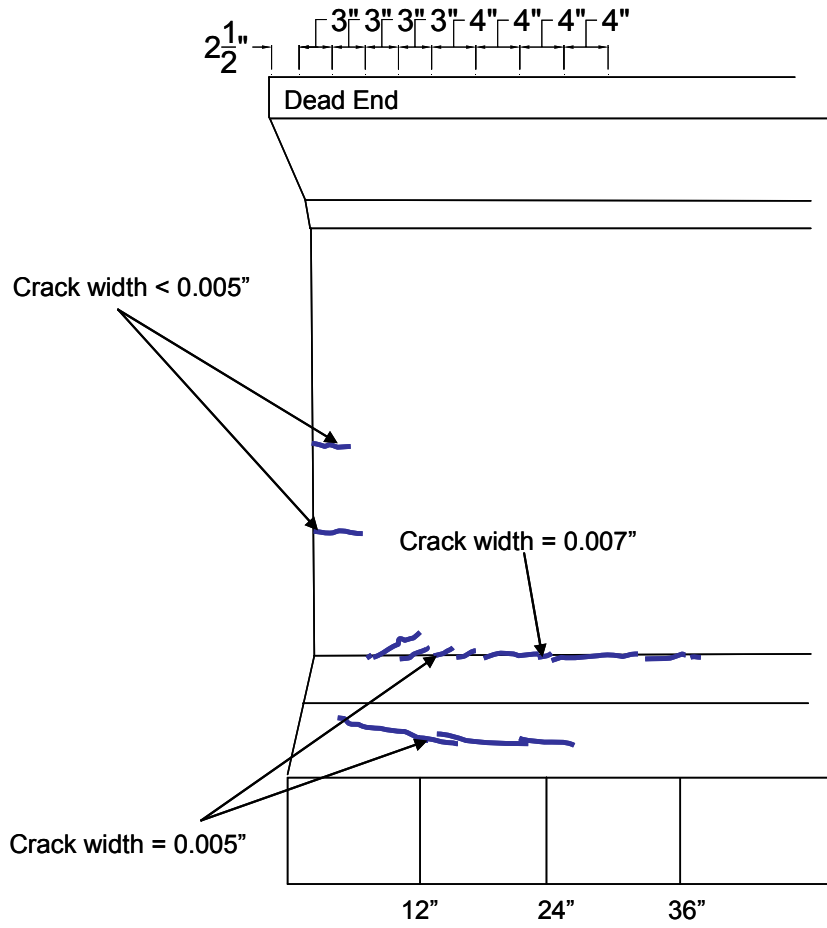


Figure 4-39: Tx70 Dead end crack pattern

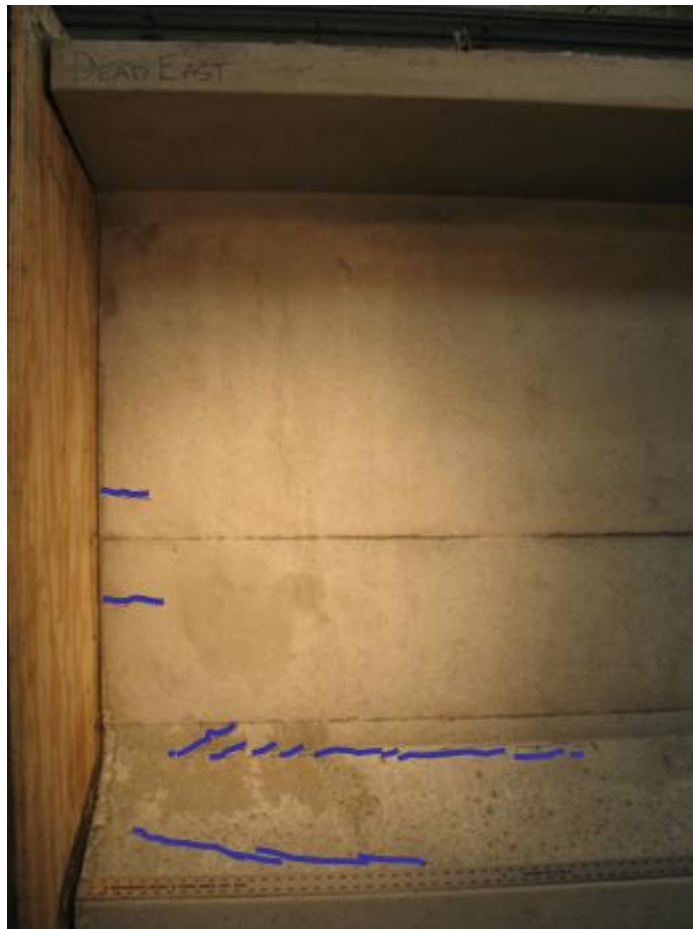


Figure 4-40: Tx70 Dead end photo with crack pattern

The crack patterns shown in Figure 4-37 and Figure 4-39 indicate that the maximum crack widths were measured near the maximum transverse reinforcing bar stress, i.e. around 2 feet into the beam. The crack width at this location in both ends is 0.007". These cracks are associated with the bursting stresses. It is also interesting to note that the spalling stresses found at the face of the girder were large enough to crack the beam. The widths of the spalling cracks were less than the lowest measurable value of 0.005" and hence those cracks can be classified as hairline cracks. Since a greater amount of transverse reinforcement

was used at the dead end, the length and widths of the cracks seen at the dead end were slightly smaller.

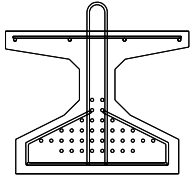
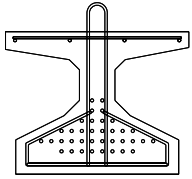
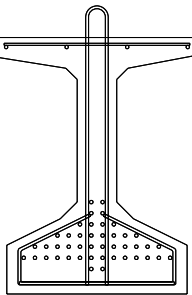
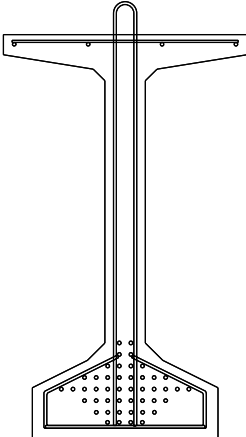
4.6.4 Tx70 Summary

Tx70 was the largest girder tested in this study. A nearly 2-million-pound prestressing force applied at an eccentricity of ~23 in., created means to study the effects of bursting and spalling stresses. Stresses inferred from the strain gauges applied to transverse reinforcing bars indicated that bursting stresses were more critical than spalling stresses. Whereas the maximum spalling stresses were measured close to the ends of the test specimen maximum bursting stresses were measured roughly 2-ft. into the beam and hence well into the 36” transfer length. Stresses in the reinforcing bars arresting spalling cracks were as high as 11 ksi, and those keeping the bursting cracks closed neared 25 ksi. It is important to note that additional reinforcement (bundled pairs of No.6 bars with the shear reinforcement) used within the $h/4$ region worked effectively in restraining spalling cracks. What is equally important to note is that the shear reinforcement used within the transfer length was the primary reason why bursting cracks were restrained.

4.7 RESULTS SUMMARY

Results from each test specimen were systematically discussed in the preceding sections. Within this section all test results will be collectively analyzed and primary conclusions of this research study will be established based on that analysis.

Table 4-8: Tx girder design summary

Section Sketch	Section Properties	Actual Applied P/S Force	Tendon Eccentricity	Cylinder Strength
<p style="text-align: center;">Tx28-I</p> 	<p>Height = 28" $A_g = 585\text{in}^2$ $I_x = 52,772\text{in}^4$ $I_y = 40,692\text{in}^4$ $y_t = 15.02''$ $y_b = 12.98''$</p>	<p>Initial: 1,591 kips</p> <p>After Losses: 1,466 kips</p>	5.01"	<p>Release: 10,025 psi</p> <p>Final: 13,825 psi</p>
<p style="text-align: center;">Tx28-II</p> 	<p>Height = 28" $A_g = 585\text{in}^2$ $I_x = 52,772\text{in}^4$ $I_y = 40,692\text{in}^4$ $y_t = 15.02''$ $y_b = 12.98''$</p>	<p>Initial: 1,692 kips</p> <p>After Losses: 1,522 kips</p>	5.01"	<p>Release: 6,475 psi</p> <p>Final: 11,375 psi</p>
<p style="text-align: center;">Tx46</p> 	<p>Height = 46" $A_g = 761\text{in}^2$ $I_x = 198,089\text{in}^4$ $I_y = 46,603\text{in}^4$ $y_t = 25.90''$ $y_b = 20.10''$</p>	<p>Initial: 1,945 kips</p> <p>After Losses: 1,732 kips</p>	10.67"	<p>Release: 6,500 psi</p> <p>Final: 13,200 psi</p>
<p style="text-align: center;">Tx70</p> 	<p>Height = 70" $A_g = 966\text{in}^2$ $I_x = 628,747\text{in}^4$ $I_y = 57,720\text{in}^4$ $y_t = 38.09''$ $y_b = 31.91''$</p>	<p>Initial: 1,974 kips</p> <p>After Losses: 1,754 kips</p>	22.91"	<p>Release: 6,675 psi</p> <p>Final: 11,575 psi</p>

4.7.1 Spalling Stresses: Summary

Table 4-8 illustrates the geometric properties and important attributes of all the specimens tested in this study. As can be seen in this table both the prestressing force and the eccentricity of the prestressing force increased with increasing beam depth. The spalling stresses inferred from the strains recorded for Tx28-I and Tx28-II were a small fraction of 1 ksi, i.e. negligibly small. As shown in Table 4-1, this agrees with the calculations from the CEB-FIP Model Code (1990). However, AASHTO LRFD Bridge Design Specifications (2007) and PCI Design Handbook (6th Ed.) guidelines include provisions for reinforcement design against spalling stresses regardless of the size of the pretensioned girder. As stated earlier, both of these provisions are incorrectly called out as bursting stress provisions when in reality the reinforcement calculated is meant to handle spalling stresses within the close proximity of the beam face. These spalling provisions are overly conservative in this case, but are in direct agreement with Guyon (1953). It was expected that as the eccentricity of the applied prestressing force increased, the spalling stresses would increase as well. Gergely et al. (1963), Uijl (1983), Stone and Breen (1984), and CEB-FIP MC 90 (summarized in Chapter 2) clearly recognize this fact. The rebar stresses induced by spalling stresses in the Tx46 reached a maximum of 6.1 ksi near the face of the girder. This level of stress was not high enough to cause noticeable cracks in the beam, but it does justify the use of spalling reinforcement. The calculations shown in Section 4.2 are for the Tx46 and they show that if the spalling stress provisions are met for this size girder, spalling stresses should easily be controlled. The Tx70 girder had a highly eccentric prestressing force (Table 4-8) and as a result the stresses in the transverse reinforcement close to the end of the beam doubled in comparison to the Tx46. The maximum value of 11 ksi in the transverse bar closest to the beam face was large enough to crack the

beam near the centroid of the section. Tuan et al. (2004) tested a 71-in. (1800 mm) deep girder that was designed in accordance with AASHTO LRFD Bridge Design Specification (2002). The maximum stress reported by the researchers was 12.9 ksi near the geometric centroid of the section and within the transverse bar closest to the beam end. Their beam also cracked near the centroid. In this regard their research findings are similar to the research findings reported in this document.

4.7.1.1 Spalling Stresses: Recommendations

The table shown below gives the total amount of spalling force resisted by the transverse bars within each beam. This force was calculated by summing the force in each reinforcing bar within the first $h/4$ of the beam.

Table 4-9: Spalling forces

Girder	$h/4$ (in)	e (in)	Total Force (kips)	Total P/S Force Applied (kips)	% of Total P/S Force Applied	Max Stress in Steel (ksi)	Cracks Present
Tx28-I Live	7	5.01	3.0	1468	0.20 %	3.36	No
Tx28-I Dead	7	5.01	3.6	1468	0.25 %	3.83	No
Tx28-II Live	7	5.01	5.9	1472	0.41 %	4.23	No
Tx28-II Dead	7	5.01	1.4	1472	0.10 %	0.93	No
Tx46 Live	11.5	10.67	6.4	1730	0.37 %	6.12	Yes
Tx46 Dead	11.5	10.67	5.2	1730	0.30 %	4.06	Yes
Tx70 Live	17.5	22.91	15.6	1849	0.84 %	11.08	Yes
Tx70 Dead	17.5	22,91	14.1	1849	0.76 %	7.95	Yes

From Table 4-9 it is apparent that even though forces remain less than 1 percent of the total prestressing force, the eccentricity of the load has an adverse effect on spalling stresses. It is interesting to note that the percentages reported for the

dead ends of the beams are smaller than those reported for the live ends. This is directly attributed to the use of more steel (20 % more) in the dead end than in the live end. While it may be tempting to recommend that the transverse reinforcement in the end regions can be designed based on a smaller percentage of the prestressing force (for example: 2% to match AASHTO LRFD (2007) post-tensioned spalling forces) based on the data reported in Table 4-9, this would be the wrong conclusion to reach. As shown in Table 4-9, different levels of prestressing force and different eccentricities were used in conducting eight tests on four girders. It is entirely possible that the most critical condition (higher prestressing force, higher eccentricity, and presence of deflected strands) may not have been considered as part of this study. In addition, the widths of the cracks seen in the spalling regions were slightly under the acceptable crack widths. If less reinforcement is used, cracks will get wider and epoxy injection and/or other remediation measures will be required. In conclusion, current AASHTO LRFD (2007) provision 5.10.10.1, currently incorrectly defined as a bursting provision, is considered to be conservative and appropriate for the design of spalling reinforcement for the Tx-family of beams tested during the course of this investigation.

4.7.2 Bursting Stresses: Summary

All four test specimens experienced significant bursting stresses upon release of the prestressing strands. The reinforcing bars resisting bursting stresses in the Tx28-I experienced a maximum stress of 22 ksi, in spite of a significantly higher concrete compressive strength at release (10,025 psi actual vs. 6,500 psi specified release strength). This was coupled with a maximum crack width of 0.005". This crack width was slightly smaller than what was seen in other girders subjected to a similar prestressing force. This is largely related to the increased

tensile capacity of the higher strength concrete at release. The crack pattern that was seen in the Tx28-I directly agrees with the smaller girders tested by Uijl (1983). Significantly higher transverse reinforcing bar stresses as well as the largest crack widths were seen in the Tx28-II girder. Transverse rebars resisting bursting stresses were stressed to 32 ksi and at the location where the maximum crack width of 0.009” was measured. As can be seen in Table 4-8, the prestressing force was slightly higher in Tx28-II in comparison to Tx28-I. The higher prestressing force and lower compressive strength of concrete at release (Table 4-8) more than likely resulted in the high transverse rebar stresses as well as slightly larger crack widths. Tx46 and Tx70 both behaved very similar to each other and in complete agreement with the previous two beams. The transverse bars in the bursting region of Tx46 reached a maximum stress of 22 ksi with a maximum crack width at this location of 0.007”. The transverse bars in the bursting region of Tx70 reached a maximum steel stress of 25 ksi with a crack width at this location of 0.007”. Table 4-10 shows a complete summary of all transverse rebar stress values and crack widths from the bursting and spalling stress regions of all the test specimens.

Table 4-10: Transverse rebar stresses and crack widths in the end regions

Girder	Applied P/S Force per Strand (kips)	Transfer Length (in)	Max Spalling Stress (ksi)	Max Spalling Crack Width (in)	Max Bursting Stress (ksi)	Max Bursting Crack Width (in)
Tx28-I	44.2	30”	0.0	0.000”	22	0.005”
Tx28-II	47.0	36”	0.0	0.000”	32	0.009”
Tx46	44.2	36”	6.1	hairline	22	0.007”
Tx70	42.9	36”	11.0	<0.005”	25	0.007”

Another point that must be recognized relates to the rapid decay of bursting stresses. The transverse reinforcing bar stresses are at their peak value at or just before the transfer length is reached. The stresses diminish very quickly after this point (Figure 4-41 and Figure 4-42). By the time the distance h is reached the transverse bars in larger beams are virtually unstressed. The shallower girders (Tx28-I and Tx28-II) are still under high transverse tensile stresses at h only because this value is less than the transfer length of the strand. This shows that the transfer length is directly related to the transverse stresses within the bursting region which agrees with the bursting provisions recommended by Uijl (1983) and the CEB Bulletins (1987, 1992).

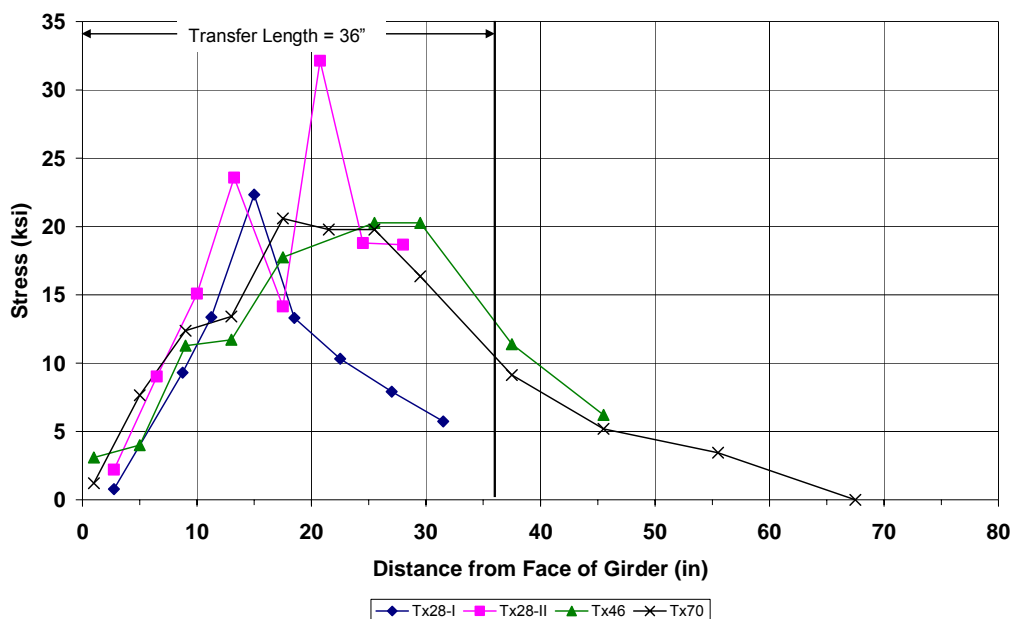


Figure 4-41: Live end bursting stresses for all Tx girders

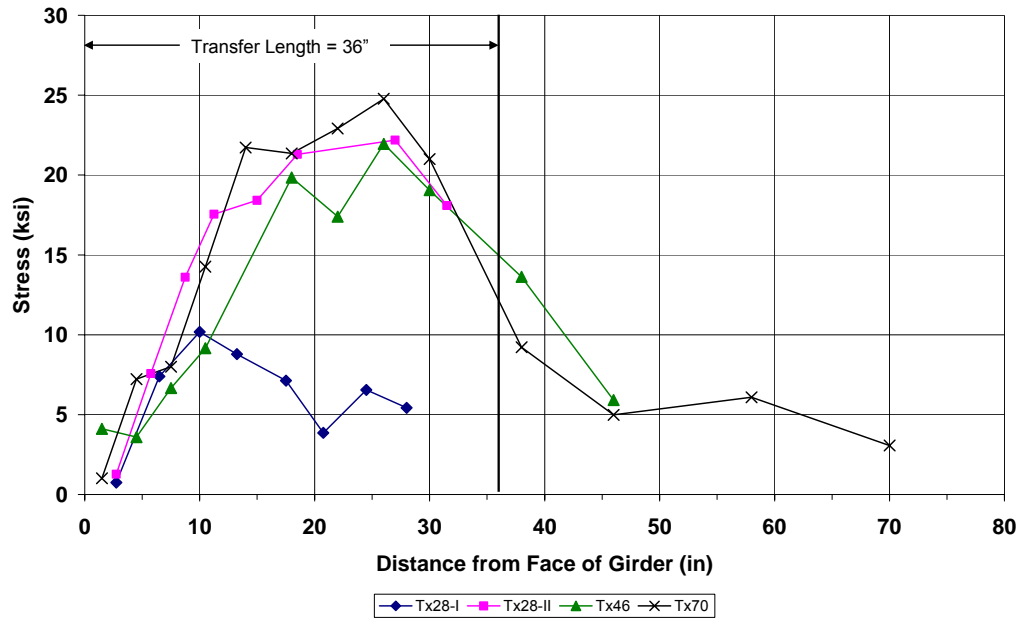


Figure 4-42: Dead end bursting stresses for all Tx girders

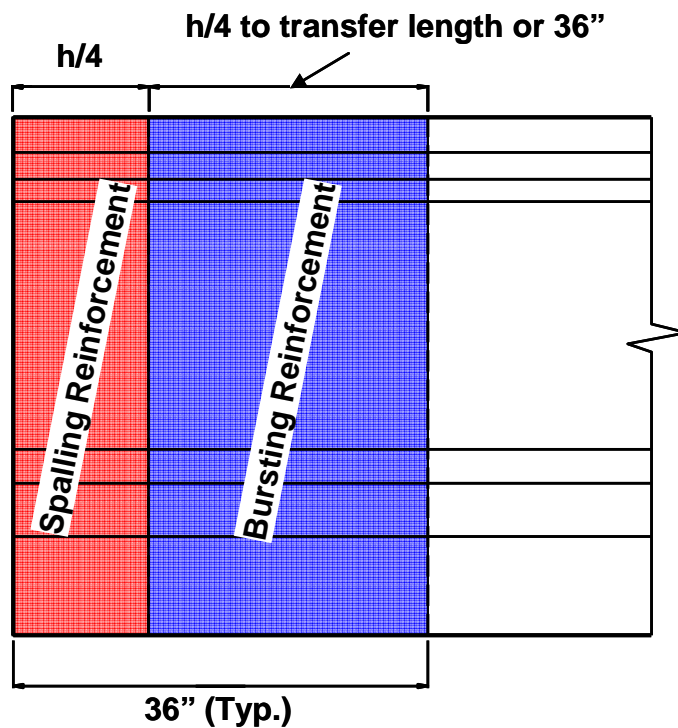
4.7.2.1 Bursting Stresses: Recommendations

The bursting forces resisted by the transverse steel in the pretensioned beam specimens are summarized in Table 4-11. As mentioned earlier the bursting stresses appear to decrease rapidly sometime before the full transfer length is reached. An examination of the crack patterns presented earlier in this chapter (Figure 4-12 - Figure 4-15, Figure 4-21 - Figure 4-24, Figure 4-29 - Figure 4-32, Figure 4-37 - Figure 4-40) indicates that cracks induced by bursting stresses are contained within the first 36 inches. In a few cases, the cracks are a few inches longer. Based on the experimental observations on the location and length of the cracks and transverse stresses inferred from the rebar strain measurements, it can be concluded that the placement of the bursting steel can be stopped at the end of transfer length. The bursting reinforcement should be placed immediately after the spalling reinforcement. The distance that the bursting steel would be placed in

should be from $h/4$ to the transfer length (Figure 4-43). Table 4-11 shows the total force in the transverse reinforcement as well as the percentage of the total prestressing force for the bursting region in each girder.

Table 4-11: Bursting forces

Girder	l_t (in)	$h/4$ to 36" (in)	Total Force (kips)	Total P/S Force Applied (kips)	% of Total P/S Force Applied	Max Stress in Steel (ksi)	Cracks Present
Tx28-I Live	30	23	32.0	1466	2.18 %	22.33	Yes
Tx28-I Dead	30	23	16.5	1466	1.13 %	10.18	Yes
Tx28-II Live	36	29	48.2	1522	3.17 %	32.13	Yes
Tx28-II Dead	36	29	38.8	1522	2.55 %	22.18	Yes
Tx46 Live	36	24.5	35.5	1732	2.05 %	20.27	Yes
Tx46 Dead	36	24.5	36.7	1732	2.12 %	22.00	Yes
Tx70 Live	36	24.5	35.4	1754	2.02 %	20.59	Yes
Tx70 Dead	36	24.5	44.0	1754	2.51 %	24.77	Yes



Location for additional transverse steel

Figure 4-43: Recommended locations for additional transverse steel

It is important to appreciate that the shear reinforcement was effective in resisting the bursting stresses. That said, in the worst case the stresses in the shear reinforcement was higher than 32 ksi. Considering the fact that the primary purpose of the shear reinforcement is to reinforce the beam against shear stresses and that at release roughly 50% of the yield stress was exploited by bursting effects, it is clear that there is a need to use additional bursting reinforcement. Figure 4-44 shows both the reinforcement of both end regions tested during the course of this research and Figure 4-45 shows the reinforcement details recommended to be used in the Tx-family of beams for the reasons explained

above. Bars S in both figures refer to the additional spalling or bursting reinforcement in the form of No.6 bars. Bars R refer to the No.4 bars used as shear reinforcement.

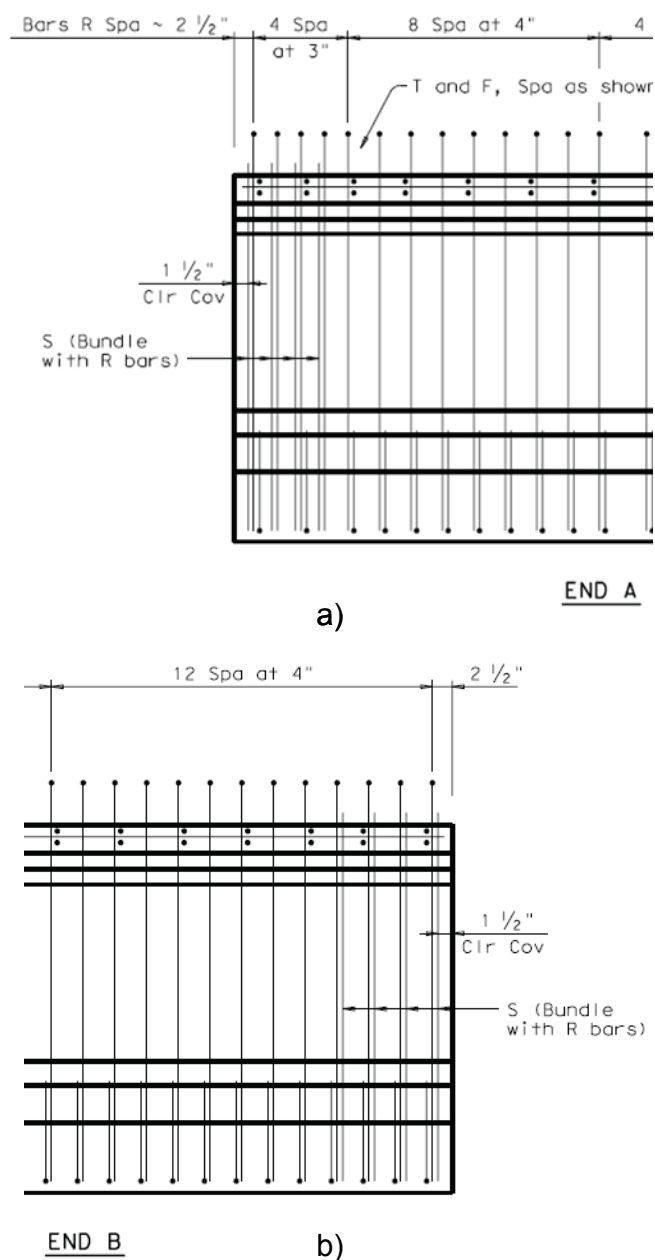


Figure 4-44: Original end region reinforcement: a) Dead end; b) Live end

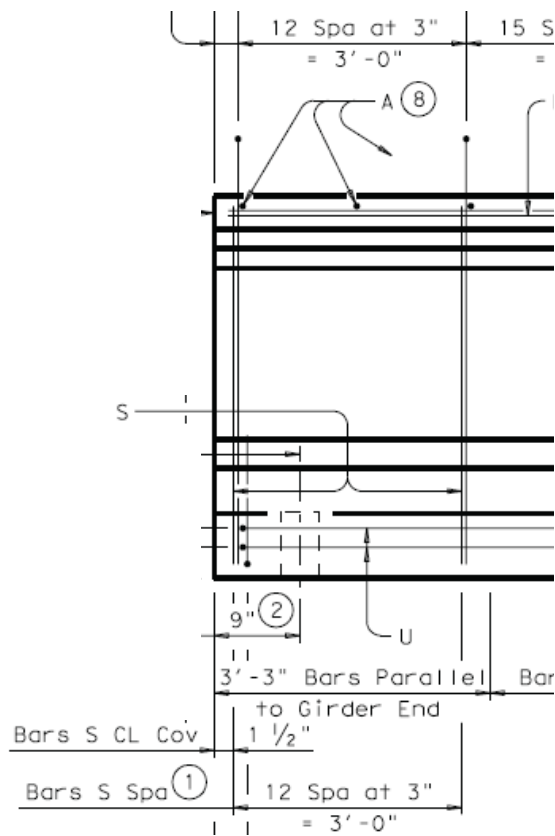


Figure 4-45: Suggested end region detail (Bars S refer to spalling and bursting reinforcement - No.6 bars)

As shown in Table 4-11 the typical load resisted by the bursting reinforcement was somewhere between 1.1 % and 3.2 % of the total prestressing force applied. Based primarily on the experimental data gathered during the course of this project, in order to be consistent with AASHTO LRFD Bridge Design Specifications (2007), and to be conservative the following recommendations are made:

5.10.10.3 – Factored Bursting Resistance (*Proposed*):

The bursting resistance of pretensioned anchorage zones provided by vertical reinforcement in the ends of pretensioned beams at the service limit state shall be taken as:

$$P_r = f_s A_s \qquad \text{Equation 4-18}$$

where:

f_s = stress in steel not exceeding 20 ksi

A_s = total area of transverse reinforcement located within the region bounded by the distance $h/4$ from the end of the beam and transfer length of the strands or 36-in. whichever is greater (in^2)

h = overall depth of precast member (in)

P_r = bursting resistance force

The resistance, (P_r) shall not be less than 4 percent of the prestressing force at transfer.

Based on the experimental evidence gathered in this investigation it is felt that if the above design recommendation is followed, cracking in the bursting region will be controlled, i.e. the widths, lengths, and the number of cracks will be reduced. In addition, transverse reinforcement placed to resist the shear stresses will not be over-taxed by having to resist the bursting stresses. This provision could be compared to the spalling provision that was already tested in this research in that it will add additional bars to be bundled with the shear reinforcement. Maximum stresses measured in the shear reinforcement in the bursting region reached 32 ksi, but if additional bundled No.6 bars were to be added the amount of transverse reinforcement would increase by a factor of 3.2 $((0.2 \cdot 2 + 0.44 \cdot 2)/(0.2 \cdot 2))$. This

increase would reduce the stress level in the transverse reinforcement by roughly 69%. In other words the stresses would reduce to 10 ksi from 32 ksi. It must be recognized that this assertion is based on calculations rather than data since bundling No.6 bars within the bursting region was not tested.

Another important comparison that can be made shows that the end-region reinforcement details given in Figure 4-45 meet the suggested design recommendations. The original designs met the PCI recommendations and contained slightly less reinforcement than those required by AASHTO LRFD specifications for spalling steel, but there was no additional bursting reinforcement. The end-region reinforcement detail suggested by the design recommendation presented above requires the use of an additional 3 to 4 in² of reinforcement for the new Tx I-girders. This amounts to an additional 10 – #6 bars within each end region. This small amount of reinforcement will not cause any major adjustments to construction, but will help control bursting cracks within the end regions of Tx family of beams.

One final point should be made regarding the code provisions and design guidelines. It is interesting to note that the current ASHTO LRFD (2007) provisions correctly define prestressed anchorage zone stresses, but only within the post-tensioned provisions. These forces shown in Figure 4-46 and Figure 4-47 are handled in pretensioned beams with the following provisions:

- a) Edge tension force – T_2 – 5.9.4.1.2 – Tension Stresses
- b) Spalling force – T_1 – 5.10.10.1 – Factored Spalling Resistance
- c) Bursting force – T_3 – 5.10.10.3 (*Proposed*) – Factored Bursting Resistance

The provisions suggested here are meant to be simple and conservative for designers to detail bursting and spalling regions of pretensioned beams.

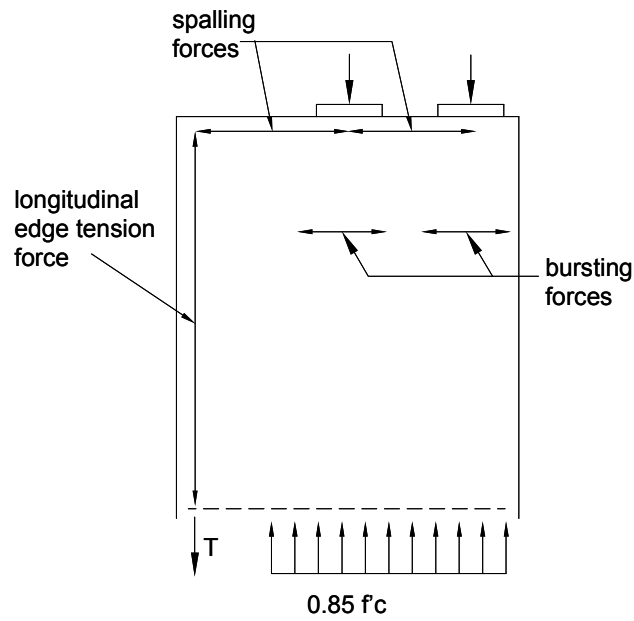


Figure 4-46: Tensile stress zones (Breen et al., 1994)

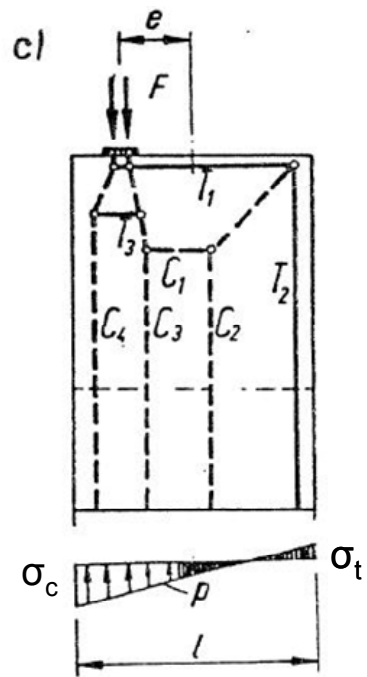


Figure 4-47: Typical strut-and-tie model for a post-tensioned beam. (Schlaich et al., 1987)

CHAPTER 5

Summary, Conclusions, and Recommendations

5.1 SUMMARY OF THE RESEARCH PROGRAM

The Texas Department of Transportation noticed inconsistencies between research results and code provisions for spalling and bursting reinforcement while developing design standards for a new family of prestressed concrete I-beams. Consequently, an interagency testing contract was established between the University of Texas at Austin and the Texas Department of Transportation to investigate end region stresses and to arrive at simple details that can be used in the new TxDOT I-Beams.

A research study was conducted at the Phil M. Ferguson Structural Engineering Laboratory at the University of Texas at Austin to investigate the cracking in end regions of prestressed I-girders at prestress transfer. This horizontal cracking near the end face of the girder is caused by the tensile forces that develop perpendicular to the line of action of the prestressing force after it has been applied. After seeing this cracking occur in multiple girders throughout the state of Texas, the Texas Department of Transportation sponsored this research to investigate this end region cracking problem. Many other states, including Florida and Washington, have experienced similar problems with their I-girders further supporting the need for experimental research. The goals of this research were to:

- i. Ensure that the cracks forming in the end regions of new I-Beams are comparable to or less severe than those in conventional AASHTO girders or TxDOT beams.

- ii. Quantify the amount of end region reinforcement that should be used in the new I-Beams to ensure that the quality of the new I-Beams, that have larger bottom flanges and greater prestressing force, is comparable to or better than the conventional AASHTO girders or TxDOT beams.

Within this research program an extensive literature review was conducted to help define the stresses found in the end regions of pretensioned girders at release and to show how they can best be controlled. In addition to research studies, AASHTO LRFD Bridge Design Specifications (2007), PCI Design Handbook (6th Edition), and CEB-FIP Model Code 1990 were all reviewed in relation to bursting, spalling, and splitting stresses in the end regions of prestressed girders.

The experimental program included the fabrication of 4 full scale beams from the new Tx-family of girders. Two 28", one 46", and one 70" deep girders were fabricated and tested. The testing of four 30-ft-long full-scale beams resulted in 8 test regions. The test regions at the two ends of each girder had different transverse reinforcement details. Each end region was comprehensively instrumented by strain gauges to capture the most critical strains. The strain gauge data collected at the release of the prestressing strands were used to prepare new design criterion to control the widths of the cracks that form in the end regions of pretensioned girders at release.

5.2 CONCLUSIONS AND RECOMMENDATIONS

The conclusions and recommendations presented herein are based on the experimental evidence gathered during the course of this research study. The primary conclusions regarding AASHTO LRFD Bridge Design Specifications can be summarized as follows:

- Provision §5.10.10.1 of AASHTO LRFD Bridge Design Specifications (2007) called “*Factored Bursting Resistance*” is actually a provision for spalling reinforcement. This code provision is named incorrectly and the naming of this section should be corrected as follows:

5.10.10.1 – Factored ~~Bursting~~ Spalling Resistance:

The ~~bursting~~ spalling resistance of pretensioned anchorage zones provided by vertical reinforcement in the ends of pretensioned beams at the service limit state shall be taken as:

$$P_r = f_s A_s$$

where:

f_s = stress in steel not exceeding 20 ksi

A_s = total area of vertical reinforcement located within the distance $h/4$ from the end of the beam (in^2)

h = overall depth of precast member (in)

P_r = bursting resistance force

The resistance shall not be less than 4 percent of the prestressing force at transfer. The end vertical reinforcement shall be as close to the end of the beam as practicable

- AASHTO LRFD Bridge Design Specifications (2007) and the PCI Design Handbook (6th Edition) both supply recommendations on how best to control the widths of the spalling cracks. Only the CEB-FIP Model Code (1990) has provisions for detailing both spalling and bursting regions. The fact that the AASHTO LRFD Bridge Design Specifications (2007) do not contain provisions for bursting reinforcement has a negative impact on the performance of pretensioned beams. While the shear reinforcement provided in pretensioned girders is effective to restrain the bursting cracks from opening, the data collected

during the course of this study demonstrated that slightly more than 50% of the capacity of shear reinforcement was exploited by bursting stresses in some cases. As such, the use of additional transverse reinforcement (i.e. bursting reinforcement) within the bursting region is recommended. Simple design guidelines to this end were developed during the course of this research study and these recommendations were based on the performance of eight test regions of four full-scale test specimens. The bursting reinforcement design recommendations were developed by studying the cracks and the transverse reinforcement stresses in bursting regions. These recommendations are as follows:

5.10.10.3 – Factored Bursting Resistance (*Proposed*):

The bursting resistance of pretensioned anchorage zones provided by vertical reinforcement in the ends of pretensioned beams at the service limit state shall be taken as:

$$P_r = f_s A_s$$

where:

f_s = *stress in steel not exceeding 20 ksi*

A_s = *total area of transverse reinforcement located within the region bounded by the distance $h/4$ from the end of the beam and transfer length of the strands or 36-in. whichever is greater (in²)*

h = *overall depth of precast member (in)*

P_r = *bursting resistance force*

The resistance, (P_r) shall not be less than 4 percent of the prestressing force at transfer.

It is important to recognize that the bursting steel is to be used in addition to spalling steel. In this way, additional transverse reinforcement provided within the transfer length will reduce the crack widths in the end region. More importantly, the stresses in the shear reinforcement will be reduced substantially and additional reinforcement provided within that region will also help improve the shear strength.

5.2.1 Spalling Stresses: Concluding Observations

- 1) For the specimens tested in this study, as the eccentricity of the prestressing force increased so did the magnitude of spalling stresses in the end regions of the pretensioned test specimens. The quantity and length of cracks also increased with increasing eccentricity.
- 2) The maximum stress seen in reinforcement closest to the face of the 70" deep girder was 11 ksi and at this location the crack width was below the measurable value of 0.005". Although the amount of spalling reinforcement provided just barely meets AASHTO LRFD provisions, the stresses measured in spalling reinforcement were less than the 20 ksi limit stipulated in the code. Since the spalling crack widths were very narrow and stress levels in the spalling reinforcement were well below the code limit, the use of the spalling reinforcement detail (additional No.6 bars bundled with No.4 shear reinforcement spaced at 3-in. o.c. within a distance $h/4$ from the beam's face) tested during the course of this study is recommended for use in the new I beams (Tx family of beams).

5.2.2 Bursting Stresses: Concluding Observations

- 1) Bursting stresses were more pronounced than spalling stresses in all of the pretensioned beams tested during the course of this research study.

- 2) The eccentricity of the prestressing force had no discernable effect on the level of bursting stresses for the pretensioned beams tested in this study. Bursting stresses appeared to be directly related to the amount of prestressing force applied and the transfer length. A maximum transverse reinforcement stress (in shear reinforcement serving as bursting reinforcement) of 32 ksi was seen coupled with crack widths of 0.009” at this location.
- 3) Each test region showed bursting stresses reaching a maximum value before the end of the transfer length is reached. These stresses then taper off to nearly zero not long after transfer length is achieved.
- 4) Shear steel was used to control the cracking within the bursting region of the beam specimens and was stressed to 20 – 30 ksi. This suggests that additional reinforcement is needed to counteract the bursting stresses as well as reduce the stresses in shear reinforcement.

5.3 RECOMMENDATIONS FOR FUTURE WORK

The recommendations for bursting reinforcement design were based on data from eight test regions in four full-scale beams. It would be desirable to check those recommendations with additional experimental data.

During the literature review phase of this research it became apparent that research on bursting and spalling stresses has been conducted on test specimens with rectangular or I-shaped cross-sections. The applicability of previous research recommendations, current research recommendations, and code provisions to other shapes (e.g. box beams, U-beams, etc.) is of great interest.

APPENDIX A

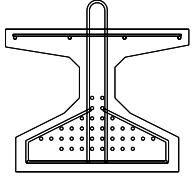
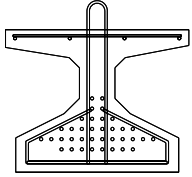
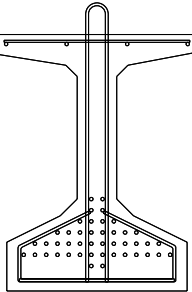
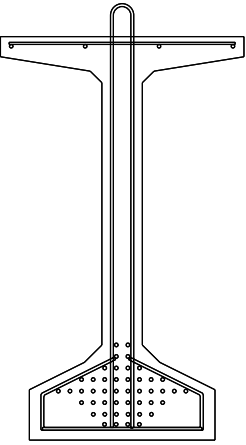
Prestressing Transfer Related Calculations

Appendix A includes the following:

- Elastic Shortening Calculations
- Calculations for Tension and Compression Limits

Elastic Shortening Calculations

Table A-1: Tx girder design summary

Section Sketch	Section Properties	Actual Applied P/S Force	Tendon Eccentricity	Cylinder Strength
<p style="text-align: center;">Tx28-I</p> 	<p>Height = 28" $A_g = 585\text{in}^2$ $I_x = 52,772\text{in}^4$ $I_y = 40,692\text{in}^4$ $y_t = 15.02''$ $y_b = 12.98''$</p>	<p>Initial: 1,591 kips</p> <p>After Losses: 1,466 kips</p>	5.01"	<p>Release: 10,025 psi</p> <p>Final: 13,825 psi</p>
<p style="text-align: center;">Tx28-II</p> 	<p>Height = 28" $A_g = 585\text{in}^2$ $I_x = 52,772\text{in}^4$ $I_y = 40,692\text{in}^4$ $y_t = 15.02''$ $y_b = 12.98''$</p>	<p>Initial: 1,692 kips</p> <p>After Losses: 1,522 kips</p>	5.01"	<p>Release: 6,475 psi</p> <p>Final: 11,375 psi</p>
<p style="text-align: center;">Tx46</p> 	<p>Height = 46" $A_g = 761\text{in}^2$ $I_x = 198,089\text{in}^4$ $I_y = 46,603\text{in}^4$ $y_t = 25.90''$ $y_b = 20.10''$</p>	<p>Initial: 1,945 kips</p> <p>After Losses: 1,732 kips</p>	10.67"	<p>Release: 6,500 psi</p> <p>Final: 13,200 psi</p>
<p style="text-align: center;">Tx70</p> 	<p>Height = 70" $A_g = 966\text{in}^2$ $I_x = 628,747\text{in}^4$ $I_y = 57,720\text{in}^4$ $y_t = 38.09''$ $y_b = 31.91''$</p>	<p>Initial: 1,974 kips</p> <p>After Losses: 1,754 kips</p>	22.91"	<p>Release: 6,675 psi</p> <p>Final: 11,575 psi</p>

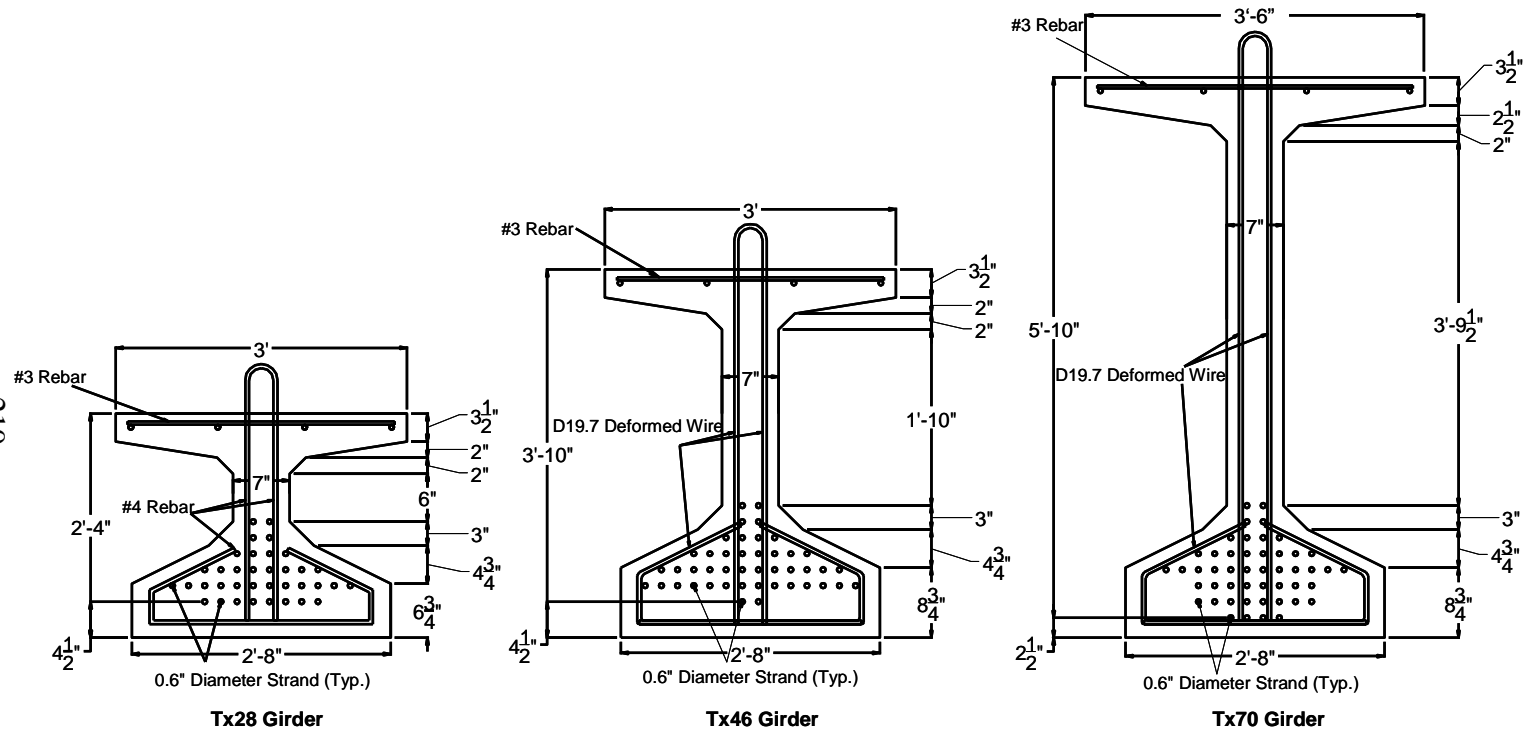


Figure A-1: Tx girder sections

Tx28-I

$$E_p = 29,500 \text{ksi}$$

$$E_{ct} = 57,000 \cdot \sqrt{10,025} = 5707 \text{ksi}$$

$$f_{cgp} = \frac{44.2k \cdot (36 \text{strands})}{585 \text{in}^2} + \frac{44.2k \cdot (36 \text{strands}) \cdot (5.24 \text{in})^2}{52,772 \text{in}^4} + \frac{5k \cdot (4 \text{strands})}{585 \text{in}^2} - \frac{5k \cdot (4 \text{strands}) \cdot (13.37 \text{in})^2}{52,772 \text{in}^4}$$

$$f_{cgp} = 3.51 \text{ksi}$$

$$\Delta f_{pES} = \frac{29,500}{5,707} \cdot 3.51 \text{ksi} = 18.2 \text{ksi}$$

Tx28-II

$$E_p = 29,500 \text{ksi}$$

$$E_{ct} = 57,000 \cdot \sqrt{6,475} = 4587 \text{ksi}$$

$$f_{cgp} = \frac{47.0k \cdot (36 \text{strands})}{585 \text{in}^2} + \frac{47.0k \cdot (36 \text{strands}) \cdot (5.24 \text{in})^2}{52,772 \text{in}^4} + \frac{5k \cdot (4 \text{strands})}{585 \text{in}^2} - \frac{5k \cdot (4 \text{strands}) \cdot (13.37 \text{in})^2}{52,772 \text{in}^4}$$

$$f_{cgp} = 3.74 \text{ksi}$$

$$\Delta f_{pES} = \frac{29,500}{4,587} \cdot 3.74 \text{ksi} = 24.0 \text{ksi}$$

Tx46

$$E_p = 29,500 \text{ksi}$$

$$E_{ct} = 57,000 \cdot \sqrt{6,500} = 4,595 \text{ksi}$$

$$f_{cgp} = \frac{44.2k \cdot (44 \text{strands})}{761 \text{in}^2} + \frac{44.2k \cdot (44 \text{strands}) \cdot (11.03 \text{in})^2}{198,089 \text{in}^4} + \frac{5k \cdot (4 \text{strands})}{761 \text{in}^2} - \frac{5k \cdot (4 \text{strands}) \cdot (24.25 \text{in})^2}{198,089 \text{in}^4}$$

$$f_{cgp} = 3.72 \text{ksi}$$

$$\Delta f_{pES} = \frac{29,500}{4,595} \cdot 3.72 \text{ksi} = 23.9 \text{ksi}$$

Tx70

$$E_p = 29,500 \text{ksi}$$

$$E_{ct} = 57,000 \cdot \sqrt{6,675} = 4,657 \text{ksi}$$

$$f_{cgp} = \frac{42.9k \cdot (46 \text{strands})}{966 \text{in}^2} + \frac{42.9k \cdot (46 \text{strands}) \cdot (23.50 \text{in})^2}{628,747 \text{in}^4} + \frac{5k \cdot (4 \text{strands})}{966 \text{in}^2} - \frac{5k \cdot (4 \text{strands}) \cdot (36.42 \text{in})^2}{628,747 \text{in}^4}$$

$$f_{cgp} = 3.75 \text{ksi}$$

$$\Delta f_{pES} = \frac{29,500}{4,657} \cdot 3.75 \text{ksi} = 23.8 \text{ksi}$$

Table A-2: Applied prestressing stress for all Tx girders

Girder	Tx28-I	Tx28-II	Tx46	Tx70
Calc. Applied P/S Stress (ksi)	203.6	216.5	203.5	197.8
Elastic Losses (ksi)	18.2	24.0	23.9	23.8
Calc. P/S Stress after Losses (ksi)	185.4	192.5	179.6	174.0

Typical Applied Prestressing Force Calculation before/after losses:

$$P = \sigma_p \cdot A_s \quad \text{Equation A-1}$$

where:

P = total applied prestressing force (kips)

A_s = cross-sectional area of strands

σ_p = stress in the strand before or after release

Table A-3: Total applied prestressing force for all Tx girders

Girder	Tx28-I	Tx28-II	Tx46	Tx70
Applied P/S Force P_o (kips)	1,591	1,692	1,945	1,974
P/S Force after Losses P_i (kips)	1,466	1,522	1,732	1,754

Tension and Compression Limit Calculations

AASHTO Allowable Prestressing Force before Prestress Transfer:

AASHTO LRFD (2007) §5.9.3-1:

$$0.75 \cdot f_{pu} = 0.75 \cdot 270 \text{ksi} = 202.5 \text{ksi} \quad \textbf{Equation A-2}$$

For low-relaxation strand

AASHTO Allowable Top Fiber Stress

AASHTO LRFD (2007) §5.9.4.1.2:

$$\sigma_t = 0.0948 \sqrt{f'_{ci}} \leq 0.2 \Rightarrow 0.0948 \sqrt{6.5 \text{ksi}} \leq 242$$

$$\sigma_t \leq 200 \text{psi with no steel}$$

$$\sigma_t = 0.24 \sqrt{f'_{ci}} \Rightarrow 0.24 \sqrt{6.5 \text{ksi}} \leq 612$$

$$\sigma_t \leq 612 \text{psi with steel}$$

Equation A-3

AASHTO Allowable Bottom Fiber Stress

AASHTO LRFD (2007) §5.9.4.1.1:

$$\sigma_b \leq 0.65 \cdot f'_{ci} \leq 0.65 \cdot 6.5 \text{ksi} \leq 4,225 \text{ksi}$$

$$\sigma_b \leq 4,225 \text{ksi}$$

Equation A-4

Tx28-I

Transfer Length (AASHTO LRFD §5.11.4.1)	
$l_t = 60 \cdot d_b$	$l_t = 36in$
Dead Load Moment due to Beam Self-Weight at Transfer Length	
$\omega_D = 0.150kcf \cdot A_g$	$\omega_D = 0.610klf$
$M_D = \frac{\omega_D \cdot l_d \cdot L_o}{2} - \frac{\omega_D \cdot l_d^2}{2}$	$M_D = 296 k \cdot in$
Top Fiber Stress at Transfer	
$f_{\max} = -\frac{P}{A} + \frac{Mc}{I} - \frac{M_D c}{I} = -\frac{P}{A} + \frac{Pec}{I_g} - \frac{M_D c}{I_g}$	
$f_{top} = -\frac{1466kips}{585in^2} + \frac{1466kips \cdot 5.01in \cdot 15.04in}{52,772in^2} - \frac{296k \cdot in \cdot 15.04in}{52,772in^2}$	
$f_{top} = -0.499ksi \text{ (compression)}$	
Bottom Fiber Stress at Transfer	
$f_{\max} = -\frac{P}{A} - \frac{Mc}{I} + \frac{M_D c}{I} = -\frac{P}{A} - \frac{Pec}{I_g} + \frac{M_D c}{I_g}$	
$f_{top} = -\frac{1466kips}{585in^2} - \frac{1466kips \cdot 5.01in \cdot 12.96in}{52,772in^2} + \frac{296k \cdot in \cdot 12.96in}{52,772in^2}$	
$f_{top} = -4.237ksi \text{ (compression)}$	
$= 0.65 f_{ci}'$	

Tx28-II

Transfer Length (AASHTO LRFD §5.11.4.1)	
$l_t = 60 \cdot d_b$	$l_t = 36in$
Dead Load Moment due to Beam Self-Weight at Transfer Length	
$\omega_D = 0.150kcf \cdot A_g$	$\omega_D = 0.610klf$
$M_D = \frac{\omega_D \cdot l_d \cdot L_o}{2} - \frac{\omega_D \cdot l_d^2}{2}$	$M_D = 296 k \cdot in$
Top Fiber Stress at Transfer	
$f_{max} = -\frac{P}{A} + \frac{Mc}{I} - \frac{M_D c}{I} = -\frac{P}{A} + \frac{Pec}{I_g} - \frac{M_D c}{I_g}$ $f_{top} = -\frac{1522kips}{585in^2} + \frac{1522kips \cdot 5.01in \cdot 15.04in}{52,772in^2} - \frac{296k \cdot in \cdot 15.04in}{52,772in^2}$ $f_{top} = -0.515ksi \text{ (compression)}$	
Bottom Fiber Stress at Transfer	
$f_{max} = -\frac{P}{A} - \frac{Mc}{I} + \frac{M_D c}{I} = -\frac{P}{A} - \frac{Pec}{I_g} + \frac{M_D c}{I_g}$ $f_{top} = -\frac{1522kips}{585in^2} - \frac{1522kips \cdot 5.01in \cdot 12.96in}{52,772in^2} + \frac{296k \cdot in \cdot 12.96in}{52,772in^2}$ $f_{top} = -4.402ksi \text{ (compression)}$ $= 0.68f'_{ci}$	
<p>* Note: The bottom fiber stress of $0.68f'_{ci}$ exceeds stress limits due to the slight overstressing during fabrication. Original strand design stress meets compression limits.</p>	

Tx46

Transfer Length (AASHTO LRFD §5.11.4.1)	
$l_t = 60 \cdot d_b$	$l_t = 36in$
Dead Load Moment due to Beam Self-Weight at Transfer Length	
$\omega_D = 0.150kcf \cdot A_g$	$\omega_D = 0.610klf$
$M_D = \frac{\omega_D \cdot l_d \cdot L_o}{2} - \frac{\omega_D \cdot l_d^2}{2}$	$M_D = 385 k \cdot in$
Top Fiber Stress at Transfer	
$f_{\max} = -\frac{P}{A} + \frac{Mc}{I} - \frac{M_D c}{I} = -\frac{P}{A} + \frac{Pec}{I_g} - \frac{M_D c}{I_g}$	
$f_{top} = -\frac{1732kips}{761in^2} + \frac{1732kips \cdot 10.67in \cdot 25.92in}{198,089in^2} - \frac{385k \cdot in \cdot 25.93in}{198,089in^2}$	
$f_{top} = 0.093ksi \text{ (tension)}$	
Bottom Fiber Stress at Transfer	
$f_{\max} = -\frac{P}{A} - \frac{Mc}{I} + \frac{M_D c}{I} = -\frac{P}{A} - \frac{Pec}{I_g} + \frac{M_D c}{I_g}$	
$f_{top} = -\frac{1732kips}{761in^2} - \frac{1732kips \cdot 10.67in \cdot 20.08in}{198,089in^2} + \frac{385k \cdot in \cdot 20.08in}{198,089in^2}$	
$f_{top} = -4.112ksi \text{ (compression)}$	
$= 0.63f'_{ci}$	

Tx70

Transfer Length (AASHTO LRFD §5.11.4.1)	
$l_t = 60 \cdot d_b$	$l_t = 36in$
Dead Load Moment due to Beam Self-Weight at Transfer Length	
$\omega_D = 0.150kcf \cdot A_g$	$\omega_D = 0.610klf$
$M_D = \frac{\omega_D \cdot l_d \cdot L_o}{2} - \frac{\omega_D \cdot l_d^2}{2}$	$M_D = 489 k \cdot in$
Top Fiber Stress at Transfer	
$f_{\max} = -\frac{P}{A} + \frac{Mc}{I} - \frac{M_D c}{I} = -\frac{P}{A} + \frac{Pec}{I_g} - \frac{M_D c}{I_g}$	
$f_{top} = -\frac{1754kips}{966in^2} + \frac{1754kips \cdot 22.91in \cdot 38.12in}{628,747in^2} - \frac{489k \cdot in \cdot 38.12in}{628,747in^2}$	
$f_{top} = 0.591ksi$ (tension) need additional steel	
Additional Bonded Reinforcement (AASHTO LRFD (2007) §C5.9.4.1.2-1)	
$T = \frac{f_{ci_{top}}}{2} \cdot b_{top} \cdot x = \frac{0.591ksi}{2} \cdot 214in^2 = 63.24kips$	
$A_s = \frac{T}{f_s} = \frac{63.24kips}{30ksi} = 2.11in^2$	
Existing $\Rightarrow 4$ strands $\Rightarrow 4 \cdot 0.217in^2 = 0.868in^2$	
Additional $\Rightarrow 2.20in^2 - 0.868in^2 = 1.33in^2$	
Try 3 - #6 bars $\Rightarrow 0.44in^2 \cdot 3 = 1.32in^2$	
Total Top Steel $\Rightarrow 0.868in^2 + 1.32in^2 = 2.19in^2$	
Bottom Fiber Stress at Transfer	
$f_{\max} = -\frac{P}{A} - \frac{Mc}{I} + \frac{M_D c}{I} = -\frac{P}{A} - \frac{Pec}{I_g} + \frac{M_D c}{I_g}$	
$f_{top} = -\frac{1754kips}{966in^2} - \frac{1754kips \cdot 22.91in \cdot 31.88in}{628,747in^2} + \frac{489k \cdot in \cdot 31.88in}{628,747in^2}$	
$f_{top} = -3.829ksi$ (compression)	
$= 0.59 f'_{ci}$	

APPENDIX B

Bursting and Spalling Steel Calculations

Appendix B includes the following:

- AASHTO LRFD Bridge Design (2007) Spalling Steel Calculations
- PCI Design Handbook (6th Edition) Spalling Steel Calculations
- CEB-FIP MC90 Spalling and Bursting Steel Calculations
- TxDOT Tx Girder Bursting and Spalling Steel Quantities

AASHTO LRFD Bridge Design (2007) Spalling Steel Calculations

§5.10.10.1 “Factored Bursting Resistance”:

The bursting resistance of pretensioned anchorage zones provided by vertical reinforcement in the ends of pretensioned beams at the service limit state shall be taken as:

$$P_r = f_s A_s \qquad \text{Equation B-1}$$

where:

f_s = stress in steel not exceeding 20 ksi

A_s = total area of vertical reinforcement located within the distance $h/4$ from the end of the beam (in^2)

h = overall depth of precast member (in)

P_r = bursting resistance force

The resistance shall not be less than 4 percent of the prestressing force at transfer.

The end vertical reinforcement shall be as close to the end of the beam as practicable.

Table B-1: AASHTO LRFD (2007) Spalling steel provision comparison

Girder	Tx28-I	Tx28-II	Tx46	Tx70
P_i (kips)	1466	1522	1732	1754
P_r (kips)	58.6	60.9	69.3	70.2
f_s (ksi)	20	20	20	20
A_s (in^2)	2.93	3.04	3.46	3.51
$h/4$ (in)	7"	7"	11.5"	17.5"

PCI Design Handbook 6th Edition Spalling Steel

Calculations

§4.2.4 “End Stresses at Transfer”:

These forces can be resisted by vertical reinforcement calculated by the following equation:

$$A_{vt} = \frac{0.021P_o h}{f_s l_t} \qquad \text{Equation B-2}$$

where:

A_{vt} = required area of stirrups at the end of a member uniformly distributed over a length $h/5$ from the end

P_o = prestress force at transfer

h = depth of member

f_s = design stress in the stirrups, usually assumed to be 30 ksi

l_t = strand transfer length

Table B-2: PCI (6th Edition) Spalling steel provision comparison

Girder	Tx28-I	Tx28-II	Tx46	Tx70
P_i (kips)	1466	1522	1732	1754
h (in)	28"	28"	46"	70"
f_s (ksi)	30	30	30	30
l_t (in)	36"	36"	36"	36"
A_{vt} (in ²)	0.80	0.83	1.55	2.39
$h/5$ (in)	5.6"	5.6"	9.2"	14"

CEB-FIP Model Code 1990 Spalling and Bursting Steel Calculations

Sample Calculation shown using the Tx46 Girder. Repeat the same procedure with other Tx Girders:

6.9.11.2 Bond Strength

$$f_{bpd} = \eta_{p1} \eta_{p2} f_{ctd} = 1.2 \cdot 0.7 \cdot \frac{242 \text{ psi}}{1.5} \quad \text{Equation B-3}$$

$$f_{bpd} = 136 \text{ psi}$$

where

$f_{ctd} = f_{ctk}(t)/1.50$ is the lower design concrete tensile strength; for the transmission length the strength at the time of release

η_{p1} = takes into account the type of prestressing tendon: $\eta_{p1} = 1.4$ for indented or crimped wires, and $\eta_{p1} = 1.2$ for 7-wire strands

η_{p2} = takes into account the position of the tendon: $\eta_{p2} = 1.0$ for all tendons with an inclination of 45° - 90° with respect to the horizontal during concreting, $\eta_{p2} = 1.0$ for all horizontal tendons which are up to 250 mm from the bottom or at least 300 mm below the top of the concrete section during concreting, and $\eta_{p2} = 0.7$ for all other cases.

6.9.11.3 Basic Anchorage Length

The basic anchorage length of an individual pretensioned tendon is

$$l_{bp} = \frac{A_{sp}}{\phi\pi} \cdot \frac{f_{ptd}}{f_{bpd}} = \frac{7 \cdot 0.6''}{36} \cdot \frac{245 \text{ ksi} / 1.15}{0.136 \text{ ksi}} \quad \text{Equation B-4}$$

$$l_{bp} = 182''$$

where

$f_{ptd} = f_{ptk}/1.15$, where f_{ptk} is yield strength of prestressing tendon

$\frac{A_{sp}}{\phi\pi} = \phi/4$ for tendons with a circular cross-section

$= 7\phi/36$ for 7-wire strands

6.9.11.4 Transmission Length

The transmission length of a pretensioned tendon is

$$l_{bpt} = \alpha_8 \alpha_9 \alpha_{10} l_{bp} \frac{\sigma_{pi}}{f_{pd}} = 1.0 \cdot 0.5 \cdot 0.5 \cdot 182'' \cdot \frac{178\text{ksi}}{196\text{ksi}} \quad \text{Equation B-5}$$

$$l_{bpt} = 41.3''$$

where

α_8 = considers the way of release: $\alpha_8 = 1.0$ for gradual release and $\alpha_8 = 1.25$ for sudden release;

α_9 considers the action effect to be verified: $\alpha_9 = 1.0$ for calculation of anchorage length when moment and shear capacity is considered, and $\alpha_9 = 0.5$ for verification of transverse stresses in anchorage zone

α_{10} considers the influence of bond situation: $\alpha_{10} = 0.5$ for strands and $\alpha_{10} = 0.7$ for indented or crimped wires;

σ_{pi} is the steel stress just after release

6.9.12 Transverse stresses in the anchorage zone of prestressed tendons

6.9.12.1 General

The anchorage zone of prestressed tendons is a discontinuity region that should be treated according to section 6.8. Should the use of the strut-and-tie model be too problematic because of the complexity of the stress field, the

verification may be performed on the basis of the stresses in a linear, uncracked member. For design purposes, the tensile stresses, due to the development and distribution of the prestressing force, are subdivided into three groups (Fig. 2.2.a).

If the strut-and-tie model is not applicable due to lack of transverse reinforcement, the verification may be performed on the basis of stress and strain analysis.

Tx28-I

6.9.12.2 Bursting

For the calculation of the bursting force the symmetric prism analogy may be used (Figure B-1).

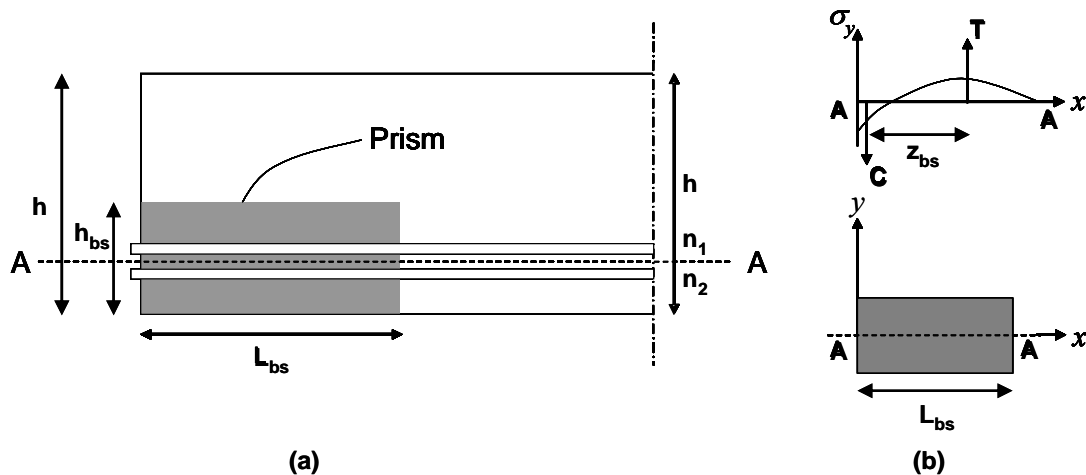


Figure B-1: For calculation of the bursting force: (a) dimensions of the symmetrical prism; (b) moment equilibrium along section A-A

(CEB-FIP, 1998)

The height and the width of the prism follow from the possible enlargement of the anchor plates (post-tensioning) or the tendon pattern (pretensioning). For multiple tendons the most unfavorable situations shall be considered: a single

tendon or a group of tendons. The bursting action shall be determined both in the vertical and in the horizontal direction.

The length of the prism is for the end anchored tendons

$$l_{bs} = h_{bs} = 15.90" \quad \text{Equation B-6}$$

And for tendons anchored by bond

$$l_{bs} = \sqrt{[h_{bs}^2 + (0.6l_{bpt})^2]} < l_{bpt} \quad \text{Equation B-7}$$

$$l_{bs} = \sqrt{[15.90^2 + (0.6 \cdot 41.3")^2]} = 29.44"$$

The internal lever arm for the bursting force is

$$z_{bs} = 0.5l_{bs} = 0.5 \cdot 29.44" = 15.6" \quad \text{Equation B-8}$$

The bursting force follows from the moment equilibrium along section A-A (Fig. 2-15(b))

$$N_{bs} = \frac{\frac{1}{2}(n_1 + n_2)t_2 - n_1t_1}{z_{bs}} \gamma_1 F_{sd}$$

$$N_{bs} = \frac{\frac{1}{2}(36.46) \cdot 7.98" - 16.46 \cdot 2.74"}{14.72"} \cdot 1.1 \cdot 44.2 \text{kips} \quad \text{Equation B-9}$$

$$N_{bs} = 301 \text{kips}$$

where

t_1 is the distance between the centroid of tendons above section A-A to the centroid of the prism

t_2 is the distance between the centroid of the concrete stress block above section A-A to the centroid of the prism

n_1, n_2 are the numbers of tendons above and below section A-A, respectively

F_{sd} is the design force per tendon

$\gamma_1 = 1.1$ is the supplementary partial safety factor against overstressing by overpumping

The maximum bursting stress follows from

$$\begin{aligned}\sigma_{bs} &= 2N_{bs} / b_{bs}l_{bs} = 2 \cdot 301k / 7'' \cdot 29.44'' \\ \sigma_{bs} &= 2.92ksi\end{aligned}\quad \text{Equation B-10}$$

where b_{bs} is the width of the prism.

For $\sigma_{bs} > f_{ctd}$ the bursting force shall be resisted by confining or net reinforcement distributed within $l_{bs}/3$ to l_{bs} from the end face, with

$$\begin{aligned}A_{bsb} &= N_{bs} / f_{sy} = 300kips / 60ksi \\ A_{bsb} &= 5.02in^2\end{aligned}\quad \text{Equation B-11}$$

6.9.12.3 Spalling

Having a section with no shear force is not possible in the Tx28 girder which implies that no spalling force exists in the girder.

$$\sigma_{sl} = 0 \text{ ksi}$$

$$A_{s,sl} = 0 \text{ in}^2$$

Tx46*6.9.12.2 Bursting*

The length of the prism is for the end anchored tendons

$$l_{bs} = h_{bs} = 18.82" \quad \text{Equation B-12}$$

And for tendons anchored by bond

$$l_{bs} = \sqrt{[h_{bs}^2 + (0.6l_{bpt})^2]} < l_{bpt} \quad \text{Equation B-13}$$

$$l_{bs} = \sqrt{[18.82^2 + (0.6 \cdot 41.3")^2]} = 31.12"$$

The internal lever arm for the bursting force is

$$z_{bs} = 0.5l_{bs} = 0.5 \cdot 31.12 = 15.6" \quad \text{Equation B-14}$$

The bursting force follows from the moment equilibrium along section A-A

(Figure B-1(b))

$$N_{bs} = \frac{1}{2} \frac{(n_1 + n_2)t_2 - n_1t_1}{z_{bs}} \gamma_1 F_{sd}$$

$$N_{bs} = \frac{1}{2} \frac{(44.46) \cdot 9.28" - 16.46 \cdot 3.73"}{15.56"} \cdot 1.1 \cdot 44.2 \text{ kips} \quad \text{Equation B-15}$$

$$N_{bs} = 412 \text{ kips}$$

The maximum bursting stress follows from

$$\sigma_{bs} = 2N_{bs} / b_{bs}l_{bs} = 2 \cdot 412 \text{ k} / 7" \cdot 31.12" \quad \text{Equation B-16}$$

$$\sigma_{bs} = 3.78 \text{ ksi}$$

where b_{bs} is the width of the prism.

For $\sigma_{bs} > f_{ctd}$ the bursting force shall be resisted by confining or net reinforcement distributed within $l_{bs}/3$ to l_{bs} from the end face, with

$$A_{bsb} = N_{bs} / f_{sy} = 412 \text{kips} / 60 \text{ksi}$$

Equation B-17

$$A_{bsb} = 6.86 \text{in}^2$$

6.9.12.3 Spalling

The spalling force may be calculated with the equivalent prism analogy (Figure B-2(a)).

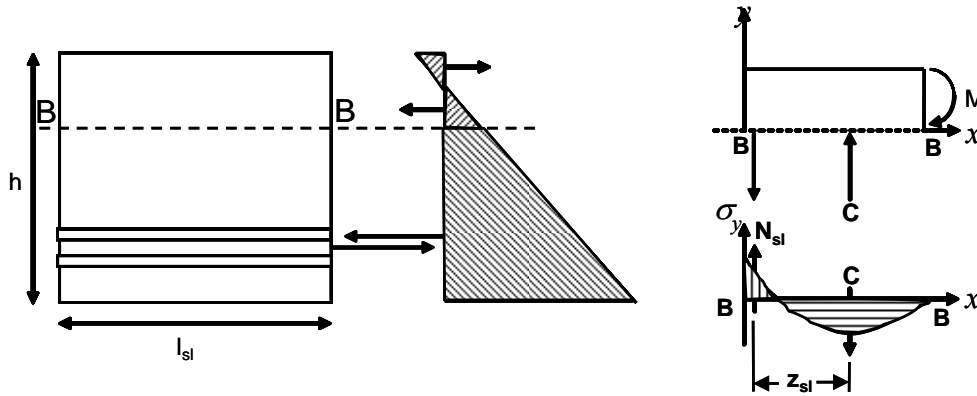


Figure B-2: For calculation of the spalling force: (a) definition of the equivalent prism; (b) moment equilibrium along section B-B (CEB-FIP, 1998)

The length of the prism is defined as, for end anchored tendons

$$l_{sl} = h$$

Equation B-18

And for tendons anchored by bond

$$l_{sl} = \sqrt{h^2 + (0.6l_{bpt})^2} < l_{bpt}$$

$$l_{sl} = \sqrt{46^2 + (0.6 \cdot 41.3'')^2} = 52.25''$$

Equation B-19

$$l_{sl} = 41.3''$$

The internal lever arm for the spalling force is

$$z_{sl} = 0.5l_{sl} = 0.5 \cdot 41.3'' = 20.65''$$

Equation B-20

Section B-B shall be chosen so that along this section no shear force results. The spalling force results from the moment equilibrium along section B-B

$$\begin{aligned} N_{sl} &= M / z_{sl} = 3.64k \cdot in / 20.65" \\ N_{sl} &= 0.18kips \end{aligned} \quad \text{Equation B-21}$$

With the moment M given by concrete stresses above section B-B.

The maximum spalling stress follows from

$$\begin{aligned} \sigma_{sl} &= 8N_{sl} / b_{sl}l_{sl} = 8 \cdot .18kips / 7" \cdot 41.3" \\ \sigma_{sl} &= 0.005ksi \end{aligned} \quad \text{Equation B-22}$$

With b_{sl} width of the cross section at section B-B.

For $\sigma_{sl} \leq f_{ct,fl} / \gamma_c$, where

$$\gamma_c = 1.5$$

$f_{ct,fl}$ is the flexural tensile strength of concrete

the spalling force shall be resisted by reinforcement

$$\begin{aligned} A_{s,sl} &= N_{sl} / f_{sy} = 0.18kips / 60ksi \\ A_{s,sl} &= 0.003in^2 \end{aligned} \quad \text{Equation B-23}$$

The spalling force resisting reinforcement shall be put parallel to the end face in its close vicinity.

Tx70*6.9.12.2 Bursting*

The length of the prism is for the end anchored tendons

$$l_{bs} = h_{bs} = 18" \quad \text{Equation B-24}$$

And for tendons anchored by bond

$$l_{bs} = \sqrt{[h_{bs}^2 + (0.6l_{bpt})^2]} < l_{bpt} \quad \text{Equation B-25}$$

$$l_{bs} = \sqrt{[18.8^2 + (0.6 \cdot 41.3")^2]} = 30.63"$$

The internal lever arm for the bursting force is

$$z_{bs} = 0.5l_{bs} = 0.5 \cdot 30.63" = 15.31" \quad \text{Equation B-26}$$

The bursting force follows from the moment equilibrium along section A-A (Figure B-1(b))

$$N_{bs} = \frac{1}{2} \frac{(n_1 + n_2)t_2 - n_1t_1}{z_{bs}} \gamma_1 F_{sd}$$

$$N_{bs} = \frac{1}{2} \frac{(46.46) \cdot 7.26" - 16.46 \cdot 4.8"}{15.31"} \cdot 1.1 \cdot 42.9 \text{kips} \quad \text{Equation B-27}$$

$$N_{bs} = 251 \text{kips}$$

The maximum bursting stress follows from

$$\sigma_{bs} = 2N_{bs} / b_{bs}l_{bs} = 2 \cdot 251 \text{k} / 7" \cdot 30.63" \quad \text{Equation B-28}$$

$$\sigma_{bs} = 2.34 \text{ksi}$$

where b_{bs} is the width of the prism.

For $\sigma_{bs} > f_{ctd}$ the bursting force shall be resisted by confining or net reinforcement distributed within $l_{bs}/3$ to l_{bs} from the end face, with

$$A_{bsb} = N_{bs} / f_{sy} = 251 \text{kips} / 60 \text{ksi}$$

$$A_{bsb} = 4.19 \text{in}^2$$

Equation B-29

6.9.12.3 Spalling

The spalling force may be calculated with the equivalent prism analogy (Figure B-2(a)).

The length of the prism is defined as, for end anchored tendons

$$l_{sl} = h$$

Equation B-30

And for tendons anchored by bond

$$l_{sl} = \sqrt{[h^2 + (0.6l_{bpt})^2]} < l_{bpt}$$

$$l_{sl} = \sqrt{[70^2 + (0.6 \cdot 41.3'')^2]} = 76.96''$$

$$l_{sl} = 41.3''$$

Equation B-31

The internal lever arm for the spalling force is

$$z_{sl} = 0.5l_{sl} = 0.5 \cdot 41.3'' = 20.65''$$

Equation B-32

Section B-B shall be chosen so that along this section no shear force results. The spalling force results from the moment equilibrium along section B-B

$$N_{sl} = M / z_{sl} = 2004 \text{k} \cdot \text{in} / 20.65''$$

$$N_{sl} = 97.05 \text{kips}$$

Equation B-33

With the moment M given by concrete stresses above section B-B.

The maximum spalling stress follows from

$$\sigma_{sl} = 8N_{sl} / b_{sl}l_{sl} = 8 \cdot 97.05 \text{kips} / 7'' \cdot 41.3''$$

$$\sigma_{sl} = 2.69 \text{ksi}$$

Equation B-34

With b_{sl} width of the cross section at section B-B.

For $\sigma_{sl} \leq f_{ct,fl} / \gamma_c$, where

$$\gamma_c = 1.5$$

$f_{ct,fl}$ is the flexural tensile strength of concrete

the spalling force shall be resisted by reinforcement

$$A_{s,sl} = N_{sl} / f_{sy} = 97.05 \text{kips} / 60 \text{ksi}$$

$$A_{s,sl} = 1.62 \text{in}^2$$

Equation B-35

The spalling force resisting reinforcement shall be put parallel to the end face in its close vicinity.

TxDOT Tx Girders – Bursting and Spalling Steel Design Quantities

Table B-3: Tx End region transverse reinforcement details (live end)

Girder	Tx28-I	Tx28-II	Tx46	Tx70
h/4	7"	7"	11.5"	17.5"
Spalling Steel	4 - #6 bars	4 - #6 bars	6 - #6 bars	8 - # 6 Bars
Spalling Steel (in ²)	1.76	1.76	2.64	3.52
Bursting Steel	16 – D19.7 bars	14 – D19.7 bars	12 – D19.7 bars	10 – D19.7 bars
Bursting Steel (in ²)	3.15	2.76	2.36	1.97

Table B-4: Tx End region transverse reinforcement details (dead end)

Girder	Tx28-I	Tx28-II	Tx46	Tx70
h/4	7"	7"	11.5"	17.5"
Spalling Steel	4 - #6 bars	4 - #6 bars	8 - #6 bars	8 - # 6 Bars
Spalling Steel (in ²)	1.76	1.76	3.52	3.52
Bursting Steel	14 – D19.7 bars	16 – D19.7 bars	12 – D19.7 bars	10 – D19.7 bars
Bursting Steel (in ²)	2.76	3.15	2.36	1.97

Table B-5: Transverse end region reinforcement comparison (dead end)

Girder	Tx28-I	Tx28-II	Tx46	Tx70
h/4	7"	7"	11.5"	17.5"
Spalling Steel (in ²)				
AASHTO	2.93	3.04	3.46	3.51
PCI (6 th Ed.)	0.80	0.83	1.55	2.39
CEB-FIP 90	0	0	0.003	1.62
Actual	1.76	1.76	3.52	3.52
Bursting Steel (in ²)				
AASHTO	N/A	N/A	N/A	N/A
PCI (6 th Ed.)	N/A	N/A	N/A	N/A
CEB-FIP 90	5.02	5.34	6.86	4.19
Actual	0.00	0.00	0.00	0.00

Table B-6: Transverse end region reinforcement comparison (live end)

Girder	Tx28-I	Tx28-II	Tx46	Tx70
h/4	7"	7"	11.5"	17.5"
Spalling Steel (in ²)				
AASHTO	2.93	3.04	3.46	3.51
PCI (6 th Ed.)	0.80	0.83	1.55	2.39
CEB-FIP 90	0	0	0.003	1.62
Actual	1.76	1.76	2.64	3.52
Bursting Steel (in ²)				
AASHTO	N/A	N/A	N/A	N/A
PCI (6 th Ed.)	N/A	N/A	N/A	N/A
CEB-FIP 90	5.02	5.34	6.86	4.19
Actual	0.00	0.00	0.00	0.00

APPENDIX C
Cylinder Test Values

Date	Time	Cylinder	Channel	Pu (kips)	fc (psi)	Temp	Maturity
Dec 15,2006	7:15 PM	28B	46	2.0	159	104.0	3500
	9:30 PM	25A	43	85.0	6768	110.2	3743.4
	9:30 PM	26A	44	57.0	4538	110.9	3771.6
	9:40 PM	27B	45	18.5	1473	104.0	3647.1
	9:45 PM	35B	47	46.0	3662	107.5	3740.1
	10:00 PM	22B	48	14.0	1115	99.1	3504.2
			AVERAGE		3511		
	10:20 PM	25B	43	90.0	7166	110.2	3819.2
	10:25 AM	26B	44	43.0	3424	111.8	3836.8
	10:30 AM	27A	45	25.0	1990	104.0	3720.2
	10:35 AM	28A	46	21.0	1672	101.6	3717.8
	10:45 AM	35A	47	10.0	796	106.9	3825.9
	10:55 AM	22A	48	3.0	239	97.8	3593.9
			AVERAGE		2548		
Dec. 16, 2006	4:15 AM	1B	43	87.0	6927	96.6	5577
	4:20 AM	7A	45	101.0	8041	92.5	5326
	4:30 AM	18B	48	97.0	7723	91.4	5073
			AVERAGE		5096		
Release							
Dec. 19, 2006	11:20 AM	2A	43	122.0	9713	73.0	10795
		5B	44	119.5	9514	72.6	10773.5
		8A	45	128.5	10231	72.6	10552.3
		12B	46	131.0	10430	72.4	10509.3
		15A	47	132.5	10549	72.7	10518.3
		21B	48	121.5	9674	72.4	10290.2
			AVERAGE		10019		

Table C-1: Tx28-I cylinder strengths

Date	Time	Cylinder	Channel	Pu (kips)	fc (psi)	Temp	Maturity
February 13, 2007	8:42 p.m.	14B	46		561	85.98	413.2
	10:00 p.m.	3B	43	25360	2019	102	546.4
	10:30 p.m.	4B	44	49020	3903	114.2	631
		18B	48	28580	2275	98.19	557.7
					3089		
	11:00 p.m.	11A	45	52420	4174	114.4	680
		28B	46	48320	3847	108.4	618.7
		35B	47	33520	2669	94.99	564.5
					3563		
	11:45 p.m.	1A	43	59910	4770	109.2	733.8
		26B	44	58120	4627	117.8	747.4
		21B	48	50990	4060	103.3	685.7
					4486		
February 14, 2007	1:00 A.M.	6B	44	62910	5009	119.4	935
		8A	45	64800	5159	116.7	911.2
		13B	46	64600	5143	110.7	965.1
		17A	47	54750	4359	92.28	776.6
					4918		
	1:45 a.m.	2A	43	72170	5746	106.5	925.2
		36B	48	69750	5553	99.75	860.1
		5B	44	71460	5689	119.8	1015.9
					5663		
	2:45 a.m.	4A	44	72420	5766	118.1	1130.2
		7A	45	75530	6014	114.7	1108.4
		12B	46	73910	5885	107.6	1051.1
					5888		
	4:00 a.m.	1B	43	83410	6641		
	4:00 a.m.	27B	45	79505	6330	110.8	1216.1
					6485		
	4:30 a.m.	5A	44	78630	6260	115	1314.2
	4:30 a.m.	25A	43	79520	6331	91.97	1179.1
					6296		
During Release	5:30 a.m.	2B	43	82210	6545		
		6A	44	84040	6691		
		7B	45	82740	6588		
		12A	46	84400	6720		
		16A	47	76220	6068		
		22B	48	79200	6306		
					6486		

Table C-2: Tx82-II cylinder tests

Date	Time	Cylinder	Channel	Pu (kips)	f'c (psi)	Temp (°F)	Maturity
March 6, 2007	12:00 AM	3A	43	0	0	91.91	644.3
		27B	45	19190	1528	107.6	703.6
		18B	48	38050	3029	111.1	745.6
					1519		
	1:30 AM	4A	44	44860	3572	113.4	824.7
		12A	46	61350	4885	112.7	907.7
		17A	47	65630	5225	100.3	829.8
					4561		
	2:15 AM	1A	43	49310	3926	108	890
		5B	44	58970	4695	117.9	920
		11A	45	71820	5718	112.5	960.1
					4780		
	3:10 AM	2A	43	77820	6196	109.1	970.20
		6B	44	80530	6412	119.8	1028.40
		7A	45	70816	5638	114.1	1077.90
		13B	46	77820	6196	111.7	1103.4
		15A	47	76180	6065	98.67	1021.9
		21B	48	80530	6412	109.9	1101.3
					6153		
	4:20 AM	25A	43	75470	6009	109.3	1098.7
		26B	44	80060	6374	120.5	1160.7
		8A	45	81700	6505	114.8	1218
		14B	46	74520	5933	110.7	1243.7
		35B	47	79740	6349	98.2	1119.6
		36B	48	84500	6728	107.8	1220.1
					6316		
	6:00 AM	1B	43	86910	6920	107.7	1286
		4A	44	80730	6428	120	1360.8
		7B	45	84590	6735	113	1394.4
		12B	46	82600	6576	105.5	1407.1
		15B	47	84940	6763	91.04	1289.9
		18A	48	84260	6709	103.7	1395.6
					6688		

Table C-3: Tx46 cylinder tests

Date	Time	Cylinder	Channel	Pu (kips)	f'c (psi)	Temp	Maturity
April 19, 2007							
April 20, 2007	1:30 AM	1A	43	14.4	1146	100.8	778.2
		27B	45	29.3	2333	109.2	779.1
		18B	48	24.5	1951	113.5	802.8
					1810		
	2:30 AM	6B	44	53460	4256		
		14B	46	42680	3398		
		15A	47	38710	3082		
					3579		
	3:45 AM	3A	43	54600	4347	111.6	1021.9
		5B	44	62120	4946	126.8	1086.4
		8A	45	62950	5012	120.6	1060.9
					4768		
	5:15 AM	2A	43	70670	5627	112.2	1177.20
		4B	44	70040	5576	127.6	1263.10
		11A	45	64820	5161	120.9	1229.50
		12B	46	61790	4920	112.1	1188.8
		16A	47	68870	5483	99.93	1134.8
		22B	48	69020	5495	120.8	1240.4
					5377		
	6:30 AM	25A	43	71750	5713	107.4	1317.7
		7A	45	71390	5684	117.3	1397.2
		17A	47	72480	5771	90.35	1249
					5722		
	8:00 AM	26B	44	79200	6306	123.3	1598
		13B	46	78420	6244	100.2	1490.9
		21B	48	75610	6020	107.5	1564.9
					6190		
	9:00 AM	1B	43	75130	5982	104.1	1594.4
		7B	45	73120	5822	111.3	1684.8
		15B	47	76990	6130	85.62	1483.3
					5978		
	10:30 AM	26A	44	80780	6432	117.8	1898
		28B	46	81660	6502	93.96	1711.8
		36B	48	83880	6678	99.03	1804.8
					6537		
	11:30 AM	25B	43	84190	6703	101.8	1824.9
		5A	44	84780	6750	115.4	2025.9
		8B	45	87290	6950	107.3	1936
		28A	46	84530	6730	91.82	1795.2
		35B	47	84790	6751	82.62	1662
		22A	48	86190	6862	97.08	1910.5
					6791		

Table C-4: Tx70 cylinder tests

APPENDIX D

Prestressing Steel Calibration Curves and Time- Temperature Curves

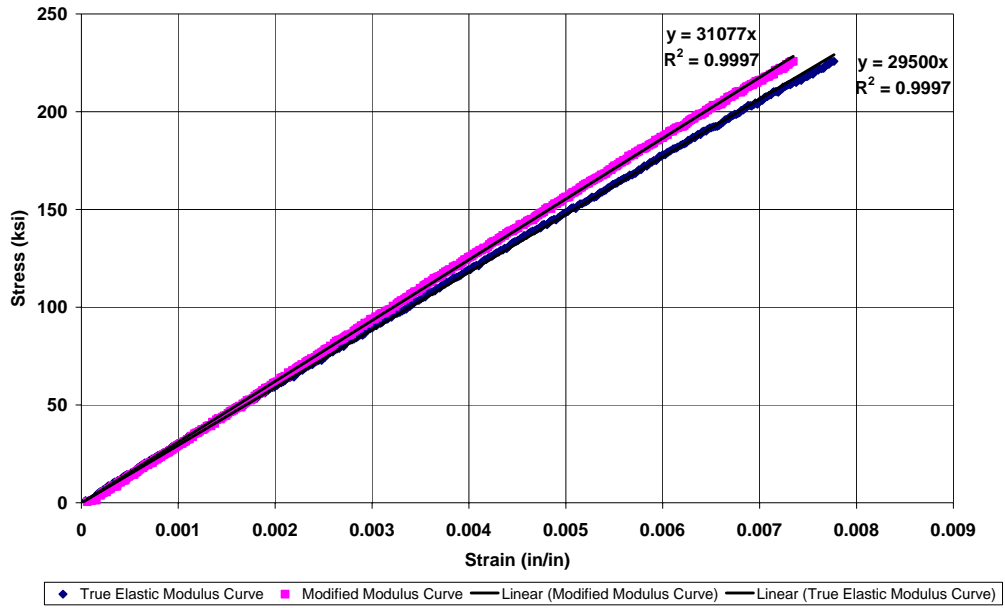


Figure D-1: Strand calibration curve for Tx70 girder

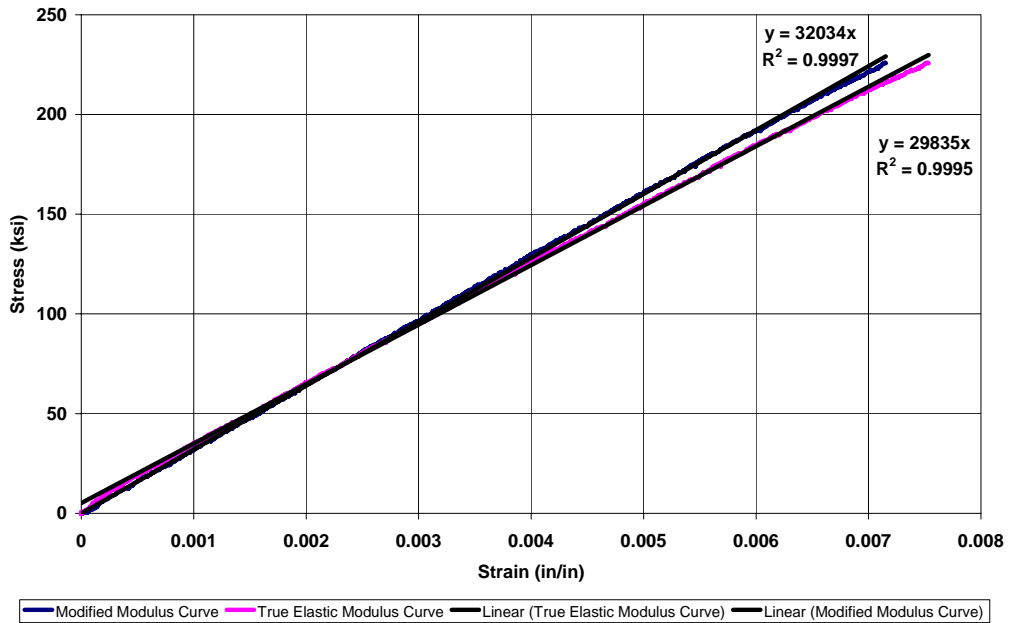


Figure D-2: Strand calibration curve for Tx28-I, Tx28-II, and Tx46 girder

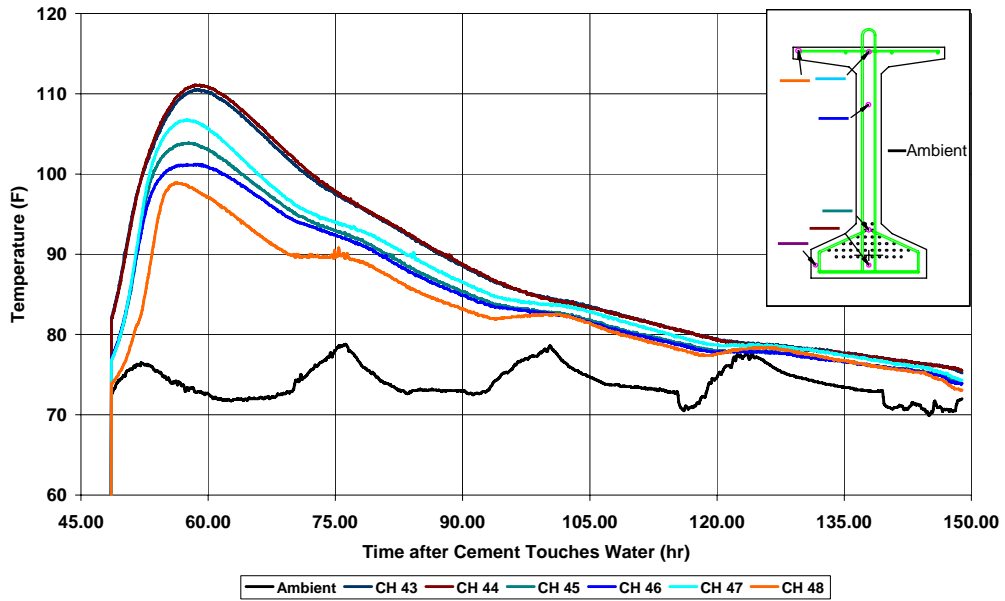


Figure D-3: Time-temperature curve for Tx28-I

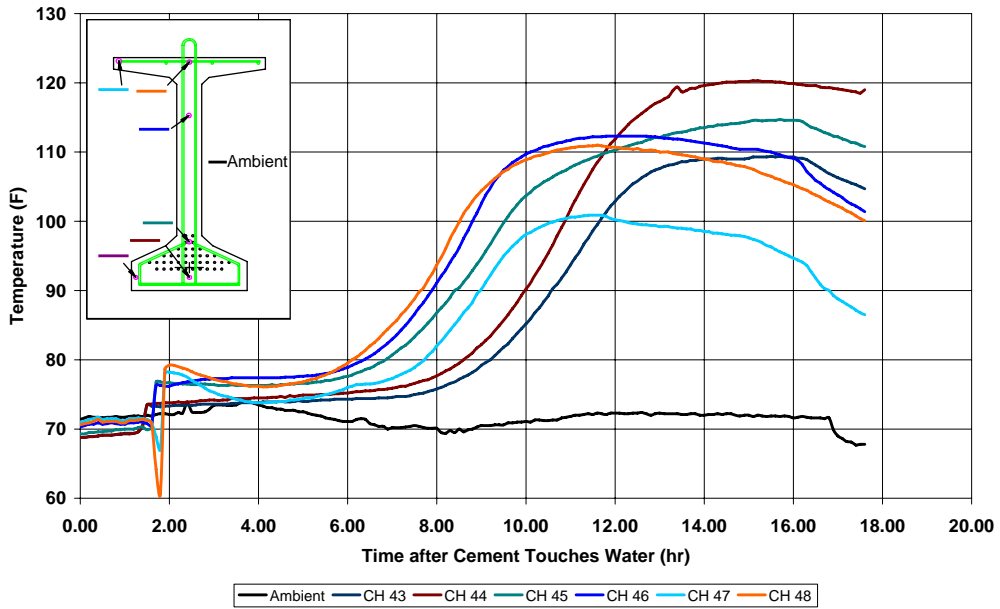


Figure D-4: Time-temperature curve for Tx46

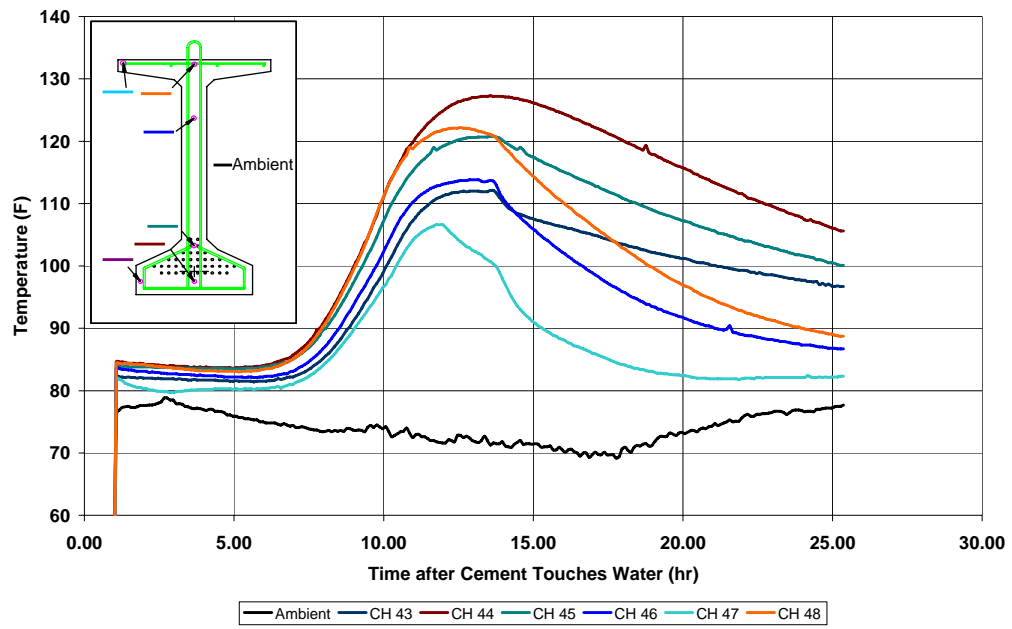


Figure D-5: Time-temperature curve for Tx70

APPENDIX E

High Capacity Prestressing Bed Design Drawings

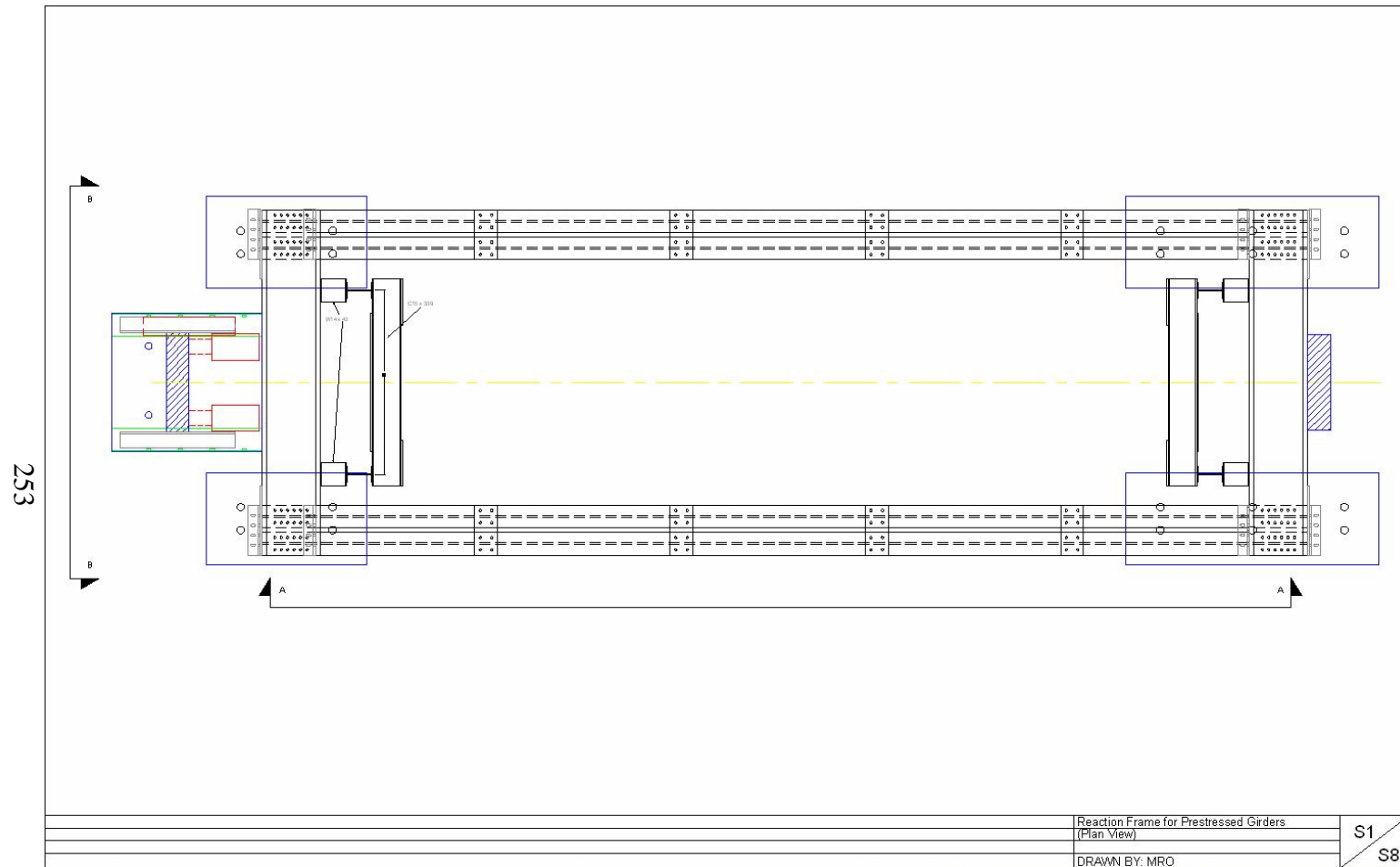


Figure E-1: High capacity prestressing bed design drawing (Plan View)

254

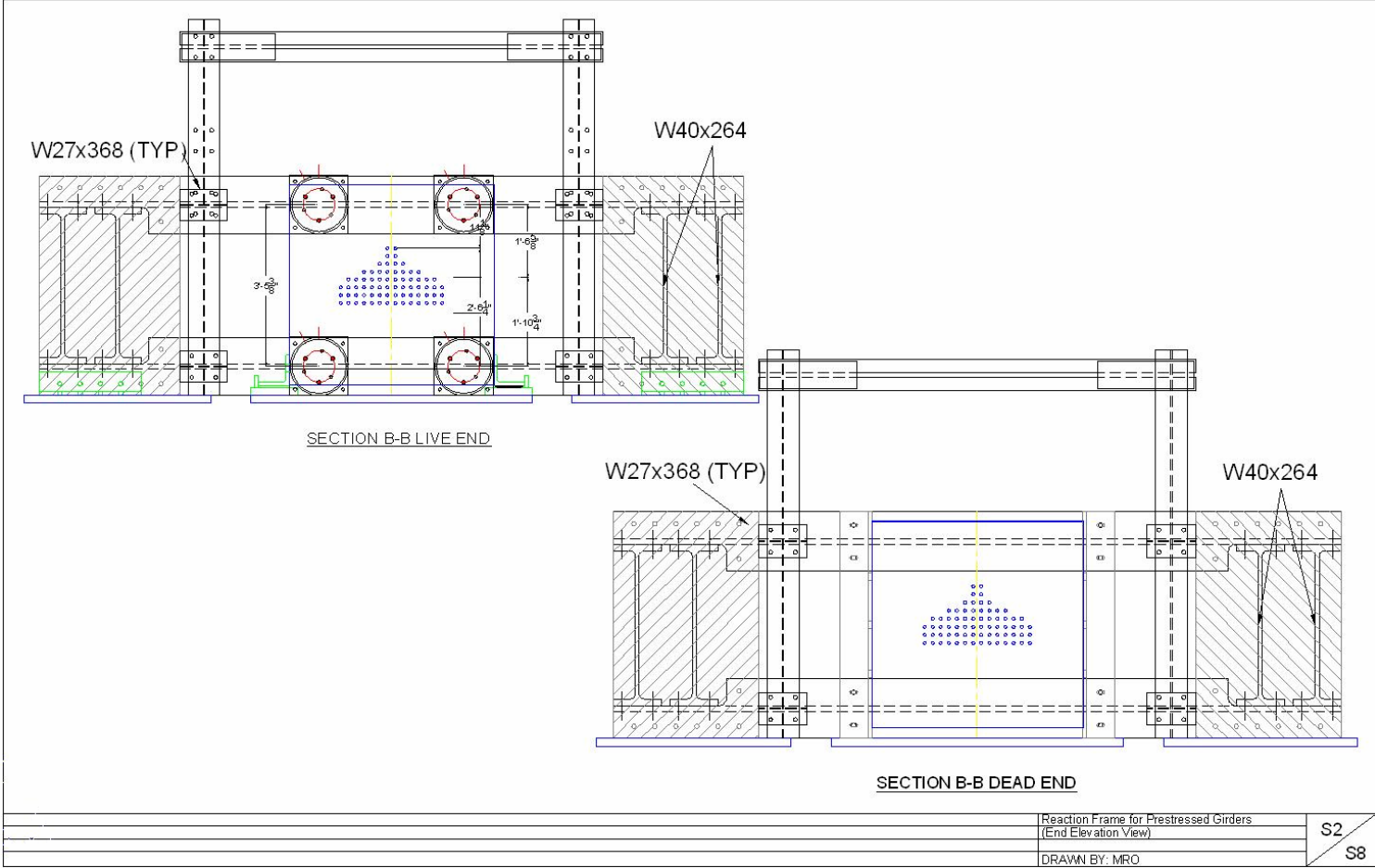


Figure E-2: High capacity prestressing bed design drawing (Elevation View)

255

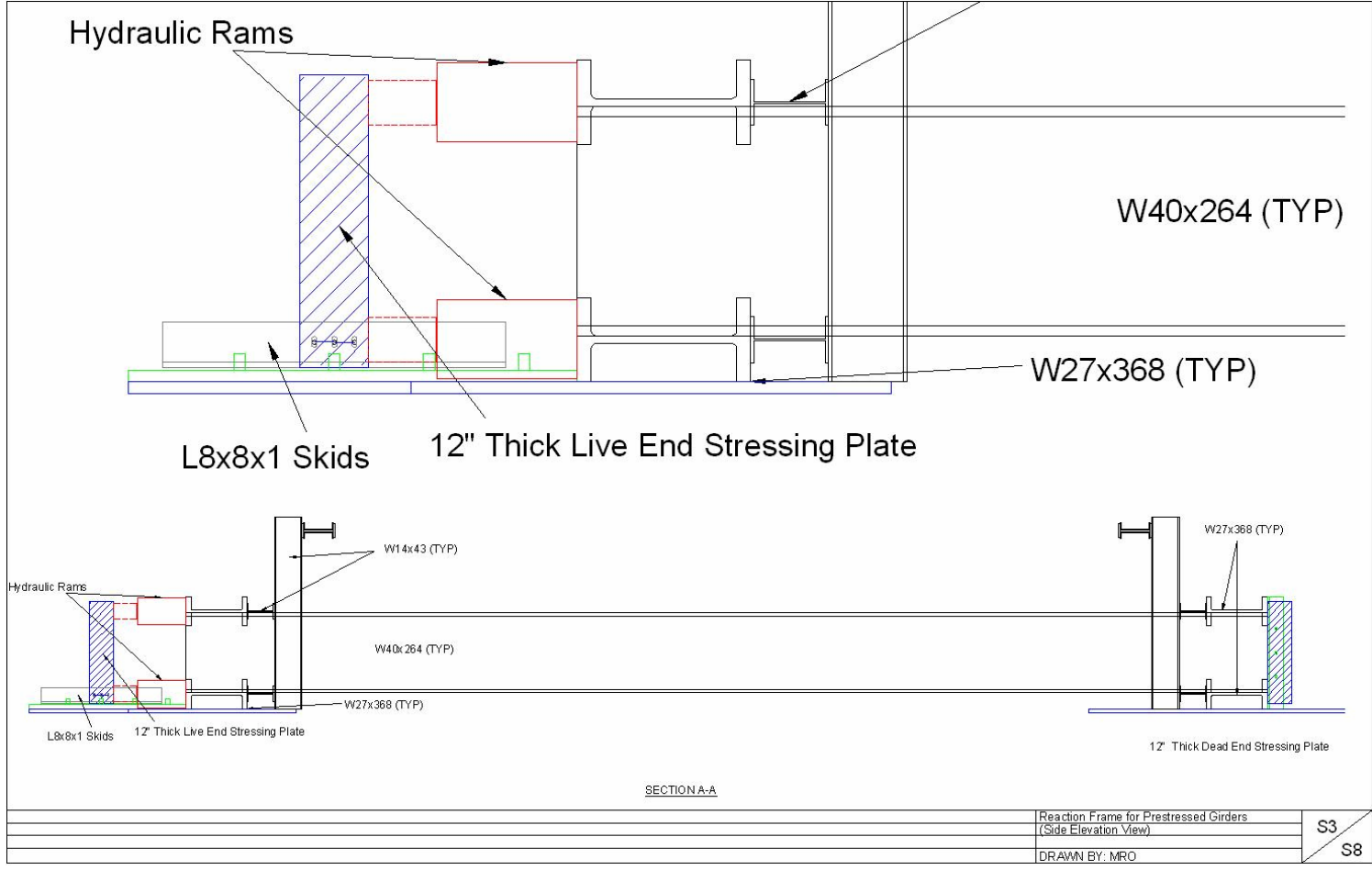


Figure E-3: High capacity prestressing bed design drawing (Elevation View)

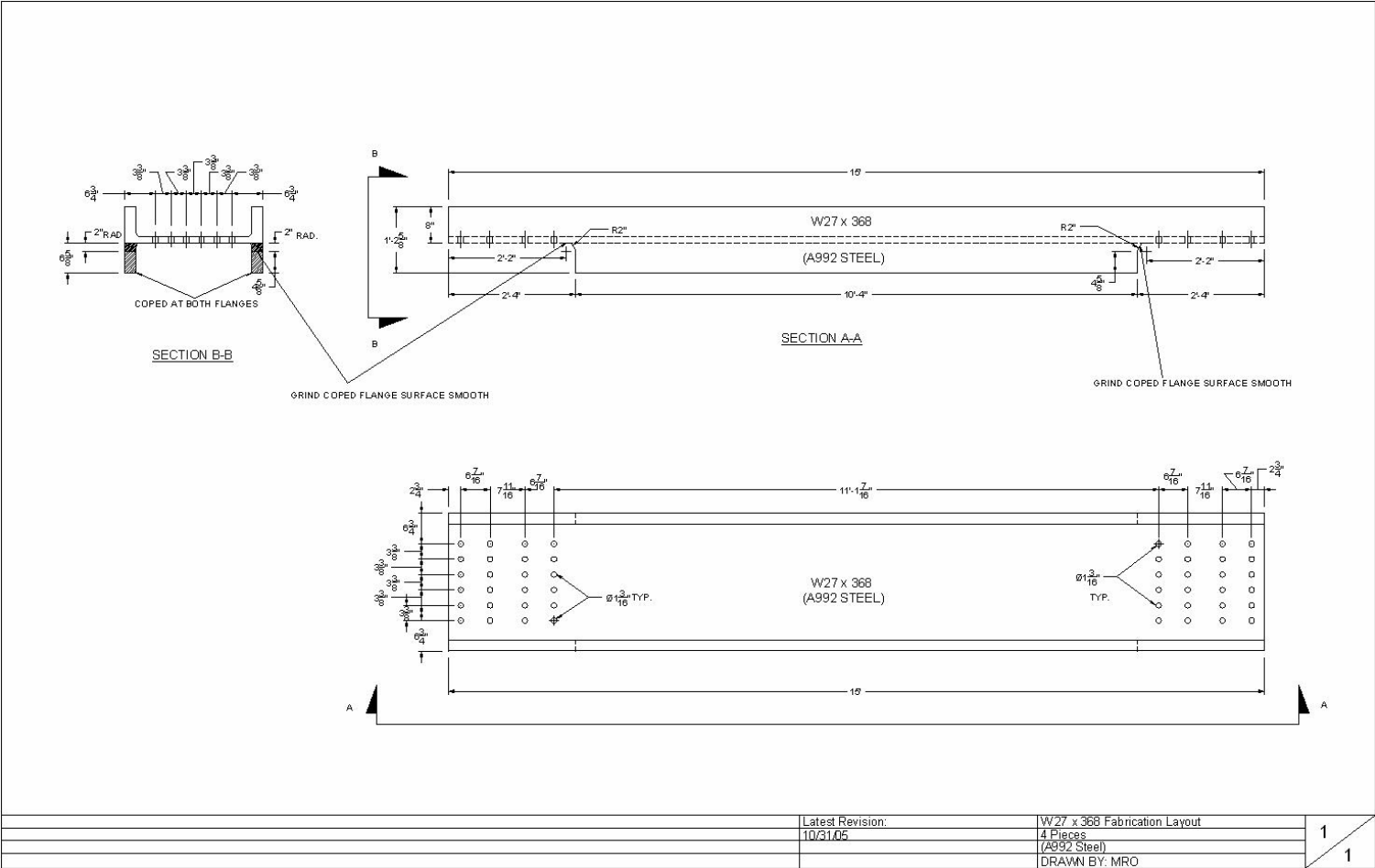
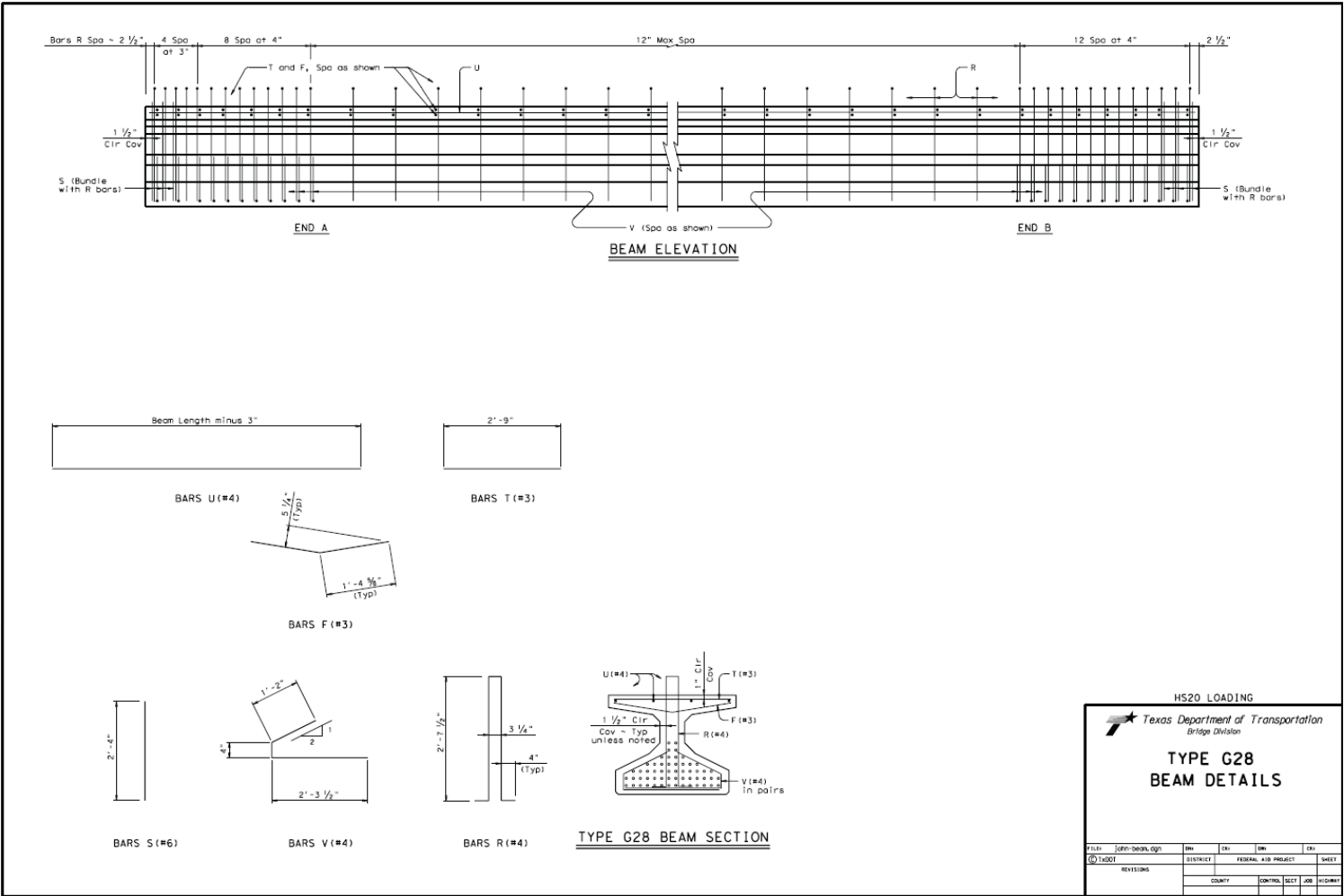


Figure E-4: High capacity prestressing bed design drawing (Typical detail drawing)

APPENDIX F

TxDOT Design Drawings for the Tx Family of Girders



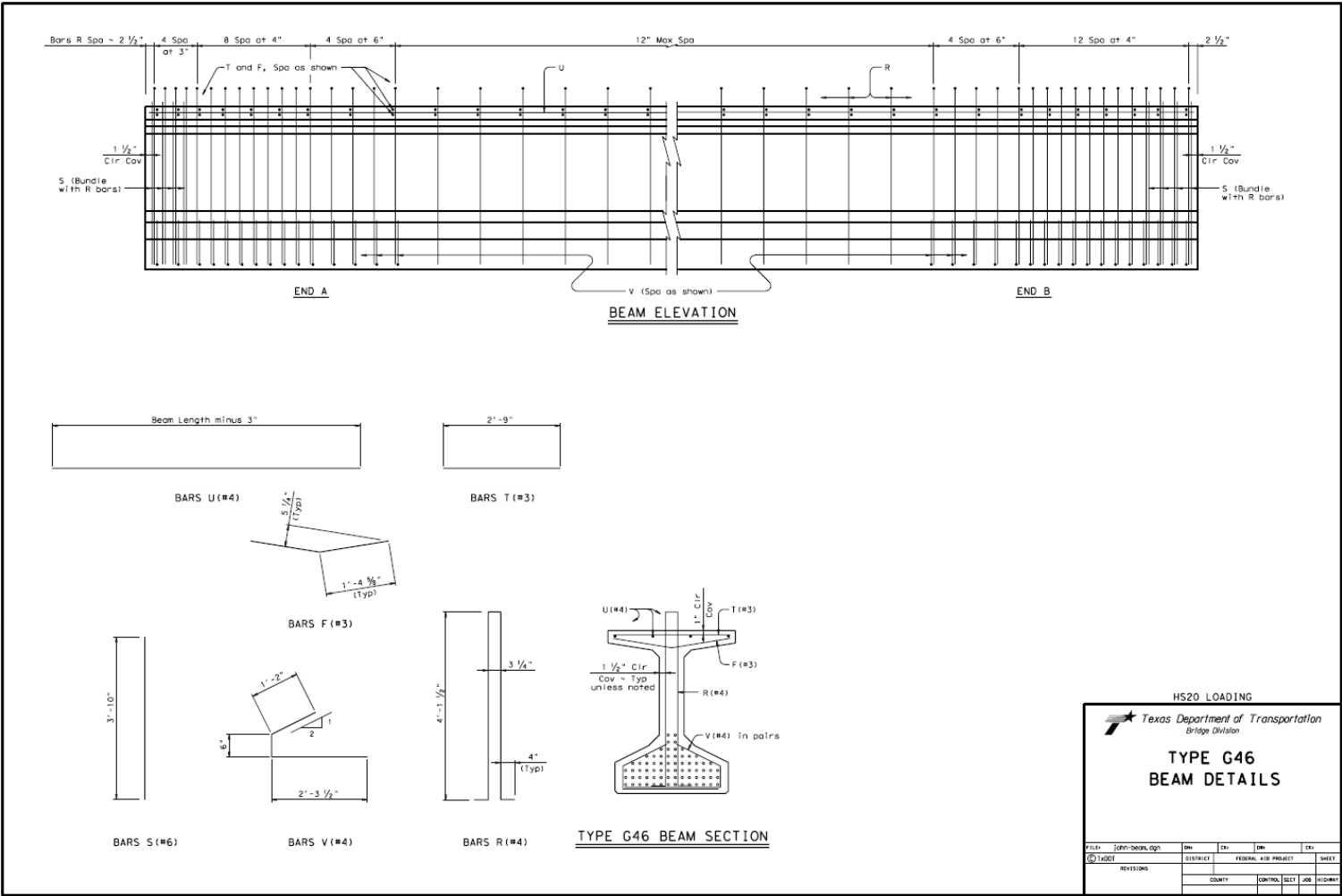
H520 LOADING

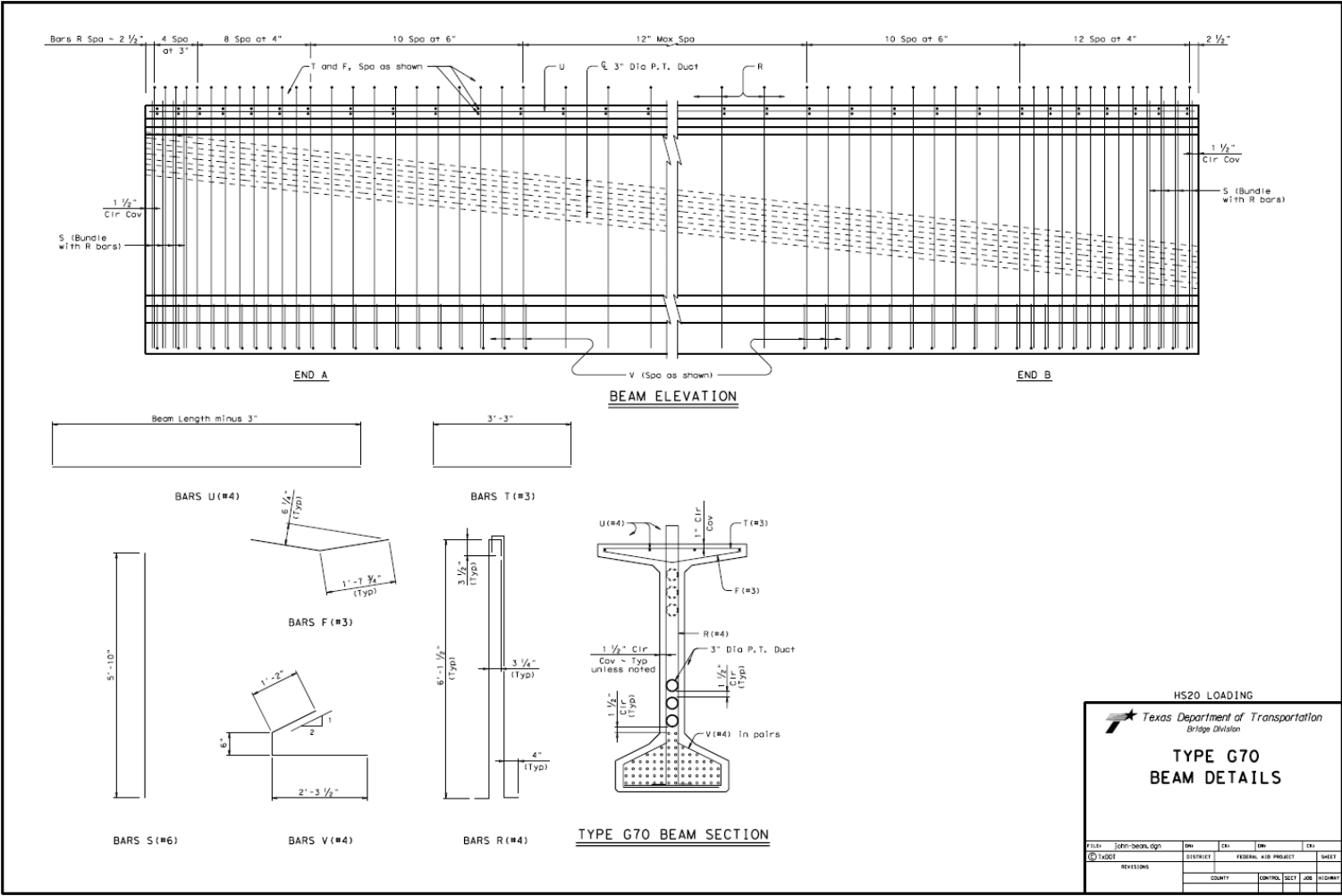
Texas Department of Transportation
Bridge Division

**TYPE G28
BEAM DETAILS**

FILE#	JOHN-BENNETT	REV	EN	REV	EN
PROJECT		DISTRICT		FEDERAL AID PROJECT	SHEET
REVISIONS		COUNTY	CONTROL	SCALE	JOB #101000

259



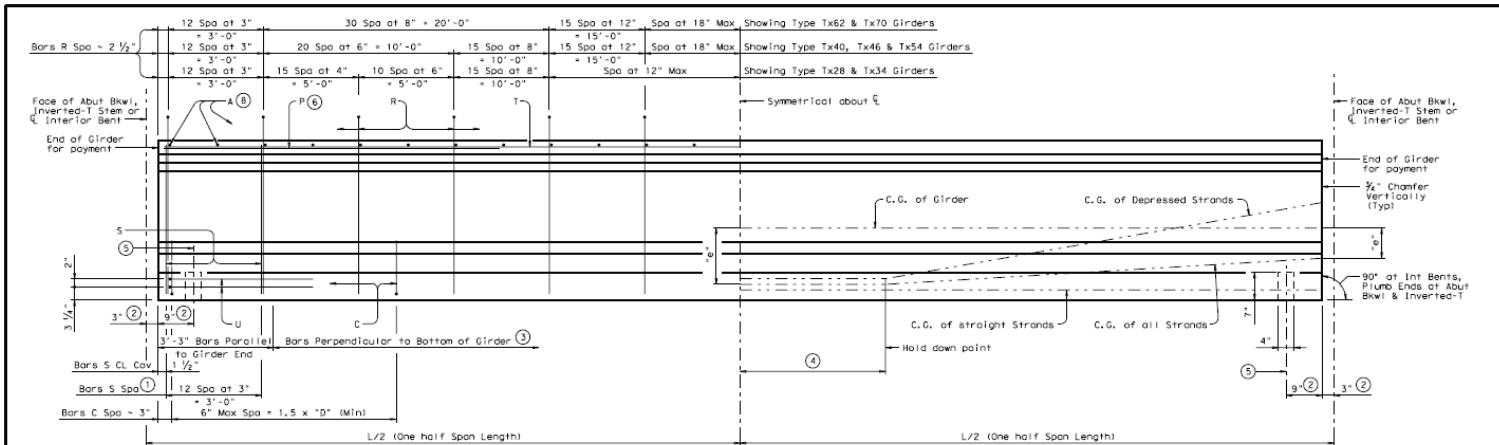


HS20 LOADING

Texas Department of Transportation
Bridge Division

**TYPE G70
BEAM DETAILS**

FILED	DATE	BY	CHK	APP	DATE
(1) 1/2001	DISTRICT	FEDERAL AID PROJECT	JOB	SHEET	NO.
REVISIONS		COUNTY	CONTRACT	SECTION	JOB
NO.	DATE	BY	CHK	APP	DATE



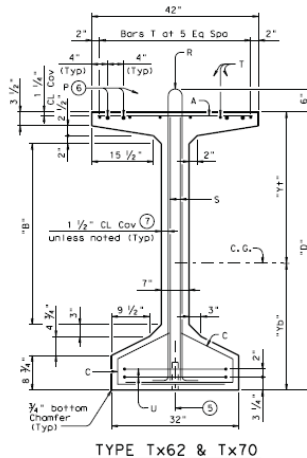
- ① Bundle with Bars R.
- ② Measured along \bar{C} of girder at interior bents; perpendicular to abutment skew or inverted-T stem.
- ③ The average of the top and bottom spacing of Bars R cannot exceed the required spacing.

GIRDER ELEVATION

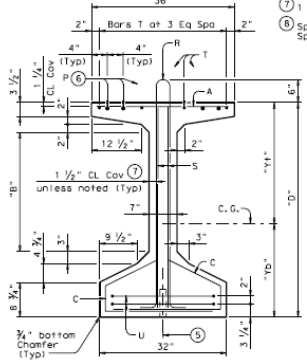
- ④ L/20, but not less than 5'-0" (-0,-2").
- ⑤ $4" \times 1\frac{1}{2}"$ Vertical Slotted Hole at doweled girder end (labeled (D) on Bridge Layout). Required for outside girder only or as shown on substructure details. Anchorage holes may be tapered ($4\frac{3}{4}" \times 1\frac{1}{2}"$) at base. If holes are formed with sheet metal, forms may be left in place.
- ⑥ Bars P (#6 x 15'-0") are only required when "e" of girder ends exceeds 0.25 x "D". At the fabricator's option bars larger than #6 may be used. When L is less than 50 ft, Bars P are to be the same length as Bars T.
- ⑦ $1\frac{1}{8}"$ Clear Cover to Bars S.
- ⑧ Space Bars A at 6" Max for girders requiring overhang bracket hangers. Space at 12" Max for all other girders. Tie to Bars R as necessary.

GIRDER DIMENSIONS AND SECTION PROPERTIES									
Girder Type	"D"	"B"	"H"	"H ₁ "	Area	"I _x "	"I _y "	Weight	
	(in.)	(in.)	(in.)	(in.)	(in. ²)	(in. ⁴)	(in. ⁴)	(pif.)	
Tx28	28	6	15.02	12.98	585	52,772	40,559	610	
Tx34	34	12	18.49	15.51	627	88,395	40,731	653	
Tx40	40	18	21.90	18.10	669	134,990	40,902	697	
Tx46	46	22	25.90	20.10	761	198,069	46,478	793	
Tx54	54	30	30.49	23.51	817	299,740	46,707	851	
Tx62	62	37 1/2"	33.72	28.28	910	463,072	57,351	948	
Tx70	70	45 1/2"	38.09	31.91	966	628,747	57,579	1,006	

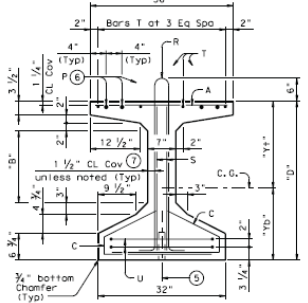
GENERAL NOTES:
 Designed in accordance with AASHTO LRFD Specifications.
 All concrete must be Class H.
 All reinforcing bars must be Grade 60.
 An equal area of deformed Welded Wire Reinforcement (WWR) (ASTM A497) may be substituted for Bars A, C, R or T unless otherwise noted.
 It is permissible for bars or strands to come in contact with materials used in forming anchor holes.



TYPE Tx62 & Tx70



TYPE Tx46 & Tx54



TYPE Tx28, Tx34 & Tx40

Texas Department of Transportation
 Bridge Division

**PRESTRESSED CONCRETE
 I-GIRDER DETAILS**

IGD

FILED	igtdetail.dgn	DATE	04/15/2007	BY	JTB	CHK	JTB	SHEET
SUBJECT		COUNT		CONTROL		JOB		NO.

PRELIMINARY
 SUBJECT TO REVISION
 DATE: May 15, 2007

BIBLIOGRAPHY

1. AASHTO, *Standard Specifications for Highway Bridges*, 8th Edition, American Association of State Highway and Transportation Officials, Washington, D.C., 1961
2. AASHTO, *LRFD Bridge Design Specifications*, Interim 2002 Edition, American Association of State Highway and Transportation Officials, Washington, D.C., 2002.
3. AASHTO, *LRFD Bridge Design Specifications*, 4th Edition, American Association of State Highway and Transportation Officials, Washington, D.C., 2007.
4. ACI Committee 318, *Building Code Requirements for Reinforced Concrete (ACI 318-05)*, American Concrete Institute, Farmington Hills, MI, 2005.
5. Adeghe, L.N., and Collins, M.P., *A Finite Element Model for Studying Reinforced Concrete Detailing Problems*. Department of Civil Engineering, University of Toronto, Publ. No. 86-12, Oct. 1986, pp. 66-74.
6. Beer, F. P., and Johnston, E. R., *Mechanics of Materials*, McGraw-Hill Inc., New York, 1992.
7. Bleich, F., "Ded gerade Stab mit Rechteckquerschnitt als ebenes Problem," *Der Bauingenieur*, No. 10, 1923, pp. 225-259.
8. Breen, J.E., Burdet, O., Roberts, C., Sanders, D., Wollmann, G., "Anchorage Zone Reinforcement for Post-Tensioned Concrete Girders," *NCHRP Report 356*, TRB, National Research Council, Washington, D.C., 1994.
9. Comité Euro-International Du Beton and the Federation Internationale de la Précontrainte, *Model Code 1990*, Comité Euro-International Du Beton, Lausanne, Switzerland, 1998.

10. Christodoulides, S.P., "The Distribution of Stresses Around the End Anchorages of Prestressed Concrete Beams," *International Association for Bridge and Structural Engineering*, Publications, Vol. 16, 1956.
11. Comité Euro-International Du Béton, *Anchorage Zones of Prestressed Concrete Members*, State-of-the-Art Report, CEB Bulletin No. 181, May 1987.
12. Comité Euro-International Du Béton, *Contributions to the Design of Prestressed Concrete Structures*, State-of-the-Art Report, CEB Bulletin No. 212, Dec. 1992.
13. Collins, M. P. and Mitchell, D., *Prestressed Concrete Structures*, Response Publications, Toronto and Montreal, Canada, 1997.
14. Fenwick, R.C., and Lee, S.C., "Anchorage Zones in Prestressed Concrete Members," *Magazine of Concrete Research*, Vol. 38, No. 135, June 1986, pp. 77-89.
15. Gergely, P., Sozen, M.A., and Siess, C.P., *The Effect of Reinforcement on Anchorage Zone Cracks in Prestressed Concrete Members*, Structural Research Series No. 271, University of Illinois, Urbana, July 1963.
16. Guyon, Y., *Prestressed Concrete*, 1st Edition, J. Wiley and Sons, Inc., New York, 1953.
17. Iyengar, K.T., "Two-Dimensional Theories of Anchorage Zone Stresses in Post-Tensioned Beams," *Journal of the American Concrete Institute*, Vol. 59, No. 10, October, 1962, pp. 1443-1466.
18. Khaleghi, B. "Splitting Resistance of Pretensioned Anchorage Zones," *Washington State Department of Transportation*, December 23, 2006, WashDOT, January, 2007, <<http://www.wsdot.wa.gov/eesc/bridge/designmemos/11-2006.htm>>.
19. Kehl, R. J., and Carrasquillo, R. L., *Investigation of the Use of Match Cure Technology in the Precast Concrete Industry*, Research Report No. 1714-2, Center for Transportation Research, The University of Texas at Austin, Aug. 1998.

20. Kupfer, H., "Bemessung von Spannbetonbauteilen", *Béton-Kalender*, 1981, Teil1, S. 1102.
21. Lin, T. Y., "Tentative Recommendations for Prestressed Concrete," *Journal of the American Concrete Institute-Proceedings*, Vol. 54, Part 2, September 1958, pp. 1232-1233.
22. Lin, T. Y. and Burns, N., *Design of Prestressed Concrete Structures*, Second Edition, John Wiley & Sons, Inc., New York, 1963.
23. Lenschow, R.J., and Sozen, M.A., "Practical Analysis of the Anchorage Zone Problem in Prestressed Beams," *Journal of the American Concrete Institute*, Vol. 62, No. 11, Nov. 1965, pp. 1421-1438.
24. Leonhardt, Fritz, *Prestressed Concrete Design and Construction*, Second Edition, Wilhelm, Ernst, and Sohn, Berlin, 1964, pp. XI.
25. Magnel, G., "Design of the Ends of Prestressed Concrete, Beams," *Concrete and Constructional Engineering*, Vol. 44, 1949.
26. Marshall, W.T., and Mattock, A.H., "Control of Horizontal Cracking in the Ends of Pretensioned Prestressed Concrete Girders," *PCI Journal*, V. 7, No. 5, October 1962, pp. 56-74.
27. MacGregor, J. G., *Reinforced Concrete Mechanics and Design*, Third Edition, Prentice Hall, New Jersey, 1997.
28. Mörsch, E., "Über die Berechnung der Gelenkquader." *Béton-und Eisen*, No. 12, 1924, pp. 156-161.
29. Nickas, W. N., "Temporary Design Bulletin C04-01", *Florida Department of Transportation*, February 3, 2004, FDOT, January, 2007, <<http://www.dot.state.fl.us/structures/memos/temporaryDesignBulletinC04-01.pdf>>.
30. PCI, *PCI Design Handbook*, Sixth Edition, Precast/Prestressed Concrete Institute, Chicago, IL, 2004.

31. Ramaswamy, G.S., and H. Goel, "Stresses in End Blocks of Prestressed Beams by Lattice Analogy," *Proceedings of the World Conference on Prestressed Concrete*, San Francisco, 1957.
32. Ruhnau, J., and Kupfer, H., "Spaltzug-, Stirnzug-, und Schubbewehrung im Eintragungsbereich von Spannbett-Trägern," *Beton-und Stahlbetonbau* 72, 1977, Heft 7, pp. 175-179, Heft 8, pp. 204-208.
33. Schlaich, J., and Schäfer, K.; and Jennewein, M., "Toward a Consistent Design of Structural Concrete," *Journal of the Prestressed Concrete Institute*, Vol. 32, No. 3, May-June 1987, pp. 74-149.
34. Sievers, H., "Über den Spannungszustand im Bereich der Ankerplatten von Spanngliedern vorgespannter Stahlbetonkonstruktionen," *Der Bauingenieur*, Vol. 31, 1956.
35. Stone, W.C., and Breen, J.E., "Behavior of Post-Tensioned Girder Anchorage Zones," *PCI Journal*, V. 29, No. 1, January-February 1984, pp. 64-109.
36. Tassi G., Erdélyi L., Bódi I., "Reliability of the stress state due to Prestressing in Factory made Elements," *Inzentrské Stavby*, 1985.
37. Tuan, C.Y., Yehia, S.A., Jongpitaksseel, N., Tadros, M.K., "End Zone Reinforcement for Pretensioned Concrete Girders," *PCI Journal*, Vol. 49, No. 3, May-June 2004, pp. 68-82.
38. Uijl, J.A. den, *Tensile Stresses in the Transmission Zones of Hollow-Core Slabs Prestressed with Pretensioned Strands*, TU Delft, Stevinlaboratory, Report No. 5-83-10, Sept. 1983.